The Dissertation Committee for Wei Yang Certifies that this is the approved version of the following dissertation:

Improvement in the Bioavailability of Poorly Water-Soluble Drugs via Pulmonary Delivery of Nanoparticles

Committee:

Robert O. Williams III, Supervisor

Keith P. Johnston, Co-Supervisor

James W. McGinity

Jason T. McConville

Nathan P. Wiederhold

Improvement in the Bioavailability of Poorly Water-Soluble Drugs via Pulmonary Delivery of Nanoparticles

by

Wei Yang, B.S.; M.S.Phr.

Dissertation

Presented to the Faculty of the Graduate School of

The University of Texas at Austin

in Partial Fulfillment

of the Requirements

for the Degree of

Doctor of Philosophy

The University of Texas at Austin

August 2009

Dedication

To my loving and ever-supportive father and mother,
Mr. Jingsen Yang and Mrs. Fengqing Wang

Acknowledgements

I would foremost like to extend my deepest gratitude to my supervising advisor, Dr. Robert O. Williams III, for providing me the opportunities over the past four years. His insightful guidance, positive attitude, and endless encouragement throughout my entire study lead me to where I am today. I would also like to thank my co-supervisor, Dr. Keith P. Johnston, for his constructive suggestions, experimental ideas, and meticulous guidance to improve my ability to communicate and write scientific papers. I sincerely appreciated the mentorship I received from Dr. James W. McGinity. His extensive and solid knowledge base, his life lessons, his enthusiasm for being a pharmaceutical scientist, and his care of students influence me immensely and will be beneficial to my career and development throughout my life. In addition, I would like to thank Dr. Jason T. McConville for his mentorship during my early years in graduate school, constant encouragement, and willingness to help whenever I have questions. I would also like to express my thankfulness to Dr. Nathan P. Wiederhold for his invaluable help in designing and conducting in vivo studies on inhaled itraconazole, insight into analysis of itraconazole delivery and pharmacokinetics, and guidance to improve my communication ability.

I am very thankful to the College of Pharmacy Staff for making my busy life easier: Ms. Yolanda Abasta, Ms. Mickie Sheppard, Ms. Claudia McClelland, Ms. Joyce McClendon, Ms. Janet Larsen, Mr. Jay Hamman, and Mr. Jim Baker.

I would also like to thank all of the past and present post doctoral fellows, graduate students for their friendship, assistance, and guidance. Specifically, I thank Dr. Jiahui Hu, Dr. Jason McConville, Ms. Jasmine Tam, Dr. Keat Theng Chow, Mr. Bo Long, Dr. Dave Miller, Dr. Jim DiNunzio, Dr. Kirk Overhoff, Dr. Troy Purvis, Dr. Michal Mateucci, Dr. Josh Engstrom, Dr. Shawn Kucera, Dr. Justin Tolman, Mr. Alan Watts, Mr. Kevin O'Donnell, Ms. Piyanuch Wonganan, Ms. Yoen Ju Son, Ms. Sandra Schilling, Ms. Nicole Nelson, Ms. Stephanie Bosselmann, Dr. Caroline Dietzsch, Dr. Dorothea Sauer, Ms. Loni Coots, and many others.

Finally, and most importantly, I express my deepest love and appreciation to my parents, Mr. Jingsen Yang and Mrs. Fengqing Wang for their unconditional love and support throughout every stage of my life. I would also like to thank my brother and all other family members for their love, care and encouragement. Lastly, I would like to extend my gratitude to my best friend Ms. Yubin Wu, my roommates Dr. Xuan Huang and Ms. Qian Wang for their friendship, care and support, which helped me went through hard times when I would need a helping hand most and without my family around.

Improvement of Bioavailability of Poorly Water-Soluble Drug via Pulmonary Delivery of Nanoparticles

Publication No._____

Wei Yang, Ph.D.

The University of Texas at Austin, 2009

Supervisors: Robert O. Williams III and Keith P. Johnston

High throughput screening techniques that are routinely used in modern drug discovery processes result in a higher prevalence of poorly water-soluble drugs. Such drugs often have poor bioavailability issues due to their poor dissolution and/or permeability to achieve sufficient and consistent systemic exposure, resulting in sub-optimal therapeutic efficacies, particularly via oral administration. Alternative formulations and delivery routes are demanded to improve their bioavailability. Nanoparticulate formulations of poorly water-soluble drugs offer improved dissolution profiles. The physiology of the lung makes it an ideal target for non-invasive local and systemic drug delivery for poorly water-soluble drugs.

In Chapter 2, a particle engineering process ultra-rapid freezing (URF) was utilized to produce nanostructured aggregates of itraconazole (ITZ), a BCS class II drug,

for pulmonary delivery with approved biocompatible excipients. The obtained formulation, ITZ:mannitol:lecithin (1:0.5:0.2, w/w), *i.e.* URF-ITZ, was a solid solution with high surface area and ability to achieve high magnitude of supersaturation. An aqueous colloidal dispersion of URF-ITZ was suitable for nebulization, which demonstrated optimal aerodynamic properties for deep lung delivery and high lung and systemic ITZ levels when inhaled by mice.

The significantly improved systemic bioavailability of inhaled URF-ITZ was mainly ascribed to the amorphous morphology that raised the drug solubility. The effect of supersaturation of amorphous URF-ITZ relative to nanocrystalline ITZ on bioavailability following inhalation was evaluated in Chapter 3. The nanoparticulate amorphous ITZ composition resulted in a significantly higher systemic bioavailability than for the nanocrystalline ITZ composition, as a result of the higher supersaturation that increased the permeation.

In Chapter 4, pharmacokinetics of inhaled nebulized aerosols of solubilized ITZ in solution versus nanoparticulate URF-ITZ colloidal dispersion were investigated, under the hypothesis that solubilized ITZ can be absorbed faster through mucosal membrane than the nanoparticulate ITZ. Despite similar ITZ lung deposition, the inhaled solubilized ITZ demonstrated significantly faster systemic absorption across lung epithelium relative to nanoparticulate ITZ in mice, due in part to the elimination of the phase-to-phase transition of nanoparticulate ITZ.

Table of Contents

List of Tables

List of Figures

Chapter 1: Inhaled Nanoparticles – A Current Review

1.1 ABSTRACT

The field of nanotechnology may hold the promise of significant improvements in the health and well being of patients, as well as in manufacturing technologies. The knowledge of this impact of nanomaterials on public health is limited so far. This paper briefly reviews the unique size-controlled properties of nanomaterials, their disposition in the body after inhalation, and the factors influencing the fate of inhaled nanomaterials. The physiology of the lung makes it an ideal target organ for non-invasive local and systemic drug delivery, especially for protein and poorly water-soluble drugs that have low oral bioavailability via oral administration. The potential application of pulmonary drug delivery of nanoparticles to the lungs, specifically in context of published results reported on nanomaterials in environmental epidemiology and toxicology is reviewed in this paper.

1.2 OVERVIEW OF NANOMATERIALS

In the current era of nanoscience, the use of nanotechnologies in commercial applications is increasing in many scientific disciplines, including electronics, sporting goods, tires, stain-resistant clothing, cosmetics, and medicine for diagnosis, imaging and drug delivery.

'Nanoscience' and 'nanotechnologies' have been defined by the Royal Society and Royal Academy of Engineering [1, 2] as follows:

"*Nanoscience is the study of phenomena and manipulation of materials at atomic, molecular and macromolecular scales, where the properties differ significantly from those at a larger scale*"; likewise, "*Nanotechnologies are the design, characterization, production and application of structures, devices and systems by controlling shape and size at nanometer scale*".

Nanomaterials, the building blocks for nanotechnology, are engineered materials with one or more components with at least one dimension measuring 100 nanometers or less. They include nanoparticles, nanofibers and nanotubes, composite materials and nano-structured surfaces. Nanoparticles, as a subset of nanomaterials, are currently defined as single particles with a diameter less than 100 nm. Agglomerates of nanoparticles can be larger than 100 nm in diameter but may be de-agglomerated with weak mechanical forces or by dispersing in a solvent. Nanofibers and nanotubes have two dimensions measuring less than 100 nm but the axial dimension can be much larger.

1.3 CHARACTERISTICS OF NANOMATERIALS

The main differentiating characteristic of nanomaterials is their size, which falls in the transitional zone between individual atoms or molecules and the corresponding bulk materials [3]. Size reduction can modify the physical and chemical properties of nanomaterials distinctively from their bulk and molecular counterparts. It is known that for a group of airborne particles with fixed mass (10 mg/m^3) and unit density (1 g/cm^3), as the particle size decreases to less than 100 nm, the number of particles increases exponentially along with the surface area, as shown in Figure 1.1. This allows a greater proportion of atoms or molecules to be orientated on the surface rather than within the interior of the material, hence allowing adjacent atoms and substances to interact more

readily. The surface-to-volume ratio determines the potential number of reactive groups; the intrinsic properties of materials at the nanosized level are emphasized compared to their larger bulk counterparts. The enhanced activities could be either beneficial (e.g. antioxidation, carrier capacity for drugs, increased uptake and interaction with biological tissues) or disadvantageous (e.g. toxicity, instability, induction of oxidative stress) depending on the intended use [4, 5].

Independent of particle size, the charges carried by the materials in contact with cell membranes and the chemical reactivity of the materials play a dominant role when the particles react with other substances or tissues [6].

Due to the attractive properties of nanomaterials (summarized in Table 1.1.), such as high strength, conductivity, solubility, durability and reactivity, they have been used in a variety of applications, including fillers, opacifiers, catalysts, semiconductors, cosmetics, microelectronics, and drug carriers [4, 7]. However, as production and use of engineered nanomaterials have expanded, the potential impact to the environment and human health must be investigated and confirmed [8].

Particle size and surface area of the nanomaterials are important characteristics from a toxicological viewpoint. Carbon black nanoparticles of similar mass and composition but with different specific surface areas (300 versus 37 m^2/g) were studied. It was found that the biological effects, such as, inflammation, genotoxicity, and histology were related to surface area and not particle mass. Similar findings have been reported regarding tumorigenic effects of inhaled particles. It was shown that the tumor incidence correlated better with specific surface area than with particle mass [9, 10]. It is

recognized that biologically available surface area is probably the most critical parameter for the effects of the nanomaterials. Additionally, particle surface chemistry, biodegradability, number, shape, and solubility are all found to be significant factors in determining harmful biological effects [3, 11, 12].

Knowledge of the effects of nanomaterials on biological systems is limited due to the relative novelty of this technology, and little has been done to assess the risks of nanomaterials to biological systems. The current paradigm in environmental epidemiology is that adverse health effects of fine and ultrafine particulates, such as those found in air pollution and some workplaces, are driven by the ultrafine particle fraction, indicating that exposure to materials in the nano-size range could cause significant public health problems, such as pulmonary and cardiovascular diseases [13-15].

1.4 THE LUNGS AS A DELIVERY TARGET FOR NANOMATERIALS

The lungs, skin, and intestinal tract are in direct contact with the environment. These organs are likely to be a first port of entry for nanomaterials into the body. Epidemiological studies showed a positive correlation between increases in atmospheric particulate concentrations and the short term increases in morbidity and mortality [15, 16]. Inhalation is the most significant exposure route for airborne nanoparticles [3, 4]. The lung consists of two functional parts, the airways (trachea, bronchi, and bronchioles) and the alveoli (gas exchange areas). The conducting zone consist of the first 16 generations of airways comprised of the trachea (generation 0), which bifurcates into the two main stem bronchi, and subdivides into progressively smaller-diameter bronchi and bronchioles. The respiratory zone consists of all structures that participate in gas exchange and begins with the respiratory bronchioles [17]. The human lungs contain

about 2300 km of airways and 500 million alveoli [18]. The surface area of the human lungs is estimated to be approximately 75-140 m^2 in adults [19-21]. The pseudostratified epithelia that constitute the barrier to absorption into the bloodstream are markedly different in airways and alveoli of the lungs. The airways are composed of a gradually thinning columnar epithelium, with the bronchial epithelium of 3-5 mm and bronchiolar epithelium of 0.5-1 mm in thickness [17, 22]. In the tracheo-bronchial region the epithelium is protected by a mucus layer [23]. Any particle deposited in this area is transported away from the lung by mucociliary clearance [24], or diffuse through the thick mucus to reach the epithelium cells. In contrast, the alveoli have a thin, single cell layer. The distance from the air in the alveolar lumen to the capillary blood flow is less than 400 nm. The large surface area of the alveoli and the intimate air-blood contact in this region make the alveoli less well protected against inhaled substances, such as nanoparticles, as compared to the airways [23].

1.5 DEPOSITION OF NANOMATERIALS IN THE RESPIRATORY TRACT

There are three principal mechanisms that lead to pulmonary deposition: inertial impaction, gravitational sedimentation, and Brownian diffusion, as summarized in Table 1.2. The inertial impaction occurs during the passage through the oropharynx and large conducting airways if the particles possess a mass median aerodynamic diameter (MMAD) more than 5 micron. When the MMAD of particles ranges from 1 to 5 microns, they are subject to sedimentation by gravitational force that occurs in smaller airways and respiratory bronchioles. Sedimentation is influenced by breath-holding. Particles with a MMAD of less than or equal to approximately 0.5 micron, they are deposited significantly by diffusion, based on the Brownian motion [23, 25, 26].

The site, extent and efficacy of particle deposition after inhalation is influenced primarily by three factors (aerosol properties and physiology) during breathing: (a) particle/droplet size (diameter), density, surface properties, or shape (i.e. fibers) [27]; (b) anatomy of the upper and lower airways and the alveolar structure; (c) ventilatory parameters with impact on the particle deposition are breath pattern (including breath-holding and presence of expiratory flow limitation), flow rates and tidal volume, determining the airflow velocity and the residence time in the respiratory tract [25, 28, 29].

Next to morphological characteristics and ventilation parameters, the particle size and geometry is most important [25]. The particle size is commonly referred to the aerodynamic diameter, which is a variable depending on the shape, density and size of the object. If aerosols contain different particles, the size distribution is usually characterized by MMAD, which is particularly important to determine whether the particles will be efficiently deposited deep into alveolar region [21, 30]. A successful deposition into deep lung requires the particles be small enough to avoid deposition by inertial impaction on upper airways and can pass through the lower airways, meanwhile be large enough to avoid exhalation [31, 32]. The optimal particle size for achieving delivery deep into alveolar region has been established to be an aerodynamic diameter between 1 and 3 microns [33]. In general, aerosol particles measuring less than 1 micron can be exhaled up to 80% after inspiration without being deposited, because of their low inertia [34, 35]. The deposition of particles in the lung; however, is bi-model and ultra fine particles (less than 100 nm) appear to settle effectively to the alveolar region with a fractional deposition of around 50%, as calculated with mathematical modeling of monodisperse particles after slow inhalation with a breath hold (see Figure 1.2.) [23, 33,

36]. This has been confirmed by controlled clinical studies evaluating deposition and effects of laboratory-generated ultra fine particles. High deposition efficiencies in the total respiratory tract of healthy subjects were found, and deposition was even greater in subjects with asthma or chronic obstructive pulmonary disease [37, 38].

Nanoparticle deposition in the respiratory tract is determined predominantly by diffusional displacement due to the thermal motion of air molecules interacting with particles in the inhaled and exhaled air streams [39, 40]. Depending on the particle size, shape and ventilation parameters, deposition occurs in all regions of the lung: the airways and the alveoli. With decreasing particle diameter below about 500 nm, the deposition increases in all regions of the lung because of the increasing diffusional mobility [33]. Nanofibers with a small diameter will penetrate deeper into the lungs, while very long fibers (more than 20 microns) are predominantly located in the upper airways [41, 42].

1.6 THE FATE OF INHALED NANOMATERIALS IN THE LUNG

The fate of inhaled nanomaterials depends on regional distribution in the lung, because disposition within the lung is a complex function of the kinetics of absorption and non-absorptive clearance mechanisms [43]. Once nanomaterials are deposited onto the lining of the respiratory tract, they first contact the mucous layer within the airways or the surfactant lining fluid layer within the alveolar region. Airway mucus (about 5 microns in depth) is a complex aqueous secretion of airways, comprising electrolytes, proteins, glycoproteins (e.g. mucins), and cell debris [44]. The components vary much depending on environmental and disease states. The surfactant lining layer (10-20 nm in thickness) that covers the alveolar surface is composed of 90% in weight of phospholipids and 10% in weight of specific proteins [45, 46]. Both airway and alveolar

surface liquids are coated with at least a monolayer of highly surface active lung surfactant, which are primarily water insoluble long chain phospholipids. They form liquid crystals but not micelles in aqueous media [22] to maintain the functions of the lungs: facilitation of gas exchange and prevention of alveoli collapse by reducing the lung air interface surface tension [47, 48].

It was found that regardless of the nature of the nanomaterials surfaces, they will be submersed into the lining fluids after their deposition [40]. Study of interactions between different nanoparticles and lung surfactant film indicated that the smaller the size of nanoparticle, the more can be incorporated into the surfactant film. However, the surface pressure of the surfactant film does not change significantly with the incorporation of nanoparticles, i.e. the size dependent incorporation of nanoparticles does not destabilize the lung surfactant film [49]. D-alpha-tocopheryl polyethylene glycol 1000 succinate (TPGS) coated nanoparticles also do not destabilize the model surfactant film, suggesting potential application of nanoparticles to lungs [50].

Once deposited within the lung lining fluid, there are separate biokinetics for lung absorption and non-absorptive clearances. The kinetics of dissolution of inhaled particulates determines whether the inhaled nanomaterials will dissolve in the epithelial lining fluid for lung absorption or whether such nanomaterials will undergo non-absorptive clearances [51]. Inhaled nanomaterials that are either lipid soluble, or soluble in intracellular or extracellular fluids undergo chemical dissolution in situ. Low molecular weight hydrophobic molecules are thought to be rapidly absorbed (within seconds) by passive diffusion through the lung epithelial membrane [52]. The kinetics of diffusion in the alveoli is much faster than that of the small airways, mainly because lung

absorption mostly occurs from the air-side surface of the alveoli to the pulmonary capillaries. The alveoli has a thin monolayer (0.1- 0.4 micron) composed of extremely broad and thin Type I cells and small compact Type II cells, and a large surface area (more than 100 m^2). Only a small portion of inhaled nanoparticles is absorbed from the tracheobronchial airways which have a much thicker layer of column-shaped epithelial cells (10–60 microns) and lower surface area (1– 2 m^2) [29]. This is supported by Fick's law. Low molecular weight hydrophilic molecules can be absorbed by active transport via specific transporters, or by passing through the tight junctions [22]. The kinetics of active absorption should depend upon the lung-regional expression and functionality of receptors or transporters. It was recently reported that the absorption of large molecule immunoglobulins of the IgG class (150 kDa) might occur in the upper airways by receptor-mediated transcytosis of IgG [53, 54]. Solutes and soluble components may be eventually cleared into blood and lymphatic circulation.

Inhaled nanomaterials that are insoluble in mucus and lining fluid, are not able to be rapidly absorbed, and may undergo physical translocation. This is different depending on lung region in which the nanoparticles have been deposited [4]. Immersion of the inhaled, slowly dissolving or insoluble nanomaterials in the fluid lining the lungs may enable them to be closely associated with epithelial cells and cells of the host-defense system for particle-cell interaction [40]. Subsequently, several post defense mechanisms, including the mucociliary escalator transport, phagocytosis by macrophages and endocytosis, are involved in the removal of deposited nanoparticles and to maintain the lung mucosal surfaces [55, 56].

The mucociliary escalator dominates clearance of nanoparticles from the upper airways. Nanoparticles that consist of slowly dissolving or insoluble materials in the airway mucus will be partly moved by action of the ciliated epithelial cells pushing the mucus along with the nanoparticles that deposited on the airway walls to the larynx, where they are swallowed to the gastrointestinal tract or excreted through the mouth [34]. The deposited nanoparticles may also be removed by coughing within 1–2 days [22]. However, Schurch et al. showed that mucus clearance can be overcome by nanoparticles, possibly due to rapid displacement of particles to the airway epithelium via surface energetics [39].

Clearance of the slowly dissolving and insoluble nanoparticles from the alveoli is predominantly by macrophage phagocytosis and endocytosis [57]. The air-side surface of each of the 500 million alveoli in the human lungs is routinely monitored by 12–14 alveolar macrophages in the lung lining fluid [18]. The uptake of deposited particles by alveolar macrophages depends on the particle size and composition of coating material. Particles of 1-3 microns in diameter are far better taken up than those of 6 microns by macrophages, which have cell diameters about 15–22 microns [58]. Particles of less than 0.26 micron can escape from phagocytosis by macrophages [59]. Due to the small size, the chance of nanoparticles undergoing phagocytosis in the alveoli is much lower than micron sized particles. The remaining nanoparticles will interact with the non-phagocytic cells of the epithelium, and the endocytic events are regulated by clathrin-coated pits and caveolae, as well as scavenger receptors (e.g., scavenger receptor SR-A). It has been suggested that caveolae and coated pits preferentially transport small and large particles, respectively, but this needs to be further verified in vivo [60]. Caveolae are indentations of the plasma membrane lined with caveolin-1, and are abundantly expressed on lung

capillaries and type l alveolar cells. Macromolecules or particles of several nanometers in radii may be transported within caveolae from lung to blood [55, 60].

Transport via pores, as suggested for lung-blood substance exchange, is another possible route of disposition of inhaled nanomaterials. Inspiratory expansion and expiratory contraction of lung alveoli may lead to the opening and closing of the caveolae. These openings measure between 40 to 100 nm in size and are thought to be involved in the transport of macromolecules, such as proteins, across the alveolar-capillary barrier [22]. Additionally, a reactive nanomaterial surface will be able to initiate chemical interactions between nanoparticles and membranes by inducing lipid peroxidation at the interface, causing changes in membrane permeability and dynamics [5]. Thus, depending on size and surface reactivity, nanoparticles may be transported across cellular and sub-cellular membranes by different mechanisms. As a result most nanoparticles will be no longer retained as free particles on the epithelium as inhaled and deposited.

1.7 SYSTEMIC TRANSLOCATION OF INHALED NANOMATERIALS

Recently, it was reported that inhaled nanomaterials may also influence organs other than the lungs. Inhaled ultrafine technetium (^{99m}Tc) labeled carbon particles, which are very similar to the ultrafine fraction of actual pollutant particles, diffused into the systemic circulation of hamsters within 5 minutes. Nemmar et al. concluded that phagocytosis by macrophages and/or endocytosis by epithelial and endothelial cells may be responsible for particle-translocation to the blood, along with other mechanisms [61]. There are recent reports that inhaled nanoparticulates have been found in the brain,

probably traveling from the nasal nerves [62]. This suggests that nanoparticles may travel to sites away from the site of deposition in the lungs.

However, no definite conclusion about the systemic translocation of inhaled nanoparticles can be drawn to date, based on the conflicting results of human and animal studies. It was reported that rapid translocation to the liver (more than 50%) of 13C-labeled nanoparticles with a diameter of 26 nm occurred within 24 hours following inhalation in a rat model [42]. In another rat study, only less than 1% iridium nanoparticles (15–20 nm in diameter) were found in secondary organs of rats, but the nanoparticles were distributed widely throughout the body to such organs as liver, spleen, kidneys, brain and heart [63]. Kato et al. [64] has provided morphological data showing that inhaled polystyrene particles are transported into the pulmonary capillary space, presumably by transcytosis; nevertheless, other research groups did not find any detectable particulates in the body other than the lungs [65, 66].

The variable results from extrapulmonary translocation of experimental nanoparticles may due to differences in the chemical composition, particle size, surface characteristics, labeling materials and experimental models reported in the different studies. Taken together evidence from the in vivo studies for alveolar translocation of inhaled nanomaterials, supports that this pathway exists in humans; however, the extent of extrapulmonary translocation is determined by characteristics of the nanomaterials. Systemic translocation of the inhaled nanomaterials could better explain the epidemiological findings of adverse cardiovascular effects found in communities with air pollution [67].

Inhaled nanoparticles may end up in systemic circulation and the lymphatic system once they reach the pulmonary interstitial sites following transcytosis across alveolar epithelial cells [4]. There is uncertainty regarding the real contribution of the lung's lymphatic pathway to systemic appearance following inhalation of nanoparticles. In the respiratory system, a vast network of lymphatic vessels drains both the airways and the alveolar regions and terminates in the hilar and mediastinal lymph nodes [68]. Lymphatic drainage is responsible for alveolar clearance of deposited drugs and particulates up to a certain particle diameter, *i.e.* 500 nm [69, 70]. In vivo pharmacokinetic studies of radiolabelled solid lipid nanoparticles (mean diameter of 200 nm) revealed significant lymphatic uptake and a high rate of distribution in periaortic, axillar and inguinal lymph nodes after inhalation in rats [71]. For the deposited nanoparticles that are insoluble in the lining fluid of the lungs, they are taken up less efficiently by the macrophages [58]. The phagocytosed nanoparticles may be destroyed once within the lysosomes of phagocytic cells. Therefore it is evident that for the nanoparticles consisting of protein drug, macrophage engulfment usually means eventual digestion of the protein [72]. The nanoparticles sequestered by the macrophages may also be transported to regional lymph nodes and may subsequently migrate to systemic circulation. Particle-loaded macrophages were seen in pulmonary lymphatic vessels and in hilar lymph nodes of animals following instillation of particulates into the airways [68]. It has been shown that transfer of nanoparticles to the lymph nodes of the lung generally increases with increasing molecular weight greater than 10–20 kDa, whereas molecules less than 10 kDa are unlikely to be involved in this pathway [73]. The extent of elimination of inhaled nanoparticles from the different pathways is highly dependant on the nanomaterial characteristics (e.g., particle size, coating, surface charges), the

amount of inhaled nanoparticles, and potential degradation by lysosomal enzymes before transport to the lymphatic circulation.

1.8 FACTORS INFLUENCING THE FATE OF NANOMATERIALS

Clearance of inhaled nanoparticles from the lungs depends mainly on particle size and, by implication, on particle surface characteristics. It was reported following three months exposure of rats to ultrafine (~20 nm) and fine (~200 nm) titanium dioxide (TiO_2) particles by inhalation, the ultrafine particles were cleared significantly more slowly, and showed more translocation to interstitial sites and to regional lymph nodes as compared to the fine TiO_2 particles [74]. Particles between about 20 and 50 nm in diameter may enter into the central nervous system and cells. In addition, alveolar macrophages on the surface of the lungs appear not be able to recognize particles of less than 70 nm as being "foreign", thus allowing them to gain access to the pulmonary interstitium, and then capillary blood flow [75].

Particle shape may also interfere with the clearance mechanisms. Nanofibers measuring more than 20 microns in one axis are too long to be phagocytosed (fibers longer than the diameter of the alveolar macrophage) and will be cleared very slowly, staying in the lungs for months and possibly years. They induce a rather general non-specific pulmonary inflammatory response, including release of chemokines, cytokines, reactive oxygen species, and other mediators, which can result in sustained inflammation and eventually fibrotic changes [3, 16].

Surface coating of nanoparticles was found to effect particle uptake. Albumin, lecithin, polysorbate 80, or peptide attachments can enhance nanoparticle uptake into

cells, whereas polyethylene glycol interferes with nanoparticle uptake into the liver [76]. Kato et al. administered intact or lecithin-coated insoluble polystyrene latex beads (240 nm in diameter) intratracheally to rats using an air jet nebulizer. Scanning electron micrographs of the rat lungs showed that both lecithin-coated and uncoated beads were incorporated into alveolar macrophages. Some of the ingested beads in the alveolar macrophages were sequestered within lysosomes. Types I, and II alveolar epithelial cells and monocytes in the capillary lumen selectively incorporated only lecithin-coated beads. These findings suggest that alveolar epithelial cells can incorporate exogenous particles, which are then transferred from the alveoli to intravascular spaces by transcytosis. The interaction between cells and the lecithin-coated particles may involve cellular ligands to recognize the lecithin by virtue of its molecular charge or hydrophilicity. Also, as observed with lecithin, albumin coating of inhaled nanoparticles appeared to facilitate nanoparticle endocytosis [64].

Moreover, surface electrostatic charge is an important factor influencing the deposition of inhaled nanoparticles. Charged nanoparticles have higher deposition efficiencies as compared to neutrally charged nanoparticles. Moderately lipophilic compounds with a positive charge at physiological conditions, such as pentamidine and verapamil, are preferentially bound to lung tissue [77]. Polycationic macromolecules show a strong interaction with cell membranes in vitro. Three polycationic paint components exhibited considerable cytotoxicity (LD50 generally below 100 mg/ml for an incubation period of 20–24 hours) in primary cultures of rat and human type II pneumocytes, alveolar macrophages and human erythrocytes. The authors argued that the multiple positive charges play an important role in the toxic mechanism [78, 79]. It was

found that nanoparticles with polar surfaces showed different translocation rates across respiratory epithelium and into circulation in a hamster model [61].

1.9 POTENTIAL APPLICATIONS OF NANOMATERIALS IN DRUG DELIVERY

Learning from environmental toxicology studies, nano-sized air pollutants, especially the spherical solid materials, easily enter the lungs and reach the alveoli, and subsequently are cleared from the lungs by different clearance mechanisms. However, due to their small size, nano-sized particles are not likely to be detected around the lung epithelial barriers. They will translocate into systemic circulation and target other organs. Since the definition for the cut-off size of airborne nanoparticles is the same as that of engineered nanoparticles (100 nm), they should share the same biokinetics upon inhalation into the lungs. Furthermore, the high surface-to-volume ratio of natural airborne and engineered nanomaterials renders them more reactive, even though they are inert as larger particles. Therefore any possible effects of the nanomaterials may be amplified once entering the body via inhalation. On the other hand, the extrapulmonary toxicity induced by inhaled nanosized air pollutants may also provide evidence for systemic delivery of nanosized pharmaceutical agents by inhalation, for the medicines not suitable for oral or parenteral administration to improve bioavailability and patient compliance.

Due to rapid advances in nanotechnology and biotechnology, nanoparticles have been considered as an effective form for delivery, and have been studied extensively to deliver the new generation of protein-, gene-based macromolecular therapeutic agents into the body, since many of the components of living cells are constructed at the nano level, such as ribosomes, membrane transporters, receptors and cell signaling systems

[80]. Nanoparticles fall in the same size range of the biological entities; therefore they can readily interact with molecules on both the cell surface and within the cell [81, 82]. Furthermore, drugs that are deposited within the lungs in nanoparticulate form have a greater chance to escape from the clearance mechanisms by the lung defense systems, compared to micro particulate form [39, 58]. Thus, drug-bearing nanoparticles have the potential to deliver drugs efficiently to the epithelium, while avoiding unwanted mucociliary clearance. In the pharmaceutical area, most nanoparticles described in the literature for drug delivery are between 50 to 500 nm in diameter [83].

Nanoparticles are useful to deliver water insoluble drugs. Despite high potency, the effectiveness of water insoluble drugs can be severely limited because the solubility is too low to reach therapeutic systemic concentrations. However, when their size is reduced to nano level, the increased particle surface-to-volume ratio helps to enhance solubility and dissolution rate in an aqueous environment. Nanoparticulate forms of drug could have an enormous benefit by significantly improving systemic bioavailability (defined as the rate and extent of therapeutically active drugs reaching the systemic circulation) and allowing a more rapid onset of therapeutic action [84].

The route of administration is as important as the drug itself for therapeutic success. Nano-based approaches to drug delivery are focused on crossing a particular physical barrier, such as the gastro-intestinal epithelium for absorption of macromolecules, blood–brain barrier; or on finding alternative and acceptable routes for the delivery of drugs expensive and vulnerable to the gastro-intestinal environment. Pulmonary delivery of drugs at the nano level is a non-invasive promising means to provide not only local lung effects but possibly high systemic bioavailability.

1.10 DELIVERY DEVICES

Aerosols are an effective method to deliver therapeutic agents to the lungs. Nebulizers, metered dose inhalers (MDIs), or dry powder inhalers (DPIs) are commonly used to generate aerosols [85, 86]. Despite the above mentioned advantages of nanoparticles, the use of a drug-bearing nanoparticle itself for delivery to lungs is severely limited because their low inertia causes them to be exhaled after inspiration. Moreover, their small size leads to particle aggregation due to their high surface energy, making handling of nanoparticles very difficult [87]. Therefore, the drug-bearing nanoparticles require carriers with MMADs suitable for efficient pulmonary delivery.

In contrast to the conventional micron sized particulate drug formulations for nebulizers, the drug-bearing nanoparticles in an aqueous colloidal dispersion are more easily incorporated into the "respirable percentage" of aerosolized droplets [88]. Therefore, more nanoparticles can be enveloped into the aerosol droplets and delivered to deep lung. For instance, assuming the particles are spherical, if the volume fraction of particles in the carrier solvent is 0.01, only about 1/100th of 3 μm carrier droplets will contain a 3 μm particle; whereas each carrier droplet would contain about ten 300 nm particles. Thus, nanoparticle colloidal dispersions, relative to microparticle dispersions, have the potential to increase the rate of drug absorption by promoting more uniform drug distribution throughout the alveoli [89, 90].

For pulmonary delivery of drug formulations in solid form, micron sized powder particles containing the drug-bearing nanoparticles were designed for deep lung delivery by using MDIs and DPIs. Sham et al. [91] developed a platform for aerosol delivery of

nanoparticles by preparing carbohydrate (e.g. lactose, mannitol) carrier particles containing nanoparticle clusters using spray drying technique. Carrier particles can be made with an appropriate MMAD to optimize alveolar deposition. Dispersion of the lactose carrier containing either gelatin or polybutylcyanoacrylate nanoparticles by a DPI showed a fine particle fraction (FPF; defined as the percentage of droplets with an aerodynamic diameter less than 4.7 μm) of about 40% and MMAD of 3 microns. Upon reaching the deep lung and contacting with the aqueous lining fluid of the lung epithelium, the carrier particles dissolved and released the nanoparticles. A novel type of effervescent carrier particle containing nanoparticles, with a MMAD suitable for deep lung delivery, was reported by Ely et al. [92]. Incorporation of effervescent technology into carrier particles adds an active release mechanism for the nanoparticles after pulmonary administration using DPI. Nanoparticles were observed to be distributed throughout the gas bubble that caused by the effervescent reaction when exposed to humidity. Another idea reported for pulmonary delivery of nanoparticles is forming trojan particles, which can be formed by incorporation of nanoparticles into a thin-walled micron sized large porous particles (LPPs) [31]. LPPs, characterized by geometric sizes larger than 5 microns and mass densities around 0.1 g/cm^3 or less, offer advantage of higher aerosolization efficiency over conventional inhaled therapeutic aerosol particles [93]. In addition, LPPs with geometric diameters of 10–20 microns can penetrate deep into the lungs and avoid macrophage engulfment by virtue of their large size [93, 94]. The trojan particles reportedly have several attractive features: they are comprised solely of nanoparticles; they are readily redispersed as nanoparticles in solution, yet the trojan particles are readily dispersed as aerosols. By using these micron sized carriers to deliver nanoparticles to deep lung, benefits of aerosolization properties of micron particles and the drug release and delivery advantages of nanoparticles can be combined.

1.11 PULMONARY DELIVERY OF THERAPEUTIC NANOMATERIALS

Drug loaded nanoparticles have the potential to be used for pulmonary delivery of therapeutics for treating lung diseases locally and exerting systemic actions. Delivery of therapeutic agents to the site of action for lung diseases may allow for efficient treatment of chronic lung infections, lung cancers, tuberculosis and other respiratory pathologies [95].

In vivo studies have observed an accumulation of nanoparticles in tumor sites after intravascular administration [96], due to the leaky blood vessel structure of tumors. Such properties make nanoparticles a very attractive delivery vehicle for lung cancer treatment. Polysorbate 80 coated nanoparticles which were loaded with doxorubicin (DOX) have been developed to treat lung cancer. The nanoparticles were then incorporated into inhalable carrier particles by a spray-freeze-drying technique [97]. DOX-loaded nanoparticles had a particle size of 173±43 nm after re-dissolving the carrier particles. Cytotoxicity was assessed by incubated cultured monolayer of two lung cancer cell lines (H460 and A549) with DOX-nanoparticle (powder form) at the concentration of 0.625 μg/mL for 24 h. The DOX-loaded nanoparticles showed enhanced cytotoxicity in a concentration dependent manner, compared to free DOX. This indicates that DOX-loaded nanoparticles are more effective than free drug. The enhanced activity of DOX-loaded nanoparticles resulted from the nanoparticles being more readily internalized by an endocytosis mechanism compared to a passive diffusion mechanism of DOX into cells. This study supports the approach of lung cancer treatment using nanoparticles as a drug delivery vector. The carrier particles containing DOX-loaded nanoparticles may be delivered by a dry powder inhaler. Development of inhalable nanoparticles loaded with

bioactive molecules is a new delivery platform which can allow targeting of lung specific diseases in the future.

Solid lipid nanoparticles (SLN) are lipophilic particulates consisting of a spherical solid lipid matrix, and can be used as an efficient and non biotoxic drug carrier for drug delivery [98]. Recently, SLN have been proposed as carriers of either diagnosis or therapeutic reagents upon encapsulation of cytotoxic drugs. Videira et al. [71] prepared lipid nanoparticles using gliceryl behenate by a melt homogenization technique and radiolabelled with ^{99m}Tc using the lipophilic chelator D,L-hexamethylpropyleneamine oxime (HMPAO). Thus obtained SLNs have a mean diameter of 180-220 nm. Biodistribution studies were carried out following ultrasonic nebulization of an aqueous dispersion of the ^{99m}Tc-HMPAO-SLN and administration of the aerosols to rats by inhalation using a mask. Dynamic images were obtained up to 4 hours post-inhalation, and showed a significant uptake of the radiolabelled SLN into the lymphatic system after inhalation, and a high rate of distribution in periaortic, axillar and inguinal lymph nodes. The results revealed an important role of the lymphatic pathway in the uptake of inhaled nanoparticulates. This study suggested the possibility of pulmonary delivery of radiolebelled SLN as a lymphoscintigraphic agent and direct delivery of cytotoxic drugs to target lung cancer, which may metastasize through lymphatic drainage.

In vivo pulmonary delivery of 5-fluorouracil (5-FU) in lipid-coated nanoparticles (LNPs) system to a hamster model was recently reported [99]. The 5-FU lipid-coated nanoparticles consisted of a core composed of 20% (w/w) 5- FU, 20% (w/w) FITC-dextran, and 60% (w/w) poly- (glutamic acid) with a shell composed of 33% (w/ w) cetyl alcohol and 67% (w/w) tripalmitin. The cores measure 600 nm in diameter and the shells

measure 200 nm in thickness. The LNPs were suspended at 5 mg/mL in 0.01% Pluronic F68 aqueous solution and atomized into droplets using an ultrasonic driver. The produced droplets were dried and then directed into a nose-only rodent aerosol exposure chamber for inhalation by hamsters at a dose of 30 mg LNPs/kg body weight (1.5 mg 5-FU/kg body weight). The pharmacokinetics of the 5-FU lipid-coated nanoparticle and total 5-FU in the lung, trachea, larynx, esophagus, and serum was studied. It was found that effective local targeting as well as sustained efficacious concentrations of 5-FU in the expected tumor sites were achieved. The results suggest using 5-FU containing lipid-coated nanoparticles for treating squamous cell carcinoma of the lung.

Besides the success in delivering macromolecules via inhalation to systemic circulation, the potential of pulmonary delivery of small molecule weight entities that encounter formidable biopharmaceutical challenges with conventional routes (e.g. oral) of administration was also explored. Itraconazole (ITZ), a poorly water soluble compound, has displayed low and erratic absorption following oral administration. It has been used for treating invasive fungal infections, which quite often gained entry to the body from lung, and may disseminate to the circulation in immune suppressed patients. Two formulations of amorphous nanoparticulate ITZ using polymers and surfactants as excipients were prepared by spray freezing into liquid (SFL) technology. One is designed for pulmonary delivery (ITZ-pulmonary). Eight milliliters of the aqueous colloidal dispersion of the ITZ-pulmonary nanoparticles (containing 200 mg of ITZ equivalent) was aerosolized by a micro pump nebulizer. The aerosols were administered to mice via inhalation exposure for 20 minutes at a dose of 30 mg/kg body weight of ITZ. The other (ITZ-oral) is for oral delivery [100]. The pharmacokinetic profiles of the two formulations were compared with the commercial product Sporanox® oral solution

(itraconazole/Janssen) after repeated dosing. ITZ-pulmonary achieved significantly greater (more than 10-fold) lung tissue concentrations compared to the Sporanox oral solution and ITZ-oral. There were no statistical differences between the two oral formulations. ITZ-pulmonary achieved significantly greater lung levels per unit serum concentration compared to the orally dosed ITZ compositions. High and sustained lung tissue concentrations were achieved via inhalation of an amorphous nanoparticulate ITZ-pulmonary formulation while maintaining serum levels above the minimum lethal concentration of Aspergillus fumigatus. This study and other related research [101, 102] showed a paradigm of treating disseminated lung infection by pulmonary delivery of nanosized therapeutics to achieve both high lung local and sufficient systemic drug concentrations to effectively improve survival.

Budesonide, another poorly water soluble drug has been prepared as a nanosuspension by high-pressure homogenization and delivered by nebulization [90]. This budesonide nanosuspension has a mean particle size about 500-600 nm, 99% of the nebulized aerosols were below 3 microns; and the nanosuspension also displayed long-term stability without aggregation or particle growth occurring over the examined period of 1 year. The manufacturing technology is feasible to scale up. These features of the budesonide nanosuspension imply the potential of successful in vivo pulmonary application. However, it is regretted that no in vivo experiments were reported to study the pharmacokinetics and effects of the budesonide nanosuspension.

1.12 CONCLUSIONS

While nanotechnology provides great promises in healthcare, the potential risk imposed by natural and engineered nanomaterials to public health has also been of

concern. This is due to their enhanced activity at the nano-scale. The potential of the lung as a natural entry route for systemic delivery of aerosols of macromolecules that are otherwise vulnerable to enzyme degradation in the gastrointestinal tract, and of water insoluble drugs, has been recognized in the pharmaceutical field. The integration of nanotechnology and pulmonary delivery of drug aerosols represents a new and exciting frontier for pharmaceutical dosage form design to increase bioavailability and patient compliance, as supported by the results of studies using nanoparticles as either diagnostic or therapeutic agents for lung and systemic diseases.

1.13 REFERENCES

1. A. Dowling, R. Clift, N. Grobert, D. Hutton, R. Oliver, O. O'Neill, J. Pethica, N. Pidgeon, J. Porritt, J. Ryan, A. Seaton, S. Tendler, M. Welland, and R. Whatmore. Nanoscience and nanotechnologies: opportunities and uncertainties, The Royal Society and the Royal Academy of Engineering London, UK, 2004.

2. P.J. Borm, D. Robbins, S. Haubold, T. Kuhlbusch, H. Fissan, K. Donaldson, R. Schins, V. Stone, W. Kreyling, J. Lademann, J. Krutmann, D. Warheit, and E. Oberdorster. The potential risks of nanomaterials: a review carried out for ECETOC. Part Fibre Toxicol. 3:11 (2006).

3. P.H. Hoet, I. Bruske-Hohlfeld, and O.V. Salata. Nanoparticles - known and unknown health risks. J Nanobiotechnology. 2:12 (2004).

4. G. Oberdorster, E. Oberdorster, and J. Oberdorster. Nanotoxicology: an emerging discipline evolving from studies of ultrafine particles. Environ Health Perspect. 113:823-839 (2005).

5. A. Nel, T. Xia, L. Madler, and N. Li. Toxic potential of materials at the nanolevel. Science. 311:622-627 (2006).

6. K.P. Lee, D.P. Kelly, P.W. Schneider, and H.J. Trochimowicz. Inhalation toxicity study on rats exposed to titanium tetrachloride atmospheric hydrolysis products for two years. Toxicol Appl Pharmacol. 83:30-45 (1986).

7. M. Meyer, O. Persson, and Y. Power. Mapping excellence in nanotechnologies, Preparatory study (Nanotechnology expert group and Eurotech data), *Report to the European Commission*, European Commission, Brussel, 2001.

8. A.P. Dowling. Development of nanotechnologies. Materials Today. 7:30-35 (2004).

9. K.E. Driscoll, L.C. Deyo, J.M. Carter, B.W. Howard, D.G. Hassenbein, and T.A. Bertram. Effects of particle exposure and particle-elicited inflammatory cells on mutation in rat alveolar epithelial cells. Carcinogenesis. 18:423-430 (1997).

10. G. Oberdorsterand C.P. Yu. Lung dosimetry--considerations for noninhalation studies. Exp Lung Res. 25:1-6 (1999).

11. D.M. Brown, M.R. Wilson, W. MacNee, V. Stone, and K. Donaldson. Size-dependent proinflammatory effects of ultrafine polystyrene particles: a role for surface area and oxidative stress in the enhanced activity of ultrafines. Toxicol Appl Pharmacol. 175:191-199 (2001).

12. A. Maynardand E. Kuempel. Airborne Nanostructured Particles and Occupational Health. Journal of Nanoparticle Research. 7:587-614 (2005).

13. K. Donaldson, L. Tran, L.A. Jimenez, R. Duffin, D.E. Newby, N. Mills, W. MacNee, and V. Stone. Combustion-derived nanoparticles: a review of their toxicology following inhalation exposure. Part Fibre Toxicol. 2:10 (2005).

14. M.C. Powelland M.S. Kanarek. Nanomaterial health effects--Part 2: Uncertainties and recommendations for the future. WMJ. 105:18-23 (2006).

15. M.C. Powelland M.S. Kanarek. Nanomaterial health effects--part 1: background and current knowledge. WMJ. 105:16-20 (2006).

16. P.J. Bormand W. Kreyling. Toxicological hazards of inhaled nanoparticles--potential implications for drug delivery. J nanosci nanotechnol. 4:521-531 (2004).

17. E. Weibel. Morphometry of the Human Lung Academic, New York, 1963.

18. K.C. Stone, R.R. Mercer, P. Gehr, B. Stockstill, and J.D. Crapo. Allometric relationships of cell numbers and size in the mammalian lung. Am J Respir Cell Mol Biol. 6:235-243 (1992).

19. P. Gehr, M. Bachenfren, and E. Weibel. The normal human lung: ultrastructure and morphometric estimations of diffusion capacity. Respiratory Physiology. 32:121-140 (1978).

20. S. Smithand J. Bernstein. Inhalation Aerosols: Physical and Biological Basis for Therapy. In A. Hickey (ed.), Lung Biology Health Diseases, Marcel Dekker, New York 1996, pp. 233–269.

21. D.A. Groneberg, C. Witt, U. Wagner, K.F. Chung, and A. Fischer. Fundamentals of pulmonary drug delivery. Respir Med. 97:382-387 (2003).

22. J.S. Patton. Mechanisms of macromolecule absorption by the lungs. Adv Drug Deliv Rev. 19:3-36 (1996).

23. H.M. Courrier, N. Butz, and T.F. Vandamme. Pulmonary drug delivery systems: recent developments and prospects. Crit Rev Ther Drug Carrier Syst. 19:425-498 (2002).

24. P. Gehr, F.H. Green, M. Geiser, V. Im Hof, M.M. Lee, and S. Schurch. Airway surfactant, a primary defense barrier: mechanical and immunological aspects. J Aerosol Med. 9:163-181 (1996).

25. T.B. Martonenand I.M. Katz. Deposition Patterns of Aerosolized Drugs within Human Lungs - Effects of Ventilatory Parameters. Pharm Res. 10:871-878 (1993).

26. P.L. Ariyananda, J.E. Agnew, and S.W. Clarke. Aerosol delivery systems for bronchial asthma. Postgrad Med J. 72:151-156 (1996).

27. J.H. Vincent, A.M. Johnston, A.D. Jones, R.E. Bolton, and J. Addison. Kinetics of deposition and clearance of inhaled mineral dusts during chronic exposure. Br J Ind Med. 42:707-715 (1985).

28. S.P. Newman, D. Pavia, N. Garland, and S.W. Clarke. Effects of various inhalation modes on the deposition of radioactive pressurized aerosols. Eur J Respir Dis Suppl. 119:57-65 (1982).

29. P.R. Byronand J.S. Patton. Drug delivery via the respiratory tract. J Aerosol Med. 7:49-75 (1994).

30. P. Byronand E. Phillips. Absorption, clearance and dissolution in the lung. In P.R. Byron (ed.), Respiratory Drug Delivery CRC, Boca Raton FL, 1990, pp. 107–141.

31. N. Tsapis, D. Bennett, B. Jackson, D.A. Weitz, and D.A. Edwards. Trojan particles: Large porous carriers of nanoparticles for drug delivery. Proc Natl Acad Sci U S A. 99:12001-12005 (2002).

32. S. Gill, R. Lobenberg, T. Ku, S. Azarmi, W. Roa, and E.J. Prenner. Nanoparticles: characteristics, mechanisms of action, and toxicity in pulmonary drug delivery - a review. J Biomed Nanotechnology. 3:107-119 (2007).

33. P.R. Byron. Prediction of drug residence times in regions of the human respiratory tract following aerosol inhalation. J Pharm Sci. 75:433-438 (1986).

34. J. Heyder, J. Gebhart, G. Rudolf, C.F. Schiller, and W. Stahlhofen. Deposition of Particles in the Human Respiratory-Tract in the Size Range 0.005-15-Mu-M. J Aerosol Sci. 17:811-825 (1986).

35. J. Heyderand G. Rudolf. Mathematical-Models of Particle Deposition in the Human Respiratory-Tract. J Aerosol Sci. 15:697-707 (1984).

36. J.S. Patton. Unlocking the opportunity of tight glycaemic control. Innovative delivery of insulin via the lung. Diabetes Obes Metab. 7 Suppl 1:S5-8 (2005).

37. P.A. Jaquesand C.S. Kim. Measurement of total lung deposition of inhaled ultrafine particles in healthy men and women. Inhal Toxicol. 12:715-731 (2000).

38. D.C. Chalupa, P.E. Morrow, G. Oberdorster, M.J. Utell, and M.W. Frampton. Ultrafine particle deposition in subjects with asthma. Environ Health Perspect. 112:879-882 (2004).

39. S. Schurch, P. Gehr, V. Im Hof, M. Geiser, and F. Green. Surfactant displaces particles toward the epithelium in airways and alveoli. Respir Physiol. 80:17-32 (1990).

40. M. Geiser, S. Schurch, and P. Gehr. Influence of surface chemistry and topography of particles on their immersion into the lung's surface-lining layer. J Appl Physiol. 94:1793-1801 (2003).

41. G. Oberdorster. Toxicokinetics and effects of fibrous and nonfibrous particles. Inhal Toxicol. 14:29-56 (2002).

42. G. Oberdorster, Z. Sharp, V. Atudorei, A. Elder, R. Gelein, A. Lunts, W. Kreyling, and C. Cox. Extrapulmonary translocation of ultrafine carbon particles following whole-body inhalation exposure of rats. J Toxicol Environ Health A. 65:1531-1543 (2002).

43. M. Sakagami. In vivo, in vitro and ex vivo models to assess pulmonary absorption and disposition of inhaled therapeutics for systemic delivery. Adv Drug Deliv Rev. 58:1030-1060 (2006).

44. J.H. Widdicombeand J.G. Widdicombe. Regulation of human airway surface liquid. Respir Physiol. 99:3-12 (1995).

45. J. Goerke. Pulmonary surfactant: functions and molecular composition. Biochim Biophys Acta. 1408:79-89 (1998).

46. J. Johansson, T. Curstedt, and B. Robertson. The proteins of the surfactant system. Eur Respir J. 7:372-391 (1994).

47. R. Veldhuizen, K. Nag, S. Orgeig, and F. Possmayer. The role of lipids in pulmonary surfactant. Biochim Biophys Acta. 1408:90-108 (1998).

48. W.R. Schief, M. Antia, B.M. Discher, S.B. Hall, and V. Vogel. Liquid-crystalline collapse of pulmonary surfactant monolayers. Biophys J. 84:3792-3806 (2003).

49. D. Stuart, R. Lobenberg, T. Ku, S. Azarmi, L. Ely, W. Roa, and E.J. Prenner. Biophysical investigation of nanoparticle interactions with lung surfactant model systems. J Biomed Nanotechnology 2:245-252 (2006).

50. L. Muand P.H. Seow. Application of TPGS in polymeric nanoparticulate drug delivery system. Colloids Surf B Biointerfaces. 47:90-97 (2006).

51. P. Borm, F.C. Klaessig, T.D. Landry, B. Moudgil, J. Pauluhn, K. Thomas, R. Trottier, and S. Wood. Research strategies for safety evaluation of nanomaterials, part V: role of dissolution in biological fate and effects of nanoscale particles. Toxicol Sci. 90:23-32 (2006).

52. J.S. Pattonand P.R. Byron. Inhaling medicines: delivering drugs to the body through the lungs. Nat Rev Drug Discov. 6:67-74 (2007).

53. G.M. Spiekermann, P.W. Finn, E.S. Ward, J. Dumont, B.L. Dickinson, R.S. Blumberg, and W.I. Lencer. Receptor-mediated immunoglobulin G transport across mucosal barriers in adult life: functional expression of FcRn in the mammalian lung. J Exp Med. 196:303-310 (2002).

54. A.J. Bitonti, J.A. Dumont, S.C. Low, R.T. Peters, K.E. Kropp, V.J. Palombella, J.M. Stattel, Y. Lu, C.A. Tan, J.J. Song, A.M. Garcia, N.E. Simister, G.M. Spiekermann, W.I. Lencer, and R.S. Blumberg. Pulmonary delivery of an erythropoietin Fc fusion protein in non-human primates through an immunoglobulin transport pathway. Proc Natl Acad Sci U S A. 101:9763-9768 (2004).

55. M. Gumbleton. Caveolae as potential macromolecule trafficking compartments within alveolar epithelium. Adv Drug Deliv Rev. 49:281-300 (2001).

56. M. Arredouani, Z. Yang, Y. Ning, G. Qin, R. Soininen, K. Tryggvason, and L. Kobzik. The scavenger receptor MARCO is required for lung defense against pneumococcal pneumonia and inhaled particles. J Exp Med. 200:267-272 (2004).

57. Y. Sibilleand H.Y. Reynolds. Macrophages and polymorphonuclear neutrophils in lung defense and injury. Am Rev Respir Dis. 141:471-501 (1990).

58. S. Chono, T. Tanino, T. Seki, and K. Morimoto. Influence of particle size on drug delivery to rat alveolar macrophages following pulmonary administration of ciprofloxacin incorporated into liposomes. J Drug Target. 14:557-566 (2006).

59. J.M. Lauwerynsand J.H. Baert. Alveolar clearance and the role of the pulmonary lymphatics. Am Rev Respir Dis. 115:625-683 (1977).

60. J. Rejman, V. Oberle, I.S. Zuhorn, and D. Hoekstra. Size-dependent internalization of particles via the pathways of clathrin- and caveolae-mediated endocytosis. Biochem J. 377:159-169 (2004).

61. A. Nemmar, H. Vanbilloen, M.F. Hoylaerts, P.H. Hoet, A. Verbruggen, and B. Nemery. Passage of intratracheally instilled ultrafine particles from the lung into the systemic circulation in hamster. Am J Respir Crit Care Med. 164:1665-1668 (2001).

62. K. Donaldson, V. Stone, C.L. Tran, W. Kreyling, and P.J. Borm. Nanotoxicology. Occup Environ Med. 61:727-728 (2004).

63. W.G. Kreyling, M. Semmler, F. Erbe, P. Mayer, S. Takenaka, H. Schulz, G. Oberdorster, and A. Ziesenis. Translocation of ultrafine insoluble iridium particles from lung epithelium to extrapulmonary organs is size dependent but very low. J Toxicol Environ Health A. 65:1513-1530 (2002).

64. T. Kato, T. Yashiro, Y. Murata, D.C. Herbert, K. Oshikawa, M. Bando, S. Ohno, and Y. Sugiyama. Evidence that exogenous substances can be phagocytized by alveolar epithelial cells and transported into blood capillaries. Cell Tissue Res. 311:47-51 (2003).

65. J.S. Brown, K.L. Zeman, and W.D. Bennett. Ultrafine particle deposition and clearance in the healthy and obstructed lung. Am J Respir Crit Care Med. 166:1240-1247 (2002).

66. N.L. Mills, N. Amin, S.D. Robinson, A. Anand, J. Davies, D. Patel, J.M. de la Fuente, F.R. Cassee, N.A. Boon, W. Macnee, A.M. Millar, K. Donaldson, and D.E. Newby. Do inhaled carbon nanoparticles translocate directly into the circulation in humans? Am J Respir Crit Care Med. 173:426-431 (2006).

67. J. Pekkanen, A. Peters, G. Hoek, P. Tiittanen, B. Brunekreef, J. de Hartog, J. Heinrich, A. Ibald-Mulli, W.G. Kreyling, T. Lanki, K.L. Timonen, and E. Vanninen. Particulate air pollution and risk of ST-segment depression during repeated submaximal exercise tests among subjects with coronary heart disease: the Exposure and Risk Assessment for Fine and Ultrafine Particles in Ambient Air (ULTRA) study. Circulation. 106:933-938 (2002).

68. D. Corry, P. Kulkarni, and M.F. Lipscomb. The migration of bronchoalveolar macrophages into hilar lymph nodes. Am J Pathol. 115:321-328 (1984).

69. L.V. Leakand V.J. Ferrans Lee. Lymphatics and lymphoil tissue. In R.G. Crystal, J.B. West, N.S. Cherniack, and E.R. Weibel (eds.), The Lung: Scientific Foundations, Raven Press, New York, 1991, pp. 779–786.

70. G.L. McIntire, E.R. Bacon, J.L. Toner, J.B. Cornacoff, P.E. Losco, K.J. Illig, K.J. Nikula, B.A. Muggenburg, and L. Ketai. Pulmonary delivery of nanoparticles of insoluble, iodinated CT X-ray contrast agents to lung draining lymph nodes in dogs. J Pharm Sci. 87:1466-1470 (1998).

71. M.A. Videira, M.F. Botelho, A.C. Santos, L.F. Gouveia, J.J. de Lima, and A.J. Almeida. Lymphatic uptake of pulmonary delivered radiolabelled solid lipid nanoparticles. J Drug Target. 10:607-613 (2002).

72. C. Lombry, D.A. Edwards, V. Preat, and R. Vanbever. Alveolar macrophages are a primary barrier to pulmonary absorption of macromolecules. Am J Physiol Lung Cell Mol Physiol. 286:L1002-1008 (2004).

73. S. Muranishi, T. Fujita, M. Murakami, and A. Yamamoto. Lymphatic transfer of macromolecules after intrapulmonary administration in the presence or absence of various absorption enhancers in rats. Pharmazie. 51:331-336 (1996).

74. G. Oberdorster, J. Ferin, and B.E. Lehnert. Correlation between particle size, in vivo particle persistence, and lung injury. Environ Health Perspect. 102 Suppl 5:173-179 (1994).

75. S.M. Moghimiand A.C. Hunter. Capture of stealth nanoparticles by the body's defences. Crit Rev Ther Drug Carrier Syst. 18:527-550 (2001).

76. P. Somasundaran, S. Chakraborty, Q. Qiang, P. Deo, J. Wang, and R. Zhang. Surfactants, polymers and their nanoparticles for personal care applications. J Cosmet Sci. 55 Suppl:S1-17 (2004).

77. P.R. Byron. Physicochemical effects on lung disposition of pharmaceutical aerosols. Aerosol Sci Tech. 18:223–229. (1993).

78. P.H. Hoet, L. Gilissen, and B. Nemery. Polyanions protect against the in vitro pulmonary toxicity of polycationic paint components associated with the Ardystil syndrome. Toxicol Appl Pharmacol. 175:184-190 (2001).

79. P.H. Hoet, L.P. Gilissen, M. Leyva, and B. Nemery. In vitro cytotoxicity of textile paint components linked to the "Ardystil syndrome". Toxicol Sci. 52:209-216 (1999).

80. V. Labhasetwar. Nanotechnology for drug and gene therapy: the importance of understanding molecular mechanisms of delivery. Curr Opin Biotechnol. 16:674-680 (2005).

81. G.C. Rao, M.S. Kumar, N. Mathivanan, and M.E. Rao. Nanosuspensions as the most promising approach in nanoparticulate drug delivery systems. Pharmazie. 59:5-9 (2004).

82. M.N. Moore. Biocomplexity: the post-genome challenge in ecotoxicology. Aquat Toxicol. 59:1-15 (2002).

83. M. Yokoyama. Drug targeting with nano-sized carrier systems. J Artif Organs. 8:77-84 (2005).

84. L. Shargeland A. Yu. Applied Biopharmaceutics & Pharmacokinetics, fourth ed., McGraw Hill, New York 1999.

85. S.P. Newman. Aerosol generators and delivery systems. Respir Care. 36:939-951 (1991).

86. P.J. Thompson. Drug delivery to the small airways. Am J Respir Crit Care Med. 157:S199-202 (1998).

87. W.C. Hinds. Aerosol Technology: Properties, Behavior, and Measurement of Airborne Particles, Wiley, New York, 1998.

88. O.N.M. McCallion, K.M.G. Taylor, M. Thomas, and A.J. Taylor. Nebulisation of monodisperse latex sphere suspensions in air-jet and ultrasonic nebulizers. Int J Pharm. 133:203–214 (1996).

89. K.D. Ostrander, H.W. Bosch, and D.M. Bondanza. An in-vitro assessment of a NanoCrystal beclomethasone dipropionate colloidal dispersion via ultrasonic nebulization. Eur J Pharm Biopharm. 48:207-215 (1999).

90. C. Jacobsand R.H. Muller. Production and characterization of a budesonide nanosuspension for pulmonary administration. Pharm Res. 19:189-194 (2002).

91. J.O.H. Sham, Y. Zhang, W.H. Finlay, W.H. Roa, and R. Lobenberg. Formulation and characterization of spray-dried powders containing nanoparticles for aerosol delivery to the lung. Int J Pharm. 269:457-467 (2004).

92. L. Ely, W. Roa, W.H. Finlay, and R. Lobenberg. Effervescent dry powder for respiratory drug delivery. Eur J Pharm Biopharm. 65:346-353 (2007).

93. D.A. Edwards, A. Ben-Jebria, and R. Langer. Recent advances in pulmonary drug delivery using large, porous inhaled particles. J Appl Physiol. 85:379-385 (1998).

94. D.A. Edwardsand C. Dunbar. Bioengineering of therapeutic aerosols. Annual review of biomedical engineering. 4:93-107 (2002).

95. S. Gelperina, K. Kisich, M.D. Iseman, and L. Heifets. The potential advantages of nanoparticle drug delivery systems in chemotherapy of tuberculosis. Am J Respir Crit Care Med. 172:1487-1490 (2005).

96. I. Brigger, C. Dubernet, and P. Couvreur. Nanoparticles in cancer therapy and diagnosis. Adv Drug Deliv Rev. 54:631-651 (2002).

97. S. Azarmi, X. Tao, H. Chen, Z. Wang, W.H. Finlay, R. Lobenberg, and W.H. Roa. Formulation and cytotoxicity of doxorubicin nanoparticles carried by dry powder aerosol particles. Int J Pharm. 319:155-161 (2006).

98. W. Mehnertand K. Mader. Solid lipid nanoparticles: production, characterization and applications. Adv Drug Deliv Rev. 47:165-196 (2001).

99. C.J. Hitzman, L.W. Wattenberg, and T.S. Wiedmann. Pharmacokinetics of 5-fluorouracil in the hamster following inhalation delivery of lipid-coated nanoparticles. J Pharm Sci. 95:1196-1211 (2006).

100. J.M. Vaughn, J.T. McConville, D. Burgess, J.I. Peters, K.P. Johnston, R.L. Talbert, and R.O. Williams, 3rd. Single dose and multiple dose studies of itraconazole nanoparticles. Eur J Pharm Biopharm. 63:95-102 (2006).

101. J.M. Vaughn, N.P. Wiederhold, J.T. McConville, J.J. Coalson, R.L. Talbert, D.S. Burgess, K.P. Johnston, R.O. Williams, 3rd, and J.I. Peters. Murine airway histology and intracellular uptake of inhaled amorphous itraconazole. Int J Pharm. 338:219-224 (2007).

102. C.A. Alvarez, N.P. Wiederhold, J.T. McConville, J.I. Peters, L.K. Najvar, J.R. Graybill, J.J. Coalson, R.L. Talbert, D.S. Burgess, R. Bocanegra, K.P. Johnston, and R.O. Williams, 3rd. Aerosolized nanostructured itraconazole as prophylaxis against invasive pulmonary aspergillosis. J Infect. 55 68-74 (2007).

1.14 DISSERTATION OBJECTIVES AND OUTLINE

High throughput screening techniques routinely used in modern drug discovery processes result in a higher prevalence of poorly water-soluble active pharmaceutical ingredient (API). Such APIs often have poor bioavailability issues due to their poor dissolution and/or permeability to achieve sufficient and consistent systemic exposure. Consequently it results in sub-optimal efficacy in patients, particularly via oral administration. Alternative formulations made by novel pharmaceutical technologies for improving the dissolution properties and thereby bioavailability of the poorly water-soluble APIs are becoming increasingly important to modern drug delivery. Alternative delivery routes are also important to enhance drug bioavailability. The overall objective of this dissertation was to formulate, fully characterize nanoparticle formulations of poorly water-soluble drug through in vitro and in vivo tests. Formulations were produced and evaluated based on current needs of clinical use, with the aid of novel particle engineering techniques and well established animal models to evaluate the bioavailability.

The use of nanotechnologies in commercial applications is increasing in many scientific disciplines. Chapter 1 reviews the unique size-controlled properties of nanomaterials, their disposition in the body after inhalation, and the factors influencing the fate of inhaled nanomaterials. The physiology of the lung makes it an ideal target organ for non-invasive local and systemic drug delivery, especially for protein and poorly water-soluble drugs. The potential application of pulmonary delivery of nanoparticle formulations of poorly water-soluble drugs is promising.

To improve the bioavailability of itraconazole (ITZ), an extremely poorly water-soluble drug which suffers erratic absorption from oral formulations, a particle engineering process ultra-rapid freezing (URF) was utilized to produce nanoparticle formulation for pulmonary delivery in Chapter 2. Biocompatible and biodegradable excipients suitable for lung use were employed to make the nanostructured aggregates containing ITZ:mannitol:lecithin=1:0.5:0.2, w/w), i.e. URF-ITZ. In which ITZ was found to molecularly dispersed in the excipients as a solid solution with high surface area and ability to achieve high magnitude of supersaturation. Aqueous colloidal dispersion of URF-ITZ was suitable for nebulization, which demonstrated optimal aerodynamic properties for deep lung delivery. Single dose inhalation of the nebulized aerosols in mice using a whole body exposure dosing apparatus demonstrated high lung and systemic ITZ levels.

The significantly improved systemic bioavailability of inhaled URF-ITZ was mainly ascribed to the amorphous morphology that raised the drug dissolution rate and saturation solubility. To evaluate the impact of supersaturation of amorphous relative to crystalline nanoparticulate formulations of ITZ on bioavailability via inhalation, a nano-sized crystalline ITZ composition was made by wet milling process (i.e. Wet-milled ITZ) to compare the bioavailability with URF-ITZ following inhalation in Chapter 3. Dissolution tests revealed that URF-ITZ achieved 4.7-times higher extent of supersaturation than nanocrystalline Wet-milled ITZ. This was translated to 3.8-times higher systemic ITZ levels in rats following a single dose inhalation of the respective nebulized aerosols using a nose-only dosing apparatus. Engineering amorphous nanoparticles of ITZ through pulmonary delivery is beneficial to improve therapeutic effects.

In Chapter 4, a 2-hydroxypropyl-β-cyclodextrin (HPβCD) solubilized ITZ solution (i.e., HPβCD-ITZ) suitable for pulmonary delivery by nebulization was made, to compare pharmacokinetics of inhaled nebulized aerosols of HPβCD-ITZ versus URF-ITZ, under the hypothesis that solubilized ITZ could be absorbed faster through a mucosal membrane than the nanoparticulate ITZ. Single dose inhalation of nebulized aerosols of HPβCD-ITZ solution and aqueous colloidal dispersion of URF-ITZ in mice produced similar ITZ lung depositions, but significantly faster systemic absorption of HPβCD-ITZ across lung epithelium than URF-ITZ. The faster absorption of solubilized ITZ across the lung mucosal surface may be due in part to the elimination of the phase-to-phase transition. However, the nanoparticle URF-ITZ offered higher systemic bioavailability due to the absorption enhancer, lecithin, contained in the formulation.

Table 1.1. Unique features of nanomaterials [16]

Size: 20-50 nm enters CNS
< 70 nm, able to escape defense system in vivo
High Surface to mass ratio
High strength, conductivity, solubility, durability and reactivity
Catalytic promotion of reactions
Ability to adsorb and carry other compounds
Ability to escape defense system in vivo
Ability to cross cellular and sub-cellular membranes
Surface coating (e.g. lecithin,albumin)
-Enhance uptake by Type I/II pneumocytes
-Transcytosis across capillary
Charged particle (higher inhaled depostition)

Table 1.2. Mechanism of Aerosol Deposition [23, 33]

Site	Size (μm)	Mechanism	Comment
Large airways	5-9 (slow inhalation) 3-6 (fast inhalation)	Impaction	Most deposition in Segmental airways
Smaller airways	1 - 5	Gravitational sedimentation	Improved with slow and deep breathe
Respiratory bronchioles	1 - 3	Gravitational sedimentation	Improved with slow and deep breathe
Alveoli	≤ 0.5	Brownian diffusion	Most exhaled

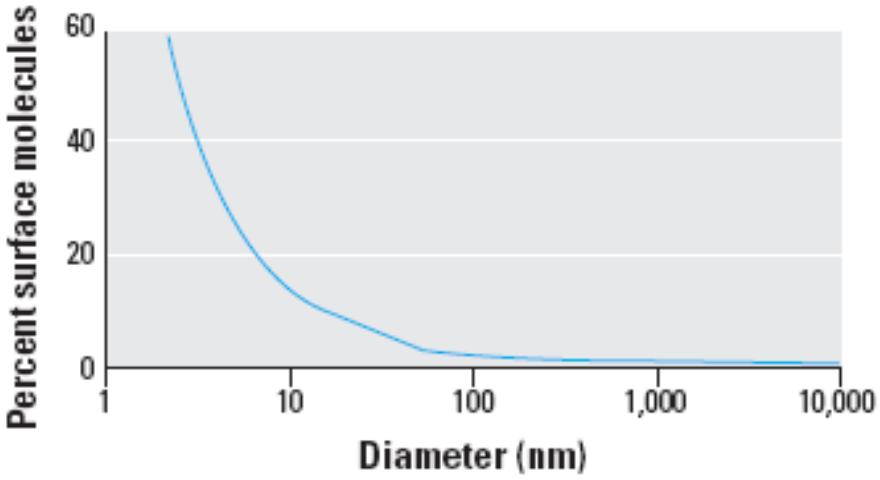

Figure 1.1. Relationship between particle size and number of molecules displayed on particle surface. The percentage of molecules displayed on the surface of the particles to the total molecules in the particles increases exponentially while particle diameter decreases in the range of 1-100 nm. At a particle diameter of 30 nm, about 10% of its molecules are displayed on the surface; whereas at 10 and 3 nm particle diameter, 20% and 50% of the total molecules in the particles may display on the surface, respectively. Increase the ratio of atoms or molecules on the surface to the total molecules of a material may enhance the chemical and biological properties of nanomaterials. The enhanced activities could be either beneficial (antioxidation, carrier capacity for drugs, increased uptake and interaction with biological tissues) or disadvantageous (toxicity, instability, induction of oxidative stress) depending on the intended use. Adapted from [4] with permission.

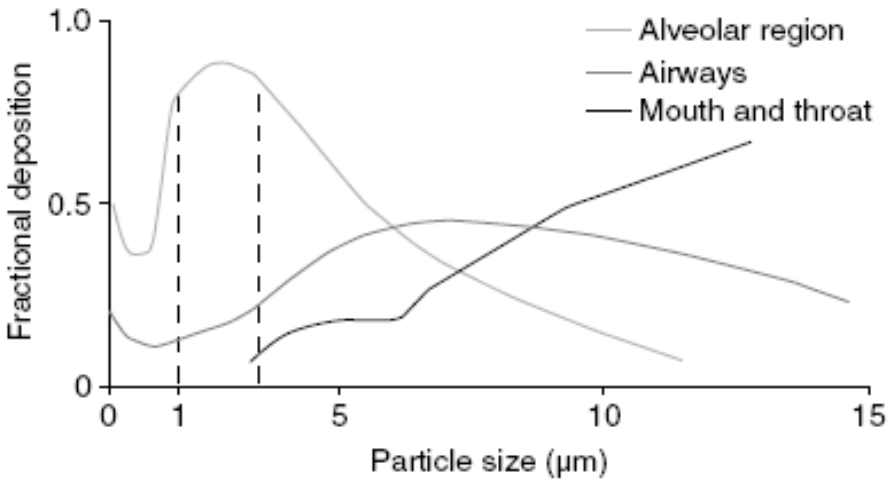

Figure 1.2. The effect of particle size on the deposition of aerosol particles in the human respiratory tract following a slow inhalation and a 5-second breath hold. Larger particles deposit in the airways or mouth and throat, whereas smaller particles deposit in the alveolar region. Particles <1 μm can be exhaled, thereby reducing deep-lung deposition. Reproduced from [36] with permission.

Chapter 2: High Bioavailability from Nebulized Itraconazole Nanoparticle Dispersions with Biocompatible Stabilizers

2.1 ABSTRACT

A nebulized dispersion of amorphous, high surface area, nano-structured aggregates of itraconazole (ITZ):mannitol:lecithin (1:0.5:0.2 w/w) yielded improved bioavailability in mice. The ultra-rapid freezing (URF) technique used to produce the nanoparticles was found to molecularly disperse the ITZ with the excipients as a solid solution. Upon addition to water, ITZ formed a colloidal dispersion suitable for nebulization, which demonstrated optimal aerodynamic properties for deep lung delivery and high lung and systemic levels when dosed to mice. The ITZ nanoparticles produced supersaturation levels 27 times the crystalline solubility upon dissolution in simulated lung fluid. A dissolution/permeation model indicated that the absorption of 3 μm ITZ particles is limited by the dissolution rate (BCS Class II behavior), while absorption is permeation limited for more rapidly dissolving 230 nm particles. The predicted absorption half-life for 230 nm amorphous ITZ particles was only 15 min, as a result of the small particle size and high supersaturation, in general agreement with the *in vivo* results. Thus, bioavailability may be enhanced, by decreasing the particle size to accelerate dissolution and increasing permeation with (1) an amorphous morphology to raise the drug solubility, and (2) permeability enhancers.

2.2 INTRODUCTION

Improving the bioavailability of active pharmaceutical ingredients (API), defined as the rate and extent of the API that reaches systemic circulation is a major goal of

pharmaceutical drug delivery. Enhancements in bioavailability may increase patient compliance. The effectiveness of poorly water soluble APIs can be severely limited when solubilities are too low to produce systemic therapeutic levels. Several strategies have been developed to improve the aqueous dissolution properties of poorly water soluble API formulations, including the use of surfactants, emulsification processes, solution based precipitation and solid state manipulation [1-6]. Amorphous particles may be designed to produce high levels of supersaturation relative to the solubility of the crystalline state [7]. Cryogenic technologies have been used to produce highly porous, amorphous, nanostructured particles with improved dissolution rates and high supersaturation drug levels relative to the solubility of the crystalline state for poorly water soluble APIs [8-10]. The Spray Freezing into Liquid (SFL) process forms a solid dispersion or solid solution composed of drug domains within a polymer matrix by spraying the drug/excipients solution directly into liquid nitrogen [8]. The URF particle engineering process utilizes rapid freezing of a drug/excipient solution onto a cryogenic substrate of desired thermal conductivity to obtain a solid dispersion/solution [10].

ITZ, a broad-spectrum antimycotic triazole has been used for both prophylaxis and treatment of invasive fungal diseases for the last two decades. ITZ is a poorly soluble weak base with a calculated log *P* of 6.2. Its aqueous solubility is estimated at approximately 1 ng/mL at neutral pH and approximately 4 μg/mL at pH 1 [11]. Given the high log *P* value, ITZ is classified as a class II drug according to the Biopharmaceutical Classification System (BCS) [12]. Sporanox® oral capsule and solution, ITZ preparations for oral administration on the market, show low oral absorption and considerably varied pharmacokinetics in immunocompromised patients,[13-15]. To treat invasive fungal infection, especially *Aspergillus* spp. infections in immunocompromised patients, ITZ

levels of greater than 0.5 μg/g of lung tissue, or 0.5 μg/mL of blood [16] is generally required.

The design of rapidly dissolving drug nanoparticles offers potential improvements in therapeutic efficacy, stability, patient compliance, and safety [17, 18]. The route of administration is as important as the drug formulation for achieving therapeutic success [19-22]. Pulmonary delivery of a wide spectrum of drug substances, including proteins/peptides, nucleic acids, and antibiotics to the lungs can be highly effective for localized treatment or prophylaxis of pulmonary diseases, including lung infections, cystic fibrosis, and asthma [23]. Pulmonary delivery is a non-invasive route that facilitates deposition of large drug doses to the lungs, and offers the potential for high systemic absorption. Efficient systemic absorption is attributed to the lung's large absorptive surface area, very thin diffusion path to the blood stream, elevated blood flow, relatively low metabolic activity, and the avoidance of hepatic first pass metabolism [24]. Particle size distribution and morphology have pronounced effects on all aspects of pulmonary drug delivery, including deposition in the respiratory tract, dissolution in the lung lining fluid and the clearance mechanism [25]. The particle size of aerosols is determined by the inhalation device and physicochemical properties of the drug formulation, such as viscosity and surface tension [26].

Pulmonary drug delivery targeted to the alveoli is advantageous and critical for systemic absorption [27]. The concept of improving bioavailability of poorly water soluble APIs by pulmonary delivery of nanostructured aggregates has been recently reported in mouse models. Inhalation of a nebulized ITZ nanoparticle composition (ITZ:polysorbate 80:poloxamer 407 = 1:0.75:0.75 by weight ratio, prepared by SFL;

namely SFL-ITZ) by mice for 20 min produced relatively high drug concentrations in lung tissue and about one third the drug level in systemic circulation compared to Sporanox® solution administered orally at the same dose [28]. Nebulization of aqueous colloidal dispersions of amorphous cyclosporin A/polysorbate 80 nanoparticles into mice produced therapeutic lung levels and systemic concentrations below toxic limits [29].

Inclusion of certain surface active excipients in pulmonary formulations may enhance bioavailability, but may also interfere with cell lipid bilayer membranes and thus raise long term safety concerns [30]. The objective of this study was to develop an ITZ nanoparticle dispersion for pulmonary delivery by nebulization that does not require the use of synthetic polymers and surfactants to achieve high supersaturation values *in vitro* and high bioavailability. Mannitol is a widely used excipient approved by the Food and Drug Administration (FDA) for inhalation purposes [31, 32]. Lecithin, currently FDA approved for pulmonary formulations, contains mainly dipalmitoylphosphatidylcholine (DPPC), the primary component of endogenous human lung surfactant [33]. We hypothesize that a high surface area nanostructured ITZ composition encompassing soluble, and/or biodegradable, and/or biocompatible materials such as mannitol and lecithin, ITZ:mannitol:lecithin = 1:0.5:0.2 (by weight ratio, namely URF-ITZ), can be inhaled by nebulization to produce high supersaturation levels rapidly in the alveolar fluid. Pulmonary delivery of the nanostructured ITZ composition may provide not only local lung deposition, but possibly high systemic bioavailability with low toxicity.

The URF-ITZ dry powder and its aqueous dispersion suitable for nebulization were characterized by a wide variety of techniques. A single dose 24-hour pharmacokinetic study was also performed in mice to assess the bioavailability of

nebulized URF-ITZ nanoparticle dispersion by inhalation and to explore the factors influencing the pharmacokinetic parameters. In order to better understand how particle size and solubility (supersaturation) may be designed to enhance absorption rates in the alveoli, a recently developed model of Tam et al. [29] was used to analyze the individual effects of dissolution.

2.3 MATERIALS AND METHODS

2.3.1 Materials

The following materials were purchased: ITZ, micronized pharmacopeial grade (Hawkins Chemical, Minneapolis, MN); mannitol and polysorbate 80 (Spectrum Chemicals, Gardena, CA); lecithin, 1,4-dioxane (Fisher Scientific, Fair Lawn, NJ); diethanolamine (VWR International, West Chester, PA); acetonitrile (EM Industries Inc., Gibbstown, NJ). All organic solvents used were HPLC grade. Other reagents used were at least ACS grade.

2.3.2 Preparation of nanostructured aggregate powder of ITZ using URF technology

For a standard batch of the formulation, lecithin (118 mg) was dissolved in a mixture of 1,4-dioxane and purified water (65/35, v/v) co-solvent system (200 mL) using a magnetic stirrer. ITZ (588 mg) and mannitol (294 mg) were subsequently dissolved in the mixture, this provided a dissolved solids ratio of ITZ:mannitol:lecithin of 1:0.5:0.2 by weight. The solution was frozen using the URF apparatus [10, 34]. Briefly, the solution was applied to the cryogenic solid substrate (which was previously cooled to -70 ℃), whereby the solution was frozen rapidly. The resultant frozen solids were collected and lyophilized using a VirTis Advantage bench top tray lyophilizer (The VirTis Company,

Inc., Gardiner, NY, USA). The dry powder was stored in a desiccator under vacuum at room temperature.

2.3.3 Preparation of physical mixture

A physical mixture consisting of ITZ:mannitol:lecithin in the weight ratio of 1:0.5:0.2 was mixed by geometric dilution and trituration using a ceramic mortar and pestle.

2.3.4 Powder X-Ray Diffraction (XRD)

The URF-ITZ powder, the physical mixture, the bulk ITZ and mannitol were examined by wide angle XRD. A Philips 1710 X-ray diffractometer with a copper target (CuKα1,λ = 1.54056 Å) and nickel filter (Philips Electronic Instruments Inc., Mahwah, NJ) was used to obtain the XRD patterns. The voltage was 40 kV and the current was 40 mA. Samples were analyzed in the 2-theta range from 10 to 50° using a step size of 0.05 2-theta degree with a dwell time of 2 sec.

2.3.5 Scanning Electron Microscopy (SEM)

SEM was used to evaluate the morphology of the samples. The samples were mounted onto an aluminum stage using conductive carbon tape. Samples were coated using a model K575 sputter coater (Emitech Products, Inc., Houston, TX) with gold/palladium for 20 sec in a high vacuum evaporator. SEM was performed using a Hitachi S-4500 field emission scanning electron microscope (Hitachi High-Technologies Corp., Tokyo, Japan) operating at an accelerating voltage of 10-15 kV. Images were

captured with Quartz PCI software (Quartz Imaging Corporation, Vancouver, BC, Canada).

2.3.6 Scanning Transmission Electron Microscopy (STEM)

The URF-ITZ powder was further characterized using STEM, by placing the dry powder on a Holey Carbon Support Film with 200 Mesh Copper Grids (Jed Pella, Inc., Redding, CA) and viewing on a JEOL 2010F transmission electron microscope (JEOL USA, Inc., Peabody, MA) equipped with an energy dispersive spectroscopy (EDS) detector for elemental characterization.

2.3.7 Thermal Analysis

Differential Scanning Calorimetry (DSC) of the URF-ITZ powder and each component was conducted using modulated temperature DSC (MTDSC), Model 2920 (TA Instruments, New Castle, DE), equipped with a refrigerated cooling system. Dry nitrogen gas was used as the purge gas through the DSC cell at a flow rate of 40 mL/min. Samples were weighed to 10-15 mg in aluminum crimped pans, Kit 0219-0041 (Perkin-Elmer Instruments, Norwalk, CT). The mass of the empty sample pan was matched with that of the empty reference pan within ±0.2 mg. Samples were heated at a ramp rate of 10 ℃/min from -30 to 200 ℃ with a modulation temperature amplitude of 1 ℃/60 sec for all studies. Data was analyzed using TA Universal Analysis 2000 software (TA Instruments, New Castle, DE). Amorphous pure ITZ was prepared by the URF process as described above. Amorphous mannitol and lecithin were prepared by quench-cooling [35]. In brief, accurately weighed mannitol and lecithin powders were heated to 200 and 150 ℃, respectively, in sealed aluminum DSC pans, the temperature was held for 15 min.

The samples were then quench-cooled in liquid nitrogen externally to the DSC instrument. DSC was conducted by placing back the samples to pre-cooled sample chamber (-50 ℃), and thermograms were recorded the same as with the other samples.

2.3.8 True Density Measurements

True density of ITZ, mannitol and lecithin was measured using an AccuPyc 1330 helium pycnometer (Micrometrics; Norcross, GA). The samples were dried overnight. Upon measurement, the samples were purged 20 times with dry helium at 19.85 psi followed by six analytical runs at 19.85 psi. The equilibration rate was 0.0050 psi/min. Measurements were performed in triplicate.

2.3.9 Particle Size Analysis by Laser Diffraction

Particle size distribution, based on volume fraction, of the URF-ITZ powder, the physical mixture and bulk ITZ was measured by laser diffraction with a Malvern Mastersizer-S (Malvern Instruments, Ltd., Worcestershire, UK). To measure the particle size distribution, powder aliquots were dispersed in 5 mL purified water, sonicated, and the dispersions were added to the sample reservoir to produce light obscuration in the range of 10–15%. Bulk ITZ was dispersed in 5 mL of a 0.1% polysorbate 80 aqueous solution for pre-wetting due to its high hydrophobicity. Sonication was used during the measurement to break up the agglomerated particles. Values reported are the average of at least three determinations.

2.3.10 Brunauer-Emmett-Teller (BET) Specific Surface Area Analysis

Specific surface area was measured using a Nova 2000 version 6.11 instrument (Quantachrome Instruments, Boynton Beach, FL). An aliquot of powder was added to a 12-mm Quantachrome bulb sample cell and degassed overnight prior to analysis. The data was then analyzed using NOVA Enhanced Data Reduction Software (version 2.13).

2.3.11 Dissolution Testing at Supersaturation Conditions

Dissolution testing at supersaturated conditions was conducted in a USP 25 dissolution apparatus model Vankel 7000 Dissolution Tester (Vankel Technology Group, Cary, NC) using 100 mL glass dissolution vessels and stirred with small paddles at 100 rpm. Simulated lung fluid containing 0.02% DPPC (Davies and Feddah, 2003, Cook et al., 2005) at 37 ℃ was used as the dissolution medium. An equivalent of 100 μg ITZ in a colloidal dispersion (equal to 100-times of equilibrium solubility of crystalline ITZ (C_{eq})) at 4 ℃ was added to the dissolution vessels (n = 6) within one second immediately after sonication. Aliquots of 2 mL of the dissolution media were taken at 5, 15, 30, 60, 120 and 180 min. All samples were filtered through a 0.2 μm GHP Acrodisc filter (Pall Corporation, East Hills, NY), and diluted with acetonitrile for content analysis. The ITZ content was determined using a Shimadzu LC-10A high performance liquid chromatography (HPLC) system (Shimadzu Corporation, Columbia, MD) equipped with an Alltech Inertsil^{TM} ODS-2 5 μm, 150 mm × 4.6 mm, C-18 column (Alltech Associates, Inc., Deerfield, IL). The mobile phase was acetonitrile:water:diethanolamine (70:30:0.05) and it eluted the ITZ peak at approximately 5.5 min at 25 ℃ with a flow rate of 1 mL/min. The ITZ absorbance was measured at a wavelength λ_{max} of 263 nm.

2.3.12 In Vitro Aerosol Performance

A colloidal dispersion of the URF-ITZ powder was prepared for nebulization by dispersing the powder in purified water (equivalent to 20 mg/mL ITZ) using ultrasonication in an ice bath. An aliquot (5 mL) of the dispersion was nebulized using an Aeroneb® Professional micropump nebulizer (Nektar Inc., Mountain View, CA) for 10 min at an air flow rate of 28.3 L/min. The flow rate was maintained by a vacuum pump (MFG Corp., Benton Harbor, MI) and calibrated by a TSI mass flow meter, Model 4000 (TSI Inc., St. Paul, MN). The *in vitro* deposition characteristics of the colloidal dispersion of URF-ITZ for nebulization, was investigated using an eight-stage Andersen cascade impactor (Thermo-Electron Corp., Symrna, GA). The cascade impactor was assembled and operated in accordance with USP General Chapter 601 to assess the drug delivered. After deposition onto the stages of the impactor, the mass deposited on each of the stages was collected and the total mass of drug on each stage was analyzed by HPLC. The aerosolization behavior was described in terms of total emitted dose (TED), mass median aerodynamic diameter (MMAD), geometric standard deviation (GSD), and percentage fine particle fraction (FPF; defined as the percentage of droplets with an aerodynamic diameter less than 4.7 μm).

2.3.13 Stability Study

The URF-ITZ powder was stored in desiccators under vacuum at room temperature, and the physical stability was assessed by XRD at 1, 3 and 12 months.

The physical stability of the colloidal dispersion of URF-ITZ for nebulization was also investigated. The colloidal dispersion of URF-ITZ for nebulization was prepared as previously described. It was allowed to equilibrate at 25 ℃ for 15 min, and then was

quench frozen using excess liquid nitrogen. The colloidal dispersion was lyophilized, and the resultant powder was investigated by XRD.

2.3.14 *In Vivo* Pulmonary Dosing of Mice

Fourteen male ICR mice (Harlan Sprague Dawley, Inc., Indianapolis, IN) were dosed by inhalation of the nebulized colloidal dispersion of the URF-ITZ (equivalent to 20 mg/mL ITZ) for 10 min in a whole-body dosing chamber as previously described (McConville et al., 2005). This restraint-free chamber was designed to hold up to 14 mice. An Aeroneb Professional micropump nebulizer was situated at the inlet of the chamber, and the colloidal dispersion of the URF-ITZ was nebulized through the inlet into the chamber with an air flow rate of 1 L/min. Following exposure to the aerosol cloud, the mice were sacrificed by carbon dioxide asphyxiation at 0.5, 1, 2, 4, 6, 10, and 24 h time points post dosing. Blood samples were taken by cardiac puncture, and the lungs were harvested. The study protocol was approved and conducted in accordance with the Institutional Animal Care and Use Committee (IACUC) guidelines at The University of Texas at Austin.

2.3.15 Plasma and Lung Analysis

Serum was separated by centrifugation at 3,000 g for 10 min in a 1.5 mL micro-centrifuge tube using a Microfuge® 18 centrifuge (Beckman Coulter, Fullerton, CA). The serum and lung samples were stored at -20 ℃ until analyzed. The homogenized lung samples were prepared by adding 1 mL of normal saline to each of the harvested lung and homogenized using tip sonication on an ice bath. Drug levels in the calibration standards, serum and homogenized lung samples were analyzed as previously indicated [28].

Briefly, to an aliquot of 250 μL serum or 250 μL of lung homogenate, 50 μL of 0.3 N barium hydroxide and 50 μL of 0.4 N zinc sulfate heptahydrate solutions were added and vortex mixed for 30 sec to precipitate water-soluble proteins. Acetonitrile (1 mL) containing 500 ng/mL ketoconazole as an internal reference standard was added to each sample followed by vortex mixing for 1.5 min. Each sample was then centrifuged at 3,000 g for 15 min. The supernatant was transferred to a clean 1.5 mL micro-centrifuge tube and dried under a stream of nitrogen gas. Each sample was reconstituted with 250 μL mobile phase (62% acetonitrile: 38% 0.05 M potassium phosphate monobasic buffer adjusted to pH 6.7 with NaOH) and analyzed by HPLC with an Alltech Inertsil^{TM} ODS-2 5 μm, 250×4.6 mm, C-18 column protected by a C-18 guard column (5 μm, 7.5×4.6 mm) (Alltech Associates, Inc., Deerfield, IL). The injection volume was 100 μL, and the wavelength of absorption was 263 nm (λ_{max}). The limit of detection and quantitation for ITZ was 10 ng/mL and 30 ng/mL, respectively. The column was maintained at 37 ℃ during the analysis. The ITZ peak eluted at approximately 18 min and the ketoconazole peak eluted at 9.3 min at a mobile phase flow rate of 1.0 mL/min.

2.3.16 Pharmacokinetic Analysis

Pharmacokinetic parameters for lung and serum were derived by noncompartmental and one-compartmental analysis, respectively. Pharmacokinetic parameters were estimated by standard methods. C_{max} was the maximal concentration observed, T_{max} was the time to C_{max}, and they were obtained from the individual concentration-time curves. The $K_{01\ absorption}$ and $K_{10\ elimination}$ rate constants were determined by linear regression of the points of the log-linear plasma concentration versus time curve. The area-under-the-concentration-time curve from time zero to infinity ($AUC_{0-\infty}$) was determined by use of the linear trapezoidal rule with extrapolation to

infinity by using the $K_{10\ elimination}$ rate constant. The $t_{1/2}$ was defined as 0.693/ rate constant K [36].

2.4 RESULTS

2.4.1 Physicochemical Properties of URF–ITZ Powder

The URF process was employed to make the nanostructured aggregate powder with an ITZ potency of 56%. ITZ is a highly crystalline hydrophobic molecule with a molecular weight of 705.64. The degree of crystallinity in the ITZ/excipient mixture has been shown to affect the solubility and dissolution rate of ITZ in the mixture [8]. The crystallinity of bulk ITZ, mannitol, URF-ITZ and the physical mixture were examined by XRD and the profiles are depicted in Figure. 1. The characteristic crystalline peaks for ITZ were found at 14.5, 17.6, 20.3, and 23.45 2-theta degrees, as seen in the bulk ITZ (purchased from the manufacturer) and physical mixture samples. The physical mixture of ITZ: mannitol: lecithin (1: 0.5: 0.2 ratio by weight) showed a qualitative reduction in crystalline intensity for both ITZ and mannitol. The URF-ITZ powder was amorphous as indicated by the absence of the characteristic crystalline peaks of ITZ and mannitol.

From the SEM images, the bulk ITZ and the physical mixture were composed of large, compact crystals at the micron-scale, ranging up to about 5 μm in length (Figures 2.2a, 2.2b). In contrast, a highly porous structure with more regularly shaped particles of the URF-ITZ powder was observed at higher magnifications in Figures 2.2c and 2.2d, displaying aggregated nanoparticles that formed a porous matrix. Closer inspection of the morphology by STEM demonstrated that the bridged, round shaped primary particles of the nanostructured aggregates were about 30-50 nm in diameter, as seen in Figure 2.3a.

2.4.2 Energy Dispersive Spectroscopy (EDS)---Elemental Characterization

The ITZ molecule ($C_{35}H_{38}Cl_2N_8O_4$) may be distinguished from other molecules present in the formulation due to the presence of two chlorine atoms; whereas mannitol contains only carbon, oxygen and hydrogen, and lecithin also contains phosphorus. Chlorine may be used as a marker to determine the distribution of ITZ molecules within the nanostructured aggregates. EDS was used to map the compositional distribution of the elements, including: carbon, oxygen and chlorine.

Elemental distribution mapping for carbon, oxygen and chlorine contained in the nanoparticle aggregates of URF-ITZ scanned by EDS are presented in Figure 2.3c, d, e along with a STEM image of the scanned nanostructured aggregates in Figure 2.3b. Element distribution images showed colored dots, representing the presence of a particular chemical element, in contrast to the black background. It can be seen that the distribution of each element is consistent with the shape and density of the aggregated nanoparticles scanned, including the presence of the pores.

2.4.3 Thermal Analysis

MTDSC was carried out to study the thermal properties of the URF-ITZ powder and its individual components. The glass transition temperature (T_g) of URF pure ITZ (no excipients; 100% potency), quench-cooled mannitol and quench-cooled lecithin were 59.6 ℃ (consistent with reports of [37, 38], 16.8 ℃ and 5.1 ℃, respectively, as shown in Figure 2.4 thermograms. The URF-ITZ powder (ITZ:mannitol:lecithin=1:0.5:0.2 ratio by weight) showed a single T_g at 44.5 ℃. The corresponding physical mixture only showed

one endothermic melting peak at 166.2 ℃. XRD was conducted on powders of the following compositions, and the results indicated that the URF pure ITZ (no excipients; 100% potency) was amorphous, URF pure mannitol was crystalline, URF pure lecithin was amorphous, URF ITZ:mannitol = 1:0.5 (ratio by weight) was amorphous, and URF mannitol:lecithin = 0.5:0.2 (ratio by weight) was partially crystalline (Figure 2.1).

2.4.4 Particle Size Distribution

The particle size distributions that measured by laser diffraction are shown in Table 2.1. The URF-ITZ powder showed a narrow size range with D_{50} and D_{90} (diameter at which the cumulative sample volume was under 50% and 90%, respectively) are less than 230 and 540 nm, respectively, compared to the corresponding values of 2.75 and 5.10 μm in the corresponding physical mixture.

2.4.5 Specific Surface Area and True Density

The specific surface area of the URF-ITZ powder was 71.48 m^2/g, in contrast to 2.20 m^2/g for the unprocessed bulk ITZ and 1.80 m^2/g for the physical mixture. The URF process rendered the ITZ/excipients about 30-40 times greater surface area as compared to that of the bulk ITZ and the physical mixture, as seen in Table 2.1.

True density of ITZ, mannitol and lecithin were determined to be 1.37, 1.50, 1.10 g/cm^3, respectively, by helium pycnometry.

2.4.6 Supersaturation Dissolution Study

The maximum concentration of dissolved ITZ in simulated lung fluid was determined under supersaturated conditions (100-times C_{eq}). The results are shown in Figure 2.5. The C_{eq} in simulated lung fluid was about 10 ng/mL after shaking at 37 ℃ for 3 days with excess ITZ present. The URF-ITZ powder showed a value of the measured concentration of dissolved ITZ *(C)* versus C_{eq} (C/C_{eq}) of 22-times at 5 min in simulated lung fluid and the highest value of 27-times at 15 min. The supersaturated ITZ concentration gradually decreased to about 7-times at 3 h. The physical mixture demonstrated about 2-times the measured C/C_{eq} at 15 and 30 min, and gradually decreased and reached a plateau at C_{eq} value after 2 h in the simulated lung fluid. The cumulative extent of supersaturation was calculated as the area-under-the-supersaturation-curve (AUSC), which was 25,000 and 2,500 ng·min/mL for URF-ITZ and the corresponding physical mixture, respectively.

2.4.7 In Vitro Aerosol Performance

The aerodynamic particle size of the colloidal dispersion of URF-ITZ for nebulization, with an equivalent of 100 mg ITZ in 5 mL, is summarized in Table 2.2. The TED was 52.97 mg out of 100 mg ITZ available for nebulization. The FPF was 66.96% with a fine particle dose (amount of aerosol droplets entering the impactor less than 4.7 μm, TED × FPF, indication of the dose delivered to the deep lung) delivered at a rate of 3.55 mg/min. The MMAD of the atomized droplets was 2.38 μm with a GSD of 2.56, which is suitable for deep lung delivery.

2.4.8 Stability Study

The crystallinity of the URF-ITZ powder was monitored using XRD and the results are depicted in Figure 2.1. There was no characteristic crystalline peak of ITZ or mannitol detected by XRD after storage for up to 12 months, indicating the powder retained its amorphous morphology when stored at room temperature and protected from humidity.

Additionally as a simulation for the period of the URF-ITZ powder dispersion to be nebulized, the absence of characteristic crystalline peaks confirmed that the URF-ITZ in the colloidal dispersion remained amorphous over the nebulization time period.

2.4.9 Single Dose, 24-h Pharmacokinetic Study in Mice

Mice inhaled the single dose aerosols of the nebulized URF-ITZ colloidal dispersion for 10 min. ITZ concentrations versus time in the blood and lung samples of the single dose 24-h pharmacokinetic study are presented in Figure 2.6. The pharmacokinetic parameters are listed in Table 2.3. In the lung samples, the C_{max} was 21.19 μg/g (wet lung tissue) at 0.5 h post dosing. The $t_{1/2}$ was 7.4 h and the $K_{elimination}$ rate constant was 0.093 h^{-1}, which may explain the ITZ lung level was maintained at 2.16 μg/g (wet lung weight) for up to 24 h. In serum, based on a one-compartmental analysis, the C_{max} was 1.64 μg/mL at 2 h after dosing. The $K_{01\ absorption}$ and $K_{10\ elimination}$ rate constants were 0.757 and 0.195 h^{-1}, respectively. The $t_{1/2\ k01}$ and $t_{1/2\ k10}$ were 0.92 and 3.55 h, respectively.

2.5 DISCUSSION

2.5.1 Characterization of URF-ITZ and Comparison to SFL-ITZ

Pulmonary delivery of the nebulized colloidal dispersion of nanostructured aggregates of URF-ITZ dramatically improved bioavailability compared to the previously reported formulation of SFL-ITZ, more specifically a faster absorption rate, shorter T_{max}, almost double the C_{max} in lung tissue, and 10-times higher C_{max} in blood were observed [28]. Both of the formulations were tested in the same animal model according to identical dosing apparatus and procedures. Further work would be needed to characterize the *in vitro* properties of the SFL-ITZ dispersions in order to understand these differences in bioavailability.

Both SFL and URF processes were able to create submicron particles of drug domains within a polymer matrix due to rapid freezing of a co-dissolved drug and excipient mixture [8, 9, 39]. Solid dispersions are systems in which drug particles are homogeneously distributed throughout a solid matrix. A solid solution results when the drug is molecularly dispersed throughout a solid matrix [40]; here, the particle size of the drug has been reduced to its absolute minimum without any crystalline drug domains [41]. Solid dispersions or solid solutions of poorly water soluble drugs have greatly enhanced extents and rates of dissolution, due to increased exposure area of drug to the dissolution media and higher Gibbs free energy of the amorphous versus crystalline states [6, 42]. This leads to significantly improved bioavailability and therefore is of interest to pharmaceutical formulation scientists.

In this study, powder XRD, MTDSC and EDS were used to differentiate between a solid dispersion and solid solution. Based on the MTDSC results, a single T_g for the

URF-ITZ powder was observed between the T_gs of the amorphous pure ITZ and mannitol. The modified Gordon–Taylor equation for ternary systems [43] was used to predict the T_g of the URF-ITZ powder:

$$T_g = \frac{w_1 T_{g1} + K_1 w_2 T_{g2} + K_2 w_3 T_{g3}}{w_1 + K_1 w_2 + K_2 w_3} \qquad (1)$$

where w_1, w_2, and w_3 are the weight fractions of lecithin, mannitol and ITZ, respectively, and T_{g1}, T_{g2} and T_{g3} are the corresponding glass transition temperatures. K is a constant calculated by

$$K_1 = \rho_1 T_{g1} / \rho_2 T_{g2},\ K_2 = \rho_2 T_{g2} / \rho_3 T_{g3} \qquad (2)$$

where ρ_1, ρ_2, and ρ_3 are the corresponding true densities. The predicted T_g' of 42.3 ℃, agrees closely with the measured T_g of 44.5 ℃ for the URF-ITZ powder.

The XRD pattern indicated that URF processed pure mannitol was partially crystalline; whereas ITZ:mannitol=1:0.5 and ITZ:mannitol:lecithin=1:0.5:0.2 (URF-ITZ) were completely amorphous. Absence of crystallinity of the drug or complete absence of a drug peak (either in DSC or XRD) indicates that the composition is a solid solution [44]. The partial crystallization of the mannitol by URF and lyophilization may be expected from its low T_g of 16.8 ℃. Kim et al. also reported similar results and difficulty in obtaining amorphous mannitol freeze-dried powder [35]. ITZ may retard mannitol crystallization from the glassy state, which is expected from a miscible polymer pair. Lecithin itself is in an amorphous form. Mannitol and lecithin may plasticize the extremely hydrophobic ITZ in the URF-ITZ powder leading to improved wettability, though also reduction of its T_g.

Moreover, EDS was performed to analyze the distribution of ITZ in the drug/excipient matrix by mapping elemental distributions. Theoretically, the ratios of the main elements (carbon, oxygen, chlorine) at any given area should be constant if ITZ, mannitol and lecithin formed a solid solution. EDS is capable of highly selective spatial resolution of chemistry, from volumes as small as 1 μm^3 [45]. The qualitative elemental distribution images suggest a generally homogenous distribution of ITZ in the scanned aggregated nanoparticles of URF-ITZ. Based on MTDSC, XRD, and EDS results, the components of the URF-ITZ composition are fully miscible and dispersed in each other at the molecular level. Thus, the URF-ITZ powder is primarily a solid solution formed by the immobilization of molecularly dispersed ITZ and excipients (mannitol, lecithin) on a timescale of milliseconds during the URF process [10, 46].

2.5.2 Role of the surfactant and mannitol

In the URF-ITZ composition, the soy lecithin is an accepted excipient for aerosol inhalation [32]. It is acceptable in the lung as the biocompatible and biodegradable substance, *i.e.* phosphatidylcholine (PC) comprises an estimated 70-80% of the naturally occurring pulmonary surfactant pool [47]. Besides playing an important role in improving the wettability of the nanoparticles containing ITZ, it may also enhance the absorption of ITZ across the lung epithelium. Phospholipids are known to penetrate cell membranes, decrease bilayer stability, and thereby induce changes in the cytoskeleton that can affect tight junctions and accelerate paracellular passage of drugs [48-50]. Codrons et al. [51] reported that incorporation of DPPC into a dry powder formulation of parathyroid hormone for pulmonary administration produced a high systemic bioavailability of 34% in rats. DPPC has also been shown to increase absorption of insulin via pulmonary delivery and enhance the hypoglycemic effect in rats relative to free insulin, when

formulated as an admixture or in liposomes [52, 53]. The addition of very small amounts of exogenous DPPC may transiently alter local PC concentrations [54], and/or accelerate the surfactant turnover process, leading to enhanced penetration of the drug molecules through the lung alveolar cells into the systemic circulation [52].

In the present study, the high systemic absorption of ITZ following pulmonary dosing may be attributed partially to the inhaled exogenous PC, as well as the small particle size. The PC from lecithin may facilitate both dissolution and permeation, via dilated pulmonary epithelial tight junctions. Thus, the selection of lecithin as an excipient in the URF-ITZ composition offers the potential of marked improvement in absorption, without adding toxicity to the formulation. Moreover, the presence of the surfactant in the ITZ nanoparticle formulations is important to stabilize the dispersion and aid in wetting upon deposition in the lungs. Nanoparticles have high surface energies, due to the high surface-to-volume ratio and tend to agglomerate. Wettability of the URF-ITZ powder is critical for forming dispersions in the aqueous medium prior to nebulization. Mannitol was chosen as the second excipient in the URF-ITZ composition, to improve wetting of the URF-ITZ powder by introducing water into the matrix to aid dissolution.

Once the drug is deposited in the aqueous lining fluid in the lung, the mannitol may quickly dissolve, resulting in a porous drug matrix. Lecithin will initially swell, causing stress relaxation of the matrix and allowing water ingress before it dissolves. These processes will help stabilize the ITZ from aggregation and precipitation during dissolution.

The URF process dramatically increased the surface area of the nanostructured aggregates of URF-ITZ to about 40 times that of the corresponding physical mixture for

dissolution. Additionally, the thinner diffusion boundary layer for the smaller particle size raises the dissolution rate [55, 56]. Furthermore, the degree of crystallization of undissolved ITZ in the particles upon exposure to the lung fluid is reduced by the rapid dissolution of the high surface area nanoparticles relative to microparticles, as examined in detail elsewhere [6]. A combination of increased intrinsic solubility and reduced chance to crystallize of undissolved ITZ in the media may provide an explanation for the URF-ITZ to produce supersaturation values more than 20-times C_{eq} in simulated lung fluid.

2.5.3 Deposition of the nanoparticles containing ITZ

It is generally accepted that aerosol droplets with aerodynamic diameters between 1-5 μm can be delivered into the alveolar lumen after inhalation [57]. Furthermore, the aerosol diameter of aqueous droplets produced by nebulizers may readily be tuned to this optimal size range [27]. Nanoparticles may be distributed more uniformly throughout the nebulized droplets than microparticles [58, 59]. For instance, if the volume fraction, *f*, of particles in the solvent is 0.01, then only about 1/100 of 3 μm carrier droplets will contain a 3 μm particle. In contrast each carrier droplet would contain about twenty-two 230 nm particles according to the relationship:

$$N_{particles}/N_{drops} = f \frac{r_{drop}^{3}}{r_{particle}^{3}} \qquad (3)$$

Thus, the rate of drug absorption may be increased for nanoparticle relative to microparticle colloidal dispersions, by promoting more uniform drug distribution throughout the alveoli [60, 61]. More specifically, for a 32.5 μg drug/g lung dose (chosen based on the ITZ C_{max} recovered from lung tissue at t=0.5 h and the corresponding blood concentration given in Figure 2.6.) delivered as 3 μm drug particles, only 1 in 75 alveoli

are estimated to receive a particle. However, approximately 30 drug particles are deposited in each alveolus when the same dose is delivered as 230 nm drug particles.

2.5.4 Absorption of ITZ as a function of the composition and particle morphology

A drug in an amorphous state will possess a higher intrinsic solubility than in its crystalline state [6, 62-64]. The URF-ITZ powder was shown to be an amorphous solid solution by DSC, XRD, and elemental mapping analysis. Furthermore, the exposure of ITZ molecules to the dissolution medium is maximized in the high surface area particles, as the soluble mannitol and lecithin dissolve in the lung lining fluid. The dispersed ITZ molecules are then available as free molecules to form a supersaturated solution [41]. After deposition of the inhaled ITZ nanoparticles in the lung lining fluid, the rate and extent of dissolution influence the permeation rate of ITZ through the lung epithelium to reach systemic circulation.

The effects of particle size, dissolution rate, extent of supersaturation and permeability on absorption of poorly water soluble drugs in the lungs were examined with a model reported recently [29]. The Noyes-Whitney equation describes the dissolution rate of ITZ spherical nanoparticles. The permeate concentration was assumed to be zero as the drug concentration in the blood may be assumed to be insignificant compared to that in the alveolar fluid and thus the permeation is irreversible [65]. The thickness of the human alveolar membrane (100-200 nm) is small versus the diameter of the alveolus (300 μm) [27, 66] and thus planar coordinates are appropriate. Consider a material balance on the fluid surrounding a drug particle in the alveolar fluid as shown in Figure 2.7. The accumulation of dissolved drug in the fluid of a single alveolus C is given

by the inlet flow from particle dissolution and the depletion by an outlet flow from drug permeation through the epithelium [29]

$$\frac{\partial C}{\partial t} = N_p D \frac{2\pi r}{V}(C_{sat} - C) - \frac{AP}{V} C \qquad (4)$$

where N_p is the number of drug particles deposited in each alveolus, D is the diffusion coefficient of the drug, P is the permeability, and V and A are the volume and surface area, respectively, of an annular layer of lung fluid in a single alveolus adjacent to the epithelium (Figure 2.7.). Absorption half-lives were determined as the time when $M_{permeated}/M_0 = 0.5$ or likewise, $r^3/ r_0^3 = 0.5$. It is instructive to consider the two boundary conditions for absorption: purely dissolution limited and purely permeation limited. For purely dissolution limited absorption ($P = \infty$ and $C \rightarrow 0$), the absorption half-life becomes

$$t_{50} \approx \frac{0.37 r_0^2}{DC_{sat}} \rho \quad (5)$$

and for purely permeation limited absorption (dissolution rate $\rightarrow \infty$ and $C=C_{sat}$)

$$t_{50} = \frac{0.5 M_0}{A_{Alv} P C_{sat}} \qquad (6)$$

where $A_{Alv} = A$ for planar geometry.

The Wilke-Chang equation was used to estimate a $D= 5.26 \times 10^{-6}$ cm^2/s [67] for ITZ. A P value of 5.61×10^{-5} cm/s was chosen based on experimental ITZ permeabilities in intestinal membranes [68]. Common permeabilities of poorly water soluble drugs with similar molecular sizes in lung cell cultures range between 10^{-6}-10^{-4} cm/s [69]. The number of drug particles deposited in the lungs was calculated from an estimated drug dose and the average particle volume. The drug dose, or the total mass of drug deposited in the lungs, was approximated to be 5.8 μg (32.5 μg/g wet lung tissue) based on the lung tissue C_{max} (21.2 μg/g) and the corresponding blood concentration (492 ng/mL) from the

single-dose pharmacokinetic study. The number of alveoli in a mouse was estimated to be ~2.25 $\times 10^7$, calculated using an alveolar surface area of 680 cm^2 [70] and alveolus diameter of 31 μm [71] for mice. Total alveolar fluid volume was estimated to be 8.3 μL, based on a human alveolar surface fluid volume of 15 mL [66, 72] and the ratio of human lung to mouse lung weight.

Figure 2.8. shows the predicted absorption half-lives for particles ranging from 50 nm to 3 μm in diameter for a wide equilibrium solubility range, from 10 ng/mL to 10 μg/mL. Particle sizes between 50-230 nm are representative of URF-ITZ particles, as determined by STEM images (Figure 2.3a) and light scattering results (Table 2.1.), whereas a particle size of 3 μm is typical of particles traditionally delivered to the lungs (Courrier et al., 2002). The t_{50} for a crystalline 3 micron ITZ particle (C_{sat}=10 ng/mL) was estimated to be 200 h (Figure 2.8G), far too slow to be appropriate for therapy. In contrast, t_{50} values for the amorphous 230 nm particles were only 14.7 min, which would be consistent with the kinetics for the studies with mice in Figure 2.6.

The t_{50} values are shown for purely dissolution limited absorption (diamonds, infinite permeability) and purely permeation limited absorption (asterisks, $C = C_{sat}$). For permeation limited absorption, t_{50} does not change with particle size for the 50 and 230 nm particles as predicted from eq. 6. However, it is much larger for a 3 μm particle deposited in an alveolus because of the larger M_o. Based on *in-vivo* lung and blood levels, only 1 in 67 alveoli would be estimated to receive a 3 μm drug particle compared to about 30 particles per alveolus for a 230 nm particle. For the 230 nm particles, the smaller M_o resulting from the more uniform distribution of particles throughout all of the alveoli is a major benefit, as it produces smaller t_{50} values relative to microparticles.

For all three C_{sat} values with 3 μm particles, the absorption rate is strongly limited by the dissolution rate as expected for a BCS Class II drug. Thus, the t_{50} decreases orders of magnitude with an increase in C_{sat} by 1000 fold, which increases the driving force for particle dissolution. Interestingly, the absorption became much more permeability limited than dissolution rate limited for the 230 nm particles, no longer exhibiting BCS Class II behavior, for all three C_{sat} values. For the high surface area 50 nm particles, the dissolution rate limited t_{50} was about two orders of magnitude shorter than the permeation limited value. With the extremely rapid dissolution rates relative to permeation, absorption times remained fairly constant versus particle diameter for sub-230 nm particles, at a given equilibrium solubility (Figure 2.8A-F).

Despite the high dissolution rate for the 230 nm crystalline particles, the t_{50} value was still undesirably long because of the effect of the low C_{sat} on the permeability. The t_{50} was reduced markedly by an increase in C_{sat} for the amorphous URF-ITZ. Yet a further improvement in permeation rates may be achieved by incorporating permeability enhancers. In fact, the increased systemic absorption rate of URF-ITZ over SFL-ITZ [28], despite the similar particle sizes, may be explained by the incorporation of lecithin in the URF-ITZ formulation, a known permeation enhancer. As a result, an order of magnitude increase in C_{max} was achieved in circulation (URF-ITZ: 1.64 μg/mL serum versus SFL-ITZ: 0.12 μg/mL) in a shorter time (T_{max} of URF-ITZ: 2 h versus SFL-ITZ: 5.35 h) as well as a higher absorption rate of ITZ from lung to blood compared to the SFL-ITZ formulation (URF–ITZ: 0.757 h^{-1} versus SFL–ITZ: 0.186 h^{-1}) [9].

2.6 CONCLUSIONS

Amorphous ITZ particles were made by the ultra-rapid freezing process with FDA approved biodegradable and biocompatible excipients to achieve a mean diameter of 230 nm, a large surface area of 71 m^2/g, and a wettable surface. The particles dissolved rapidly in simulated lung fluid to produce supersaturation levels up to 27-times of C_{eq} for the crystalline form. Nebulized aqueous colloidal dispersions of the ITZ nanoparticles exhibited aerodynamic characteristics suitable for deep lung delivery. An *in vivo* single dose 24-h pharmacokinetics study of the nebulized ITZ nanoparticle dispersion demonstrated substantial lung deposition and systemic absorption with blood levels reaching a peak of 1.6 μg/mL serum in 2 h.

To investigate the mechanism of drug absorption in the alveolar epithelium, a dissolution/permeation model was used to elucidate the effects of particle size and solubility. ITZ microparticles (3 μm) exhibited BCS Class II behavior for poorly soluble drugs with high permeabilities, where the absorption was influenced strongly by the dissolution rate. However, for 230 nm particles, the dissolution became sufficiently fast such that the concentration in the alveolar fluid reached saturation, and consequently, the absorption became permeation limited. Therefore, a microparticle formulation with BCS Class II behavior, may exhibit a completely different kind of behavior when reformulated at the nanoscale.

Four strategies were used to raise the bioavailability. The aqueous nebulized droplets were optimized to deposit the drug in the deep lungs. The decrease in particle size (increase in surface area) enhanced the dissolution rate as well as the uniformity of the distribution of drug dose among the alveoli. The increase in C_{sat} with the formation of

an amorphous polymorph, raised the driving force for permeation through the alveolar membrane. The fourth and final approach was to raise the membrane flux with lecithin, a known permeation enhancer. For the permeation limited absorption of the 50-230 nm URF-ITZ nanoparticles, the presence of lecithin may have contributed to the enhanced systemic levels observed in the *in-vivo* results. Pulmonary delivery of the ITZ nanoparticle aerosols offers the potential to treat invasive fungal infections more effectively in patient populations that have poor prognosis.

2.7 ACKNOWLEDGEMENTS

The authors are grateful to Dr. Troy Purvis for his help with HPLC analysis. This material is based upon work supported in part by the STC Program of the National Science Foundation under Agreement No. CHE-9876674, the Welch Foundation, and the Process Science and Technology Center of the University of Texas.

2.8 REFERENCES

1. G.V. Betageriand K.R. Makarla. Enhancement of dissolution of glyburide by solid dispersion and lyophilization techniques. International Journal of Pharmaceutics. 126:155-160 (1995).

2. S. Mawson, M.Z. Yates, M.L. ONeill, and K.P. Johnston. Stabilized polymer microparticles by precipitation with a compressed fluid antisolvent .2. Poly(propylene oxide)- and poly(butylene oxide)-based copolymers. Langmuir. 13:1519-1528 (1997).

3. T.L. Rogers, K.P. Johnston, and R.O. Williams, 3rd. Solution-based particle formation of pharmaceutical powders by supercritical or compressed fluid CO2 and cryogenic spray-freezing technologies. Drug Dev Ind Pharm. 27:1003-1015 (2001).

4. M. Sarkari, J. Brown, X. Chen, S. Swinnea, R.O. Williams, 3rd, and K.P. Johnston. Enhanced drug dissolution using evaporative precipitation into aqueous solution. Int J Pharm. 243:17-31 (2002).

5. J. Hu, K.P. Johnston, and R.O. Williams, 3rd. Nanoparticle engineering processes for enhancing the dissolution rates of poorly water soluble drugs. Drug Dev Ind Pharm. 30:233-245 (2004).

6. M.E. Matteucci, B.K. Brettmann, T.L. Rogers, E.J. Elder, R.O. Williams, 3rd , and K.P. Johnston. Design of Potent Amorphous Drug Nanoparticles for Rapid Generation of Highly Supersaturated Media. Molecular pharmaceutics. 4:782-793 (2007).

7. B.C. Hancockand M. Parks. What is the true solubility advantage for amorphous pharmaceuticals? Pharmaceutical research. 17:397-404 (2000).

8. J.M. Vaughn, X. Gao, M.J. Yacaman, K.P. Johnston, and R.O. Williams, 3rd. Comparison of powder produced by evaporative precipitation into aqueous solution (EPAS) and spray freezing into liquid (SFL) technologies using novel Z-contrast STEM and complimentary techniques. Eur J Pharm Biopharm. 60:81-89 (2005).

9. J.T. McConville, K.A. Overhoff, P. Sinswat, J.M. Vaughn, B.L. Frei, D.S. Burgess, R.L. Talbert, J.I. Peters, K.P. Johnston, and R.O. Williams, 3rd. Targeted High Lung Concentrations of Itraconazole Using Nebulized Dispersions in a Murine Model. Pharmaceutical research (2006).

10. K.A. Overhoff, J.D. Engstrom, B. Chen, B.D. Scherzer, T.E. Milner, K.P. Johnston, and R.O. Williams, 3rd. Novel ultra-rapid freezing particle engineering process for enhancement of dissolution rates of poorly water-soluble drugs. Eur J Pharm Biopharm. 65:57-67 (2007).

11. J. Peeters, P. Neeskens, J.P. Tollenaere, P. Van Remoortere, and M.E. Brewster. Characterization of the interaction of 2-hydroxypropyl-beta-cyclodextrin with itraconazole at pH 2, 4, and 7. Journal of pharmaceutical sciences. 91:1414-1422 (2002).

12. G.L. Amidon, H. Lennernas, V.P. Shah, and J.R. Crison. A theoretical basis for a biopharmaceutic drug classification: the correlation of in vitro drug product dissolution and in vivo bioavailability. Pharmaceutical research. 12:413-420 (1995).

13. D. Smith, V. van de Velde, R. Woestenborghs, and B.G. Gazzard. The pharmacokinetics of oral itraconazole in AIDS patients. J Pharm Pharmacol. 44:618-619 (1992).

14. J.A. Barone, J.G. Koh, R.H. Bierman, J.L. Colaizzi, K.A. Swanson, M.C. Gaffar, B.L. Moskovitz, W. Mechlinski, and V. Vandevelde. Food Interaction and Steady-State Pharmacokinetics of Itraconazole Capsules in Healthy Male-Volunteers. Antimicrobial Agents and Chemotherapy. 37:778-784 (1993).

15. J.M. Poirier, S. Hardy, F. Isnard, P. Tilleul, J. Weissenburger, and G. Cheymol. Plasma itraconazole concentrations in patients with neutropenia: advantages of a divided daily dosage regimen. Therapeutic Drug Monitoring. 19:525-529 (1997).

16. J.D. Sobel. Practice guidelines for the treatment of fungal infections. For the Mycoses Study Group. Infectious Diseases Society of America. Clinical Infectious Diseases. 30:652 (2000).

17. M. Ebbesenand T.G. Jensen. Nanomedicine: techniques, potentials, and ethical implications. J Biomed Biotechnol. 2006:51516 (2006).

18. W. Yang, J.I. Peters, and R.O. Williams, 3rd. Inhaled Nanoparticles – A Current Review. Int J Pharm. DOI: 10.1016/j.ijpharm.2008.02.011: (2008).

19. S.J. Lin, J. Schranz, and S.M. Teutsch. Aspergillosis case - Fatality rate: Systematic review of the literature. Clinical Infectious Diseases. 32:358-366 (2001).

20. B. Mehrad, G. Paciocco, F.J. Martinez, T.C. Ojo, M.D. Iannettoni, and J.P. Lynch, 3rd. Spectrum of Aspergillus infection in lung transplant recipients: case series and review of the literature. Chest. 119:169-175 (2001).

21. T.A. Clarkand R.A. Hajjeh. Recent trends in the epidemiology of invasive mycoses. Current Opinion in Infectious Diseases. 15:569-574 (2002).

22. N. Singhand S. Husain. Aspergillus infections after lung transplantation: clinical differences in type of transplant and implications for management. Journal of Heart and Lung Transplantation. 22:258-266 (2003).

23. D.A. Edwardsand C. Dunbar. Bioengineering of therapeutic aerosols. Annu Rev Biomed Eng. 4:93-107 (2002).

24. A.L. Adjeand P.K. Gupta. Inhalation Delivery of Therapeutic Peptides and Proteins. In A.A.F. Mahmoud (ed.), Parasitic Lung Diseases, Marcel Rcel Dekker Inc., New York, 1997, pp. 89-125.

25. A.H.L. Chow, H.H.Y. Tong, P. Chattopadhyay, and B.Y. Shekunov. Particle engineering for pulmonary drug delivery. Pharmaceutical Research. 24:411-437 (2007).

26. O.N. McCallion, K.M. Taylor, M. Thomas, and A.J. Taylor. Nebulization of fluids of different physicochemical properties with air-jet and ultrasonic nebulizers. Pharmaceutical research. 12:1682-1688 (1995).

27. H.M. Courrier, N. Butz, and T.F. Vandamme. Pulmonary drug delivery systems: Recent developments and prospects. Critical Reviews in Therapeutic Drug Carrier Systems. 19:425-498 (2002).

28. J.M. Vaughn, J.T. McConville, D. Burgess, J.I. Peters, K.P. Johnston, R.L. Talbert, and R.O. Williams, 3rd. Single dose and multiple dose studies of itraconazole nanoparticles. Eur J Pharm Biopharm. 63:95-102 (2006).

29. J. Tam, J.T. McConville, R.O. Williams, 3rd, and K.P. Johnston. Amorphous Cyclosporin Nanodispersions for Enhanced Pulmonary Deposition and Dissolution. Journal of pharmaceutical sciences (Submitted).

30. J.S. Patton, J.G. McCabe, S.E. Hansen, and A.L. Daugherty. Absorption of human growth hormone from the rat lung. Biotechnol Ther. 1:213-228 (1989).

31. C. Bosquillon, C. Lombry, V. Preat, and R. Vanbever. Influence of formulation excipients and physical characteristics of inhalation dry powders on their aerosolization performance. Journal of Controlled Release. 70:329-339 (2001).

32. http://www.accessdata.fda.gov/scripts/cder/iig/getiigWEB.cfm.

33. J. Goerke. Pulmonary surfactant: functions and molecular composition. Biochim Biophys Acta. 1408:79-89 (1998).

34. J.C. Evans, B.D. Scherzer, C.D. Tocco, G.B. Kupperblatt, J.N. Becker, D.L. Wilson, S.A. Saghir, and E.J. Elder. Preparation of nanostructured particles of poorly water soluble drugs via a novel ultra-rapid freezing technology. in: S Svenson (Ed), Polymeric Drug Delivery – Polymeric Matrices and Drug Particle Engineering. :ACS Symposium Series 924, American Chemical Society, Washington, DC, pp320–328 (2006).

35. A.I. Kim, M.J. Akers, and S.L. Nail. The physical state of mannitol after freeze-drying: effects of mannitol concentration, freezing rate, and a noncrystallizing cosolute. Journal of pharmaceutical sciences. 87:931-935 (1998).

36. M. Rowlandand T. Tozer. Absorption and disposition kinetics. In M. Rowlandand T. Tozer (eds.), Clinical pharmacokinetics: Concepts and applications, Lippincott Williams & Wilkins, Baltimore, 1995, pp. 11–52.

37. K. Six, G. Verreck, J. Peeters, P. Augustijns, R. Kinget, and G. Van den Mooter. Characterization of glassy itraconazole: a comparative study of its molecular mobility below T(g) with that of structural analogues using MTDSC. Int J Pharm. 213:163-173 (2001).

38. G. Verreck, K. Six, G. Van den Mooter, L. Baert, J. Peeters, and M.E. Brewster. Characterization of solid dispersions of itraconazole and hydroxypropylmethylcellulose prepared by melt extrusion--Part I. Int J Pharm. 251:165-174 (2003).

39. K.A. Overhoff, A. Moreno, D.A. Miller, K.P. Johnston, and R.O. Williams, 3rd. Solid dispersions of itraconazole and enteric polymers made by ultra-rapid freezing. Int J Pharm. 336:122-132 (2007).

40. S.G. Kapsiand J.W. Ayres. Processing factors in development of solid solution formulation of itraconazole for enhancement of drug dissolution and bioavailability. Int J Pharm. 229:193-203 (2001).

41. C. Leunerand J. Dressman. Improving drug solubility for oral delivery using solid dispersions. Eur J Pharm Biopharm. 50:47-60 (2000).

42. A. Martin. Physical Pharmacy. Fourth ed., Williams&Wilkins, Baltimore, 1993.

43. G. Van den Mooter, M. Wuyts, N. Blaton, R. Busson, P. Grobet, P. Augustijns, and R. Kinget. Physical stabilisation of amorphous ketoconazole in solid dispersions with polyvinylpyrrolidone K25. Eur J Pharm Sci. 12:261-269 (2001).

44. F. Damian, N. Blaton, L. Naesens, J. Balzarini, R. Kinget, P. Augustijns, and G. Van den Mooter. Physicochemical characterization of solid dispersions of the antiviral agent UC-781 with polyethylene glycol 6000 and Gelucire 44/14. Eur J Pharm Sci. 10:311-322 (2000).

45. L.W. Sarver. SEM and EDS analyze materials. Adv Mater Process. 150:19-21 (1996).

46. J.D. Engstrom, E.S. Lai, B.S. Ludher, B. Chen, T.E. Milner, R.O. Williams, 3rd, G.B. Kitto, and K.P. Johnston. Formation of Stable Submicron Protein Particles by Thin Film Freezing. Pharmaceutical research. : (In Press).

47. M.A. Myers, D.A. Thomas, L. Straub, D.W. Soucy, R.W. Niven, M. Kaltenbach, C.I. Hood, H. Schreier, and R.J. Gonzalez-Rothi. Pulmonary effects of chronic exposure to liposome aerosols in mice. Exp Lung Res. 19:1-19 (1993).

48. P. Ott, M.J. Hope, A.J. Verkleij, B. Roelofsen, U. Brodbeck, and L.L. van Deenen. Effect of dimyristoyl phosphatidylcholine on intact erythrocytes. Release

of spectrin-free vesicles without ATP depletion. Biochim Biophys Acta. 641:79-87 (1981).

49. B. Roelofsen, F.A. Kuypers, J.A. Op den Kamp, and L.L. van Deenen. Influence of phosphatidylcholine molecular species composition on stability of the erythrocyte membrane. Biochem Soc Trans. 17:284-286 (1989).

50. T. Lindmark, Y. Kimura, and P. Artursson. Absorption enhancement through intracellular regulation of tight junction permeability by medium chain fatty acids in Caco-2 cells. J Pharmacol Exp Ther. 284:362-369 (1998).

51. V. Codrons, F. Vanderbist, B. Ucakar, V. Preat, and R. Vanbever. Impact of formulation and methods of pulmonary delivery on absorption of parathyroid hormone (1-34) from rat lungs. Journal of pharmaceutical sciences. 93:1241-1252 (2004).

52. F.Y. Liu, Z. Shao, D.O. Kildsig, and A.K. Mitra. Pulmonary delivery of free and liposomal insulin. Pharmaceutical research. 10:228-232 (1993).

53. R. Mitra, I. Pezron, Y. Li, and A.K. Mitra. Enhanced pulmonary delivery of insulin by lung lavage fluid and phospholipids. Int J Pharm. 217:25-31 (2001).

54. W. Bernhard, H.P. Haagsman, T. Tschernig, C.F. Poets, A.D. Postle, M.E. vanEijk, and H. vonderHardt. Conductive airway surfactant: Surface-tension function, biochemical composition, and possible alveolar origin. American Journal of Respiratory Cell and Molecular Biology. 17:41-50 (1997).

55. A.P. Tinke, K. Vanhoutte, R. De Maesschalck, S. Verheyen, and H. De Winter. A new approach in the prediction of the dissolution behavior of suspended particles by means of their particle size distribution. Journal of pharmaceutical and biomedical analysis. 39:900-907 (2005).

56. M.T. Crisp, C.J. Tucker, T.L. Rogers, R.O. Williams, and K.P. Johnston. Turbidimetric measurement and prediction of dissolution rates of poorly soluble drug nanocrystals. Journal of Controlled Release. 117:351-359 (2007).

57. P. Byronand E. Phillips. Absorption, clearance and dissolution in the lung. In P.R. Byron (ed.), Respiratory Drug Delivery CRC, Boca Raton FL, 1990, pp. 107–141.

58. H.K. Chanand I. Gonda. Development of a Systematic Theory of Suspension Inhalation Aerosols .2. Aggregates of Monodisperse Particles Nebulized in Polydisperse Droplets. International Journal of Pharmaceutics. 41:147-157 (1988).

59. B.E. Rabinow. Nanosuspensions in drug delivery. Nature Reviews Drug Discovery. 3:785-796 (2004).

60. C. Jacobsand R.H. Muller. Production and characterization of a budesonide nanosuspension for pulmonary administration. Pharmaceutical research. 19:189-194 (2002).

61. K.D. Ostrander, H.W. Bosch, and D.M. Bondanza. An in-vitro assessment of a NanoCrystal beclomethasone dipropionate colloidal dispersion via ultrasonic nebulization. Eur J Pharm Biopharm. 48:207-215 (1999).

62. W.L. Chiou. Pharmaceutical applications of solid dispersion systems: X-ray diffraction and aqueous solubility studies on griseofulvin-polyethylene glycol 6000 systems. Journal of pharmaceutical sciences. 66:989-991 (1977).

63. K. Yamashita, T. Nakate, K. Okimoto, A. Ohike, Y. Tokunaga, R. Ibuki, K. Higaki, and T. Kimura. Establishment of new preparation method for solid dispersion formulation of tacrolimus. Int J Pharm. 267:79-91 (2003).

64. D.J. van Drooge, W.L. Hinrichs, and H.W. Frijlink. Anomalous dissolution behaviour of tablets prepared from sugar glass-based solid dispersions. J Control Release. 97:441-452 (2004).

65. J.S. Pattonand P.R. Byron. Inhaling medicines: delivering drugs to the body through the lungs. Nat Rev Drug Discov. 6:67-74 (2007).

66. J. Patton. Mechanisms of macromolecule absorption by the lungs. Adv Drug Del Rev. 19:3–36 (1996).

67. W.L. McCabe, J.C. Smith, and P. Harriott. Unit Operations of Chemical Engineering, McGraw Hill Inc., Boston, MA, 2001.

68. M.V. Varma, K. Sateesh, and R. Panchagnula. Functional role of P-glycoprotein in limiting intestinal absorption of drugs: contribution of passive permeability to P-glycoprotein mediated efflux transport. Molecular pharmaceutics. 2:12-21 (2005).

69. B. Forbesand C. Ehrhardt. Human respiratory epithelial cell culture for drug delivery applications. Eur J Pharm Biopharm. 60:193-205 (2005).

70. A. Geelhaarand E.R. Weibel. Morphometric estimation of pulmonary diffusion capacity. 3. The effect of increased oxygen consumption in Japanese Waltzing mice. Respiration physiology. 11:354-366 (1971).

71. H. Lumand W. Mitzner. A species comparison of alveolar size and surface forces. J Appl Physiol. 62:1865-1871 (1987).

72. R.W. Niven. Pharmaceutical Inhalation Aerosol Technology, Marcel Dekker, Inc., New York, 1992.

Table 2.1. Particle size distributions and specific surface areas (SSA) of URF-ITZ (URF processed ITZ:mannitol:lecithin = 1:0.5:02) powders, Physical Mixture (physical mixture of ITZ:mannitol:lecithin = 1:0.5:02) and bulk ITZ.

	Particle Size (μm)			
Samples	D(v, 0.1)	D(v, 0.5)	D(v, 0.9)	SSA (m^2/g)
URF-ITZ	0.09	0.23	0.54	71.48
Physical Mixture	1.45	2.75	5.1	1.80
Bulk ITZ	1.6	2.89	4.95	2.20

Table 2.2. Cascade impaction data for URF-ITZ (URF processed ITZ:mannitol:lecithin = 1:0.5:02) powder, aerosolized using the Aeroneb® Professional micropump nebulizer at an air flow-rate of 28.3 L/min for 10 min.

Total Emitted Dose (mg)	52.97
Fine Particle Fraction (%)	66.96
Fine Particle Dose (mg/min)	3.55
Mass Median Aerodynamic Diameter (MMAD) (μm)	2.38
Geometric Standard Deviation (GSD)	2.56

Table 2.3. Pharmacokinetic parameters for lung deposition and serum concentration in male outbred ICR mice (25 g) after inhalation of nebulized URF-ITZ (URF processed ITZ: mannitol: lecithin = 1: 0.5: 02) nanoparticles dispersion following single dose administration.

	SFL-ITZ*		URF-ITZ	
Pharmacokinetic parameter	Lung[a]	Serum[b]	Lung[a]	Serum[b]
C_{max} (μg/g)	13.4	0.12	21.19	1.64
T_{max} (h)	1	5.35	0.5	2
$t_{1/2\ K01}$ (h)		3.73		0.92
$t_{1/2\ K10}$ (h)	5.5	3.7	7.44	3.55
$K_{01\ absorption}$ (h^{-1})		0.186		0.76
$K_{10\ elimination}$ (h^{-1})	0.13	0.188	0.093	0.2
AUC_{0-24} (μg·h/mL)			126.74	5.53
$AUC_{0-\infty}$ (μg·h/mL)	85.8	1.69	149.94	5.60

* Data of SFL-ITZ were adapted from [28] for comparison purposes.
[a] Based on non-compartmental analysis of the lung tissue concentrations versus time.
[b] Calculated based on one-compartmental analysis of the serum concentrations versus time for extravascular administration.

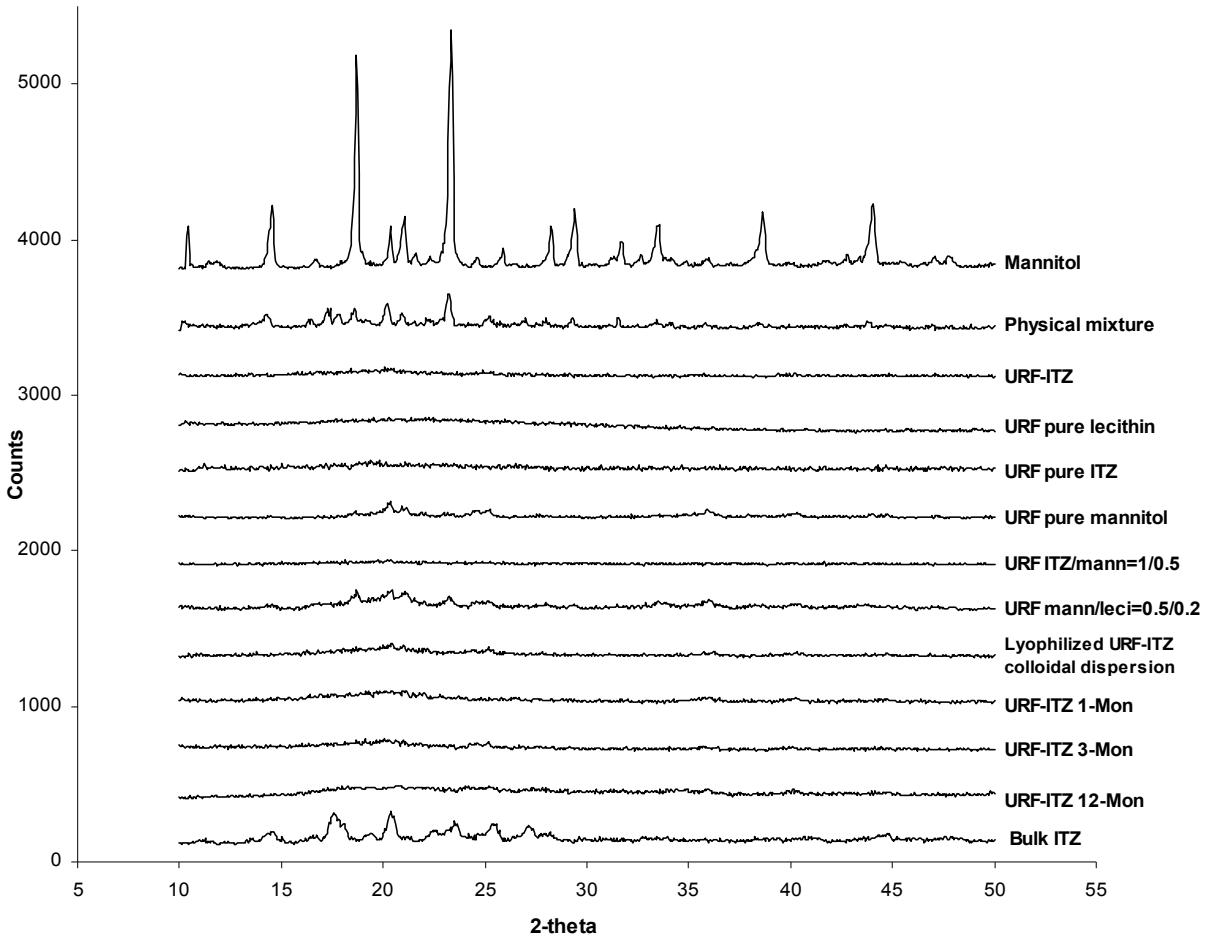

Figure 2.1. X-ray powder diffraction patterns (from the top to bottom): micronized bulk mannitol, Physical Mixture (physical mixture of ITZ:mannitol:Lecithin = 1:0.5:0.2), URF-ITZ (URF processed ITZ:mannitol:Lecithin = 1:0.5:0.2), URF processed lecithin, ITZ, mannitol, ITZ:mannitol = 1:0.5 (ratio in weight), mannitol:lecithin = 0.5 :0.2 (ratio in weight), respectively, re-lyophilized powder from a fast frozen colloidal dispersion of the URF-ITZ (20 mg ITZ/mL) after sitting at room temperature for 15 min, URF-ITZ powders after stored in desiccators under vacuum at room temperature for 1, 3 and 12 months, respectively, micronized bulk ITZ.

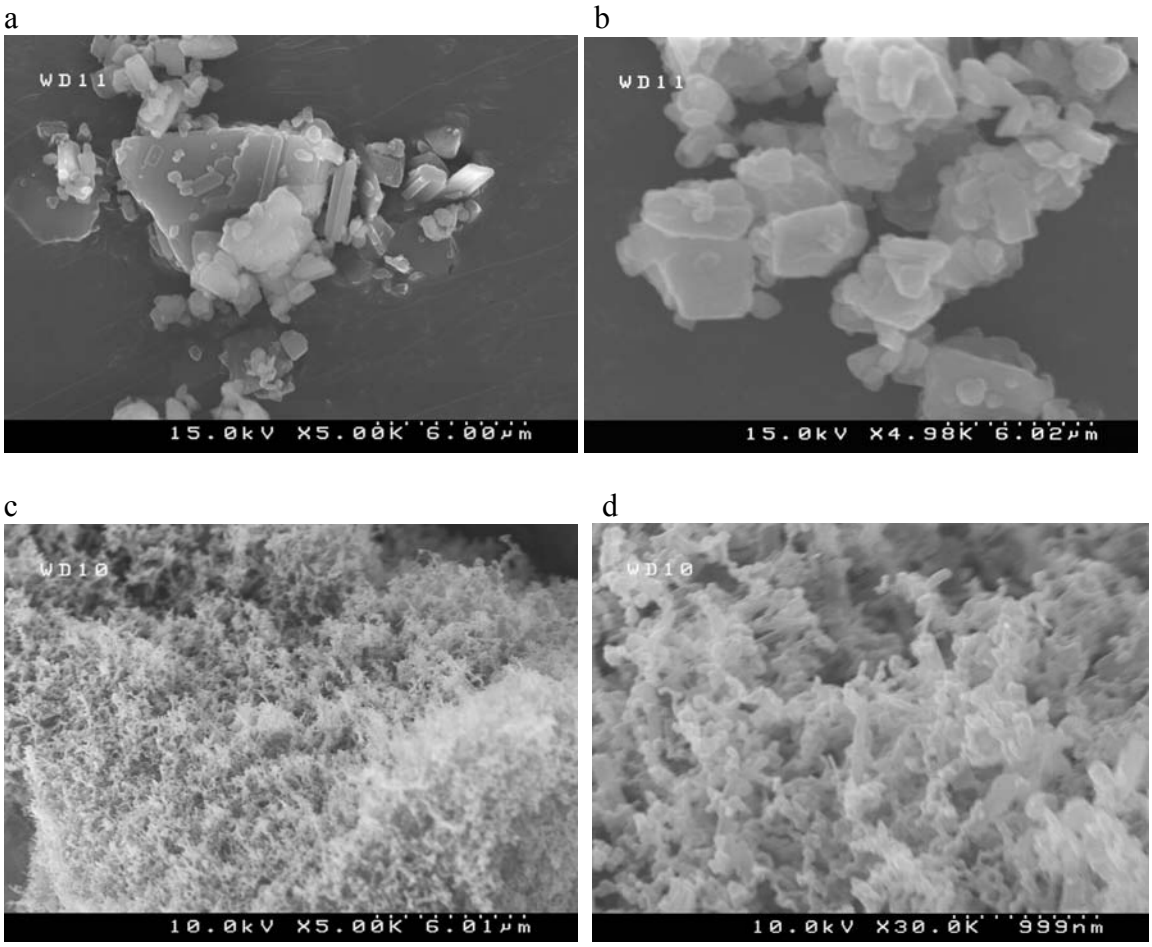

Figure 2.2. SEM images of (a) Bulk ITZ at a magnification of 5k (b) Physical Mixture of ITZ: mannitol: Lecithin = 1: 0.5: 0.2 at a magnification of 5k (c) URF-ITZ (URF processed ITZ: mannitol: Lecithin = 1: 0.5: 0.2) at a magnification of 5k (d) URF-ITZ at a magnification of 30k.

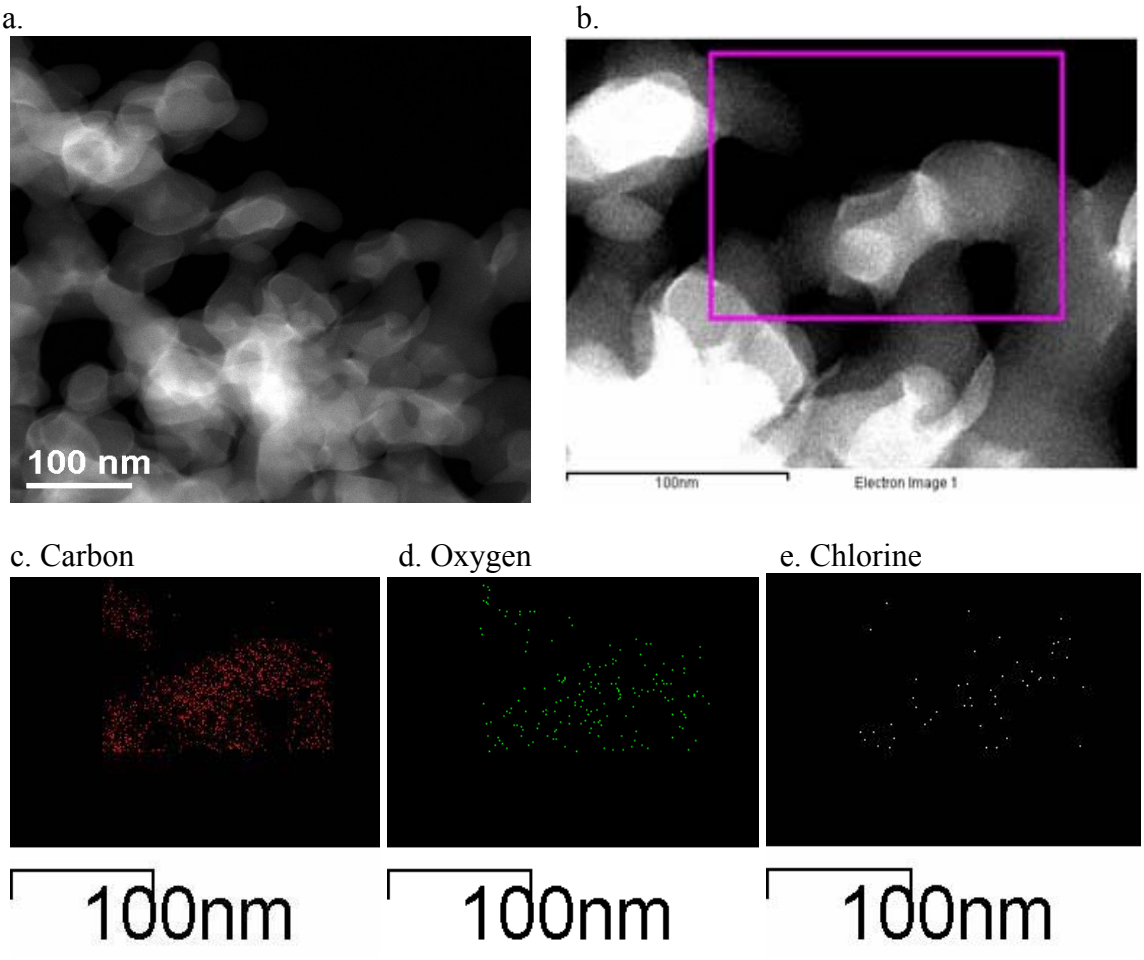

Figure 2.3. (a) STEM image of nanoparticles of URF-ITZ (URF processed ITZ:mannitol:Lecithin = 1:0.5:0.2). (b) STEM image of nanoparticles of URF-ITZ at a higher magnification for elemental analysis by area scan using energy dispersive spectroscopy. The particles within the pink frame were scanned for elemental distribution. (c) Carbon atoms distribution in the scanned nanoparticles (d) Oxygen atoms distribution in the scanned nanoparticles (e) Chlorine atoms distribution in the scanned nanoparticles.

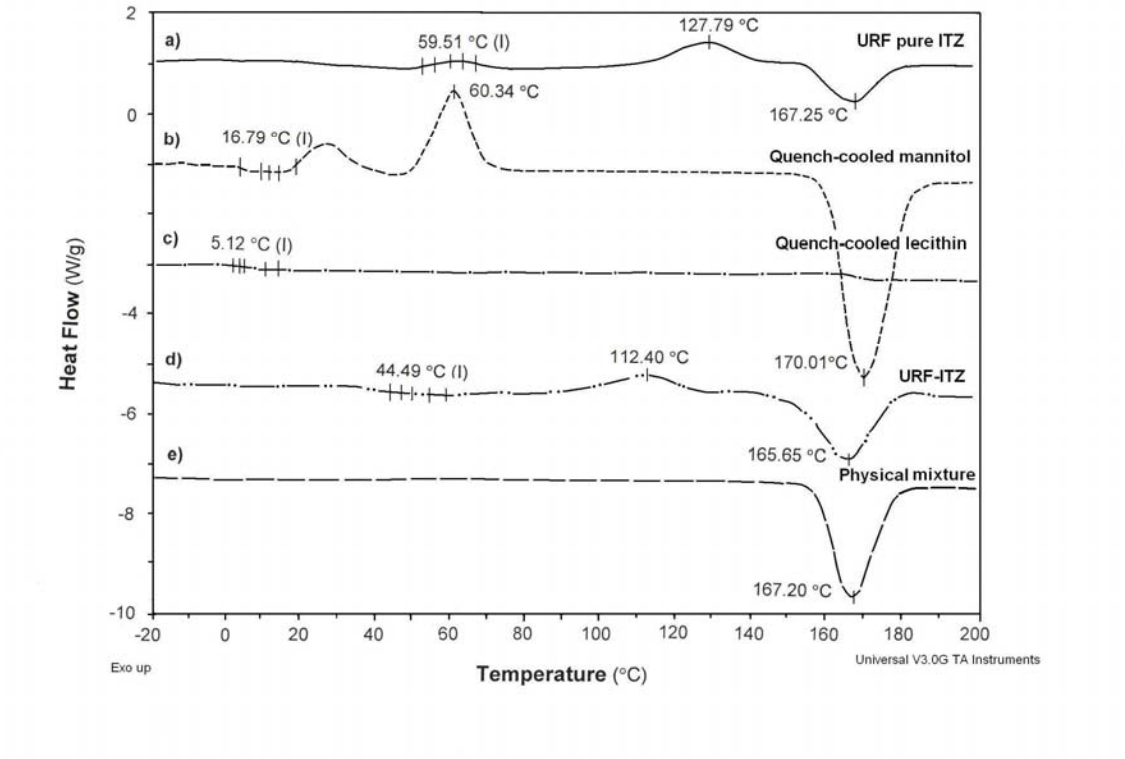

Figure 2.4. DSC profiles of (a). URF processed pure ITZ, (b). Quench-cooled mannitol, (c). Quench-cooled lecithin, (d). URF-ITZ (ITZ:mannitol:lecithin = 1:0.5:0.2 ratio in weight), (e). Physical mixture of ITZ:mannitol:lecithin = 1:0.5:0.2 ratio in weight.

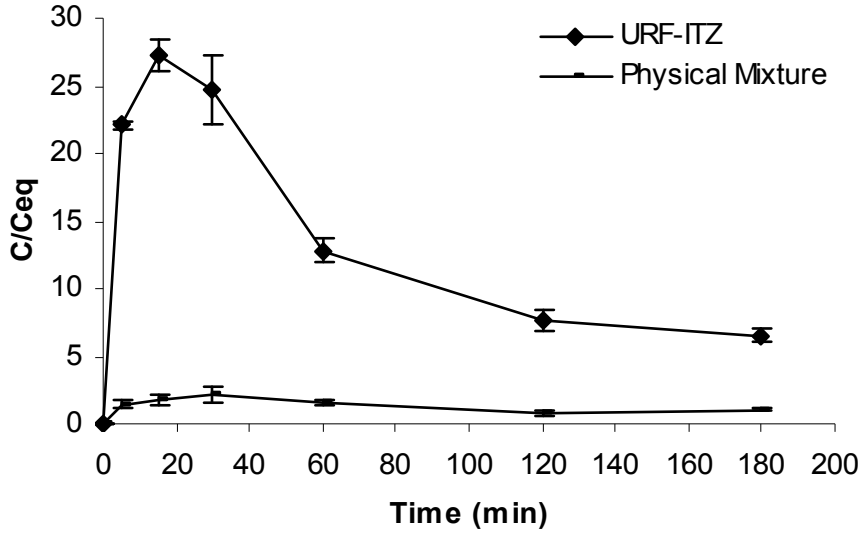

Figure 2.5. Dissolution profiles of URF-ITZ (URF processed ITZ: mannitol: Lecithin = 1: 0.5: 0.2) and Physical Mixture (ITZ: mannitol: Lecithin = 1: 0.5: 0.2) in simulated lung fluid (pH=7.4) at supersaturation conditions (e.g. 100-times equilibrium solubility of crystalline ITZ was added) using 100-mL vessels and small paddle apparatus at 100 rpm and 37 ℃.

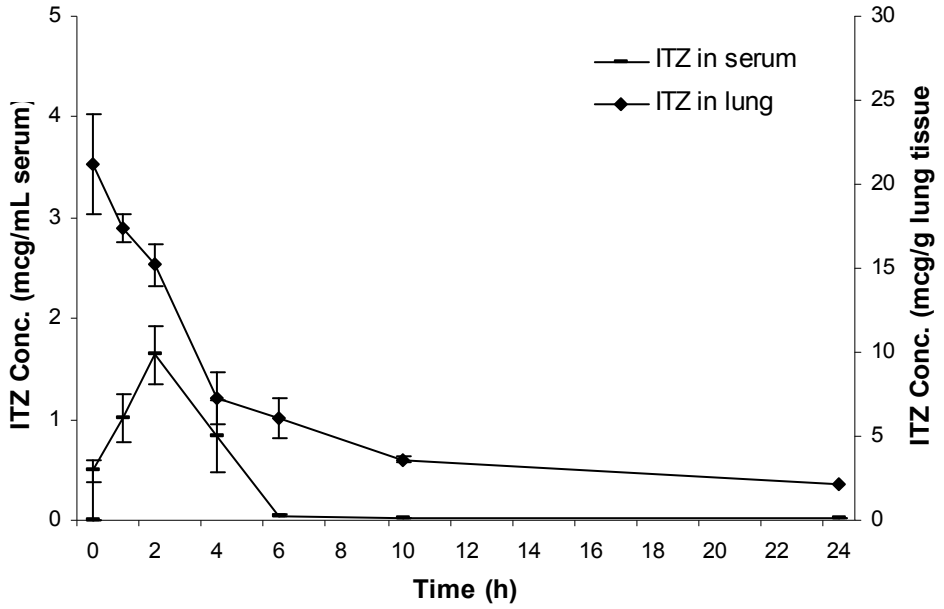

Figure 2.6. Serum concentration and lung deposition of ITZ in male outbred ICR mice after inhalation of nebulized URF-ITZ (URF processed ITZ: mannitol: Lecithin = 1: 0.5: 0.2, ratio by weight) colloidal dispersion by single dose administration (an equivalent dose exposure of 100 mg/kg by aerosolization over a 10 minute period). Data is presented as Mean±SD.

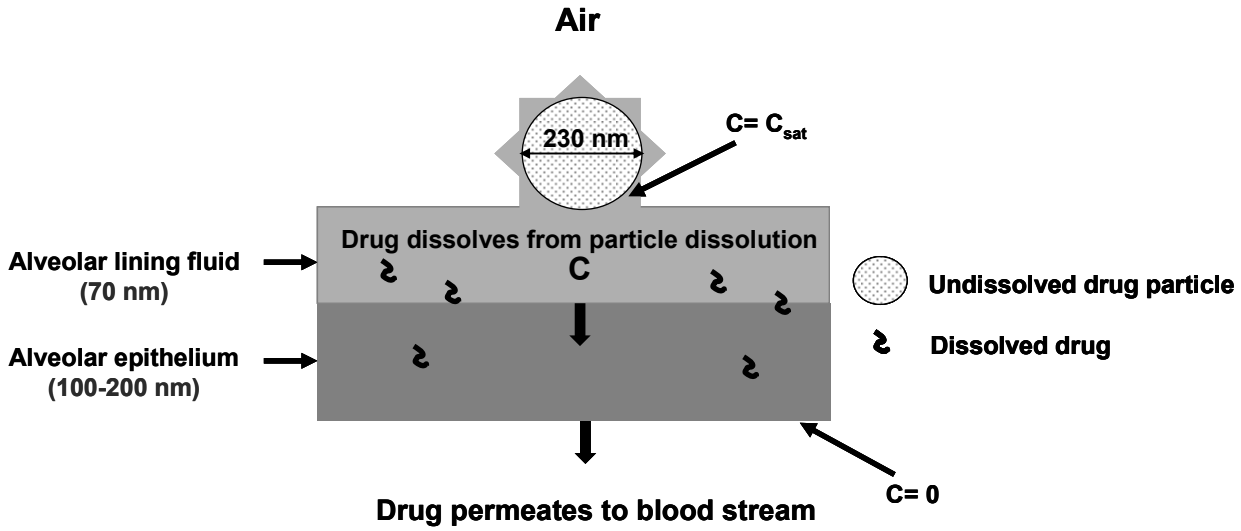

Figure 2.7. Schematic of material balance used in dissolution/permeation model. The concentration of dissolved drug in the alveolar fluid of a single alveolus, C, is given by the inlet flow from particle dissolution and the depletion by an outlet flow from drug permeation through the epithelium

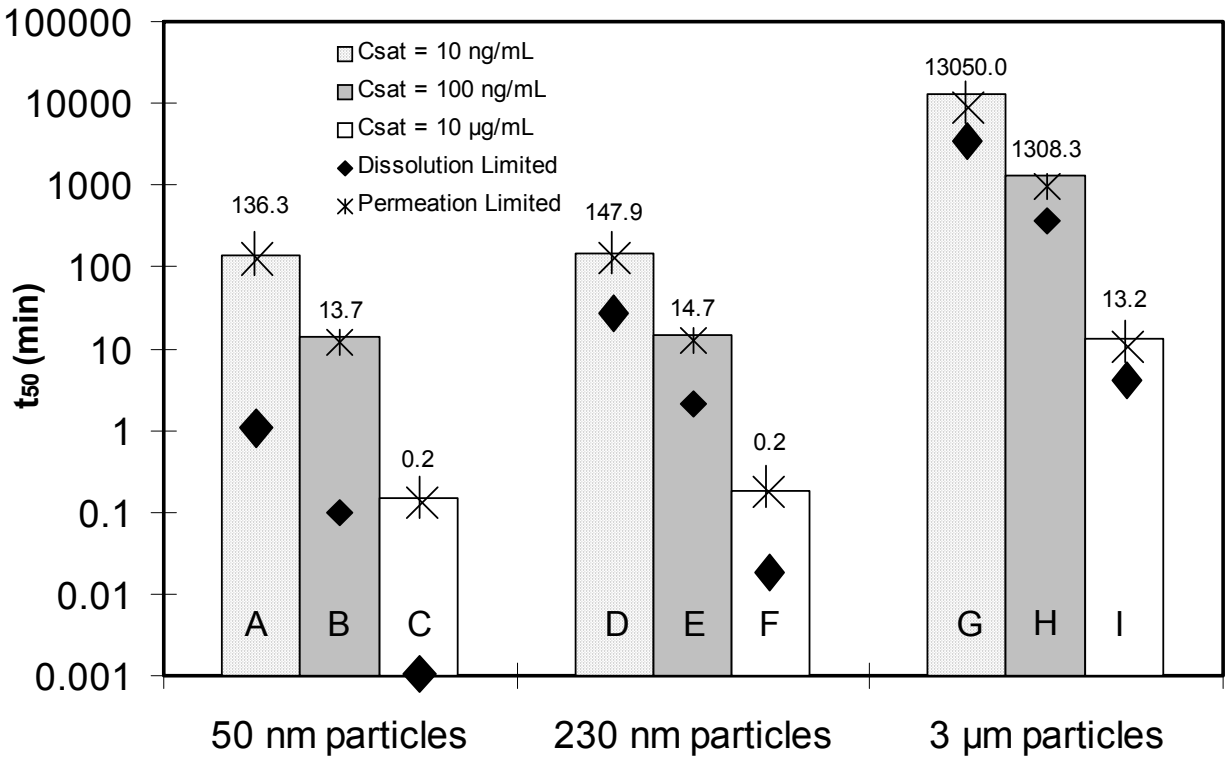

Figure 2.8. Predicted absorption half lives (time for 50% of drug to dissolve and permeate through lung epithelium) for various particle sizes and solubilities. The values are also shown for purely dissolution limited absorption (diamonds, infinite permeability) and purely permeation limited absorption (asterisks, $C = C_{sat}$).

Chapter 3: Comparison of the Bioavailability of Amorphous versus Crystalline Itraconazole Nanoparticles via Pulmonary Administration in Rats

3.1 ABSTRACT

The effect of supersaturation on bioavailability of inhaled nebulized aerosols is compared for amorphous versus crystalline nanoparticulate dispersions. The nanocrystalline formulations of itraconazole (ITZ) were made using wet milling (*i.e.* Wet-milled ITZ), whereas nano-structured aggregates (ITZ:mannitol:lecithin =1:0.5:0.2, weight ratio) were made using an ultra-rapid freezing process (*i.e.* URF-ITZ). Dissolution tests revealed the extent of supersaturation was 4.7-times higher for URF-ITZ versus Wet-milled ITZ, though their dissolution rates were similar. The aerodynamic performances of both aqueous colloidal dispersions were comparable and suitable for deep lung delivery. Single-dose 24-hr pharmacokinetic studies were conducted in Sprague-Dawley rats following inhalation of the nebulized colloidal dispersions (equivalent to 20 mg ITZ/mL dispersion in 5 mL) using a nose-only dosing apparatus. Lung depositions following inhalation were similar for both compositions. In systemic circulation, Wet-milled ITZ and URF-ITZ achieved C_{max} of 50.4 and 177.5 ng/mL at 2.7 and 4 hr, and AUC_{0-24} of 662 and 2543 ng·hr/mL, respectively, based on one-compartmental analysis. Pulmonary delivery of the nanoparticulate amorphous ITZ composition resulted in significantly higher systemic bioavailability than for the nanocrystalline ITZ composition, as a result of the higher supersaturation that increased the permeation of ITZ.

3.2 INTRODUCTION

Modern drug discovery processes, which routinely use high throughput screening techniques, appear to result in a higher prevalence of lead compounds with increased molecular weight and lipophilicity [1, 2]. Such drug molecules pose challenges to formulate therapeutically effective products for clinical use, since they often have poor bioavailability issues due to their poor dissolution or poor permeability to achieve sufficient and consistent systemic exposure. Consequently this results in sub-optimal efficacy in patients, particularly when delivered via the oral administration [3, 4].

To address the issues of low aqueous solubility, solubilization and micronization have commonly been used to increase dissolution rate and thereby oral bioavailability of such drugs. Attempts to solubilize and stabilize these drugs using salt formation [5], co-solvents [6], micellar solutions [7], or inclusion complexes with cyclodextrins [8] have been of limited success. The increased amount of excipients required to formulate the poorly water-soluble drugs may potentially increase side effects, resulting in low patient compliance. Alternatively, invasive dosage forms such as parenteral formulations have to be developed to address the challenges being presented. However, with even less pharmaceutically acceptable excipient options, increased solubilization of drug is practically limited [9].

For the means of micronization, although particle size reduction of the poorly water-soluble drugs increases their dissolution rate by increasing drug surface area, it does not increase equilibrium solubility. Often for drugs with very low aqueous solubility, the achieved increase in dissolution rate is limited and insufficient to provide significant enhancement of bioavailability [3].

However, drug particles in the 100 nm range dissolve more quickly and to a greater extent (*i.e.*, higher equilibrium solubility) than micronized drug particles, as described by the Noyes-Whitney and Ostwald-Freundlich equations [10]. Both particle dissolution kinetics and solubility are size dependent. Thus, the dissolution of drug nanoparticles *in vivo* is usually accompanied by an increase in bioavailability [11, 12]. On the other hand, the potential for increased Van der Waals interactions and electrostatic attraction between ultrafine particles can reduce the effective surface area for dissolution and therefore counteract improvements in bioavailability [13]. Colloidal dispersions of drug nanocrystals with a typical mean particle size between 200 and 500 nm and stabilized by a suitable stabilizer (*i.e.* nanosuspension) [4], have therefore been developed as an alternative approach.

The effectiveness of nanosuspensions of poorly water-soluble drugs in enhancing bioavailability has been proved in animal models and clinical trials with various administration routes, including oral [14, 15], pulmonary [16-18], ocular [19, 20] and parenteral delivery due to their particle size sufficiently small to be injected intravenously [21-23]. Among these, of particular interest is inhalation delivery, because of the following advantages of this noninvasive delivery route: (1) potential for high systemic absorption with an enormous absorptive surface area of approximately 100 m^2, very thin diffusion path to the blood stream and rich vasculature that facilitate rapid delivery of large drug doses; (2) targeted lung local action with reduced systemic side effects relative to other routes of administration, and (3) relatively low metabolic activity and avoidance of hepatic first-pass metabolism [24, 25].

Several studies predicted, from thermodynamics, the potential impact of polymorphs on bioavailability based on *in vitro* dissolution profiles and/or thermal analysis for oral delivery [26-28]. The amorphous form of a drug has a higher thermodynamic chemical potential than its crystalline counterpart [29]. The higher thermodynamic activity of the drug can produce supersaturated solutions [28, 30], thereby providing an opportunity to enhance absorption and bioavailability. In most experimental studies, supersaturation values of micron sized particles are less than 5-times C_{eq}, despite predictions from calorimetric measurements of the heat capacity (used to determine the free energy) that they can be much larger [26, 31]. Significantly higher supersaturation values approaching 100 were achieved for amorphous nanoparticles relative to microparticles, as the microparticles crystallize in the solid state before they dissolve and produce high supersaturation [32]. The experimental supersaturation values approached the large values calculated from the heat capacity glassy solid measured by DSC [28], unlike previous studies with microparticles where supersaturation values are typically below 5.

Amorphous nanostructured formulations of poorly water-soluble drugs for pulmonary delivery have also been developed to enhance therapeutic effectiveness [33, 34]. Vaughn et al. reported that inhaled aerosols in mice of a nebulized ITZ amorphous nanoparticulate composition (ITZ: polysorbate 80: poloxamer 407 = 1:0.75:0.75 by weight ratio, prepared by Spray Freezing into Liquid technology; namely SFL-ITZ) for 20 min, achieved a lung tissue C_{max} of 13.4 μg/g wet lung weight and an AUC_{inf} of 99.7 μg·hr/mL, and a serum C_{max} of 0.12 μg/mL [35]. Inhalation of another ITZ nanostructured composition (ITZ: poloxamer 407: polysorbate 80 = 1: 0.16: 0.13 by weight ratio, prepared by Evaporative Precipitation into Aqueous Solution technology;

namely EPAS-ITZ) which had a crystalline morphology, in the same mouse model produced a high lung C_{max} of 16.8 μg/g wet lung weight and an AUC_{inf} of 85.8 μg·hr/mL, but no systemic ITZ level was reported [36]. Despite the similar lung depositions of inhaled ITZ, in a subsequent prophylaxis study using a mouse model of invasive pulmonary aspergillosis, the nebulized aerosols of SFL-ITZ led to higher survival than for EPAS-ITZ for both short (8 days) and long-term survival (20 days) [37]. This improvement in survival may have resulted from a higher supersaturation of ITZ in the lung fluid for the amorphous SFL-ITZ, compared to crystalline EPAS-ITZ formulation.

To our knowledge, so far no study has assessed the effects of amorphous versus crystalline nanoparticulate formulations of a poorly water-soluble drug on *in vivo* bioavailability following lung delivery. In the present study, we evaluate the impact of the *in vitro* solubility advantage of amorphous versus crystalline nanoparticulate formulations of poorly water-soluble drug on bioavailability following pulmonary administration. We hypothesize that the supersaturation produced by inhaled amorphous nanoparticles of a poorly water-soluble drug will produce a higher systemic absorption and thereby enhanced bioavailability, relative to the nanocrystalline counterpart. ITZ was chosen as a model poorly water-soluble drug, because of its extremely high lipophilicity, *i.e.* an estimated aqueous solubility of about 1 ng/mL at neutral pH and a calculated octanol/water partition coefficient (Clog P) value of 6.2 [38]. A nano-sized crystalline ITZ composition was made by wet ball milling process (*i.e.* Wet-milled ITZ). The amorphous nano-structured aggregates of ITZ composition (ITZ: mannitol: lecithin =1: 0.5: 0.2 by weight ratio) with a large, wettable surface made by ultra-rapid freezing process (*i.e.* URF-ITZ) was reported previously [34]. We compare both the physiochemical properties *in vitro* and the bioavailability after inhalation in rats. Given

that pulmonary delivery has become an increasingly attractive route of application for poorly water-soluble drugs, the ability to provide greater insight into formulation design for improved bioavailability will be of widespread interest.

3.3 MATERIALS AND METHODS

3.3.1 Materials

The following materials were purchased: ITZ, micronized B.P. grade (Hawkins Chemical, Minneapolis, MN); mannitol and lecithin (Spectrum Chemicals, Gardena, CA); 1,4-dioxane and acetonitrile (Fisher Scientific, Fair Lawn, NJ); diethanolamine (VWR International, West Chester, PA). All organic solvents used were HPLC grade. Other reagents used were at least of ACS grade.

3.3.2 Preparation of Crystalline ITZ Nanoparticulates and Amorphous Nanostructured Aggregate of ITZ

The crystalline ITZ nanoparticulates were prepared by wet ball milling in a ceramic jar with Zirconia grinding media (1/2" Radius end cylinder) (U.S. Stoneware, East Palestine, OH). Three grams of the commercially available ITZ powder (mean particle size of 5 μm in diameter, 100% < 17.7 μm) was added 15 mL of purified water and milled at 100 rpm 20 °C under nitrogen gas for 10 days. Thus obtained slurry was combined with several successive washings of the ceramic jar and milling media using purified water to make a dispersion of the milled ITZ; which was then quickly frozen by dripping into liquid nitrogen and lyophilized to obtain dry powder by using a VirTis Advantage bench top tray lyophilizer (The VirTis Company, Inc., Gardiner, NY, USA). Thus obtained Wet-milled ITZ dry powder was stored in a desiccator under vacuum (~15% relative humidity) at room temperature.

Amorphous nanostructured aggregate URF-ITZ powder was prepared using the ultra-rapid freezing (URF) technology, as described previously [34]. In brief, lecithin was dissolved in a mixture of 1, 4-dioxane and purified water (65/35, v/v) co-solvent system using a magnetic stirrer. Mannitol and ITZ were subsequently dissolved in the mixture, in a weight ratio of ITZ:mannitol:lecithin = 1:0.5:0.2. The solution was rapidly frozen after applied to the URF apparatus that pre-cooled to about −70 °C [39]. The frozen solids were collected, lyophilized and stored the same as described above.

3.3.3 Scanning Electron Microscopy (SEM)

SEM was used to evaluate the morphology of the samples. The samples were mounted onto an aluminum stage using conductive carbon tape. Samples were coated using a model K575 sputter coater (Emitech Products, Inc., Houston, TX) with gold/palladium for 20 sec in a high vacuum evaporator. SEM was performed using a Hitachi S-4500 field emission scanning electron microscope (Hitachi High-Technologies Corp., Tokyo, Japan) operating at an accelerating voltage of 10-15 kV. Images were captured with Quartz PCI software (Quartz Imaging Corporation, Vancouver, BC, Canada).

3.3.4 Powder X-Ray Diffraction (XRD)

The crystallinity of the dried powders of Wet-milled ITZ and URF-ITZ were examined by wide angle XRD. A Philips 1710 X-ray diffractometer with a copper target (CuKa1,λ = 1.54056 Å) and nickel filter (Philips Electronic Instruments Inc., Mahwah, NJ) was used to obtain the XRD patterns. Dried powder was pressed onto a glass slide to

from a level surface. Samples were analyzed in the 2-theta range from 10 to 50° using a step size of 0.05 2-theta degree with a dwell time of 2 sec.

3.3.5 Modulated Temperature Differential Scanning Calorimetry (MTDSC)

Thermal properties of the powder samples were investigated using a TA Instruments Model 2920 DSC (New Castle, DE), equipped with a refrigerated cooling system. Dry nitrogen gas was used as the purge gas through the DSC cell at a flow rate of 40 mL/min. Samples were weighed to 10-15 mg in aluminum crimped pans (Kit 0219-0041, Perkin-Elmer Instruments, Norwalk, CT). The mass of the empty sample pan was matched with that of the empty reference pan within ±0.2 mg. Samples were heated at a ramp rate of 10 ℃/min from 0 to 200 ℃ with a modulation temperature amplitude of 1 ℃/60 sec. Data was analyzed using TA Universal Analysis 2000 software (TA Instruments, New Castle, DE).

3.3.6 Particle Size Analysis

Particle size distribution, based on volume fraction, of the colloidal dispersions of Wet-milled ITZ and URF-ITZ was measured by static light scattering with a Malvern Mastersizer-S (Malvern Instruments, Ltd., Worcestershire, UK). The colloidal dispersion of URF-ITZ (equivalent to 20 mg ITZ/mL) was prepared by dispersing an aliquot of URF-ITZ powder (~ 170 mg) in 5 mL purified water by sonication on an ice bath. The colloidal dispersion of Wet-milled ITZ was prepared by dispersing an aliquot of Wet-milled ITZ powder (~ 100 mg) in 5 mL aqueous solution containing 1% mannitol and 0.4% lecithin to make the compositions same as the URF-ITZ dispersion. To measure the particle size distribution, the respective dispersion was then diluted with about 500 mL of

purified water to produce light obscuration in the range of 10–15%. Values reported are the average of at least three measurements.

3.3.7 Brunauer-Emmett-Teller (BET) Specific Surface Area Analysis

Specific surface area was measured using a Nova 2000 version 6.11 instrument (Quantachrome Instruments, Boynton Beach, FL) with nitrogen as the adsorbate gas. An aliquot of powder was added to a 12-mm Quantachrome bulb sample cell and degassed for a minimum of 8 hr prior to analysis. Six points were taken over a range of relative pressures from 0.05 to 0.35. The data was then analyzed with the BET equation using NOVA Enhanced Data Reduction Software (version 2.13).

3.3.8 Dissolution Testing Under Supersaturated Conditions

Dissolution testing at supersaturated conditions was conducted in a USP 25 dissolution apparatus model Vankel 7000 Dissolution Tester (Vankel Technology Group, Cary, NC) using 100 mL glass dissolution vessels and stirred with small paddles at 100 rpm. Simulated lung fluid containing 0.02% dipalmitoylphosphatidylcholine [40, 41] was used as the dissolution medium and pre-heated to 37 ℃. Aliquots of the URF-ITZ and Wet-milled ITZ colloidal dispersions (equivalent of 80 μg ITZ, equal to 100-times of the equilibrium solubility (C_{eq}) of crystalline ITZ) were added to the dissolution vessels (n = 6), respectively, within one second immediately after preparation. Aliquots of 2 mL of the dissolution media were taken at 5, 15, 30 min, 1, 2, 3, 6, 12 and 24 hr. The samples were immediately filtered through a 0.2 μm GHP Acrodisc filter (Pall Corporation, East Hills, NY), and diluted with acetonitrile for content analysis. The ITZ content was quantified using a Shimadzu LC-10A high performance liquid chromatography (HPLC)

system (Shimadzu Corporation, Columbia, MD) equipped with an Alltech Inertsil™ ODS-2 5 μm, 150 mm × 4.6 mm, C-18 column (Alltech Associates, Inc., Deerfield, IL). The mobile phase was acetonitrile:water:diethanolamine (70:30:0.05) and it eluted the ITZ peak at approximately 5.5 min at 25 ℃ with a flow rate of 1 mL/min. The ITZ absorbance was measured at a wavelength λ_{max} of 263 nm. The supersaturation levels are reported as the drug concentration divided by the crystalline equilibrium solubility. Supersaturation was plotted versus time and area-under-the-supersaturation-curve (AUSC) was calculated by the linear trapezoidal rule.

3.3.9 *In Vitro* Aerosol Performance

An aliquot (5 mL) of the colloidal dispersions of the Wet-milled ITZ and URF-ITZ (equivalent to 20 mg/mL ITZ) were nebulized using an Aeroneb® Professional micropump vibrating mesh nebulizer (Nektar Inc., Mountain View, CA) for about 10 min. The *in vitro* deposition characteristics of the colloidal dispersions of Wet-milled ITZ and URF-ITZ for nebulization, was investigated using an eight-stage Andersen cascade impactor (Thermo-Electron Corp., Symrna, GA). The cascade impactor was assembled and operated in accordance with USP General Chapter 601 to assess the drug delivered. The flow rate of the nebulized aerosols was maintained by a vacuum pump (MFG Corp., Benton Harbor, MI) that was calibrated by a TSI mass flowmeter (Model 4000, TSI Inc., St. Paul, MN) to an air flow rate of 28.3 L/min. After deposition onto the stages of the impactor, the mass deposited on each of the impactor pieces was collected and the total mass of drug was quantified by HPLC. The aerosolization behavior was described in terms of total emitted dose (TED), mass median aerodynamic diameter (MMAD), geometric standard deviation (GSD), and percentage fine particle fraction (FPF; defined as the percentage of droplets with an aerodynamic diameter less than 4.7 μm). The

MMAD and GSD were obtained by plotting the cumulative mass found on the stages of the impactor as a function of the logarithm of the impactor stage cut-off diameter.

3.3.10 *In Vivo* Pulmonary Dosing of Rats

With approval and in accordance with the Institutional Animal Care and Use Committee (IACUC) guidelines at The University of Texas at Austin, *in vivo* studies were conducted using jugular vein pre-catheterized CD® IGS Sprague-Dawley rats (Charles River Laboratories, Inc., Wilmington, MA), weighing 275 to 325 grams. Throughout the study the rats were housed individually, subjected to 12 h -12 h light and darkness cycles, with access to food and water *ad libitum*. The catheters were flushed daily with heparinized normal saline. After acclimatization for 3 days, eight rats in each formulation group were dosed by inhalation of the nebulized colloidal dispersions of the Wet-milled ITZ or URF-ITZ (equivalent to 20 mg/mL ITZ), respectively, for 10 min in a nose-only dosing apparatus, as shown in Figure 3.1. An Aeroneb® Professional micropump nebulizer was situated at the inlet of the dosing tube, and the nebulized drug aerosols went through the dosing tube with an air flow rate of 1 L/min. Following exposure to the aerosol cloud, serial blood samples (approximately 0.3 mL each) were withdrawn through the jugular vein catheter at 0, 0.5, 1, 1.5, 2, 2.5, 3, 4, 6, 8, 12 and 24 hr post dosing and placed into a pre-heparinized microcentrifuge tube. Equal volumes of saline were replaced after each sampling. Two rats in each dosing group were sacrificed immediately upon finishing inhalation to harvest the lungs for determining the lung deposition of the inhaled drug. The lungs of the other rats were harvested at 24 hr upon completing blood sampling.

3.3.11 Plasma and Lung Analysis

Plasma was separated by centrifugation at 3,000 g for 10 min in a 1.5 mL micro-centrifuge tube using a Microfuge® 18 centrifuge (Beckman Coulter, Fullerton, CA). The plasma and lung samples were stored at -80 ℃ until HPLC analysis. The lung homogenates were prepared by adding 1 mL of normal saline to a portion of about 0.5 g of the harvested lung and using a homogenizer (Omni International, Marietta, GA) in an ice bath. Drug levels of the calibration standards, plasma, and homogenized lung samples were analyzed using the following procedures. Briefly, to an aliquot of 250 μL plasma or 250 μL of lung homogenate, 50 μL of 0.3 N barium hydroxide, and 50 μL of 0.4 N zinc sulfate heptahydrate solutions were added and vortex mixed for 30 sec to precipitate water-soluble proteins. Acetonitrile (1 mL), containing 500 ng/mL ketoconazole as an internal reference standard, was added to each sample followed by vortex mixing for 1.5 min. Each sample was then centrifuged at 3,000 g for 15 min. The supernatant was transferred to a clean 1.5 mL micro-centrifuge tube and dried under a stream of nitrogen gas. Each sample was reconstituted with 250 μL mobile phase (62% acetonitrile: 38% 0.05 M potassium phosphate monobasic buffer adjusted to pH 6.7 with NaOH) and analyzed by HPLC with an Alltech Inertsil™ ODS-2 5 μm, 250 × 4.6 mm, C-18 column protected by a C-18 guard column (5 μm, 7.5×4.6 mm) (Alltech Associates, Inc., Deerfield, IL). The injection volume was 100 μL, and the wavelength of absorption was 263 nm (λ_{max}). The limit of detection and quantitation for ITZ was 10 ng/mL and 30 ng/mL, respectively. The column was maintained at 37 ℃ during the analysis. The ITZ peak eluted at approximately 18 min, and the ketoconazole peak eluted at 9.3 min at a mobile phase flow rate of 1.0 mL/min.

3.3.12 Pharmacokinetic and Statistical Analysis

Plots of the log concentration of ITZ in plasma versus time exhibited a first-order absorption phase and a first-order elimination phase. A one-compartmental model for extravascular administration was therefore selected to assess the pharmacokinetic parameters of ITZ in rat plasma using WinNonlin Professional Version 2.1 (Pharsight Corporation, Mountain View, CA). All results are presented as mean±SD. Student's *t* tests were conducted using SigmaPlot version 7 (Systat Software, Inc., Chicago, IL), to determine the significance between the two dosing groups. For all tests, statistical significance was defined by $p < 0.05$.

3.4 RESULTS AND DISCUSSION

3.4.1 Physicochemical Properties of Wet-milled ITZ and URF-ITZ Formulations

3.4.1.1 Morphology and Particle Size Distribution

In the widely used wet milling process, comminution continually fractures drug crystals to reduce the particle size. The efficiency depends upon the nature of the grinding medium, the wetting of the solid, and the hardness of the drugs [42]. In the present study, because of the limited achievable rolling speed of the mill and hardness of ITZ, it took 10 days to reduce the particle size from an average size of 5 μm (100% < 17.7 μm) to nano-size level. The low solubility of ITZ may be advantageous in suppressing crystal growth during and after the milling process, and the hardness (*i.e.* the high melting point) may favor comminution. From the SEM image in Figure 3.2(a), Wet-milled ITZ was composed of fractured, irregular shaped particles with various sizes, ranging from about 150 to 600 nm in length. This is consistent with a report that NanoCrystals of

beclomethsaone dipropiante can be prepared by ball milling a 5% w/w drug suspension in 2.5% PVA over a day, resulting in a mean size of 267 nm [42].

In contrast with Wet-milled ITZ, URF-ITZ powder exhibited a highly porous structure with more regularly round-shaped particles as shown in Figure 3.2(b). The SEM displayed aggregated nanoparticles that formed a porous matrix. Both the milling and URF process dramatically reduced ITZ particles to nano-size range compared to bulk micron-sized ITZ particles shown in Figure 3.2(c).

With the particle size reduction, the specific surface area of the Wet-milled ITZ and URF-ITZ powder were found to be 38.6 and 31.7 m^2/g, respectively, which correspond to effective particle diameters of 150 and 190 nm (Table 3.1), assuming the particles were monodisperse and in spherical shape. The surface area of the bulk particles of 2.20 m^2/g was 15 times smaller.

However, the particle size distribution analysis using static laser light scattering showed D(v, 0.5) and D(v, 0.9) (diameter at which the cumulative sample volume was under 50% and 90%, respectively) values of 0.57 and 1.22 μm, respectively, for Wet-milled ITZ in colloidal dispersion (Table 3.1). This value is larger than that inferred from the measured surface area and SEM. Though the primary particle size of Wet-milled ITZ is ~190 nm from the surface area, the potential for increased Van der Waals interactions and electrostatic attraction between ultrafine particles can lead to aggregates ranging from loose flocculates to completely fused particles [13]. It is possible that some of the primary particles formed aggregates that were detected by static light scattering. Nevertheless, over 80% of the particles had a diameter of 1 micron or less.

In comparison, the URF-ITZ colloidal dispersion showed a narrow and smaller range with D(v, 0.5) and D(v, 0.9) of 0.25 and 0.59 μm, respectively. The stable and relatively uniform particle sizes resulted from the rapid nucleation during ice formation in URF and arrested growth as the solution freezes as discussed previously [34].

3.4.1.2 Crystalline State Evaluation

From the XRD diffraction profiles in Figure 3.3, ITZ exhibited intense characteristic crystalline peaks at 14.35, 17.46, 20.31, and 23.41 2-theta degrees, as seen in the micron-sized bulk ITZ (as purchased from the manufacturer). The XRD patterns of Wet-milled ITZ were found to be superimposable to the spectra of the micronized crystalline ITZ but with smaller peak heights. Reducing particle size can result in XRD peak broadening and halo formation, due to lost long-range crystalline order, without complete transition to an amorphous form [43]. It was also reported that XRD profiles of asulacrine nanocrystals with a mean particle size of 130 nm made by high pressure homogenization were not affected, with similar peak intensities as for micron-sized drug [22]. The XRD patterns of nanocrystal therefore seem material-specific and are related to the crystalline microstructure (crystal size, micro-strain and defects) of individual substances [43]. Therefore, the reduction in XRD peak intensity of Wet-milled ITZ is most likely due to particle size reduction.

For XRD of URF-ITZ powder in Figure 3.3, broad, diffuse haloes were present with an absence of the characteristic crystalline peaks, indicating a highly amorphous morphology [29]. The crystallinity was examined further with MTDSC as shown in Figure 3.4. The URF-ITZ powder exhibited a glass transition at around 50 ℃, one

exothermic recrystallization peak, and finally a single endothermic melting peak at 165.7 ℃. These results further confirmed the amorphous nature of URF-ITZ seen by XRD. In contrast, an exothermic peak was not present for Wet-milled ITZ, but only a single endothermic peak at 163.4 ℃, corresponding to the melting of ITZ. However, the melting peak of Wet-milled ITZ was not as sharp as for bulk ITZ and shifted slightly.

Milling processes may generate amorphous domains on the particle surface [44]. Despite the long time period for milling the ITZ, the crystallinity was high and the amorphous content undetectable according to the XRD and DSC results.

3.4.2 Supersaturation of Wet-milled ITZ and URF-ITZ Colloidal Dispersions in Simulated Lung Fluid

Dissolution of the ITZ colloidal dispersions in simulated lung fluid with pH 7.4 at 37 ℃ was conducted under supersaturated conditions (100-times C_{eq} equivalent ITZ were added) as shown in Figure 3.5. The C_{eq} in simulated lung fluid was measured to be 10 ng/mL after shaking at 37 ℃ for 3 days with excess crystalline ITZ present. For the URF-ITZ, C/C_{eq} reached 22-times at 5 min and a maximum value of about 26-times at 15 and 30 min. The supersaturation levels gradually decreased to about 7-times at 2 hr, and 5-times at 24 hr. In contrast, the supersaturation for Wet-milled ITZ only reached about 3-times the measured C/C_{eq} at 30 min, fell to about 2-times at 6 hr and then gradually declined to about unity, the equilibrium ratio at 24 hr. The cumulative extent of supersaturation was calculated as the AUSC, which was 1785 and 383 ng·hr/mL for URF-ITZ and Wet-milled ITZ, respectively. The much larger C_{sat} at various times and AUSC for the amorphous URF-ITZ have the potential to enhance bioavailability of this poorly water soluble drug.

Formation of a high energy amorphous or semicrystalline state can increase the predicted solubility, in many cases up to 100 times that of its crystalline form [26, 31]. The URF-ITZ formulation has been previously identified to be a solid solution of ITZ molecularly dispersed in mannitol and lecithin matrix [34]. Once the solid solution was exposed to the aqueous simulated lung fluid, the excipients dissolved very rapidly and the high surface area ITZ domains quickly supersaturated the dissolution medium. Because of the maximal achievable surface area for dissolution obtained by solid solution [45], the dissolution rate and C_{sat} value of URF-ITZ colloidal dispersion could be much higher than the nanocrystalline ITZ colloidal dispersion upon added to a dissolution medium. The elevated C_{sat} value of URF-ITZ might therefore be responsible for the 4.7-times higher amount of solvated ITZ molecules in the simulated lung fluid than Wet-milled ITZ.

The driving force for dissolution depends on the drug solubility within a given environment (*i.e.* lung fluid) C_{sat} and the concentration gradient between C_{sat} at the particle surface and C in the bulk solution phase. Particle dissolution is governed by several factors that can be described by the Noyes-Whitney equation:

$$dM/dt = AD(C_{sat} - C)/h$$

where dM/dt is the fraction of mass dissolved per unit time, A is the surface area available for dissolution, D is the diffusion coefficient, and h is the thickness of the diffusion boundary layer. Nanoparticles often dissolve more quickly due to the extensive enhancement in surface area, the smaller h which is proportional to the particle diameter and the higher C_{sat} because of particle curvature according to the Kelvin equation [46-48]. The nano-sized URF-ITZ and Wet-milled ITZ both dissolved rapidly and reached a

maximum concentration within 30 min, as well as supersaturation relative to equilibrium solubility of the micronized ITZ. The *D* value was the same for both formulations, and the the available surface areas *A* were similar. Also the *h* values which are closely related to particle size [49] were similar. Thus the higher dissolution rate for the amorphous ITZ is due to the higher C_{sat} values.

3.4.3 *In Vitro* Aerosol Performance of Wet-milled ITZ and URF-ITZ Aqueous Colloidal Dispersions

Pulmonary drug delivery targeted to the alveoli is advantageous and critical for systemic absorption [50], as the distance from the air in the alveolar lumen to the capillary blood flow is less than 400 nm [51]. The efficacy of pulmonary delivery of drug to the deep lung is largely determined by the particle size distribution of aerosol droplets [52]. The inhaled aerosol should possess a narrow range of aerodynamic diameters between 1-5 micron to pass through the filter of the mouth and throat to be effectively delivered inside the lung [25]. The aerodynamic particle size of the nebulized colloidal dispersions of Wet-milled ITZ and URF-ITZ for inhalation, with an equivalent of 100 mg ITZ in 5 mL, is summarized in Table 3.2. The TED of Wet-milled ITZ and URF-ITZ were 51.73 and 56.40 mg out of 100 mg ITZ available for nebulization, respectively. Their corresponding FPF were 47.28 and 54.39% with the respective fine particle dose (defined as the amount of aerosol droplets entering the impactor less than 4.7 μm, TED × FPF, indication of the dose delivered to the deep lung) delivered at a rate of 2.45 and 3.07 mg/min. The MMAD of the atomized droplets of Wet-milled ITZ and URF-ITZ colloidal dispersions were 2.78 and 2.36 μm with GSD of 3.06 and 2.66, respectively, which are suitable for deep lung delivery.

In this study, the aerodynamic diameter is goverened by the easily controllable nebulization of the aqueous droplets, which contain much smaller dispersed particles of drug. It was reported that the Aeroneb® Professional micropump nebulizer produced an aqueous mist of fine droplets with sizes ranging between 1 and 4 μm [36]. Nanoparticles with a diameter of less than 1 μm are more easily incorporated in the respirable aerosolized droplets with MMAD of 1–5 μm [53, 54]. Furthermore, the viscosities of the colloidal dispersions are similar to those of the water. The low viscosity facilitates the formation of small and uniform droplets [55]. Since both URF-ITZ and Wet-milled ITZ colloidal dispersions contain submicron particles, the aerodynamic performance of the nebulized fine aerosol droplets is similar to that of pure water.

3.4.4 Pharmacokinetics of Inhaled Wet-milled ITZ and URF-ITZ in Rats

With the same compositions and comparable *in vitro* aerodynamic performance of the nebulized aerosols of Wet-milled ITZ and URF-ITZ colloidal dispersions, their *in vivo* performance was subsequently explored in a rat model. Rats were exposed nose-only to a single dose aerosols of the nebulized colloidal dispersions (equivalent to 100 mg of ITZ total), respectively, for about 10 min. Drug concentration profiles in lung tissue and blood following a single inhalation dose are presented in Figures 3.6 and 3.7. Upon completing inhalation of the nebulized compositions (0 hr post dosing), 12.28±0.60 and 11.01±4.26 μg/g wet lung weight of ITZ were found deposited in lungs from Wet-milled ITZ and URF-ITZ dosing groups, respectively. At 24 hr post dosing, these values were 562±443 and 455±237 ng/g wet lung weight, respectively.

Once deposited in the lungs, the nanoparticles underwent dissolution in the lung lining fluid to release free ITZ molecules for lung local action or were further absorbed

through lung alveolar epithelium to systemic circulation. The corresponding pharmacokinetic parameters in blood are summarized in Table 3.3. In plasma, based on a one compartmental analysis, the C_{max} for Wet-milled ITZ and URF-ITZ dosing group were 50.4 and 177.5 ng/mL at 2.7 and 4.0 hr after dosing, respectively. The AUC_{0-24} of Wet-milled ITZ and URF-ITZ were 662 and 2543 ng·hr/mL, respectively. In URF-ITZ dosing group, after reaching the C_{max}, a plateau of the high ITZ level was maintained from 2.5 to 6 hr, similar to a sustained release profile. At all the sampling time points, the ITZ levels in rats inhaled URF-ITZ were significantly higher than those inhaled Wet-milled ITZ.

Despite the comparable lung deposition levels of the inhaled aerosols of the two ITZ colloidal dispersions, the cumulative ITZ concentrations absorbed into blood from rats was about 3.8-times higher for the URF-ITZ versus Wet-milled ITZ. From Fick's first law, the systemic absorption rate of a drug from the lung epithelium is given by $P \times A \times C$, where P is membrane permeability, A is the available surface area over which the drug is spread, C is the drug concentration in the lung lining fluids. The drug concentration in blood is assumed to be insignificant compared to the lung concentration and the transfer from lung to blood is irreversible [56]. For the Wet-milled ITZ and URF-ITZ colloidal dispersions, many factors were fairly constant include the composition, aerodynamic performance, lung depositions, total drug dose, permeability and absorption area. The absorption has been shown to be permeation limited for both amorphous and crystalline ITZ nanoparticles of the sizes on the order of 200-600 nm with a combined dissolution/permeation material balance in the lung fluid [34]. Here the dissolution is essentially instantaneous relative to the permeation. In this case, the flux of ITZ into systemic circulation would be directly proportional to the dissolved concentration C_{sat}.

This prediction was observed in the current study. The 3.8-times larger AUC of URF-ITZ in the systemic circulation versus Wet-milled ITZ was on the same order as the 4.7-times larger supersaturation level (thermodynamic activity) measured in the *in vitro* dissolution test.

The biopharmaceutical consequences of solubility differences of polymorphs are directly related to the solubility difference [57]. It was reported that polymorphs of chloramphenicol palmitate with a measured solubility ratio of about 4.0 induced about 6-times difference in C_{max} in human after oral administration [58]; whereas no significant difference in pharmacokinetics was observed after a single oral dose of polymorphs of mefenamic acid with measured solubility ratio of about 1.3 [57]. Therefore, to achieve clinically meaningful biopharmaceutical consequences of solubility differences, the solubility ratios need to be about two fold higher [26]. Compared to the crystalline counterpart, the formation of significantly higher levels of supersaturation offered by amorphous formulations of drugs with poor/erratic bioavailability, enhances total drug absorption (AUC) and C_{max} while reducing t_{max} as observed for oral [59, 60], topical [61] and pulmonary [62] administrations. The use of amorphous form of poorly water-soluble drugs has widened the window of achievable pharmacokinetic performance enormously.

3.4.5 Lung Clearance of the Deposited Nanoparticles Containing ITZ

In addition to influencing aerosol deposition and dissolution in the lung lining fluid, particle size distribution and morphology also may influence the clearance mechanism [44, 63]. The lungs have very efficient clearance mechanisms for foreign particles. The MMAD of Wet-milled ITZ and URF-ITZ aerosols favor deposition in the deep lung, bypassing the mucociliary clearance in the airways. Compared to Wet-milled

ITZ, the deposited amorphous URF-ITZ nanoparticles dissolve more quickly upon exposure to the lung lining fluid. Furthermore the rapid dissolution may minimize crystallization of undissolved particles of URF-ITZ in the lung fluid, which would otherwise lower the supersaturation [64, 65]. The more rapid dissolution and resulting higher supersaturation with minimal time for crystallization of undissolved solid results in reduced clearance of URF-ITZ relative to Wet-milled ITZ particles by the lung defense system. These factors favor the observed significantly enhanced bioavailability of URF-ITZ.

For those deposited particles have not completely dissolved, they would mainly be cleared from the alveoli via endocytosis by epithelial and endothelial cells, and phagocytosis by macrophages [66, 67]. The efficiency of clearance of the inhaled particles is size-dependent. Alveolar macrophages preferentially uptake particles of approximately 1 to 3 μm in diameter [25, 68]. Phagocytosis of 1 μm particles has been observed as early as 15 min after nebulization [69]. Furthermore, 30–60% of 1–3 μm particles have been observed to be phagocytosed 2–4 h post intra-tracheal instillation, with complete pulmonary clearance of particles within 24 h [70]. After 24 hr post inhalation the ITZ levels in the lung were similar for the URF-ITZ and Wet-milled ITZ, even though the former was absorbed at a level of ~4 times higher. Thus the much larger amount of unabsorbed Wet-milled ITZ particles must have been cleared by the lung defense system. The aggregates of the Wet-milled ITZ of 590 nm in mean diameter measured by light scattering are more vulnerable to uptake by macrophage clearance than the smaller URF-ITZ particles, so that ITZ levels in lung at 24 hr post inhalation were both significantly reduced.

3.5 CONCLUSION

For an aqueous colloidal dispersion of amorphous nanoparticulate ITZ, rapid dissolution produced a supersaturation ~4.7-times larger than for a dispersion of crystalline nanoparticulates made by wet milling with the same composition and similar particle surface area. The aerodynamic diameters for both dispersions were suitable for deep lung delivery by nebulization, and similar to values produced for pure water. However, the increase in the systemic bioavailability for the amorphous versus crystalline dispersion of about 3.8 was approximately the same as the increase in supersaturation measured *in vitro* in the simulated lung fluid. The experimentally observed similarity in the values of bioavailability and supersaturation would be predicted for a permeability controlled model, where dissolution is very rapid, as suggested previously [34]. The high supersaturation, favored by rapid dissolution of amorphous nanoparticles, prior to particle clearance or crystallization favors the high permeability into the bloodstream. Pulmonary delivery of amorphous nanoparticle formulations of extremely poorly water-soluble drugs, especially for high-dose drugs (e.g. ITZ), is thus beneficial for both local and systemic therapy.

3.6 ACKNOWLEDGEMENTS

This material is supported in part by the STC Program of the National Science Foundation under Agreement No. CHE987664. We would like to thank Mr. Kevin O'Donnell for his assistance with animal study.

3.7 REFERENCES

1. C.A. Lipinski. Drug-like properties and the causes of poor solubility and poor permeability. Journal of Pharmacological and Toxicological Methods. 44:235-249 (2000).

2. C.A. Lipinski, F. Lombardo, B.W. Dominy, and P.J. Feeney. Experimental and computational approaches to estimate solubility and permeability in drug discovery and development settings. Adv Drug Deliver Rev. 23:3-25 (1997).

3. R.H. Muller, C. Jacobs, and O. Kayser. Nanosuspensions as particulate drug formulations in therapy Rationale for development and what we can expect for the future. Adv Drug Deliver Rev. 47:3-19 (2001).

4. V.B. Patravale, A.A. Date, and R.M. Kulkarni. Nanosuspensions: a promising drug delivery strategy. J Pharm Pharmacol. 56:827-840 (2004).

5. S. Agharkar, S. Lindenbaum, and T. Higuchi. Enhancement of Solubility of Drug Salts by Hydrophilic Counterions - Properties of Organic Salts of an antimalarial Drug. J Pharm Sci. 65:747-749 (1976).

6. K. Amin, R.M. Dannenfelser, J. Zielinski, and B. Wang. Lyophilization of polyethylene glycol mixtures. J Pharm Sci. 93:2244-2249 (2004).

7. V.P. Torchilin. Micellar nanocarriers: Pharmaceutical perspectives. Pharmaceut Res. 24:1-16 (2007).

8. R.A. Rajewskiand V.J. Stella. Pharmaceutical applications of cyclodextrins. 2. In vivo drug delivery. J Pharm Sci. 85:1142-1169 (1996).

9. R. Liu. Water-insoluble drug formulation, CO Interpharm Press, Englewood, 2000.

10. D.J.W. Grantand H.G. Brittian. Physical Characterisation of Pharmaceutical Solids, Marcel Dekker, New York, 1995.

11. R.J. Hintzand K.C. Johnson. The Effect of Particle-Size Distribution on Dissolution Rate and Oral Absorption. Int J Pharm. 51:9-17 (1989).

12. P. Borm, F.C. Klaessig, T.D. Landry, B. Moudgil, J. Pauluhn, K. Thomas, R. Trottier, and S. Wood. Research strategies for safety evaluation of nanomaterials, part V: role of dissolution in biological fate and effects of nanoscale particles. Toxicol Sci. 90:23-32 (2006).

13. N. Blagden, M. de Matas, P.T. Gavan, and P. York. Crystal engineering of active pharmaceutical ingredients to improve solubility and dissolution rates. Adv Drug Deliver Rev. 59:617-630 (2007).

14. G.G. Liversidgeand K.C. Cundy. Particle-Size Reduction for Improvement of Oral Bioavailability of Hydrophobic Drugs .1. Absolute Oral Bioavailability of Nanocrystalline Danazol in Beagle Dogs. Int J Pharm. 125:91-97 (1995).

15. R. Mauludin, R.H. Muller, and C.M. Keck. Development of an oral rutin nanocrystal formulation. Int J Pharm. 370:202-209 (2009).

16. P.C. Chiang, J.W. Alsup, Y.R. Lai, Y.D. Hu, B.R. Heyde, and D. Tung. Evaluation of Aerosol Delivery of Nanosuspension for Pre-clinical Pulmonary Drug Delivery. Nanoscale Research Letters. 4:254-261 (2009).

17. C. Jacobsand R.H. Muller. Production and characterization of a budesonide nanosuspension for pulmonary administration. Pharmaceut Res. 19:189-194 (2002).

18. W.K. Kraft, B. Steiger, D. Beussink, J.N. Quiring, N. Fitzgerald, H.E. Greenberg, and S.A. Waldman. The pharmacokinetics of nebulized nanocrystal budesonide suspension in healthy volunteers. Journal of Clinical Pharmacology. 44:67-72 (2004).

19. M.A. Kassem, A.A.A. Rahman, M.M. Ghorab, M.B. Ahmed, and R.M. Khalil. Nanosuspension as an ophthalmic delivery system for certain glucocorticoid drugs. Int J Pharm. 340:126-133 (2007).

20. R. Pignatello, C. Bucolo, P. Ferrara, A. Maltese, A. Puleo, and G. Puglisi. Eudragit RS100 (R) nanosuspensions for the ophthalmic controlled delivery of ibuprofen. European Journal of Pharmaceutical Sciences. 16:53-61 (2002).

21. K. Peters, S. Leitzke, J.E. Diederichs, K. Borner, H. Hahn, R.H. Muller, and S. Ehlers. Preparation of a clofazimine nanosuspension for intravenous use and evaluation of its therapeutic efficacy in murine Mycobacterium avium infection. Journal of Antimicrobial Chemotherapy. 45:77-83 (2000).

22. S. Ganta, J.W. Paxton, B.C. Baguley, and S. Garg. Formulation and pharmacokinetic evaluation of an asulacrine nanocrystalline suspension for intravenous delivery. Int J Pharm. 367:179-186 (2009).

23. J.E. Kipp. The role of solid nanoparticle technology in the parenteral delivery of poorly water-soluble drugs. Int J Pharm. 284:109-122 (2004).

24. A.L. Adjeand P.K. Gupta. Inhalation Delivery of Therapeutic Peptides and Proteins. In A.A.F. Mahmoud (ed.), Parasitic Lung Diseases, Marcel Rcel Dekker Inc., New York, 1997, pp. 89-125.

25. H.M. Courrier, N. Butz, and T.F. Vandamme. Pulmonary drug delivery systems: recent developments and prospects. Crit Rev Ther Drug Carrier Syst. 19:425-498 (2002).

26. B.C. Hancockand M. Parks. What is the true solubility advantage for amorphous pharmaceuticals? Pharmaceut Res. 17:397-404 (2000).

27. B.C. Hancockand G. Zograf. Characteristics and significance of the amorphous state in pharmaceutical systems. J Pharm Sci. 86:1-12 (1997).

28. M.E. Matteucci, M.A. Miller, R.O. Williams, and K.P. Johnston. Highly Supersaturated Solutions of Amorphous Drugs Approaching Predictions from Configurational Thermodynamic Properties. Journal of Physical Chemistry B. 112:16675-16681 (2008).

29. L.R. Hildenand K.R. Morris. Physics of amorphous solids. J Pharm Sci. 93:3-12 (2004).

30. G.V. Betageriand K.R. Makarla. Enhancement of dissolution of glyburide by solid dispersion and lyophilization techniques. Int J Pharm. 126:155-160 (1995).

31. P. Gupta, G. Chawla, and A.K. Bansal. Physical stability and solubility advantage from amorphous celecoxib: The role of thermodynamic quantities and molecular mobility. Molecular Pharmaceutics. 1:406-413 (2004).

32. M.E. Matteucci, B.K. Brettmann, T.L. Rogers, E.J. Elder, R.O. Williams, and K.P. Johnston. Design of potent amorphous drug nanoparticles for rapid generation of highly supersaturated media. Molecular Pharmaceutics. 4:782-793 (2007).

33. J.M. Tam, J.T. McConville, R.O. Williams, 3rd, and K.P. Johnston. Amorphous cyclosporin nanodispersions for enhanced pulmonary deposition and dissolution. Journal of pharmaceutical sciences:DOI 10.1002/jps.21367 (2008).

34. W. Yang, J. Tam, D.A. Miller, J. Zhou, J.T. McConville, K.P. Johnston, and R.O. Williams. High bioavailability from nebulized itraconazole nanoparticle dispersions with biocompatible stabilizers. Int J Pharm. 361:177-188 (2008).

35. J.M. Vaughn, J.T. McConville, D. Burgess, J.I. Peters, K.P. Johnston, R.L. Talbert, and R.O. Williams, 3rd. Single dose and multiple dose studies of itraconazole nanoparticles. Eur J Pharm Biopharm. 63:95-102 (2006).

36. J.T. McConville, K.A. Overhoff, P. Sinswat, J.M. Vaughn, B.L. Frei, D.S. Burgess, R.L. Talbert, J.I. Peters, K.P. Johnston, and R.O. Williams. Targeted

high lung concentrations of itraconazole using nebulized dispersions in a murine model. Pharmaceutical Research. 23:901-911 (2006).

37. B.J. Hoeben, D.S. Burgess, J.T. McConville, L.K. Najvar, R.L. Talbert, J.I. Peters, N.P. Wiederhold, B.L. Frei, J.R. Graybill, R. Bocanegra, K.A. Overhoff, P. Sinswat, K.P. Johnston, and R.O. Williams. In vivo efficacy of aerosolized nanostructured itraconazole formulations for prevention of invasive pulmonary aspergillosis. Antimicrob Agents Ch. 50:1552-1554 (2006).

38. J. Peeters, P. Neeskens, J.P. Tollenaere, P. Van Remoortere, and M.E. Brewster. Characterization of the Interaction of 2-hydroxypropyl-beta-cyclodextrin with itraconazole at pH 2, 4, and 7. J Pharm Sci. 91:1414-1422 (2002).

39. K.A. Overhoff, J.D. Engstrom, B. Chen, B.D. Scherzer, T.E. Milner, K.P. Johnston, and R.O. Williams, 3rd. Novel ultra-rapid freezing particle engineering process for enhancement of dissolution rates of poorly water-soluble drugs. Eur J Pharm Biopharm. 65:57-67 (2007).

40. R.O. Cook, R.K. Pannu, and I.W. Kellaway. Novel sustained release microspheres for pulmonary drug delivery. Journal of Controlled Release. 104:79-90 (2005).

41. N.M. Daviesand M.R. Feddah. A novel method for assessing dissolution of aerosol inhaler products. International journal of pharmaceutics. 255:175-187 (2003).

42. T.S. Wiedmann, L. DeCastro, and R.W. Wood. Nebulization of NanoCrystals(TM): Production of a respirable solid-in-liquid-in-air colloidal dispersion. Pharmaceut Res. 14:112-116 (1997).

43. Z. Deng, S. Xu, and S. Li. Understanding a relaxation behavior in a nanoparticle suspension for drug delivery applications. Int J Pharm. 351:236-243 (2008).

44. A.H.L. Chow, H.H.Y. Tong, P. Chattopadhyay, and B.Y. Shekunov. Particle engineering for pulmonary drug delivery. Pharmaceutical Research. 24:411-437 (2007).

45. C. Leunerand J. Dressman. Improving drug solubility for oral delivery using solid dispersions. European Journal of Pharmaceutics and Biopharmaceutics. 50:47-60 (2000).

46. P. Borm, F.C. Klaessig, T.D. Landry, B. Moudgil, J. Pauluhn, K. Thomas, R. Trottier, and S. Wood. Research strategies for safety evaluation of nanomaterials, part V: role of dissolution in biological fate and effects of nanoscale particles. Toxicological Sciences. 90:23-32 (2006).

47. M.T. Crisp, C.J. Tucker, T.L. Rogers, R.O. Williams, 3rd, and K.P. Johnston. Turbidimetric measurement and prediction of dissolution rates of poorly soluble drug nanocrystals. J Control Release. 117:351-359 (2007).

48. M.E. Matteucci, M.A. Hotze, K.P. Johnston, and R.O. Williams. Drug nanoparticles by antisolvent precipitation: Mixing energy versus surfactant stabilization. Langmuir. 22:8951-8959 (2006).

49. A.P. Tinke, K. Vanhoutte, R. De Maesschalck, S. Verheyen, and H. De Winter. A new approach in the prediction of the dissolution behavior of suspended particles by means of their particle size distribution. Journal of pharmaceutical and biomedical analysis. 39:900-907 (2005).

50. H.M. Courrier, N. Butz, and T.F. Vandamme. Pulmonary drug delivery systems: Recent developments and prospects. Critical Reviews in Therapeutic Drug Carrier Systems. 19:425-498 (2002).

51. R. Altiereand D. Thompson. hysiology and pharmacology of the airways. In A. Hickey (ed.), Inhalation aerosols—Physical and biological basis for therapy Marcel Dekker, Inc., New York, 1996, pp. 85–138.

52. T.B. Martonenand I.M. Katz. Deposition Patterns of Aerosolized Drugs within Human Lungs - Effects of Ventilatory Parameters. Pharmaceut Res. 10:871-878 (1993).

53. L.A. Dailey, T. Schmehl, T. Gessler, M. Wittmar, F. Grimminger, W. Seeger, and T. Kissel. Nebulization of biodegradable nanoparticles: impact of nebulizer technology and nanoparticle characteristics on aerosol features. Journal of Controlled Release. 86:131-144 (2003).

54. O.N. McCallion, K.M. Taylor, M. Thomas, and A.J. Taylor. Nebulization of fluids of different physicochemical properties with air-jet and ultrasonic nebulizers. Pharmaceutical Research. 12:1682-1688 (1995).

55. B.Y. Shekunov, P. Chattopadhyay, D. Yim, D. Cippola, and B. Boyd. Formulation and in vitro performance of drug-lipid nanosuspensions for pulmonary delivery, *Conference on Respiratory Drug Delivery*, Boca Raton, Florida, 2006, pp. 609-612.

56. J.S. Pattonand P.R. Byron. Inhaling medicines: delivering drugs to the body through the lungs. Nature reviews. 6:67-74 (2007).

57. A.J. Aguiarand J.E. Zelmer. Dissolution behavior of polymorphs of chloramphenicol palmitate and mefenamic acid. J Pharm Sci. 58:983-987 (1969).

58. A.J. Aguiar, J. Krc, Jr., A.W. Kinkel, and J.C. Samyn. Effect of polymorphism on the absorption of chloramphenicol from chloramphenicol palmitate. J Pharm Sci. 56:847-853 (1967).

59. K. Yamashita, T. Nakate, K. Okimoto, A. Ohike, Y. Tokunaga, R. Ibuki, K. Higaki, and T. Kimura. Establishment of new preparation method for solid dispersion formulation of tacrolimus. Int J Pharm. 267:79-91 (2003).

60. D.A. Miller, J.T. McConville, W. Yang, R.O. Williams, 3rd, and J.W. McGinity. Hot-melt extrusion for enhanced delivery of drug particles. Journal of pharmaceutical sciences. 96:361-376 (2007).

61. V. Sanna, E. Gavini, M. Cossu, G. Rassu, and P. Giunchedi. Solid lipid nanoparticles (SLN) as carriers for the topical delivery of econazole nitrate: in-vitro characterization, ex-vivo and in-vivo studies. J Pharm Pharmacol. 59:1057-1064 (2007).

62. P. Sinswat, K.A. Overhoff, J.T. McConville, K.P. Johnston, and R.O. Williams. Nebulization of nanoparticulate amorphous or crystalline tacrolimus - Single-dose pharmacokinetics study in mice. European Journal of Pharmaceutics and Biopharmaceutics. 69:1057-1066 (2008).

63. W. Yang, J.I. Peters, and R.O. Williams. Inhaled nanoparticles - A current review. Int J Pharm. 356:239-247 (2008).

64. M.E. Matteucci, B.K. Brettmann, T.L. Rogers, E.J. Elder, R.O. Williams, 3rd , and K.P. Johnston. Design of Potent Amorphous Drug Nanoparticles for Rapid Generation of Highly Supersaturated Media. Molecular pharmaceutics. 4:782-793 (2007).

65. M.E. Matteucci, J.C. Paguio, M.A. Miller, R.O. Williams, and K.P. Johnston. Highly Supersaturated Solutions from Dissolution of Amorphous Itraconazole Microparticles at pH 6.8. Molecular Pharmaceutics. 6:375-385 (2009).

66. K. Donaldson, V. Stone, C.L. Tran, W. Kreyling, and P.J. Borm. Nanotoxicology. Occupational and environmental medicine. 61:727-728 (2004).

67. A. Nemmar, H. Vanbilloen, M.F. Hoylaerts, P.H. Hoet, A. Verbruggen, and B. Nemery. Passage of intratracheally instilled ultrafine particles from the lung into the systemic circulation in hamster. American journal of respiratory and critical care medicine. 164:1665-1668 (2001).

68. W.G. Kreyling, M. Semmler, F. Erbe, P. Mayer, S. Takenaka, H. Schulz, G. Oberdorster, and A. Ziesenis. Translocation of ultrafine insoluble iridium particles

from lung epithelium to extrapulmonary organs is size dependent but very low. J Toxicol Environ Health A. 65:1513-1530 (2002).

69. P. Forsgren, J. Modig, B. Gerdin, B. Axelsson, and M. Dahlback. Intrapulmonary Deposition of Aerosolized Evans Blue-Dye and Liposomes in an Experimental Porcine Model of Early Ards. Ups J Med Sci. 95:117-136 (1990).

70. H.Y. Zhou, Y.L. Zhang, D.L. Biggs, M.C. Manning, T.W. Randolph, U. Christians, B.M. Hybertson, and K.Y. Hg. Microparticle-based lung delivery of INH decreases INH metabolism and targets alveolar macrophages. J Controlled Release. 107:288-299 (2005).

Table 3.1. Particle size distributions, specific surface areas (SSA) and the calculated particle sizes based on SSA of Wet-milled ITZ (wet milling processed pure ITZ) and URF-ITZ (URF processed ITZ:mannitol:lecithin = 1:0.5:02) powders.

Samples	Particle Size (μm)			Specific Surface Area (m^2/g)	Calculated Particle Size (μm)
	D(v, 0.1)	D(v, 0.5)	D(v, 0.9)		
Wet-milled ITZ	0.16	0.57	1.22	31.7	0.19
URF-ITZ	0.10	0.25	0.59	38.6	0.15

Table 3.2. Cascade impaction data for nebulized aerosols of Wet-milled ITZ colloidal dispersion (ITZ:mannitol:lecithin = 1:0.5:0.2, weight ratio) and URF-ITZ colloidal dispersion (ITZ:mannitol:lecithin = 1:0.5:0.2, weight ratio) (equivalent to 100 mg of total ITZ), using the Aeroneb Professional micropump nebulizer at an air flow rate of 28.3 L/min for 10 min.

	Wet-milled ITZ	URF-ITZ
Total Emitted dose (mg)	51.73	56.40
Respirable Fraction[#] (%)	74.54	72.95
Fine Particle Fraction* (%)	47.28	54.39
Available Dose (mg/min)	3.86	4.11
Mass Median Aerodynamic Diameter (MMAD) (μm)	2.78	2.36
Geometric Standard Deviation (GSD)	3.06	2.66

[#] Defined as the % mass of drug in aerosol droplets < 9 μm
[*] Defined as the % mass of drug in aerosol droplets < 4.7μm

Table 3.3. Pharmacokinetic parameters for plasma ITZ concentration in rats after a single dose inhalation of nebulized aerosols of Wet-milled ITZ colloidal dispersion (ITZ:mannitol:lecithin = 1:0.5:0.2, weight ratio) and URF-ITZ colloidal dispersion (ITZ:mannitol:lecithin = 1:0.5:0.2, weight ratio).

Pharmacokinetic parameters	Wet-milled ITZ	URF-ITZ
C_{max} (ng/mL)	50.4	177.5
T_{max} (hr)	2.7	4
$K_{01\ absorption}$ (/hr)	0.98	0.55
$K_{10\ elimination}$ (/hr)	0.09	0.08
$T_{1/2\ absorption}$ (hr)	0.71	1.27
$T_{1/2\ elimination}$ (hr)	7.82	8.16
$AUC_{0–24}$ (ng·hr/mL)	662	2543

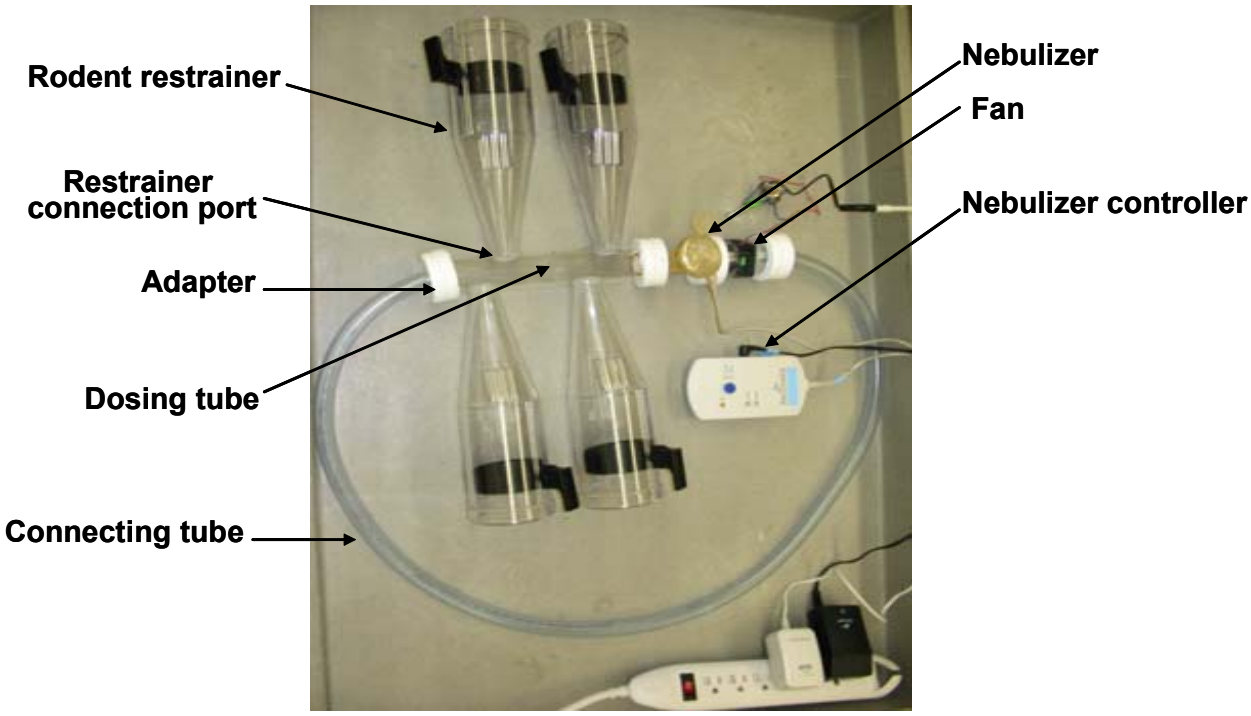

Figure 3.1. Picture of the nose-only dosing apparatus for rodents

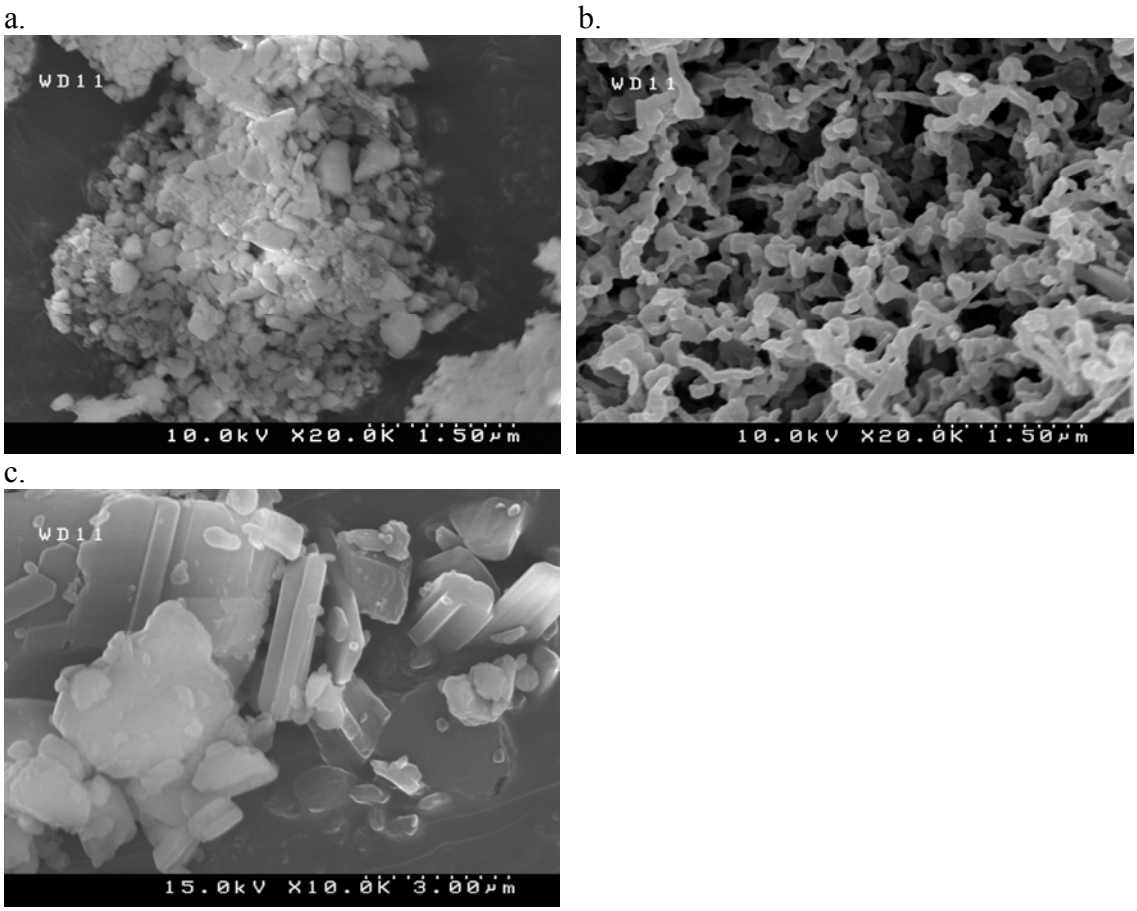

Figure 3.2. SEM images of (a) Wet-milled ITZ (wet milling processed pure ITZ) powder at a magnification of 20k (b) URF-ITZ (URF processed ITZ:mannitol:lecithin = 1:0.5:0.2, weight ratio) powder at a magnification of 20k (c) bulk ITZ as received at a magnification of 10k.

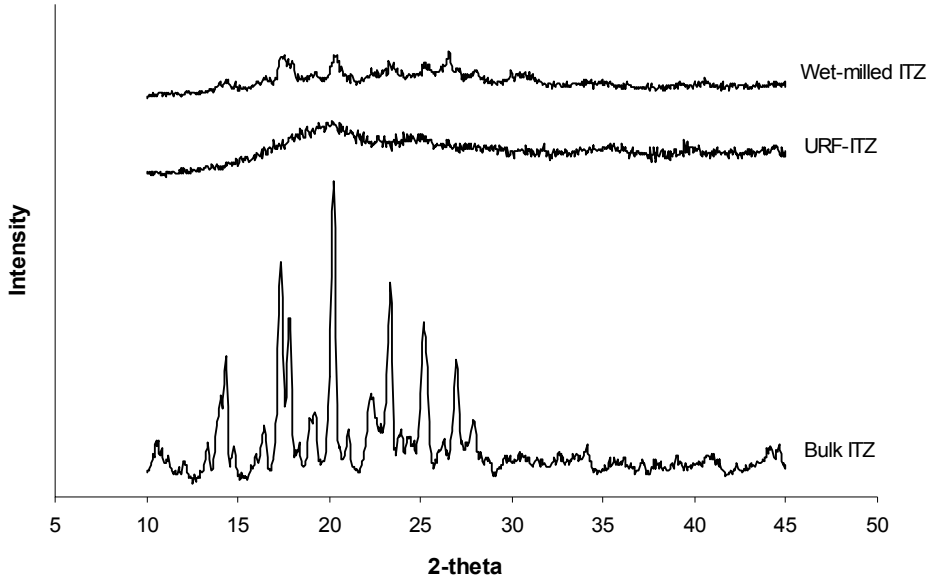

Figure 3.3. X-ray powder diffraction patterns (from the top to bottom): Wet-milled ITZ (wet milling processed pure ITZ), URF-ITZ (URF processed ITZ:mannitol:Lecithin = 1:0.5:0.2), micronized bulk ITZ.

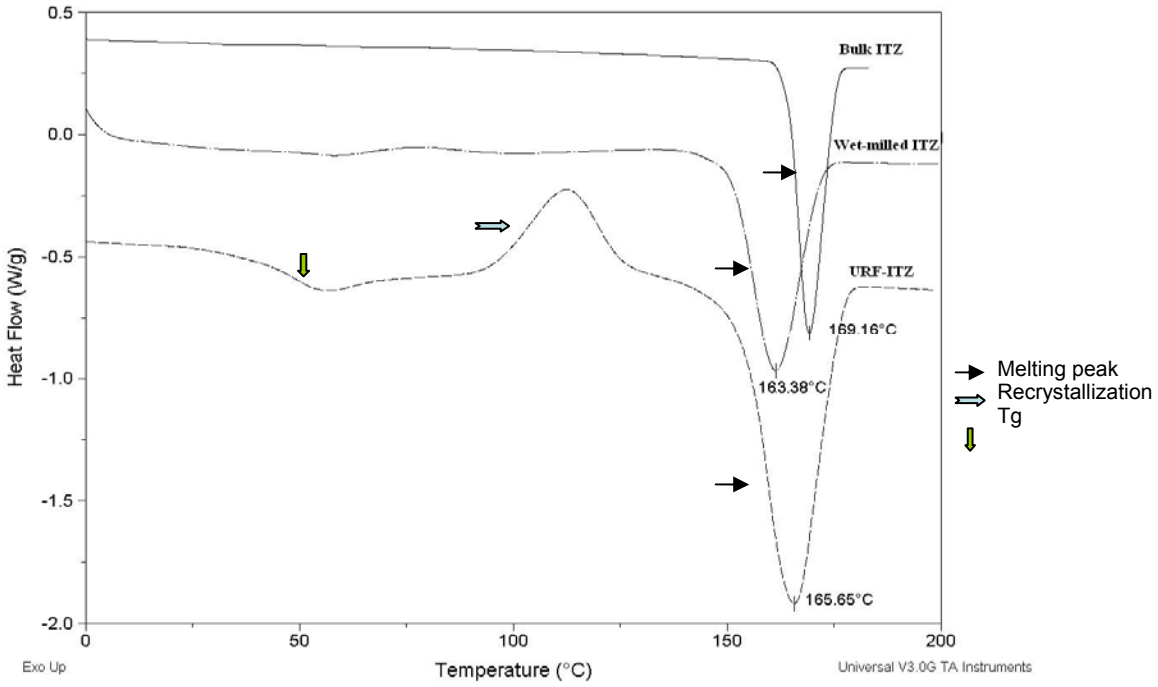

Figure 3.4. DSC profiles of bulk ITZ, Wet-milled ITZ (wet milling processed pure ITZ) powder and URF-ITZ (URF processed ITZ:mannitol:lecithin = 1:0.5:0.2, weight ratio) powder.

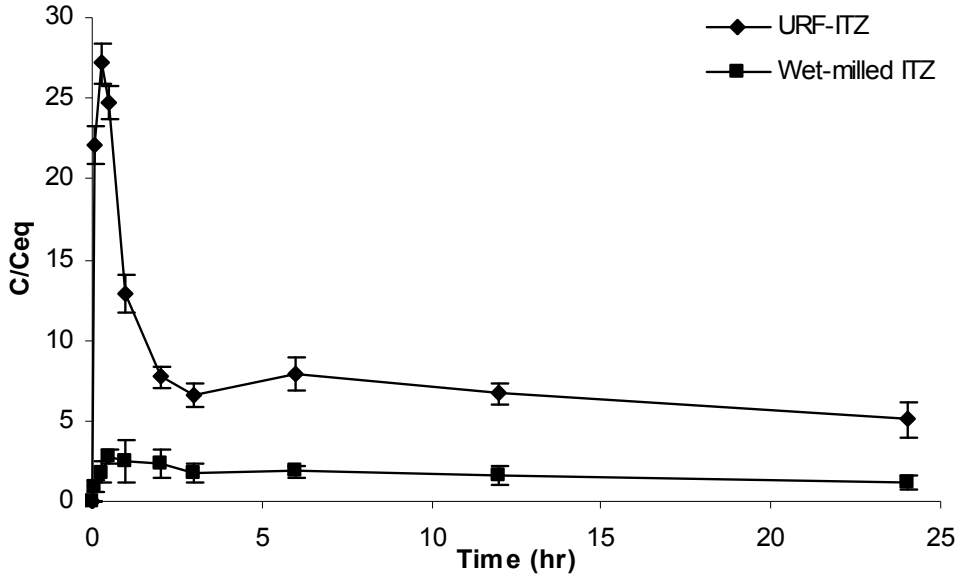

Figure 3.5. Dissolution profiles of Wet-milled ITZ colloidal dispersion (ITZ:mannitol:lecithin = 1:0.5:0.2, weight ratio) and URF-ITZ colloidal dispersion (ITZ:mannitol:lecithin = 1:0.5:0.2, weight ratio) in simulated lung fluid (pH=7.4) at supersaturation conditions (*i.e.* 100-times equilibrium solubility of micronized crystalline ITZ was added) using 100-mL vessels and small paddle apparatus at 100 rpm and 37 ℃.

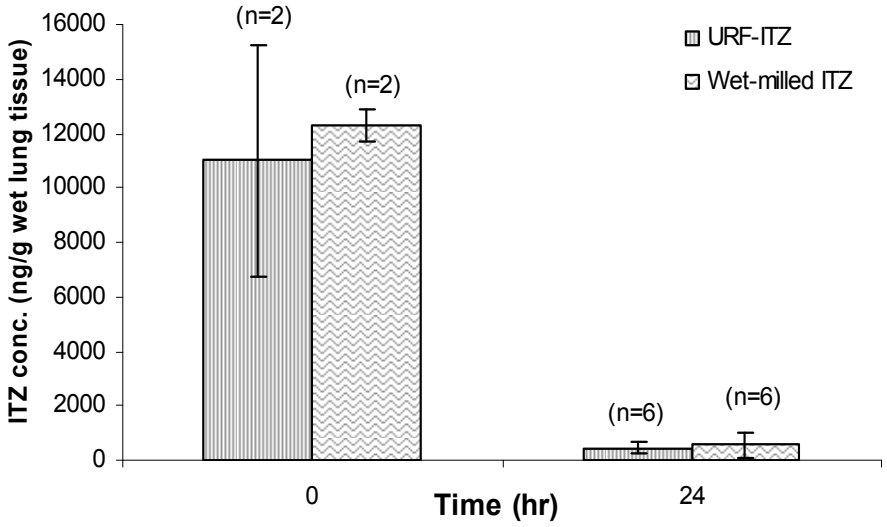

Figure 3.6. Lung deposition of ITZ in rats at 0 and 24 hr post inhalation of a single-dose nebulized aqueous Wet-milled ITZ colloidal dispersion (ITZ:mannitol:lecithin = 1:0.5:0.2, weight ratio) and URF-ITZ colloidal dispersion (ITZ:mannitol:lecithin = 1:0.5:0.2, weight ratio). Data are presented as Mean±SD.

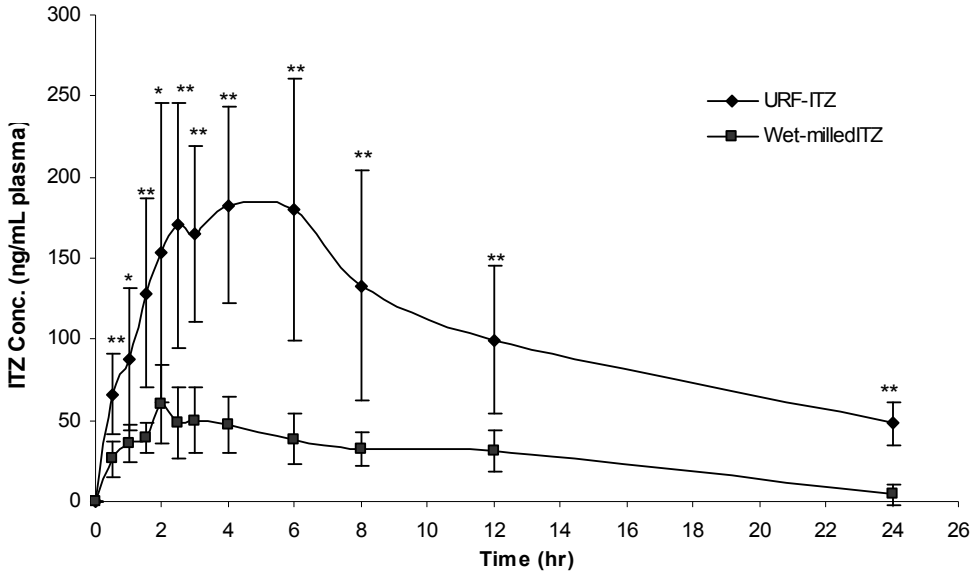

Figure 3.7. Plasma concentration of ITZ in rats after a single-dose inhalation of nebulized aqueous Wet-milled ITZ colloidal dispersion (ITZ:mannitol:lecithin = 1:0.5:0.2, weight ratio) and URF-ITZ colloidal dispersion (ITZ:mannitol:lecithin = 1:0.5:0.2, weight ratio). Data are presented as Mean±SD, n=6.
* $p < 0.05$, ** $p < 0.01$

Chapter 4: In Vitro Characterization and Pharmacokinetics in Mice following Pulmonary Delivery of Itraconazole as a Cyclodextrin Solubilized Solution

4.1 ABSTRACT

This study aims to make a 2-hydroxypropyl-β-cyclodextrin (HPβCD) solubilized itraconazole (ITZ) solution (i.e., HPβCD-ITZ) suitable for pulmonary delivery by nebulization, and compare the pharmacokinetics of inhaled nebulized aerosols of HPβCD-ITZ versus a colloidal dispersion of an ITZ nanoparticulate formulation (i.e., URF-ITZ). Solid state characterizations of lyophilized HPβCD-ITZ by differential scanning calorimetry (DSC), Fourier Transform Infrared Spectroscopy (FTIR), and X-ray photoelectron spectroscopy (XPS) indicated the formation of dynamic inclusion complexes between ITZ and HPβCD. Nebulized aerosols of both HPβCD-ITZ and a colloidal dispersion of URF-ITZ were confirmed suitable for deep lung delivery. Single doses of the nebulized aerosols (equivalent to 5.3 mg ITZ/mL in 5 mL) in mice produced similar ITZ lung depositions and pharmacokinetic profiles, with ITZ lung levels of approximately 4 μg/g wet lung weight upon completion of nebulization and remained above 0.5 μg/g at 24 hr. HPβCD-ITZ demonstrated faster systemic absorption of ITZ across lung epithelium than URF-ITZ, with T_{max} values of 1.5 and 3.0 hr, and $AUC_{0-\infty}$ of 2513 and 3717 ng·hr/mL, respectively. The fast absorption of solubilized ITZ across lung mucosal surface may be due in part to the elimination of the phase-to-phase transition.

4.2 INTRODUCTION

The incidence of invasive fungal infections has continued to increase over the last decade especially among high risk patients including those undergoing chemotherapy, solid organ or hematopoietic stem cell transplantation, and patients in intensive care units [1, 2]. The azole antifungals, which inhibit lanosterol 14-α-demethylase resulting in reductions in ergosterol within the fungal cell membrane, are a mainstay in the treatment of invasive fungal infecitons. Itraconazole (ITZ) is an appealing antifungal triazole for both prophylaxis and treatment in neutropenic and other immunocompromised patients, because of its broad spectrum of activity and enhanced potency against commonly occurring fungal pathogens including *Candida* and *Aspergillus* species [3].

ITZ has a well-defined correlation between its *in vitro* minimal inhibitory concentration (MIC) activity and clinical performance in the treatment of candidiasis [4]. For susceptible organisms (MIC < 0.125 μg/ml), 89% of patients are cured clinically when ITZ plasma concentration is greater than 0.5 μg/mL. For *Aspergillus* sp. infections in immunocompromised patients, ITZ trough levels greater than 0.5 μg/g in lung tissue, or greater than 0.5 μg/mL in blood [5] are generally required. However, being classified as a Biopharmaceutical Classification System (BCS) class II compound, ITZ is practically insoluble in water (estimated aqueous solubility is approximately 1 ng/mL at neutral pH and 6 μg/mL at pH 1) [6]. The low solubility presents significant challenges in formulating sufficiently bioavailable dosage forms of ITZ, irrespective of routes of administration. A number of formulation approaches have been assessed in order to improve the pharmaceutical performance of ITZ [7], such as solubilization in surfactants to form self-emulsifying drug delivery systems [8, 9], solid state manipulation using particle engineering technologies [10-12], and formation of drug/cyclodextrin (CD)

inclusion complexes. Among these formulation approaches, the first to be commercialized was Sporanox® oral capsules, in which ITZ is molecularly dispersed with hydroxypropylmethylcellulose forming a solid solution [6]. However, the oral bioavailability is low, with erratic absorption influenced by food intake [13]. An alternative oral solution (Sporanox®, ITZ/HPβCD inclusion complex containing 10 mg/mL of ITZ and 400 mg/mL of HPβCD) further increased bioavailability to about 30% higher than the capsule formulation [14]. However, the significant gastrointestinal adverse effects caused by HPβCD, including osmotic diarrhea [15], led to limited patient acceptance. Newer formulations and/or delivery systems of ITZ with greater therapeutic efficacy and lower toxicity are still in demand.

The lungs are often the primary port of entry into the body and site of infection for many life-threatening opportunistic fungi in immuno-compromised patients [16]. However, pulmonary infections may not respond well to systemic therapy with oral dosage forms due to insufficient drug diffusion into pulmonary tissues and lumen [17]. An increase in the amount of drug doses intended to compensate for poor diffusion may lead to systemic toxicity. Delivering antifungal drugs as aerosols by the pulmonary route allows high drug concentrations targeted directly at the site of infection, while minimizing potential systemic toxicity.

Production of drug-loaded nanoparticles such as nanosuspensions for the poorly-water soluble drugs is an alternative and promising approach to overcome their low aqueous solubilities and the consequential low bioavailabilities [18]. Moreover, drug-loaded nanoparticles have the potential to be used for pulmonary delivery of therapeutics for treating lung diseases locally as well as for systemic actions. Pulmonary delivery of

nanoparticle formulations of poorly water-soluble drugs showed promising results in several *in vitro* investigations [19, 20], *in vivo* studies [21], and in a clinical trial of a nebulized nanocrystal suspension of budesonide (75–300 nm) [22].

Nanoparticle formulations of ITZ for deep lung delivery have been designed and prepared by particle engineering technologies in our laboratory, namely evaporative precipitation of aqueous solution (EPAS) [23] and spray freezing into liquid (SFL) [24]. Single and multi dose inhalation of nebulized aerosols of these ITZ nanoparticle colloidal dispersions with a suitable aerodynamic diameter for deep lung delivery, demonstrated therapeutically effective ITZ concentrations in mouse lung, superior to the Sporanox® oral solution [25, 26]. In addition, the inhaled ITZ formulations demonstrated prophylactic effects against invasive pulmonary aspergillosis in murine models [27, 28].

A novel nanostructured ITZ solid solution formulation, URF-ITZ (ITZ:mannitol:lecithin=1:0.5:0.2, weight ratio) was recently developed using the ultra-rapid freezing (URF) technology [29]. Inhalation of nebulized URF-ITZ aqueous colloidal dispersion, containing the same amount ITZ loading as the previously reported ITZ pulmonary formulations on the same murine model [25], produced significantly enhanced lung drug deposition and more than 10-fold higher ITZ level in the systemic circulation. The improved bioavailability was mainly attributed to the smaller nano-scaled particle size (primary particles of 30-50 nm in diameter), and the presence of lecithin, which had facilitated permeation of ITZ through the lung epithelium [30].

CDs have been reported to facilitate faster systemic absorption and improved bioavailability of poorly water-soluble drugs after pulmonary administration of aerosols

or solutions as compared to equipotent alternative formulations or routes of administration [31, 32]. A recent study reported that pulmonary delivery of a nebulized Vfend® I.V. aqueous solution of voriconazole (a triazole analog of ITZ) solubilized with sulfobutylether-β-cyclodextrin (SBEβCD) to rodents, attained a high lung deposition and a high systemic peak drug level within 30 min, similar to the intravenous administration profile [33]. The presence of the solubilized form of voriconazole molecules in a SBEβCD aqueous solution was thought to contribute to the rapid and complete absorption, and high systemic drug concentrations following pulmonary administration.

Based on the results of the bioavailability studies of inhaled nanoparticulate ITZ and CD-solubilized voriconazole formulations, we hypothesized that inhalation of an effectively solubilized form of poorly-water soluble drug could lead to faster absorption through the lung mucosal epithelium as compared to the nanoparticulate form, which requires a drug dissolution process prior to absorption. Our aims were two-fold: (1) to prepare and characterize a CD solubilized ITZ solution formulation suitable for pulmonary delivery by nebulization; (2) to investigate the pharmacokinetic profiles of the inhaled aerosol of the CD solubilized form of ITZ compared to a nanoparticulate colloidal dispersion of this triazole in mice following nebulization in a whole-body exposure dosing apparatus.

4.3 MATERIALS AND METHODS

4.3.1 Materials

Crystalline ITZ (micronized pharmacopeial grade) was purchased from Hawkins Chemical (Minneapolis, MN, USA). Hydroxyitraconazole was purchased from BDG

Synthesis (Wellington, New Zealand). Mannitol and lecithin (NF grade) were from Spectrum Chemicals (Gardena, CA). 2-hydroxypropyl-β-cyclodextrin (HPβCD) was kindly provided by Roquette America Inc. (Keokuk, IA). 1,4-dioxane, acetonitrile, and diethanolamine were purchased from Fischer Chemicals (Gibbstown, NJ, USA). All organic solvents used were of HPLC grade. Other chemicals utilized in this study were at least of ACS grade. Blank mice serum for chromatography analysis method validation was supplied by Invitrogen (Camarillo, CA, USA).

4.3.2 Preparation of Nanostructured Aggregates Powder of ITZ Using URF Technology

The amorphous nanostructured aggregate powder URF-ITZ, was prepared using URF technology as described previously [29]. In brief, ITZ, mannitol, and lecithin (in a weight ratio of 1:0.5:0.2) were dissolved in a mixture of 1,4-dioxane and purified water (65/35, v/v) co-solvent system. The solution was then applied to the cryogenic solid substrate (which was previously cooled to -70 °C) of the URF apparatus. The rapidly frozen solids were collected and lyophilized using a VirTis Advantage bench top tray lyophilizer (The VirTis Company, Inc., Gardiner, NY, USA). The resultant dry powder was stored in a desiccator under vacuum at room temperature. Amorphous pure ITZ was also prepared by the URF process as described above.

4.3.3 Characterization of HPβCD and HPβCD-ITZ Solutions

A series of concentrations of HPβCD solutions in purified water were prepared. Viscosity of the solutions was measured using a Cannon-Fenske Routine viscometer (Cannon Instrument Company, State College, PA, USA) at 25 °C.

Considering the osmolarity of the formulation to be delivered to the lungs, a sodium chloride (NaCl) solution in water with the proper osmolarity, was used to prepare the HPβCD solutions. The osmolality of the HPβCD-ITZ solution was measured by the freezing point depression method using a μOsmette Micro Osmometer (Precision Systems Inc., Natick, MA).

The pH of the filtrates of the dispersions of ITZ in HPβCD was determined using an Orion 350 PerpHecT® Advanced Benchtop pH Meter (Thermo Fisher Scientific, Waltham, MA).

4.3.4 Solubility Studies

To study solubility differences between crystalline and amorphous ITZ in HPβCD, excess amounts of micronized crystalline ITZ or amorphous pure ITZ were added to 5 mL of 15% HPβCD in purified water. A 2-min sonication by a probe sonicator (Branson Sonifier 450, Danbury, CT) was used to facilitate the dispersion of the powders into the aqueous phase. The formed dispersions were then shaken at 100 rpm, at 25 °C for up to 2 days. Aliquots of 200 μL of the suspension were withdrawn at 0, 0.5, 1, 2, 3, 5, 8, 24, 48 hr. All samples were filtered through 0.2 μm GHP Acrodisc syringe filters (Pall Corporation, East Hills, NY) and appropriately diluted with a solvent mixture of acetonitrile:water (70:30, v/v) for content analysis. The ITZ content was determined using a Shimadzu LC-10A high performance liquid chromatography (HPLC) system (Shimadzu Corporation, Columbia, MD) equipped with an Alltech Inertsil^{TM} ODS-2 5 μm, 150 mm × 4.6 mm, C-18 column (Alltech Associates, Inc., Deerfield, IL). The ITZ peak was eluted at approximately 5.5 min using a mobile phase consisting of acetonitrile:water:diethanolamine (70:30:0.05, v/v/v) at a flow rate of 1 mL/min, column

temperature of 25 °C, and an absorption wavelength λ_{max} of 263 nm. Values reported are the average of three measurements.

4.3.5 Preparation of Solid State ITZ-HPβCD Inclusion Complex

Aliquots of the ITZ in 15% HPβCD dispersion were sampled at 24 hr after dispersion and equilibration at room temperature, and filtered through 0.2 μm Acrodisc filters (Pall Corporation, East Hills, NY). The filtrates (designated as HPβCD-ITZ solution) were frozen and then lyophilized using the VirTis Advantage bench top tray lyophilizer (The VirTis Company, Inc., Gardiner, NY, USA) to obtain dry powders.

4.3.6 Preparation of Physical Mixture

A physical mixture consisting of micronized crystalline ITZ and HPβCD powder was prepared by gently mixing ITZ and HPβCD powders for 5 min using a spatula in a glass mortar to obtain a homogeneous blend at the same weight ratio as the lyophilized HPβCD-ITZ inclusion complex, based on the equilibrium solubility of ITZ per mL of 15% HPβCD solution.

4.3.7 Thermal Analysis

All the powders were dried in desiccator for at least one day before thermal analysis. Differential scanning calorimetry (DSC) of the lyophilized HPβCD-ITZ dry powder, physical mixture, and each pure component was conducted using modulated temperature DSC (MTDSC), Model 2920 (TA Instruments, New Castle, DE), equipped with a refrigerated cooling system. Dry nitrogen gas was used as the purge gas through the DSC cell at a flow rate of 40 mL/min. Samples weighing 10-15 mg in crimped

aluminum pans (Kit 0219-0041, Perkin-Elmer Instruments, Norwalk, CT) were used. The mass of the empty sample pan was matched with that of the empty reference pan within ±0.2 mg. Samples were heated at a ramp rate of 10 °C/min from 0 to 250 °C with a modulation temperature amplitude of 1 °C /60 sec for all studies. Data was analyzed using the TA Universal Analysis 2000 software (TA Instruments, New Castle, DE).

4.3.8 Fourier Transform Infrared Spectroscopy (FTIR)

ITZ, HPβCD, physical mixture powders, and the lyophilized HPβCD-ITZ dry powder were analyzed by FTIR to evaluate potential interactions. The samples were prepared by weighing approximately 4 mg of the material for analysis, homogenously dispersing in dried KBr of about 300 mg using a mortar and pestle, and compressing the powder under vacuum with a compression force of 10 tons using a 13 mm diameter round flat face punch for three minutes to produce a pellet compacts. The sample was placed in the IR light path and the IR spectra were recorded using a Thermo Mattson Infinity Gold FTIR with Spectra-Tech Thermal ARK module from 400 to 4000 cm^{-1} in transmission mode equipped with a KBr beamsplitter and DTGS detector having a resolution of 1 cm^{-1}.

4.3.9 X-ray Photoelectron Spectroscopy (XPS)

XPS analysis was performed on the lyophilized powder comprised of HPβCD/ITZ inclusion complexes sampled at 1, 24 and 48 hr after dispersion, as well as physical mixture in order to verify the amount of ITZ present on the powder surfaces. The XPS measurements were conducted with an AXIS HS photoelectron spectrometer (Kratos Analytical, UK) equipped with a monochromated Al Kα x-ray source (hv =

1486.6 eV) operating at 10 kV and 15 mA (150 W). The vacuum in the sample chamber was maintained below 10^{-7} torr during analysis. The analysis area was approximately 1 mm^2. For each sample, a take-off angle of the photoelectrons perpendicular to the sample holder was used throughout. The data for the atomic surface composition were converted into molecular surface composition under the assumptions that all molecular species on the surface are present in "patches" with a depth of at least the depth of analysis (~5 nm for the powders), and the surface can be regarded as linear combination of the different molecular species.

4.3.10 Aerosol Particle Size Analysis Using a Cascade Impactor

The colloidal dispersion of URF-ITZ powder was prepared for nebulization by dispersing the powder in purified water using ultrasonication in an ice bath. An aliquot (5 mL) of the URF-ITZ colloidal dispersion and HPβCD-ITZ aqueous solution were nebulized using an Aeroneb® Professional micropump nebulizer (Nektar Therapeutics, San Carlos, CA) with an air flow rate of 28.3 L/min. The characterization of aerodynamic droplet size distribution was conducted according to the guidelines in USP 30 Section 601 [34].

Aerodynamic droplet size distributions were determined using a USP Apparatus 1 non-viable eight-stage cascade impactor (Thermo-Anderson, Symrna, GA) with a spacer to quantify total emitted dose (TED) from the nebulizer output, mass median aerodynamic diameter (MMAD), geometric standard deviation (GSD), and percentage fine particle fraction (FPF; defined as the percentage of droplets with an aerodynamic diameter less than 4.7 μm). Fiberglass filters (81 mm diameter) (ThermoFisher Scientific, Franklin, MA) were set atop each impactor plate to absorb the aerosolized suspensions

and prevent overload of the plates. Each stage was rinsed with a known volume of the washing solution (acetonitrial/water=70/30, v/v). Each filter was placed in a separate container with a known volume of the washing solution and sonicated for 30 min to dissolve ITZ. Samples were filtered using 0.2 μm GHP Acrodisc syringe filters prior to quantification of drug contents using HPLC.

4.3.11 Single-dose Pulmonary Administration to Mice

Male outbred ICR (Institute for Cancer Research) mice (Harlan Sprague Dawley, Inc., Indianapolis, IN) weighing 25–28 g were acclimated in a whole-body dosing chamber as previously described [26] for 20 min/day for 2 days prior to dosing. This restraint-free chamber was designed to hold up to 14 mice. An Aeroneb® Professional micropump nebulizer was fitted at the inlet of the chamber, and the aerosols were delivered through the inlet into the chamber with an air flow rate of 1 L/min. Nebulized aerosols of HPβCD-ITZ solution and URF-ITZ colloidal dispersion were inhaled by the mice for approximately 18 min in the whole-body dosing chamber. Following exposure to the aerosol cloud, six mice were euthanized by carbon dioxide narcosis at 0, 0.5, 1, 1.5, 2, 3, 4, 6, 10, and 24 hr post dosing. Samples taken immediately upon completion of aerosolization were assigned to the zero time point. Blood samples were taken by cardiac puncture, and the lungs were collected following exsanguination. The study protocol was approved and conducted in accordance to the Institutional Animal Care and Use Committee (IACUC) guidelines at The University of Texas at Austin. Throughout the study the animals were maintained in accordance with the American Association for Accreditation of Laboratory Animal Care guidelines.

4.3.12 Chromatographic Analysis

Whole blood samples were centrifuged at 3000 g for 15 min to obtain the serum. Serum samples and whole lungs were stored at -80°C until assayed. Lungs were thawed and homogenized with 1 mL of purified water using an Omni Ruptor 250 ultrasonication homogenizer (Omni International, Marietta, GA) with power output setting at 40 and pulser at 60.

Calibration standards, serum, and homogenized lung samples were analyzed as described previously [29]. Briefly, serum samples of 250 µL were transferred to clean 2-mL microcentrifuge tubes. To each microcentrifuge tube, 50 µL of 0.3 N barium hydroxide and 50 µL 0.4 N zinc sulfate heptahydrate solutions were added and vortex mixed for 30 sec to precipitate water-soluble proteins. Acetonitrile (1 mL) containing about 500 ng/mL voriconazole as an internal standard was added to each sample followed by vortex mixing for 1.5 min. Samples were then centrifuged at 3000 g for 15 min. The supernatant from each vial was transferred to a clean 1.5 mL centrifuge tube and dried in an aluminum heating block (70 °C) under a stream of nitrogen gas. The samples were reconstituted with 250 µL mobile phase (0.05 M phosphate buffer, pH 6.7: acetonitrile = 38:62, v/v), vortex mixed for 1 min, and centrifuged at 6000 g for 5 min. An aliquot of 150 µL was pipetted into HPLC vial spring inserts and analyzed using Shimadzu HPLC system with an Alltech Inertsil^{TM} ODS-2 5 µm, 250 × 4.6 mm, C-18 column connected to a C-18 guard column (5 µm, 7.5×4.6 mm) (Alltech Associates, Inc., Deerfield, IL) maintained at 37 °C. The voriconazole, hydroxyitraconazole (HyITZ) and ITZ peaks were eluted at approximately 5.3, 8.5 and 18.2 min, respectively, at a flow rate of 1 mL/min, injection volume of 100 µL, and an absorption wavelength of 225 nm. The limit

of detection and quantification for HyITZ and ITZ were 10 ng/mL and 30 ng/mL, respectively.

4.3.13 Pharmacokinetic Analysis

Pharmacokinetics of 24-hr lung and serum was assessed for the pulmonary delivery of nebulized aerosols of HPβCD-ITZ aqueous solution and URF-ITZ colloidal dispersion to mice. A noncompartmental model was used to determine pharmacokinetic profiles for the ITZ concentrations in lung tissue using WinNonlin Professional Version 2.1 (Pharsight Corporation, Mountain View, CA). Using this method of analysis, T_{max} and C_{max} were determined directly from the empirical data; area under the plasma concentration-time curve (AUC) was calculated by the linear trapezoidal rule. Plots of the log concentration of ITZ and HyITZ in serum versus time revealed a first-order absorption phase and a first-order elimination phase. A one-compartmental analysis was therefore used. The $K_{10\ elimination}$ rate constants were determined by linear regression of the points of the log-linear plasma concentration versus time curve. The $K_{01\ absorption}$ rate constants were determined by residual method. The $t_{1/2}$ was defined as 0.693/rate constant K.

4.3.14 Statistical Analysis

Drug concentrations in lung tissue and serum were presented as mean with standard deviation (SD) (n = 6) at each sampling time point. The data were statistically analyzed by one-way Analysis of Variance (ANOVA) followed by Tukey's post hoc analysis using OriginPro 7.5 (OriginLab Corporation, Northampton, MA), and Microsoft Excel 2003. A *p*-value of < 0.05 was considered as statistically significant.

4.4 RESULTS AND DISCUSSION

To improve the bioavailability resulting from poor water solubility, CDs and their derivatives have been used as a means to increase aqueous solubility. CDs are characteristic of a truncated cone shape with a hydrophilic exterior surface and a nonpolar cavity interior [35]. This structure allows CDs to form non-covalent host–guest dynamic inclusion complexes with drug molecules of proper sizes and polarities, leading to enhanced apparent aqueous solubility, dissolution rate, chemical stability, and bioavailability [36, 37].

Having a external and internal diameters of 1.53 nm and 0.78 nm, respectively, βCD provides the right fit for ITZ molecule, as the cavity internal diameter is comparable to the dimensions of substituted phenyl groups which contribute to the lipophilicity of ITZ and other azoles [15]. HPβCD and SBEβCD are chemically modified βCD with enhanced aqueous solubility and safety profiles, and there is a vast experience of use in pharmaceutical applications [38]. Despite their safety profiles, pharmaceutical dosage forms should contain as little CD as possible. Moreover, to make an ITZ solution with acceptable amount of CD for nebulization, enhancement of the complexation capacity of the chosen CD is of practical importance. HPβCD and SBEβCD were therefore tested in this study to select a more efficient complexing agent for solubilizing ITZ.

4.4.1 Solubility Studies and In Vitro Solution Characterization

The phase solubility studies of ITZ in various concentrations of CDs and derivatives at different pHs have been extensively investigated and reported in literature

[39, 40]. For pulmonary delivery systems, it is crucial that the formulations are physiologically compatible with the lungs. Our preliminary experiments found that higher equilibrium solubility of ITZ can be achieved in HPβCD as compared to SBEβCD solutions at neutral pH conditions. This result is consistent with other reports investigating interactions between CDs and antifungal azoles [40, 41]. HPβCD was therefore chosen as the functional excipient to formulate ITZ in our study due to its stronger solubilizing.

The viscosity of the CD-containing solution is a barrier for pulmonary administration by the Aeroneb® Professional micropump nebulizer. In order to aerosolize the ITZ-CD formulation completely within a reasonable dosing duration, it is necessary to find a suitable HPβCD concentration for the nebulizer. As can be seen from Figure 4.1., viscosity of HPβCD solutions increases along with its concentrations. Greater than 30 min and approximately 17 min were required to nebulize 5 mL of 20% and 15% w/v HPβCD solutions with measured viscosities of 1.40 and 1.19 cP, respectively. The 15% w/v HPβCD solution was selected to formulate the ITZ nebulization solution, to be comparable with the URF-ITZ formulation which takes about 10 min to nebulize 5 mL of the dispersion.

The equilibrium solubility of crystalline ITZ was significantly enhanced from 1 ng/mL in water [6] to 0.15 mg/mL in 15% w/v HPβCD aqueous solution in this study, which was in agreement with the work of Brewster et al. [40]. Despite the significant increase of ITZ concentration in HPβCD aqueous solution, the complexation efficiency was low, and was limited by the allowed amount of HPβCD in this formulation. To further increase complexation efficiency of ITZ, amorphous pure ITZ, which has a higher

intrinsic solubility than its crystalline counterpart [42], was employed to make the ITZ inclusion complex with HPβCD. As shown in Figure 4.2., a concentration of 5.4 mg/mL of ITZ was achieved immediately after dispersing amorphous ITZ in 15% HPβCD solution, presumably due to the supersaturation rendered by the amorphous state. Compared to crystalline ITZ, amorphous pure ITZ brought about a 34-times increase in equilibrium solubility in 15% w/v HPβCD solution. An equilibrium level of 5.3 mg/mL was attained at 2 hr and was maintained up to 24 hr as a mixed effect of HPβCD-ITZ inclusion complex formation, supersaturation stabilized by HPβCD via nucleation, and crystal growth inhibition [43]. At 48 hr, the ITZ concentration decreased slightly to 4.6 mg/mL, which could be attributed to precipitation of supersaturated ITZ in the system.

Osmolarity is one of the important parameters to be considered for physiological compatibility of pulmonary formulations. Sodium chloride (NaCl) was used to adjust the osmolarity of HPβCD aqueous solutions. The filtered HPβCD-ITZ solution that was sampled at 24 hr containing 5.3 mg/mL of ITZ, 150 mg/mL of HPβCD and 0.54 mg/mL of NaCl was found to be isotonic with an osmolality ranging from 290 to 310 mOsm/kg and a measured pH of 6.8. The lung lining fluid was reported to be either isotonic or slightly hypotonic and slightly acidic (pH 6.9) relative to plasma [44], hence the good compatibility of the HPβCD-ITZ solution with the lung fluid was evident. With considerably high levels of dissolved ITZ and a physiological pH value, the HPβCD-ITZ isotonic solution was shown to be suitable for *in vivo* dosing as solubilized form of ITZ.

4.4.2 Solid State Analysis of Inclusion Complexes

4.4.2.1 DSC

DSC is used in pharmaceutical area to establish the identity and purity of solid-state systems and detect interaction of the components. Incorporation of a guest molecule in CD cavity can cause disappearance or shifting of its melting, boiling and sublimation points [45]. The thermograms of the pure components, physical mixture and lyophilized powder of HPβCD-ITZ are presented in Figure 4.3. Micronized crystalline ITZ demonstrated a single, defined endotherm at 171.9 °C, corresponding to its melting point. The thermogram of pure HPβCD powder exhibited a broad endothermic peak between 50-120 °C, corresponding to the dehydration of HPβCD [46], since βCD did not produce any peaks of interest when examined by DSC [47]. In the physical mixture, the characteristic melting peak of ITZ appeared at 168.3 °C but with much lower intensity due to the dilution by HPβCD, indicating the absence of significant drug–cyclodextrin interactions. For the dry powder of HPβCD-ITZ, no appreciable endothermic event associated with the melting of ITZ was observed, suggesting the formation of true inclusion complexes between ITZ molecules and HPβCD at a weight ratio of 5.3: 150 (molar ratio of 1:12).

4.4.2.2 FTIR analysis

FTIR spectra of pure ITZ, pure HPβCD, physical mixture (ITZ: HPβCD= 5.3: 150, weight ratio), and lyophilized dry powder of HPβCD-ITZ are presented in Figure 4.4. The characteristic bands of pure ITZ occurred at 3126 and 3069 cm^{-1} due to absorption of the NH_2 groups; at 2962 cm^{-1} due to CH_2 stretching and the large peak at 1698 cm^{-1} due to C=O stretching. The wave numbers observed at 1609 and 1425 cm^{-1}

were assigned to the C=N and C-N bonds respectively. The bands at 1510 and 1451 cm^{-1} are due to C-H deformation. These characteristic bands are consistent with previous reports [48]. The fingerprint region (1400-600 cm^{-1}) contains a large number of bands characteristic of vibration within the molecule. Changes in the FTIR spectra such as shift of characteristic bands, disappearance or reduction in intensity, and appearance of new bands might be related to possible drug-CD interaction and/or amorphization of the product [49].

The spectral pattern of the physical mixture corresponds to the sum of the band positions of the FTIR spectra of both ITZ and HPβCD although the intensity of the ITZ bands are low due to the low weight ratio of ITZ. The results indicated no or minor interaction between ITZ and HPβCD molecules in the physical mixture. In contrast, the spectra of the dry powder of HPβCD-ITZ demonstrated complete smoothing of the ITZ characteristic bands that were seen in the physical mixture spectra. Additionally, smoothing was evident for bands situated between wave numbers of 1170-1010 cm^{-1} as compared to those of the pure HPβCD and physical mixture, indicating interactions occurring in the HPβCD-ITZ dry powder.

4.4.2.3 XPS analysis

XPS is a surface sensitive technique used to probe the elemental composition of the surfaces with an analysis depth of less than 100 Å [50]. ITZ molecule ($C_{35}H_{38}Cl_2N_8O_4$) is distinguished from HPβCD molecules (empirical formula: $C_{42}H_{70-n}O_{35}(C_3H_7)_n$) present in the HPβCD/ITZ systems due to the presence of two chlorine atoms and eight nitrogen atoms in the ITZ molecule, which can be used as probing markers. As βCD has an external diameter of 1.53 nm and internal diameter of

0.78 nm, encapsulated ITZ in its cavity can not be detected by XPS but ITZ molecules situated on the outside surface can be probed by its elemental markers.

The atomic concentration (%) of carbon, oxygen, nitrogen and chlorine on the surface of the lyophilized dry powders of HPβCD/ITZ inclusion complex sampled at 1, 24 and 48 hr after dispersing amorphous ITZ in 15% HPβCD as well as the physical mixture are presented in Table 4.1. The detection of 4.99% nitrogen and 0.65% chlorine on the surface of the physical mixture demonstrated the presence of free ITZ molecules. A decrease in chlorine and nitrogen content is observed in the HPβCD/ITZ inclusion complex sampled at 1 hr, suggesting that considerable portion of ITZ molecules hidden from the surface. In the HPβCD/ITZ inclusion complexes sampled at 24 and 48 hr, chlorine and nitrogen were no longer quantifiable, suggesting the majority of the ITZ molecules in the systems were encapsulated inside the HPβCD cavities and also possibly within micelles formed by HPβCD aggregation [51]. XPS data provided evidence of interactions between ITZ and HPβCD molecules by ruling out the existence of free, unencapsulated ITZ molecules from the powder surface.

Based on the solid state characterizations by DSC, FTIR and XPS, it can be concluded that in the HPβCD-ITZ solution sampled at 24 hr, the majority of ITZ molecules were encapsulated, forming dynamic inclusion complexes. ITZ molecules inside the CD cavities were in equilibrium with free ITZ molecules in the solution. The focus of this study is the *in vivo* pharmacokinetic profiles following pulmonary administration of solubilized ITZ molecules as compared to ITZ nanoparticles. In consideration of the time to attain and maintain a high concentration of ITZ in solution, and based on the observations from the solubility studies and solid state characterizations,

the filtrate sampled at 24 hr from the amorphous ITZ dispersion in 15% HPβCD isotonic solution (ITZ:HPβCD=5.3:150 by weight ratio) was selected as the solubilized ITZ solution for *in vivo* dosing.

4.4.3 Aerodynamic Particle Size Analysis

HPβCD-ITZ solution and URF-ITZ colloidal dispersion (equivalent to 5.3 mg/mL of ITZ) as depicted in Figure 4.5. were aerosolized using an Aeroneb® Professional micropump nebulizer. The aerodynamic particle size distributions of the nebulized aerosols were measured using the 8-stage Anderson cascade impactor with an air-flow rate of 28.3 L/min. The nebulizer produced an aqueous mist of fine droplets with sizes ranging between 1 and 4 μm, which falls within the optimal size range of 1-5 μm for effective aerosol delivery into the deep lung after inhalation [52]. The aerodynamic parameters of the aerosols are summarized in Table 4.2. The TED of aerosolized HPβCD-ITZ solution and URF-ITZ colloidal dispersion were 22.04 and 21.78 mg, respectively out of the total of 27 mg ITZ available for nebulization. Their corresponding fine particle doses were 11.58 and 11.93 mg. Fine particle dose was defined as TED × FPF, the amount of aerosol droplets entering the impactor that was less than 4.7 μm, representing the dose delivered to the deep lung. The MMAD of the aerosol droplets from nebulized HPβCD-ITZ solution and URF-ITZ colloidal dispersion were 3.19 and 2.80 μm, respectively with GSD of 2.28 and 2.83, respectively, indicating their suitability for deep lung delivery.

4.4.4 Pharmacokinetic Study of Single Dose Inhalation in Mice

The mice were exposed to the single dose aerosols of the nebulized HPβCD-ITZ solution and URF-ITZ colloidal dispersion (equivalent to 27 mg of ITZ total) for a duration of 18 and 11 min, respectively. The longer nebulization time of the HPβCD-ITZ solution was due to its higher viscosity. The concentration-time profile of ITZ in lung tissue obtained from the single dose 24-hr pharmacokinetic study is illustrated in Figure 4.6. Immediately upon finishing nebulization of the compositions (0 hr post dosing), a C_{max} of 3.38±1.16 and 4.86±2.67 μg/g wet lung weight of ITZ was measured in lungs from the HPβCD-ITZ solution and URF-ITZ colloidal dispersion dosing groups, respectively. The elimination of ITZ from lungs appeared to be 2-phased with an initial rapid elimination/distribution phase from 0 to 4 hr with $K_{distribution}$ rate constants of 0.143 and 0.238 hr^{-1} and corresponding $t_{1/2}$s of 4.87 and 2.91 hr for HPβCD-ITZ and URF-ITZ, respectively. This was followed by slow elimination from 6 to 24 hr with $K_{elimination}$ rate constants of 0.022 and 0.025 hr^{-1} and the corresponding $t_{1/2}$ of 30.9 and 28.0 hr for HPβCD-ITZ and URF-ITZ, respectively (Table 4.3.). The fast elimination of ITZ from lung tissue coincided with absorption into the systemic circulation. At 24 hr post dosing, their corresponding ITZ levels in the lungs were 0.98±0.40 and 0.65±0.29 μg/g wet lung weight, respectively, probably due to slow elimination. Their AUC_{0-24} values were calculated to be 32.0 and 27.2 μg·hr/mL, respectively. The C_{max} of deposited ITZ in lung after a single dose inhalation of nebulized HPβCD-ITZ solution and URF-ITZ colloidal dispersion were not statistically different, although the latter exhibited a higher mean value. This could partly be attributed to variation in rodent behavior within the dosing apparatus and breathing patterns since the two formulations demonstrated comparable MMADs (both within the 1- 4 μm range).

The drug concentration-time profiles of ITZ and its main metabolite hydroxyl-itraconazole (HyITZ) in serum are illustrated in Figures 4.7. and 4.8., and the pharmacokinetic parameters of ITZ and HyITZ are listed in Table 4.4. The C_{max} of ITZ for the HPβCD-ITZ solution and URF-ITZ colloidal dispersion dosing groups were 0.48±0.11 and 0.55±0.084 μg/mL measured at 1.5 and 3 hr after dosing, respectively. Their corresponding $K_{01\ absorption}$ and $K_{10\ elimination}$ rate constants were 0.679 and 0.718 hr^{-1}, and 0.144 and 0.168 hr^{-1}, respectively, indicating a much faster absorption and slower elimination of ITZ from HPβCD-ITZ solution as compared to URF-ITZ nanoparticle dispersion. The corresponding $AUC_{0-\infty}$ values were 3.26 and 4.17 μg·hr/mL.

Upon absorption into systemic circulation, ITZ is primarily metabolized in the liver by a large number of pathways producing more than 30 metabolites. The major metabolite, HyITZ, has considerable antifungal activity similar to that of ITZ and contributes to the overall potent antifungal properties of ITZ [53, 54]. In this study, the C_{max} of HyITZ for HPβCD-ITZ and URF-ITZ dosing group were 0.49±0.14 and 0.64±0.17 μg/mL at 2 and 4 hr post dosing, respectively, exhibiting a lag-time between 30 to 60 minutes with respect to the t_{max} of the parent compound. The K_{01} and K_{10} rate constants of HyITZ in serum are very similar to those of ITZ. Their $AUC_{0-\infty}$ values were 3.98 and 5.26 μg·hr/mL, respectively. HyITZ reached higher plasma concentrations than the parent compound, in agreement with the literature [55]. However, HyITZ levels in lung tissues were not quantifiable because they were below the detection limit of the HPLC method. This is because drug-metabolizing enzymes exist in much lower concentrations in the lungs than the liver and gastrointestinal tract [56].

The pharmacokinetic profile of inhaled HPβCD-ITZ in the lungs and blood differed substantially from the findings by Tolman and coworkers [33] who administered a single dose (6.25 mg/mL, 5 mL) of nebulized voriconazole solubilized in SBEβCD solution (prepared by diluting the Vfend® I.V. aqueous solution) to mice. The rapid absorption of voriconazole into systemic circulation was observed with t_{max} values of 20 to 30 min in plasma after completion of dosing, similar to pharmacokinetics following intravenous drug administration [33]. Moreover, elimination of voriconazole from lung tissue was relatively fast such that the drug level was undetectable after 6–8 hr while the plasma levels remained quantifiable for up to 24 hr post dosing. In contrast, inhalation of HPβCD-ITZ aerosols resulted in ITZ t_{max} of 1.6 hr in blood and ITZ levels in lung were still high at about 1 μg ITZ/g wet lung weight at 24 hr post dosing. This is a notable finding since both of the triazoles were solubilized in solutions of βCD derivatives and the *in vivo* experiment conditions were similar.

Literature regarding the pulmonary applications of cyclodextrin in formulating poorly-water soluble drugs is limited, despite increasing interest in pulmonary delivery of therapeutics. Little has been reported about the pharmacokinetics of drugs and CDs following pulmonary administration. The most significant barrier to absorption of inhaled drug is the pulmonary epithelium [57]. Cabral Marques et al. [58] studied the absorption of several cyclodextrin derivatives themselves following intratracheal instillation into rabbits. Interestingly, the bioavailabilities of intratracheal instilled βCD, dimethyl-βCD and HPβCD were found to be as high as 66, 74 and 80%, respectively. These values were considerably higher than CD absorption following oral administration. The systemic absorption of CD molecules from the gastrointestinal tract is limited because of their bulkiness and hydrophilicity [59]. However, CDs can permeate the pulmonary Calu-3

cells, suggesting the ability of HPβCD to be absorbed into systemic circulation from the lungs [60]. The t_{max} in plasma for HPβCD was reported to be about 113 min as compared to 20-30 min for βCD and dimethyl-βCD, and the plasma elimination of the three CDs seemed to be independent of the route of administration [58]. In our study, the pharmacokinetic profile of nebulized HPβCD-ITZ in serum showed an initial lag phase prior to reaching C_{max} at about 90 min and a prolonged post-peak decline such that ITZ levels were still detectable at 24 hr. These features were well matched with the reported pharmacokinetic profile of pure HPβCD following lung administration [58]. Therefore, it appears that the pharmacokinetics of ITZ from the inhaled HPβCD-ITZ formulation seemed to have been modified to follow the pharmacokinetics of HPβCD.

However, the present findings contradict previous reports which had demonstrated the absence of influence of CD on pharmacokinetics of drugs. Previous researchers attempted to use HPβCD as a carrier to modify pulmonary absorption of small, hydrophobic molecules, with a hypothesis that inclusion of a guest molecule within HPβCD that can also be absorbed would present a larger entity for absorption. Marques et al. [58] made an HPβCD-salbutamol complex, with the intent of slowing the pulmonary absorption of salbutamol in rabbits. Unexpectedly, the pulmonary absorption of salbutamol was not significantly extended by HPβCD complexation. The authors suggested that drug-HPβCD complexes with larger stability constants may display extended absorption profiles with a decrease in the apparent rate of drug absorption. A subsequent study [61] employed HPβCD for delaying the absorption of rolipram and testosterone (with stability constants of 260 and 12 000 M^{-1}, respectively, versus 60-70 M^{-1} for salbutamol) in rats. It was also observed that HPβCD exerted little effect on rolipram absorption and no effect on testosterone absorption *in vivo*. The authors

suggested that rapid dissociation of the drugs from HPβCD may be occurring *in vivo* due to the potential competition of endogenous cholesterol with these drugs for the CDs.

To explore the potential reasons for the discrepancy in pharmacokinetics observed between the above reported studies and our current work, the movement of the inhaled HPβCD-ITZ aerosols from deposition into alveoli to absorption into systemic circulation was examined mechanistically.

Each droplet of the nebulized aerosol of HPβCD-ITZ contains many ITZ molecules predominantly encapsulated inside HPβCD as demonstrated *in vitro*. The inhaled aerosol deposited mainly in lung alveoli as characterized by their MMAD. In the alveoli, the nebulized droplets containing HPβCD-ITZ coalesced into the thin layer of lung lining fluid. Total alveolar fluid volume for mice was estimated to be 10 μL, based on the alveolar surface area of 680 cm^2 for mice [62] as compared to a total alveolar surface area of 1,022,000 cm^2 and average alveolar surface fluid volume of 15 mL in a human [56, 63]. Moreover, based on the lung drug deposition of 3.38 μg ITZ/g wet lung weight upon completing nebulization and an average mouse lung weight of 0.16 g, an estimated mass of 0.54 μg ITZ (equal to 0.1 μL of the HPβCD-ITZ solution used) was deposited in each mouse lung. The deposition of inhaled HPβCD-ITZ has insignificant influence on the volume of lung lining fluid. Therefore ITZ concentration in the lung lining fluid is estimated to be 54 μg/mL (i.e. 0.54 μg ITZ/10 μL total alveolar fluid volume), which is dramatically higher than the equilibrium solubility of ITZ of about 10 ng/mL in simulated lung fluid as previously reported [29]. Meanwhile, the inhaled HPβCD-ITZ was diluted 100-times following lung deposition. HPβCD-ITZ is present as dynamic inclusion complexes without irreversible covalent bonds. The ITZ molecules

contained within the HPβCD cavities were in equilibrium with free ITZ molecules in the lining fluid. The major driving force for drug release from these dynamic inclusion complexes is simple dilution [64, 65]. Only at rare occasions when the binding stability constants are greater than 10^5 M^{-1}, the persistence of the drug and CD interaction was probable despite dilution. Generally, the stability constant values are found within the range of $10 - 1\times10^3$ M^{-1} while values of 1×10^4 M^{-1} were seen occasionally. With reported binding stability constants of ITZ/HPβCD 1:1 complexes of 1000-2000 M^{-1} at pH 7 [6, 66], dissociation of ITZ from the inclusion complexes may presumably occur easily owing to the significant concentration decrease of free ITZ molecules.

Once ITZ was released from the host HPβCD, it followed its inherent pharmacokinetics and was absorbed across the mucosal membrane [67, 68]. For drugs with low solubility, the mass transport of the drugs across the GI tract mucosal absorption surface was proposed to be equal to the solubility times the permeability [69]. Applying this equation to lung epithelium, the systemic absorption rate of a drug deposited within the lungs is determined by the product of its membrane permeability (P), the available surface area over which it is spread (A), and the drug concentration in the fluids (C), *i.e.* absorption rate = P × A × C. The drug concentration in blood is assumed to be insignificant as compared to the lung concentration and the transfer from lung to blood is irreversible [70]. Since the inhaled aerosol droplets mainly deposited in the lung alveoli where the barrier is the thinnest [56], the value for A is fixed. Since HPβCD-ITZ in the lung lining fluid was still effectively solubilized, solubilization was not a rate-limiting step any more. Thus, permeability of ITZ through lung epithelium seemed to be the factor controlling the rate of molecular transport. It is widely accepted that small, mildly hydrophobic molecules can show extremely rapid absorption kinetics from the lungs [57].

Typical drug molecules with a log P value (octanol–water partition coefficient) greater than 1 are expected to be absorbed, with absorption half-lives (*i.e.*, the time required for half of the total number of molecules deposited in the lungs to disappear from the tissue) of approximately 1 minute or so [71]. According to this principle, with a molecular weight of 349.3 and moderate lipophilicity (log P =1.8) [72], voriconazole was well matched with the criteria for high permeability across mucosal membranes. This may explain the rapid and high extent distribution of voriconazole from lung to systemic circulation after its delivery to the deep lung. In contrast, ITZ molecule is larger (MW: 705.6) and has a calculated log P value of 6.2 [6] suggesting its poor permeability. Classified as a BCS class II drug, ITZ was deemed to have high membrane permeability. However, this is relative to its extremely low solubility. In the absence of poor solubility, permeability seems to have emerged as the primary factor that hindered drug absorption across the mucosal membrane.

Tolman et al. [33] used an approximation of the drug partition coefficient (based on the lung-to-plasma ratios of C_{max} and $AUC_{0–6}$) with the calculated values between 1.4 - 1.6 to explain the fast absorption and distribution of voriconazole across lung mucosal surfaces to systemic circulation with minimal drug retained in lung tissue. Accordingly, after inhalation of the nebulized aerosols of HPβCD-ITZ, the calculated partition coefficients for C_{max} and AUC were 9.7 and 12.7, respectively, suggesting a relatively poor transport of ITZ from lung to systemic circulation. The calculated partition coefficients for the inhaled URF-ITZ colloidal dispersion were 9.9 and 7.3, respectively, falling into the same range. Therefore, it was apparent that the calculated partition coefficient of ITZ was independent of the formulations used in this study.

Based on the dynamic equilibrium between free ITZ and the inclusion complexes, there should still be a considerable portion of ITZ remaining as HPβCD-ITZ complexes in the lung lining fluid. It could be possible that ITZ was carried across the lung epithelium together with HPβCD by paracellular diffusion due to the hydrophilicity of HPβCD [57]. However, the apparent permeability coefficient of HPβCD is rather low, based on the typical measured permeabilities of molecules with similar sizes and hydrophilicities in lung cell culture, which range from 10^{-7} to 10^{-8} cm/s [73]. Thus, HPβCD-ITZ inclusion complexes may move across the lung epithelium fairly slowly. It is reported that the time required for HPβCD to reach the maximum plasma level was 113 min (1.9 hr) in rabbit after intratracheal instillation [58], which approximate the ITZ T_{max} of 1.5 hr in serum in the present study. Absorption of ITZ as HPβCD-ITZ inclusion complexes from lung epithelium could be one of the potential mechanisms contributing to the total transport of ITZ from lung to blood after inhalation of nebulized HPβCD-ITZ solution.

In comparison, upon deposition of the inhaled aerosol droplets containing URF-ITZ (ITZ:mannitol:lecithin=1:0.5:0.2, weight ratio) nanoparticles in the lung lining fluid, they underwent rapid dissolution and were able to attain and maintain high magnitude of supersaturation, as indicated in simulated lung fluid *in vitro* [29]. The rate and extent of dissolution, as well as permeability across mucosal membrane influenced the absorption rate of ITZ through the lung epithelium to reach systemic circulation. Worthy to note is the role of lecithin which contains mainly dipalmitoylphosphatidylcholine (DPPC), the primary component of endogenous human lung surfactant [74]. Besides playing an important role in improving the wettability of the nanoparticles containing ITZ, lecithin also acted as a permeation enhancer. It could induce changes in the cytoskeleton which

affect tight junctions and accelerate paracellular passages of drugs [75], resulting in enhanced permeation of ITZ molecules through lung epithelium into systemic circulation. In the present study, the higher C_{max} and AUC of ITZ in serum of mice inhaled nebulized URF-ITZ colloidal dispersion, compared to mice inhaled HPβCD-ITZ solution, may be attributed to the permeation enhancement of lecithin in the URF-ITZ composition.

Since ITZ in HPβCD-ITZ solution is effectively solubilized, it was immediately available for absorption. The elimination of the phase-to-phase transition which limited bioavailability [37], rendered HPβCD-ITZ about 1.3 hr faster in reaching t_{max} as compared to URF-ITZ colloidal dispersion that required a prior dissolution step of the nanoparticle matrices.

In our previous report, where mice inhaled a nebulized URF-ITZ colloidal dispersion at a single dose of 100 mg ITZ equivalent (5 mL × 20 mg ITZ/mL dispersion), an ITZ C_{max} of 21.19 μg/g wet lung weight and 1.64 μg/mL in serum was achieved [29]. In this study, under the identical *in vivo* experimental conditions, except for the reduction of ITZ dosage to about one-fourth of the previously used dose, very similar drug concentration-time curves in lung and serum were observed with C_{max} values of 4.86 μg/g wet lung weight and 492 ng/mL, respectively. Those values were almost proportional to the dose reduction, suggesting non-saturable absorption of inhaled URF-ITZ colloidal dispersion from lung to systemic circulation over a wide concentration range. This implies the capacity to choose a flexible dosing regimen.

4.5 CONCLUSION

An aqueous solution containing 5.3 mg/mL of ITZ in inclusion complex with HPβCD suitable for deep lung delivery using the Aeroneb® micropump nebulizer was made of amorphous ITZ without other excipients. Inhalation of nebulized aerosols of the aqueous ITZ solution and a nanoparticulate ITZ colloidal dispersion produced similar ITZ lung depositions due to comparable aerodynamic properties of the aerosols. Solubilized ITZ exhibited faster systemic absorption than the nanoparticulate ITZ colloidal dispersion due to the elimination of phase-to-phase transition that required for ITZ release from nanoparticulates. Permeability of ITZ across the lung epithelium becomes the rate-limiting factor that hindered the solubilized ITZ from achieving rapid systemic absorption, as compared to other reported inhaled drug solutions.

4.6 REFERENCES

1. T.A. Clarkand R.A. Hajjeh. Recent trends in the epidemiology of invasive mycoses. Current Opinion in Infectious Diseases. 15:569-574 (2002).

2. T.F. Patterson. Advances and challenges in management of invasive mycoses. Lancet. 366:1013-1025 (2005).

3. K. De Beuleand J. Van Gestel. Pharmacology of itraconazole. Drugs. 61:27-37 (2001).

4. J.H. Rex, M.A. Pfaller, J.N. Galgiani, M.S. Bartlett, A. Espinel-Ingroff, M.A. Ghannoum, M. Lancaster, F.C. Odds, M.G. Rinaldi, T.J. Walsh, and A.L. Barry. Development of interpretive breakpoints for antifungal susceptibility testing: conceptual framework and analysis of in vitro-in vivo correlation data for fluconazole, itraconazole, and candida infections. Subcommittee on Antifungal Susceptibility Testing of the National Committee for Clinical Laboratory Standards. Clin Infect Dis. 24:235-247 (1997).

5. J.D. Sobel. Practice guidelines for the treatment of fungal infections. For the Mycoses Study Group. Infectious Diseases Society of America. Clinical Infectious Diseases. 30:652 (2000).

6. J. Peeters, P. Neeskens, J.P. Tollenaere, P. Van Remoortere, and M.E. Brewster. Characterization of the Interaction of 2-hydroxypropyl-beta-cyclodextrin with itraconazole at pH 2, 4, and 7. J Pharm Sci. 91:1414-1422 (2002).

7. W. Yang, N.P. Wiederhold, and R.O. Williams, 3rd. Drug delivery strategies for improved azole antifungal action. Expert Opin Drug Deliv. 5:1199-1216 (2008).

8. J.Y. Hong, J.K. Kim, Y.K. Song, J.S. Park, and C.K. Kim. A new self-emulsifying formulation of itraconazole with improved dissolution and oral absorption. J Control Release. 110:332-338 (2006).

9. M.J. Park, S. Ren, and B.J. Lee. In vitro and in vivo comparative study of itiraconazole bioavailability when formulated in highly soluble self-emulsifying system and in solid dispersion. Biopharm Drug Dispos. 28:199-207 (2007).

10. K. Six, T. Daems, J. de Hoon, A. Van Hecken, M. Depre, M.P. Bouche, P. Prinsen, G. Verreck, J. Peeters, M.E. Brewster, and G. Van den Mooter. Clinical study of solid dispersions of itraconazole prepared by hot-stage extrusion. Eur J Pharm Sci. 24:179-186 (2005).

11. D.A. Miller, J.T. McConville, W. Yang, R.O. Williams, 3rd, and J.W. McGinity. Hot-melt extrusion for enhanced delivery of drug particles. Journal of pharmaceutical sciences. 96:361-376 (2007).

12. D.A. Miller, J.C. DiNunzio, W. Yang, J.W. McGinity, and R.O. Williams. Targeted intestinal delivery of supersaturated itraconazole for improved oral absorption. Pharmaceutical research. 25:1450-1459 (2008).

13. J.A. Barone, J.G. Koh, R.H. Bierman, J.L. Colaizzi, K.A. Swanson, M.C. Gaffar, B.L. Moskovitz, W. Mechlinski, and V. Vandevelde. Food Interaction and Steady-State Pharmacokinetics of Itraconazole Capsules in Healthy Male-Volunteers. Antimicrob Agents Ch. 37:778-784 (1993).

14. p.l. Sporanox®. Package insert. Sporanox capsules/oral solution/Sporanox I.V. (itraconazole).

15. J.S. Hostetler, L.H. Hanson, and D.A. Stevens. Effect of cyclodextrin on the pharmacology of antifungal oral azoles. Antimicrob Agents Chemother. 36:477-480 (1992).

16. K.A. Marr, R.A. Carter, F. Crippa, A. Wald, and L. Corey. Epidemiology and outcome of mould infections in hematopoietic stem cell transplant recipients. Clin Infect Dis. 34:909-917 (2002).

17. J. Li, C.R. Rayner, R.L. Nation, R.J. Owen, D. Spelman, K.E. Tan, and L. Liolios. Heteroresistance to colistin in multidrug-resistant Acinetobacter baumannii. Antimicrob Agents Chemother. 50:2946-2950 (2006).

18. R.H. Muller, C. Jacobs, and O. Kayser. Nanosuspensions as particulate drug formulations in therapy Rationale for development and what we can expect for the future. Adv Drug Deliver Rev. 47:3-19 (2001).

19. C. Jacobsand R.H. Muller. Production and characterization of a budesonide nanosuspension for pulmonary administration. Pharmaceut Res. 19:189-194 (2002).

20. K.D. Ostrander, H.W. Bosch, and D.M. Bondanza. An in-vitro assessment of a NanoCrystal (TM) beclomethasone dipropionate colloidal dispersion via ultrasonic nebulization. European Journal of Pharmaceutics and Biopharmaceutics. 48:207-215 (1999).

21. W. Yang, J.I. Peters, and R.O. Williams. Inhaled nanoparticles - A current review. International journal of pharmaceutics. 356:239-247 (2008).

22. W.K. Kraft, B. Steiger, D. Beussink, J.N. Quiring, N. Fitzgerald, H.E. Greenberg, and S.A. Waldman. The pharmacokinetics of nebulized nanocrystal budesonide suspension in healthy volunteers. Journal of Clinical Pharmacology. 44:67-72 (2004).

23. E.J. Elder, J.E. Hitt, T.L. Rogers, C.J. Tucker, S. Saghir, G.B. Kupperblatt, S. Svenson, and J.C. Evans. Particle engineering of poorly water soluble drugs by controlled precipitation. Acs Sym Ser. 924:292-304 (2006).

24. J.M. Vaughn, X. Gao, M.J. Yacaman, K.P. Johnston, and R.O. Williams, 3rd. Comparison of powder produced by evaporative precipitation into aqueous solution (EPAS) and spray freezing into liquid (SFL) technologies using novel Z-contrast STEM and complimentary techniques. Eur J Pharm Biopharm. 60:81-89 (2005).

25. J.M. Vaughn, J.T. McConville, D. Burgess, J.I. Peters, K.P. Johnston, R.L. Talbert, and R.O. Williams, 3rd. Single dose and multiple dose studies of itraconazole nanoparticles. Eur J Pharm Biopharm. 63:95-102 (2006).

26. J.T. McConville, K.A. Overhoff, P. Sinswat, J.M. Vaughn, B.L. Frei, D.S. Burgess, R.L. Talbert, J.I. Peters, K.P. Johnston, and R.O. Williams, 3rd. Targeted high lung concentrations of itraconazole using nebulized dispersions in a murine model. Pharm Res. 23:901-911 (2006).

27. B.J. Hoeben, D.S. Burgess, J.T. McConville, L.K. Najvar, R.L. Talbert, J.I. Peters, N.P. Wiederhold, B.L. Frei, J.R. Graybill, R. Bocanegra, K.A. Overhoff, P. Sinswat, K.P. Johnston, and R.O. Williams. In vivo efficacy of aerosolized nanostructured itraconazole formulations for prevention of invasive pulmonary aspergillosis. Antimicrob Agents Ch. 50:1552-1554 (2006).

28. C.A. Alvarez, N.P. Wiederhold, J.T. McConville, J.I. Peters, L.K. Najvar, J.R. Graybill, J.J. Coalson, R.L. Talbert, D.S. Burgess, R. Bocanegra, K.P. Johnston, and R.O. Williams, 3rd. Aerosolized nanostructured itraconazole as prophylaxis against invasive pulmonary aspergillosis. J Infect. 55 68-74 (2007).

29. W. Yang, J. Tam, D.A. Miller, J. Zhou, J.T. McConville, K.P. Johnston, and R.O. Williams. High bioavailability from nebulized itraconazole nanoparticle dispersions with biocompatible stabilizers. International journal of pharmaceutics. 361:177-188 (2008).

30. F.Y. Liu, Z. Shao, D.O. Kildsig, and A.K. Mitra. Pulmonary delivery of free and liposomal insulin. Pharm Res. 10:228-232 (1993).

31. K. Koushik, D.S. Dhanda, N.P. Cheruvu, and U.B. Kompella. Pulmonary delivery of deslorelin: large-porous PLGA particles and HPbetaCD complexes. Pharm Res. 21:1119-1126 (2004).

32. Z.H. Shao, Y.P. Li, T. Chermak, and A.K. Mitra. Cyclodextrins as Mucosal Absorption Promoters of Insulin .2. Effects of Beta-Cyclodextrin Derivatives on Alpha-Chymotryptic Degradation and Enteral Absorption of Insulin in Rats. Pharmaceut Res. 11:1174-1179 (1994).

33. J.A. Tolman, N.A. Nelson, Y.J. Son, S. Bosselmann, N.P. Wiederhold, J.I. Peters, J.T. McConville, and R.O. Williams, 3rd. Characterization and pharmacokinetic analysis of aerosolized aqueous voriconazole solution. Eur J Pharm Biopharm. 72:199-205 (2009).

34. USP. Aerosols, Nasal Sprays, Metered-dose Inhalers, and Dry Powder Inhalers USP 31 - NF 26 The United States Pharmacopeial Convention, Rockville, MD, 2008.

35. J. Pitha, L. Szente, and J. Szejtli. Molecular encapsulation of drugs by cyclodextrins and congeners. In S.D. Bruck (ed.), Controlled drug delivery, CRC Press, Inc., Boca Raton, Fla, 1983.

36. M.E. Brewster, J.W. Simpkins, M.S. Hora, W.C. Stern, and N. Bodor. The Potential Use of Cyclodextrins in Parenteral Formulations. Journal of Parenteral Science and Technology. 43:231-240 (1989).

37. D.A. Stevens. Itraconazole in cyclodextrin solution. Pharmacotherapy. 19:603-611 (1999).

38. V.J. Stellaand Q. He. Cyclodextrins. Toxicol Pathol. 36:30-42 (2008).

39. A.H. Al-Marzouqi, I. Shehatta, B. Jobe, and A. Dowaidar. Phase solubility and inclusion complex of itraconazole with beta-cyclodextrin using supercritical carbon dioxide. J Pharm Sci. 95:292-304 (2006).

40. M.E. Brewster, R. Vandecruys, J. Peeters, P. Neeskens, G. Verreck, and T. Loftsson. Comparative interaction of 2-hydroxypropyl-beta-cyclodextrin and sulfobutylether-beta-cyclodextrin with itraconazole: phase-solubility behavior and stabilization of supersaturated drug solutions. Eur J Pharm Sci. 34:94-103 (2008).

41. M.E. Brewster, P. Neeskens, and J. Peeters. Solubilization of itraconazole as a function of cyclodextrin structural space. Journal of Inclusion Phenomena and Macrocyclic Chemistry. 57:561-566 (2007).

42. T. Loftsson, M. Masson, and J.F. Sigurjonsdottir. Methods to enhance the complexation efficiency of cyclodextrins. Stp Pharma Sciences. 9:237-242 (1999).

43. T. Loftssonand M. Masson. The effects of water-soluble polymers on cyclodextrins and cyclodextrin solubilization of drugs. Journal of Drug Delivery Science and Technology. 14:35-43 (2004).

44. D. Valeyre, P. Soler, G. Basset, P. Loiseau, J. Pre, P. Turbie, J.P. Battesti, and R. Georges. Glucose, K+, and Albumin Concentrations in the Alveolar Milieu of Normal Humans and Pulmonary Sarcoidosis Patients. Am Rev Respir Dis. 143:1096-1101 (1991).

45. H.M.C. Marques, J. Hadgraft, and I.W. Kellaway. Studies of cyclodextrin inclusion complexes .1. the salbutamol-cyclodextrin complex as studied by phase solubility and DSC International journal of pharmaceutics. 63:259-266 (1990).

46. M. Echezarreta-Lopez, J.J. Torres-Labandeira, L. Castineiras-Seijo, L. Santana-Penin, and J.L. Vila-Jato. Complexation of the interferon inducer, bropirimine, with hydroxypropyl-beta-cyclodextrin. Eur J Pharm Sci. 9:381-386 (2000).

47. S. Jonesand G. Parr. The acetotoluides as models for studying cyclodextrin inclusion complexes International journal of pharmaceutics. 36:223-231 (1987).

48. D.I. Nesseem. Formulation and evaluation of itraconazole via liquid crystal for topical delivery system. J Pharm Biomed Anal. 26:387-399 (2001).

49. A.H. Al-Marzouqi, H.M. Elwy, I. Shehadi, and A. Adem. Physicochemical properties of antifungal drug-cyclodextrin complexes prepared by supercritical carbon dioxide and by conventional techniques. J Pharm Biomed Anal. 49:227-233 (2009).

50. C. Dahlberg, A. Millqvist-Fureby, and M. Schuleit. Surface composition and contact angle relationships for differently prepared solid dispersions. European Journal of Pharmaceutics and Biopharmaceutics. 70:478-485 (2008).

51. M.E. Brewsterand T. Loftsson. Cyclodextrins as pharmaccutical solubilizers. Adv Drug Deliver Rev. 59:645-666 (2007).

52. P. Byronand E. Phillips. Absorption, clearance and dissolution in the lung. In P.R. Byron (ed.), Respiratory Drug Delivery CRC, Boca Raton FL, 1990, pp. 107–141.

53. J. Heykants, A. Vanpeer, V. Vandevelde, P. Vanrooy, W. Meuldermans, K. Lavrijsen, R. Woestenborghs, J. Vancutsem, and G. Cauwenbergh. The Clinical Pharmacokinetics of Itraconazole - an Overview. Mycoses. 32:67-87 (1989).

54. J.M. Poirierand G. Cheymol. Optimisation of itraconazole therapy using target drug concentrations. Clinical Pharmacokinetics. 35:461-473 (1998).

55. L. Willems, R. van der Geest, and K. de Beule. Itraconazole oral solution and intravenous formulations: a review of pharmacokinetics and pharmacodynamics. J Clin Pharm Ther. 26:159-169 (2001).

56. J. Patton. Mechanisms of macromolecule absorption by the lungs. Advanced Drug Delivery Review 19:3–36 (1996).

57. J. Patton, C. Fishburn, and J. Weers. The lungs as a portal of entry for systemic drug delivery. Proc Am Thorac Soc. 1:338-344 (2004).

58. H.M.C. Marques, J. Hadgraft, I.W. Kellaway, and G. Taylor. Studies of Cyclodextrin Inclusion Complexes .3. The Pulmonary Absorption of Beta-Cyclodextrin, Dm-Beta-Cyclodextrin and Hp-Beta-Cyclodextrin in Rabbits. International journal of pharmaceutics. 77:297-302 (1991).

59. T. Irieand K. Uekama. Pharmaceutical applications of cyclodextrins .3. Toxicological issues and safety evaluation. J Pharm Sci. 86:147-162 (1997).

60. L. Matilainen, T. Toropainen, H. Vihola, J. Hirvonen, T. Jarvinen, P. Jarho, and K. Jarvinen. In vitro toxicity and permeation of cyclodextrins in Calu-3 cells. Journal of Controlled Release. 126:10-16 (2008).

61. D.A. Wall, J. Marcello, D. Pierdomenico, and A. Farid. Administration as Hydroxypropyl-Beta-Cyclodextrin Complexes Does Not Slow Rates of Pulmonary Drug Absorption in Rat. Stp Pharma Sciences. 4:63-68 (1994).

62. A. Geelhaarand E.R. Weibel. Morphometric estimation of pulmonary diffusion capacity. 3. The effect of increased oxygen consumption in Japanese Waltzing mice. Respiration physiology. 11:354-366 (1971).

63. R.W. Niven. Pharmaceutical Inhalation Aerosol Technology, Marcel Dekker, Inc., New York, 1992.

64. R.A. Rajewskiand V.J. Stella. Pharmaceutical applications of cyclodextrins. 2. In vivo drug delivery. J Pharm Sci. 85:1142-1169 (1996).

65. V.J. Stella, V.M. Rao, E.A. Zannou, and V. Zia. Mechanisms of drug release from cyclodextrin complexes. Adv Drug Deliver Rev. 36:3-16 (1999).

66. I. Shehatta, A. Al-Marzouqi, B. Jobe, and A. Dowaidar. Enhancement of aqueous solubility of itraconazole by complexation with cyclodextrins using supercritical carbon dioxide. Canadian Journal of Chemistry-Revue Canadienne De Chimie. 83:1833-1838 (2005).

67. J.S. Hostetler, L.H. Hanson, and D.A. Stevens. Effect of hydroxypropyl-beta-cyclodextrin on efficacy of oral itraconazole in disseminated murine cryptococcosis. J Antimicrob Chemother. 32:459-463 (1993).

68. C.R. Bradford, A.G. Prentice, D.W. Warnock, and J.A. Copplestone. Comparison of the multiple dose pharmacokinetics of two formulations of itraconazole during remission induction for acute myeloblastic leukaemia. J Antimicrob Chemother. 28:555-560 (1991).

69. D.M. Oh, R.L. Curl, and G.L. Amidon. Estimating the Fraction Dose Absorbed from Suspensions of Poorly Soluble Compounds in Humans - a Mathematical-Model. Pharmaceut Res. 10:264-270 (1993).

70. J.S. Pattonand P.R. Byron. Inhaling medicines: delivering drugs to the body through the lungs. Nature reviews. 6:67-74 (2007).

71. P.R. Byronand J.S. Patton. Drug delivery via the respiratory tract. J Aerosol Med. 7:49-75 (1994).

72. M.A. Thiel, A.S. Zinkernagel, J. Burhenne, C. Kaufmann, and W.E. Haefeli. Voriconazole concentration in human aqueous humor and plasma during topical or combined topical and systemic administration for fungal keratitis. Antimicrob Agents Ch. 51:239-244 (2007).

73. B. Forbesand C. Ehrhardt. Human respiratory epithelial cell culture for drug delivery applications. European Journal of Pharmaceutics and Biopharmaceutics. 60:193-205 (2005).

74. J. Goerke. Pulmonary surfactant: functions and molecular composition. Biochim Biophys Acta. 1408:79-89 (1998).

75. T. Lindmark, Y. Kimura, and P. Artursson. Absorption enhancement through intracellular regulation of tight junction permeability by medium chain fatty acids in Caco-2 cells. J Pharmacol Exp Ther. 284:362-369 (1998).

Table 4.1. XPS analysis of surface elemental content of the physical mixture, and lyophilized powders of HPβCD/ITZ inclusion complexes sampled at 1, 24 and 48 hr after dispersion of amorphous ITZ in 15% (w/v) HPβCD.

Tested Powder	Atomic Concentration %			
	C 1s	O 1s	N 1s	Cl 2p
Physical Mixture	64.78	29.58	4.99	0.65
HPβCD/ITZ Inclusion Complex-1 hr	61.92	36.98	0.98	0.12
HPβCD/ITZ Inclusion Complex-24 hr	63.11	36.83	0.06	0
HPβCD/ITZ Inclusion Complex-48 hr	62.77	37.23	0	0

Table 4.2. Andersen Cascade Impactor data for nebulized HPβCD-ITZ solution (ITZ:HPβCD = 5.3:150, weight ratio) and URF-ITZ (ITZ:mannitol:lecithin = 1:0.5:0.2, weight ratio) colloidal dispersion (equivalent to 5.3 mg/mL of ITZ) using the Aeroneb® Professional micropump nebulizer with an airflow rate of 28.3 L/min.

	HPβCD-ITZ	URF-ITZ
Total Emitted dose (mg)	22.04	21.78
Respirable Fraction[#] (%)	82.52	82.41
Fine Particle Fraction* (%)	52.56	54.77
Available Dose (mg/min)	1.07	1.68
Mass Median Aerodynamic Diameter (MMAD) (μm)	3.19	2.80
Geometric Standard Deviation (GSD)	2.28	2.83

[#] Defined as the % mass of drug in aerosol droplets < 9 μm
* Defined as the % mass of drug in aerosol droplets <4.7μm

Table 4.3. Pharmacokinetic parameters of ITZ deposited in mice lung after inhalation of nebulized aerosols of HPβCD-ITZ solution (ITZ: HPβCD = 5.3:150, weight ratio) and URF-ITZ (ITZ:mannitol:lecithin = 1:0.5:0.2, weight ratio) colloidal dispersion (equivalent to 5.3 mg/mL of ITZ) in a whole-body exposure dosing apparatus.

Pharmacokinetic Parameter	HPβCD-ITZ	URF-ITZ
C_{max} (μg/g)	3.38±1.16	4.87±2.67
T_{max} (hr)	0	0
$K_{distribution}$ (hr^{-1})	0.143	0.238
$T_{1/2\ distribution}$ (hr)	4.87	2.91
$K_{elimination}$ (hr^{-1})	0.022	0.025
$T_{1/2\ elimination}$ (hr)	30.9	28
AUC_{0-24} (μg·hr/mL)	32.0	27.2

Table 4.4. Pharmacokinetic parameters of ITZ and HyITZ in mice serum after inhalation of nebulized aerosols of HPβCD-ITZ solution (ITZ: HPβCD = 5.3:150, weight ratio) and URF-ITZ (ITZ:mannitol:lecithin = 1:0.5:0.2, weight ratio) colloidal dispersion (equivalent to 5.3 mg/mL of ITZ) in a whole-body exposure dosing apparatus.

	ITZ		HyITZ	
Pharmacokinetic Parameters	HPβCD-ITZ	URF-ITZ	HPβCD-ITZ	URF-ITZ
C_{max} (μg/mL)	0.48±0.11	0.55±0.084	0.49±0.14	0.64±0.17
T_{max} (hr)	1.5	3.0	2.0	4.0
K_{01} (/hr)	0.679	0.718	0.973	0.858
K_{10} (/hr)	0.144	0.168	0.166	0.151
$T_{1/2\ K01}$ (hr)	1.02	0.97	0.71	0. 81
$T_{1/2\ K10}$ (hr)	4.83	4.13	4.18	4.58
$AUC_{0-\infty}$ (μg·hr/mL)	3.26	4.17	3.98	5.26

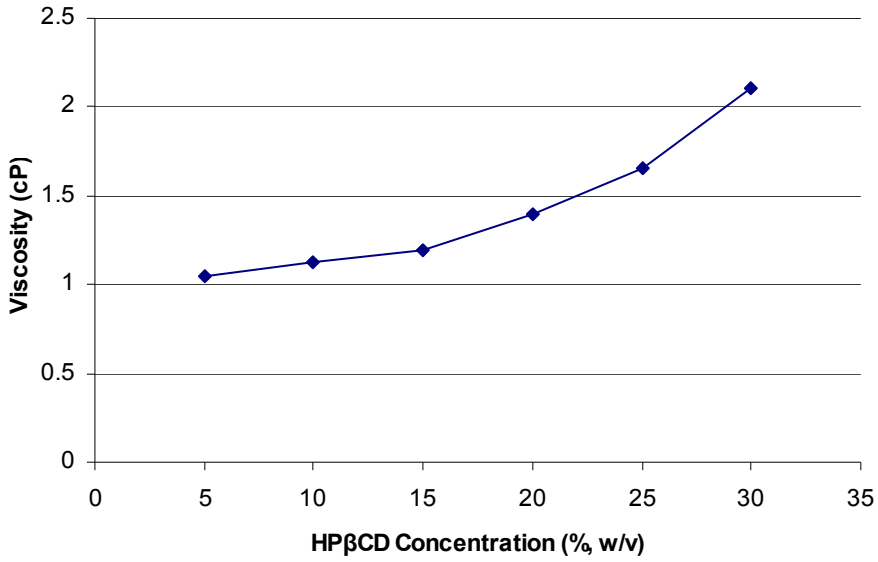

Figure 4.1. Viscosity of HPβCD aqueous solutions at various concentrations.

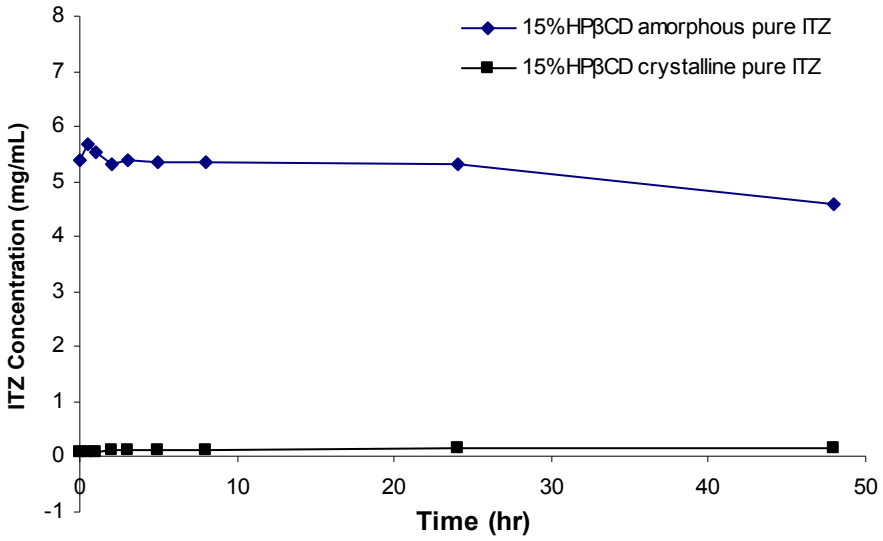

Figure 4.2. Time-concentration profiles for crystalline and amorphous ITZ in 15% HPßCD isotonic aqueous solution.

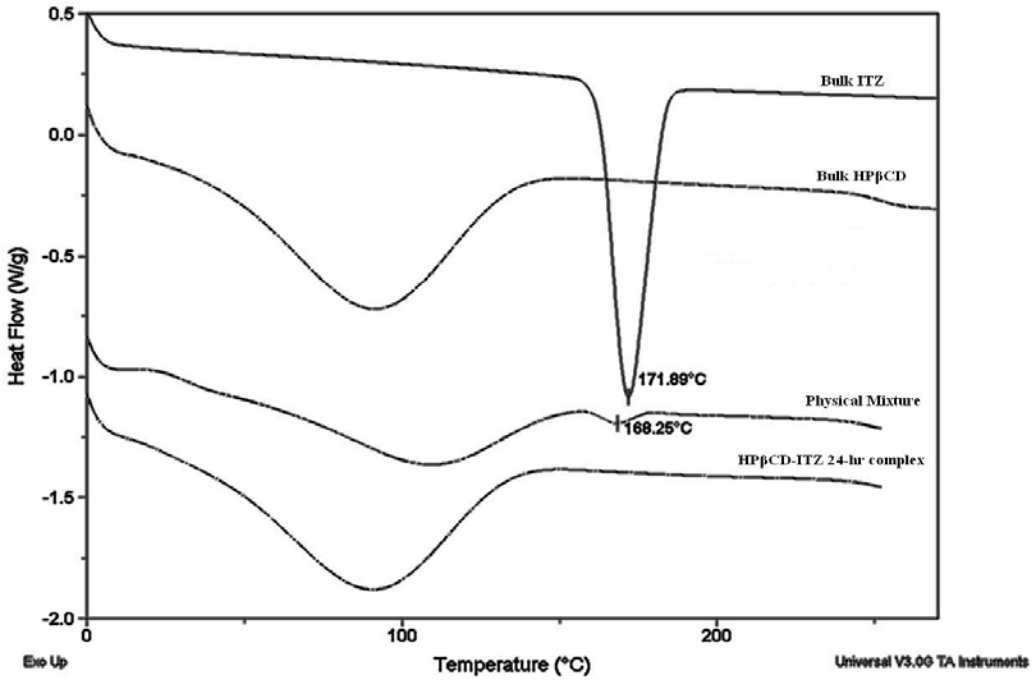

Figure 4.3. Differential Scanning Calorimetry (DSC) thermograms of bulk crystalline ITZ, bulk HPβCD, Physical Mixture (ITZ:HPβCD= 5.3:150, weight ratio), and lyophilized HPβCD-ITZ (ITZ:HPβCD= 5.3:150, weight ratio) powder.

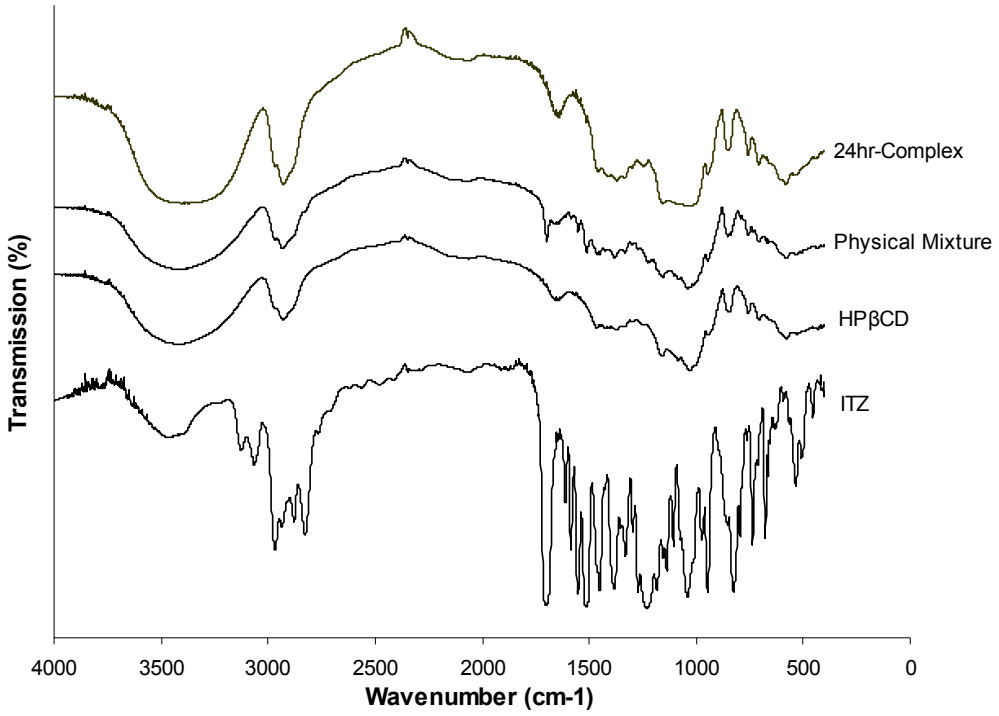

Figure 4.4. Fourier transform infrared spectroscopy (FTIR) spectra of pure crystalline ITZ, pure HPβCD, Physical Mixture (ITZ:HPβCD= 5.3:150, weight ratio), and lyophilized HPβCD-ITZ (ITZ:HPβCD= 5.3:150, weight ratio) powder.

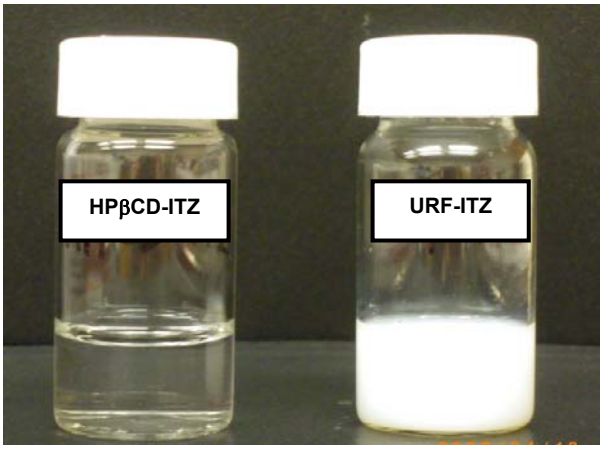

Figure 4.5. Photographs of HPβCD-ITZ solution (ITZ: HPβCD = 5.3:150, weight ratio) and URF-ITZ (ITZ:mannitol:lecithin = 1:0.5:0.2, weight ratio) colloidal dispersion (equivalent to 5.3 mg/mL of ITZ) employed for *in vivo* pulmonary dosing to mice by nebulization.

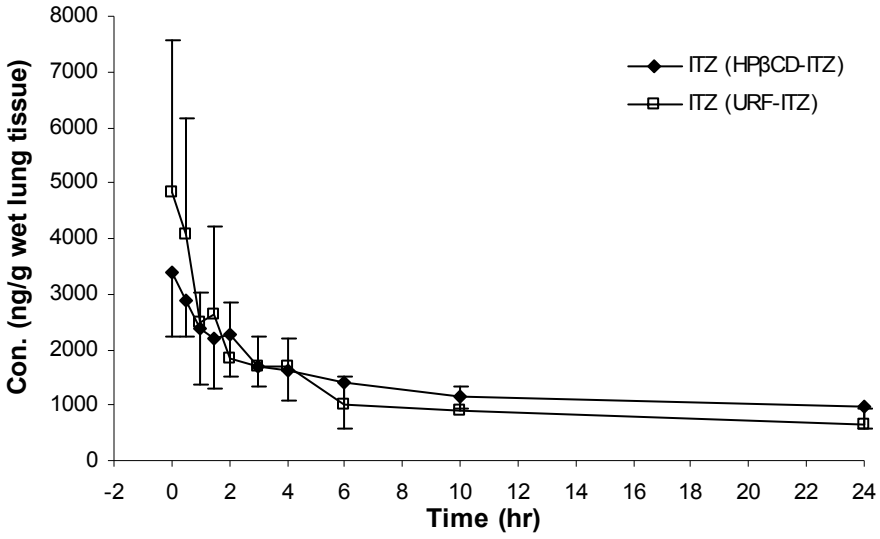

Figure 4.6. Concentration-time profile of ITZ in mice lung after inhalation of nebulized aerosols of HPβCD-ITZ solution (ITZ: HPβCD = 5.3:150, weight ratio) and URF-ITZ (ITZ:mannitol:lecithin = 1:0.5:0.2, weight ratio) colloidal dispersion (equivalent to 5.3 mg/mL of ITZ) in a whole-body exposure dosing apparatus. Data are presented as mean with standard deviation (n=6) at each time point.

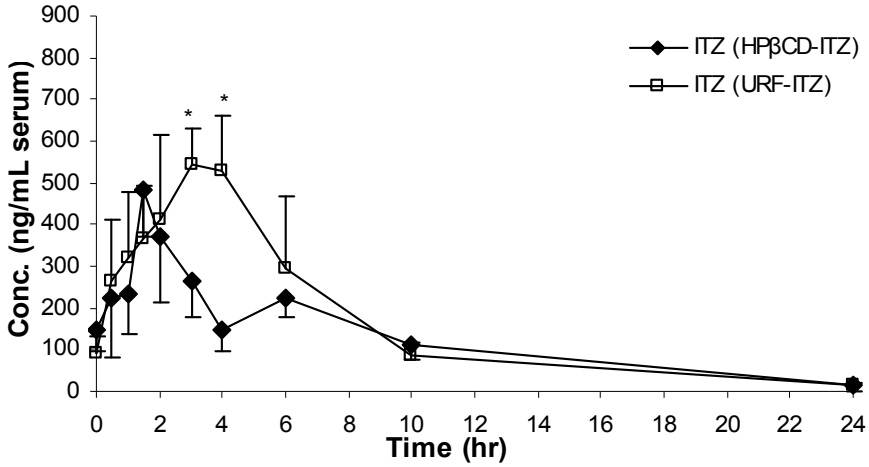

Figure 4.7. Concentration-time profile of ITZ in mice serum after inhalation of nebulized aerosols of HPβCD-ITZ solution (ITZ: HPβCD = 5.3:150, weight ratio) and URF-ITZ (ITZ:mannitol:lecithin = 1:0.5:0.2, weight ratio) colloidal dispersion (equivalent to 5.3 mg/mL of ITZ) in a whole-body exposure dosing apparatus. Data are presented as mean with standard deviation (n=6) at each time point.
* $p<0.05$

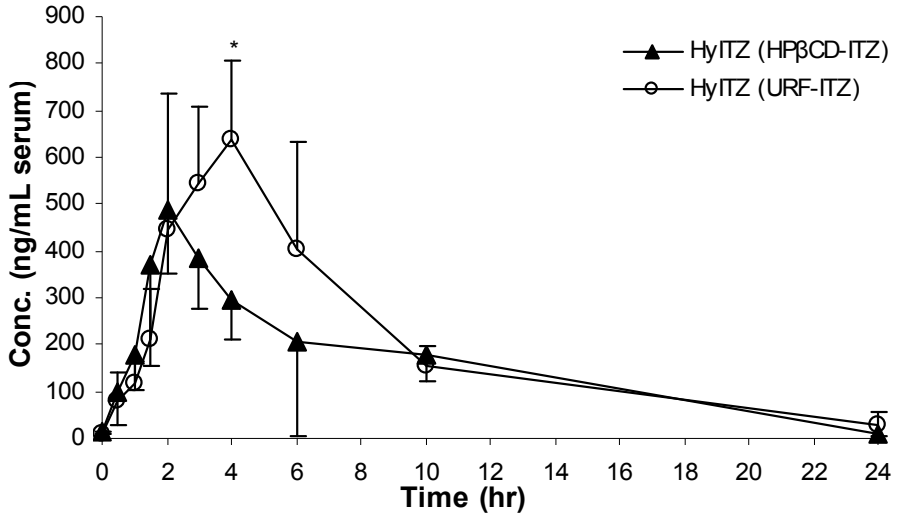

Figure 4.8. Concentration-time profile of HyITZ in mice serum after inhalation of nebulized aerosols of HPβCD-ITZ solution (ITZ: HPβCD = 5.3:150, weight ratio) and URF-ITZ (ITZ:mannitol:lecithin = 1:0.5:0.2, weight ratio) colloidal dispersion (equivalent to 5.3 mg/mL of ITZ) in a whole-body exposure dosing apparatus. Data are presented as mean with standard deviation (n=6) at each time point.
* $p<0.05$

Appendix A: Prophylaxis Study of Inhaled Itraconazole against Invasive Pulmonary Aspergillosis

A.1 INTRODUCTION

The ultimate aim of developing new itraconazole (ITZ) formulation and alternative administration route compared to the conventional formulations is to improve bioavailability of drug and thereby therapeutic effect. For treating invasive aspergillosis, survival in fungal infected animal model is probably the most meaningful difference can be shown between the control and the fungal infected group.

As characterized in previous chapters, aqueous colloidal dispersion of URF-ITZ nanostructured aggregates (URF nanotechnology processed ITZ:mannitol:lecithin =1:0.5:0.2 by weight ratio) has demonstrated excellent in vitro properties for deep lung deliver by nebulization. Furthermore, single-dose inhalation of the nebulized aerosols of the URF-ITZ aqueous colloidal dispersion produced considerable lung deposition (more than 20 μg/g wet lung tissue) and systemic ITZ level (1.64 μg/mL) in mice [1]. Based on the promising pharmacokinetic profiles of the inhaled URF-ITZ and prophylaxis studies of previously developed pulmonary ITZ formulations [2, 3], we are therefore interested to see the preventing effect of inhaled URF-ITZ against invasive fungal infections on Aspergillus fumigatus inoculated immunosuppressed mouse model.

A.2 ANIMAL MODEL

An established murine model of invasive pulmonary aspergillosis was used as previously described [2, 4]. Female ICR mice (Harlan Sprague Dawley, Inc.,

Indianapolis, IN) were immunosuppressed by intraperitoneal cyclophosphamide (250 mg/kg) and subcutaneous cortisone acetate (250 mg/kg) two days prior to inoculation. Both cyclophosphamide (200 mg/kg intraperitoneal) and cortisone acetate (250 mg/kg subcutaneously) were re-administered on day 3 post-inoculation, and mice received antibiotic prophylaxis with ceftazidime 50 mg/kg/day. This study was approved by the Institutional Animal Care Use Committee at the University of Texas Health Science Center at San Antonio, and all animals were handled in accordance with the American Association for Accreditation of Laboratory Animal Care.

For inoculation, mice were placed inside an acrylic chamber, and A. fumigatus conidia were introduced by aerosolizing the conidial suspension with a small particle nebulizer (Hudson Micro Mist, Hudson RCI, Temecula, CA) driven by compressed air [4]. A standard exposure time of 1 hour was used to allow for complete aerosolization of the conidial suspension. Starting inocula were assessed by colony forming unit (CFU) enumeration from mice one hour post-inoculation.

A.3 ANTIFUNGAL THERAPY

Mice were assigned to three treatment groups: inhaled nebulized aerosol of URF-ITZ (ITZ:mannitol:lecithin=1:0.5:0.2 by weight ratio) colloidal dispersion (20 mg/mL × 10 mL, twice daily), amphotericin B deoxycholate (1 mg/kg interperitoneally daily; Apothecon, Princeton, NJ), or aerosolized purified water as control in a whole-body exposure dosing chamber [5] using a Aeroneb® Pro micropump nebulizer with air-flow of 1 L/min to blow the aerosol into the chamber. Prophylaxis was begun two days prior to pulmonary inoculation and continued for a total of 10 days (day 7 post-inoculation).

Animals that appeared moribund prior to the end of the study were euthanized by halothane and death was recorded as occurring the next day.

The prophylaxis study of inhaled URF-ITZ colloidal dispersion in fungal infected mice model was performed by Dr. Nathan Wiederhold in the University of Texas Health Science Center at San Antonio.

A.4 SURVIVAL RESULTS

The prophylaxis study results are presented in Figure A.1. URF-ITZ dosing group showed similar survival rate compared to mice dosed amphotericin B in both short term (8 days) and long term (12 days). However, both of the antifungal treatment groups demonstrated lower percent survival than the control group which inhaled nebulized water. The 8 days survival on therapy in control group was 75%, which may indicate the fungal infection mouse model was not successful. The URF-ITZ and amphotericin B administration groups were 55 and 50%, respectively. This may imply possible toxic side effects associated with the antifungal agents used in this study. Further investigation of the drug interactions on this specific mouse model is needed.

A.5 REFERENCES

1. W. Yang, J. Tam, D.A. Miller, J. Zhou, J.T. McConville, K.P. Johnston, and R.O. Williams. High bioavailability from nebulized itraconazole nanoparticle dispersions with biocompatible stabilizers. Int J Pharm. 361:177-188 (2008).

2. C.A. Alvarez, N.P. Wiederhold, J.T. McConville, J.I. Peters, L.K. Najvar, J.R. Graybill, J.J. Coalson, R.L. Talbert, D.S. Burgess, R. Bocanegra, K.P. Johnston, and R.O. Williams. Aerosolized nanostructured itraconazole as prophylaxis against invasive pulmonary aspergillosis. J Infection. 55:68-74 (2007).

3. B.J. Hoeben, D.S. Burgess, J.T. McConville, L.K. Najvar, R.L. Talbert, J.I. Peters, N.P. Wiederhold, B.L. Frei, J.R. Graybill, R. Bocanegra, K.A. Overhoff, P. Sinswat, K.P. Johnston, and R.O. Williams. In vivo efficacy of aerosolized nanostructured itraconazole formulations for prevention of invasive pulmonary aspergillosis. Antimicrob Agents Ch. 50:1552-1554 (2006).

4. D.C. Sheppard, G. Rieg, L.Y. Chiang, S.G. Filler, J.E. Edwards, and A.S. Ibrahim. Novel inhalational murine model of invasive pulmonmy aspergillosis. Antimicrobial Agents and Chemotherapy. 48:1908-1911 (2004).

5. J.T. McConville, R.O. Williams, T.C. Carvalho, A.N. Iberg, K.P. Johnston, R.L. Talbert, D. Burgess, and J.I. Peters. Design and evaluation of a restraint-free small animal inhalation dosing chamber. Drug Development and Industrial Pharmacy. 31:35-42 (2005).

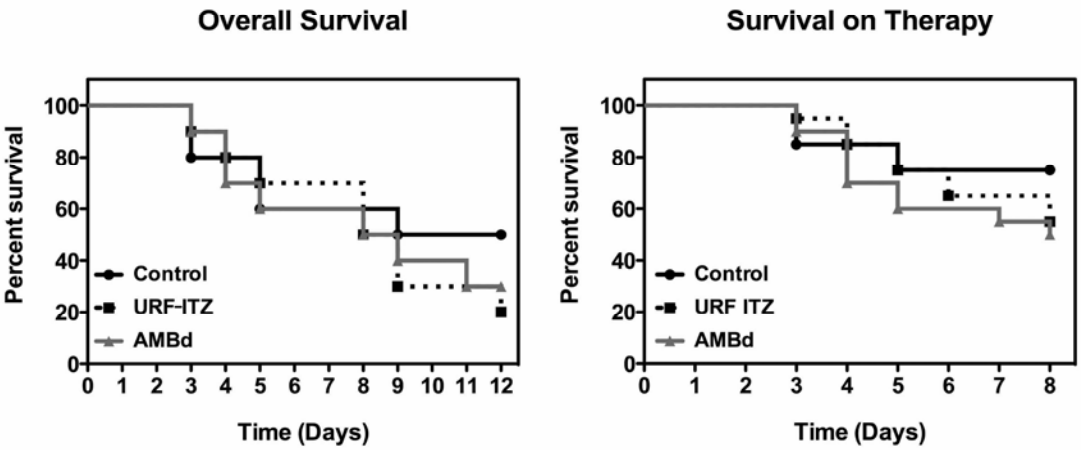

Group	Percent Surv.	Median Surv.
Control	50	10.5
URF−ITZ	20	8.5
AMBd	30	8.5

Group	Percent Surv.	Median Surv.
Control	75	> 8
URF−ITZ	55	> 8
AMBd	50	8

Figure A.1. Survival curves for immunosuppressed mice that inhaled nebulized aerosol of URF-ITZ (ITZ:mannitol:lecithin=1:0.5:0.2 by weight ratio) colloidal dispersion (20 mg/mL × 10 mL, twice daily), amphotericin B deoxycholate, or control (aerosolized purified water) and challenged by pulmonary inoculation with *A. fumigatus*.

Appendix B: Study of Interaction of Cyclophosphamide and Inhaled Itraconazole

B.1 INTRODUCTION

Aqueous colloidal dispersion of URF-ITZ (URF nanotechnology processed ITZ:mannitol:lecithin=1:0.5:0.2) has demonstrated excellent in vitro properties for deep lung deliver by nebulization. Furthermore, single-dose inhalation of the nebulized aerosols of the URF-ITZ aqueous colloidal dispersion produced considerable lung deposition and systemic itraconazole (ITZ) level (1.64 μg/mL) in mice [1]. Because of the promising pharmacokinetic profiles of the inhaled URF-ITZ, prophylaxis studies of inhaled URF-ITZ on fungi inoculated immunosuppressed mice were conducted in the University of Texas Health Science Center at San Antonio. However, the prophylaxis study showed no significant improvement of the survival rate in mice administered ITZ compared to the control.

To establish the immunosuppressed mouse model, a combination of cortisone acetate and cyclophosphamide (CY) were employed. CY is a phosphoramide form of nitrogen mustard commonly used in cancer treatment. In addition, its toxicity to lymphocytes has made it an important immunosuppresent agent in hematopoietic stem cell transplant therapies [2], and more recently in treatment of inflammatory conditions such as systemic lupus erythematosis and rheumatoid arthritis, etc. [3]. The parent drug itself is not cytotoxic. It must be activated by hepatic cytochrome P450 (CYP) enzymes and undergoes three metabolic pathways: (1) urinary elimination as unchanged CY, which account for about 25-30% of the drug metabolism; (2) detoxification via CYP

3A4/5 to dechloroethyl-cyclophosphamide (DCCY), which account for about 5-10%; and (3) the major metabolic pathway---activation via CYP 2A6, 2B6, 3A4, 3A5, 2C9, 2C18, and 2C19 to 4-hydroxycyclophosphamide (HCY) [4]. HCY is then converted by beta-elimination to toxins acrolein, which is primarily responsible for urothelial toxicity, and phosphoramide mustard (PM), responsible for antineoplastic activity. Other metabolites include o-carboxyethyl-phosphoramide mustard (CEPM), 4-keto-cyclophosphamide (ketoCY), and hydroxypropyl-phosphoramide mustard (HPPM) [3, 5]. The schematic of CY metabolic pathways is shown in Figure B.1.

Antifungal azole drugs function by inhibiting the fungal CYP enzyme 14-α-sterol-demethylase which is involved in cell membrane biosynthesis [6]. ITZ is a known potent inhibitor of CYP 3A4 and has many clinically significant drug interactions associated with this enzyme inhibition [7]; whereas fluconazole is a relatively potent inhibitor of CYP 2C9 [8].

Published toxicity data from a randomized trial comparing fluconazole with ITZ as antifungal prophylaxis in hematopoietic cell transplant recipients demonstrated a disequilibrium in CY metabolites, and renal and hepatic toxicities in patients who received the azole drugs concurrent with CY-containing regimens [9, 10]. Coadministration of high-dose fluconazole (400 mg daily) with CY was associated with greater exposure to CY and DCCY, whereas ITZ (2.5 mg/kg 3 times daily) was associated with greater exposure to HCY, ketoCY, and CEPM [9]. In addition, concurrent fluconazole was associated with less renal and hepatic toxicity, and a trend to improved survival at day 20 [11]. Recipients of ITZ demonstrated higher exposure to toxic metabolites than recipients of fluconazole, suggesting differential inhibition of hepatic CYP450 isoenzymes can affect CY metabolism and conditioning-related toxicities [12].

We therefore suspect that drug interaction between CY and ITZ occurred in the prophylaxis studies, and the resultant toxic metabolites lead to the unexpected lower survival rate of the fungal infected immunosuppressed mice with ITZ therapy. This study is designed to confirm this hypothesis.

To quantify the metabolites of CY, LC-MS need to be used. However, HCY and AldoCY are very unstable ($t_{1/2}$ = ~4 min). Moreover, PM and acrolein are toxic and unstable; they might bind to protein or react with tissue, hard to extract out, and easily decompose [13, 14]. CEPM is the only chemically stable major CY metabolite formed between the activation of CY to HCY and the ultimate formation of glutathione conjugates of acrolein and PM. ITZ can inhibit P4503A4, then the inactivation pathway product DCCY may be decrease [15]. Based on these, CEMP and DCCY were selected as markers to monitor the change of CY toxic metabolites with concomitant ITZ therapy.

B.2 MATERIALS AND METHODS

B.2.1 Materials

CY is produced by Baxter Health Corporation (Deerfield, IL). CEPM and DCCY were purchased from Eno Research Chemicals and Custom Synthesis Eno Research & Consulting Services, LLC (Hillsborough, NC). Cortisone acetate was purchased from Sigma. Ceftazidime is manufactured by Sandoz GmbH for Hospira Worldwide Inc., (Lake Forest, IL). ITZ was purchased from Hawkins Chemical (Minneapolis, MN).

B.2.2 *In vivo* study design

The immunosuppressed mouse model will be established as follows. Mice (weighing between 18 - 22 g, female) with access to sterile food and water ad libitum, will be rendered immunosuppressed by intraperitoneal CY (250 mg/kg) and subcutaneous cortisone acetate (250 mg/kg) on Day-1. Both CY (200 mg/kg intraperitoneally) and cortisone acetate (250 mg/kg subcutaneously) were re-administered on Day-6. The mice will inhale ITZ aerosols from Day-1 for 10 days, 100 mg ITZ equivalent in 5 mL × 2 each time, twice per day. The immunosuppressed mice need housing in the barrier facility to ensure the health and safety. In addition, mice will receive a daily dose of the antibiotic ceftazidime (50 mg/kg) subcutaneously (0.2 mL/mouse) to prevent bacteria infection from Day-1. The mice will be divided into 5 groups as following.

Group 1: Aerosolized ITZ + Cyclophosphamide & cortisone acetate (same immunosuppression regimen used in the prophylaxis study)

Group 2: Aerosolized ITZ + cortisone acetate (no Cyclophosphamide)

Group 3: Cyclophosphamide + cortisone acetate (no aerosolized ITZ)

Group 4: Cortisone acetate alone

Group 5: Normal mice without any treatment

The treatment of the mice listed schematically in Figure B.2.

B.2.3 Sampling of blood

Blood samples will be taken by cardiac puncture and place into tubes containing EDTA (ethylenediaminetetraacetic acid), mixed and centrifuged immediately after withdrawn. Plasma will be immediately removed, frozen and stored at -80 °C until analysis.

B.2.4 Analysis of CY metabolites by using mass spectrometry-HPLC (LC-MS)

The Applied Biosystems 4000 Q Trap LC-MS/MS system with ESI, APCI and nanospray sources coupled with Shimadzu LC-20AD HPLC system (Shimadzu, Columbia, MD) located in the Analytical Instrumentation Facility Core (PHR 1.110) at The University of Texas at Austin was employed for quantitation of CY stable metabolites DCCY and CEPM, as well as ITZ. The LC-MS/MS method development was performed by Dr. Herng-Hsiang Lo in the CRED Analytical Instrumentation Facility Core supported by NIEHS center grant ES07784.

B.2.5 Bioassays of mice plasma and organ histology

Plasma creatinine, BUN, bilirubin (total and indirect), alanine aminotransferase (ALT), aspartate aminotransferase (AST), Alkaline phosphatase (ALP) will be analyzed by IDEXX for toxicity analysis.

Livers and kidneys will be collected and fixed in formaldehyde; Tissue slices may be prepared by IDEXX when necessary for histology study.

B.3 RESULTS

LC-MS methods for determining the amount of ITZ, DCCY and CEPM have been established by Dr. Stony Lo. The standard curves are presented in Figures B.3, B.4, and B.5. For ITZ, there is a good linearity in the range of 50-1000 picogram (pg) can be detected by the LC-MS system used. DCCY and CEPM demonstrated good linearity in the range of 100-2000 pg and 50-1000 pg, respectively.

B.4 REFERENCES

1. W. Yang, J. Tam, D.A. Miller, J. Zhou, J.T. McConville, K.P. Johnston, and R.O. Williams. High bioavailability from nebulized itraconazole nanoparticle dispersions with biocompatible stabilizers. Int J Pharm. 361:177-188 (2008).

2. M.E. de Jonge, A.D.R. Huitema, S. Rodenhuis, and J.H. Beijnen. Clinical pharmacokinetics of cyclophosphamide. Clin Pharmacokinet. 44:1135-1164 (2005).

3. T.F. Kalhorn, S. Ren, W.N. Howald, R.F. Lawrence, and J.T. Slattery. Analysis of cyclophosphamide and five metabolites from human plasma using liquid chromatography-mass spectrometry and gas chromatography-nitrogen-phosphorus detection. J Chromatogr B. 732:287-298 (1999).

4. S.M. Yule, D. Walker, M. Cole, L. McSorley, S. Cholerton, A.K. Daly, A.D.J. Pearson, and A.V. Boddy. The effect of fluconazole on cyclophosphamide metabolism in children. Drug Metab Dispos. 27:417-421 (1999).

5. G.J. Pass, D. Carrie, N. Boylan, S. Lorimore, E. Wright, B. Houston, C.J. Henderson, and C.R. Wolf. Role of hepatic cytochrome P450s in the pharmacokinetics and toxicity of cyclophosphamide: Studies with the hepatic cytochrome P450 reductase null mouse. Cancer Res. 65:4211-4217 (2005).

6. G.P. Bodey. Azole Antifungal Agents. Clin Infect Dis. 14:S161-S169 (1992).

7. D.E. Colburn, F.J. Giles, D. Oladovich, and J.A. Smith. In vitro evaluation of cytochrome P450-mediated drug interactions between cytarabine, idarubicin, itraconazole and caspofungin. Hematology. 9:217-221 (2004).

8. T. Kantola, J.T. Backman, M. Niemi, K.T. Kivisto, and P.J. Neuvonen. Effect of fluconazole on plasma fluvastatin and pravastatin concentrations. Eur J Clin Pharmacol. 56:225-229 (2000).

9. K.A. Marr, W. Leisenring, F. Crippa, J.T. Slattery, L. Corey, M. Boeckh, and G.B. McDonald. Cyclophosphamide metabolism is affected by azole antifungals. Blood. 103:1557-1559 (2004).

10. I. Oren, J.M. Rowe, H. Sprecher, A. Tamir, N. Benyamini, L. Akria, A. Gorelik, N. Dally, T. Zuckerman, N. Haddad, R. Fineman, and E.J. Dann. A prospective randomized trial of itraconazole vs fluconazole for the prevention of fungal infections in patients with acute leukemia and hematopoietic stem cell transplant recipients. Bone Marrow Transplantation. 38:127-134 (2006).

11. A. Upton, J.S. McCune, K.A. Kirby, W. Leisenring, G. McDonald, A. Batchelder, and K.A. Marr. Fluconazole coadministration concurrent with cyclophosphamide conditioning may reduce regimen-related toxicity postmyeloablative hematopoietic cell transplantation. Biol Blood Marrow Transplant. 13:760-764 (2007).

12. G.B. McDonald, J.T. Slattery, M.E. Bouvier, S. Ren, A.L. Batchelder, T.F. Kalhorn, H.G. Schoch, C. Anasetti, and T. Gooley. Cyclophosphamide metabolism, liver toxicity, and mortality following hematopoietic stem cell transplantation. Blood. 101:2043-2048 (2003).

13. S. Ren, T.F. Kalhorn, G.B. McDonald, C. Anasetti, F.R. Appelbaum, and J.T. Slattery. Pharmacokinetics of cyclophosphamide and its metabolites in bone marrow transplantation patients. Clin Pharmacol Ther. 64:289-301 (1998).

14. U. Schuler, P. Waidelich, H. Kolb, T. Wagner, and G. Ehninger. Pharmacokinetics and Metabolism of Cyclophosphamide Administered after Total-Body Irradiation of Bone-Marrow Transplant Recipients. Eur J Clin Pharmacol. 40:521-523 (1991).

15. L. Yuand D.J. Waxman. Role of cytochrome P450 in oxazaphosphorine metabolism - Deactivation via N-dechloroethylation and activation via 4-hydroxylation catalyzed by distinct subsets of rat liver cytochromes P450. Drug Metab Dispos. 24:1254-1262 (1996).

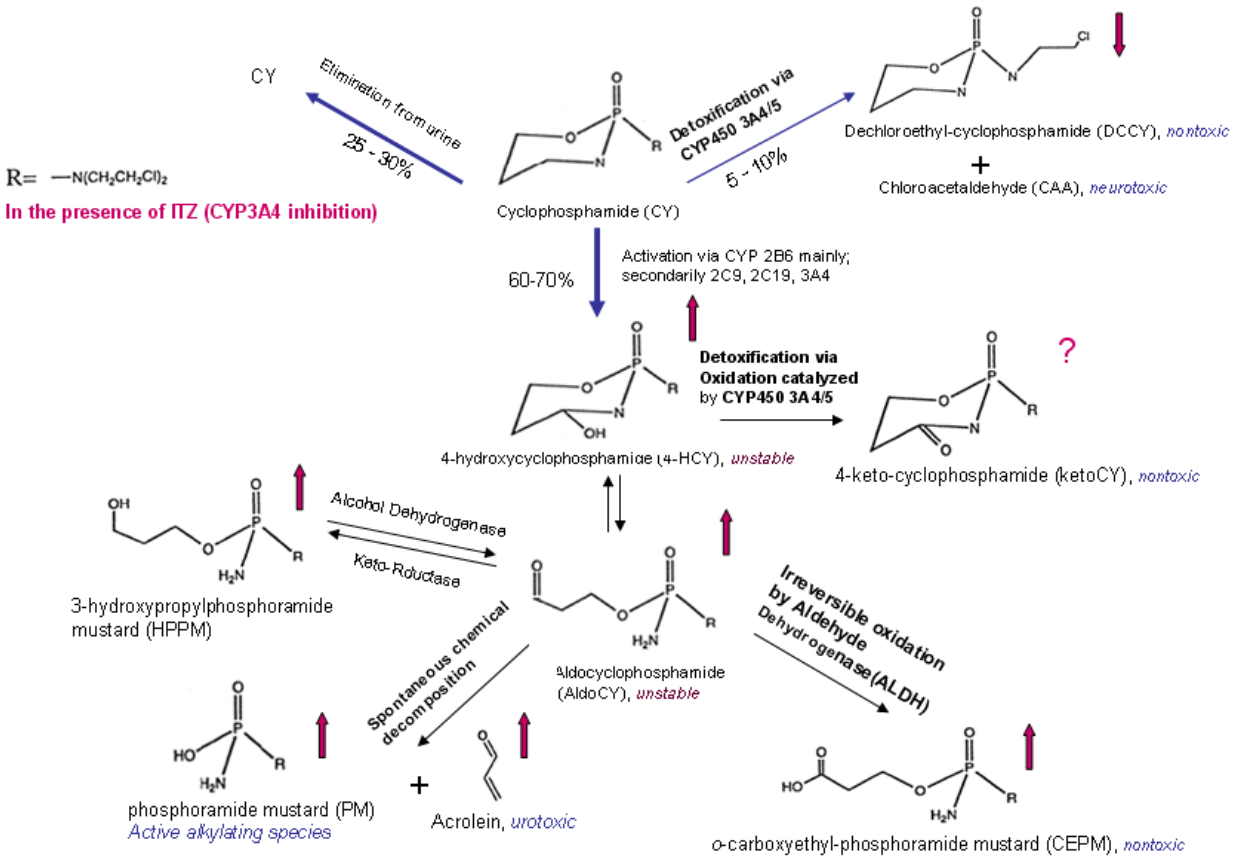

Figure B.1. Partial metabolic pathways of cyclophosphamide (CY). Chloroacetaldehyde (CAA), acrolein, and phosphoramide mustard (PM) are cytotoxins, but acrolein and PM are the major toxins because of the abundance of their formation. HCY (4-hydroxy-cyclophosphamide) is formed primarily in the liver but circulates in blood, entering cells as its tautomer aldocyclophosphamide (AldoCY). Acrolein and PM are formed from AldoCY when it decomposes through beta-elimination. Other metabolites include *o*-carboxyethylphosphoramide mustard (CEPM), deschloroethyl-cyclophosphamide (DCCY), 4-ketocyclophosphamide (KetoCY), hydroxypropyl-phosphoramide mustard (HPPM).

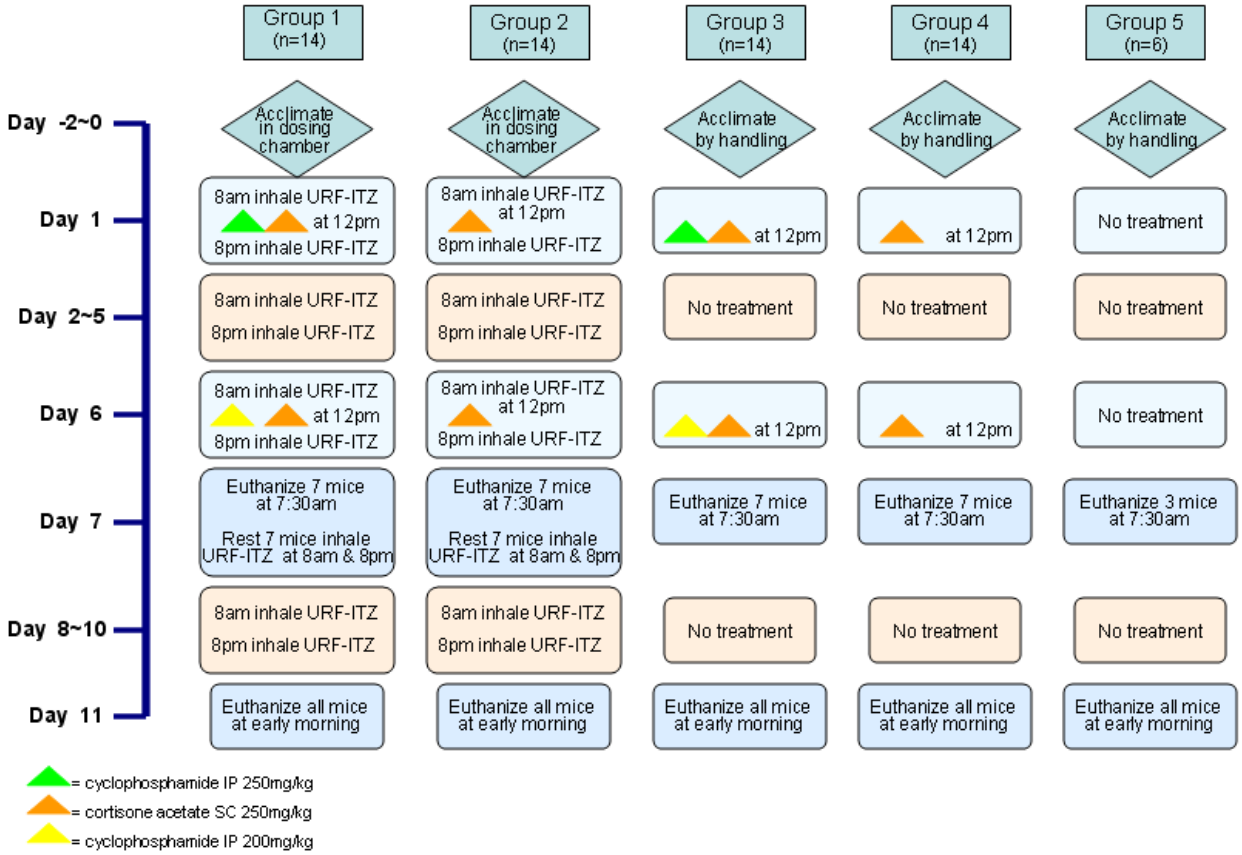

Figure B.2. Flowchart of timeline for the animal experiment

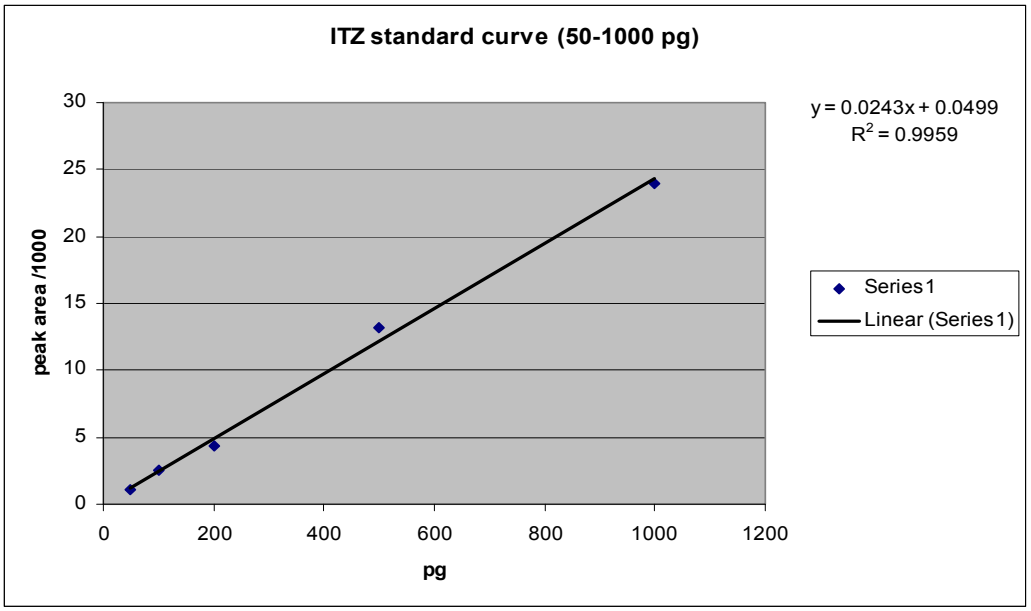

Figure B.3. ITZ standard curve in the concentration range of 50-1000 pg determined by LC-MS.

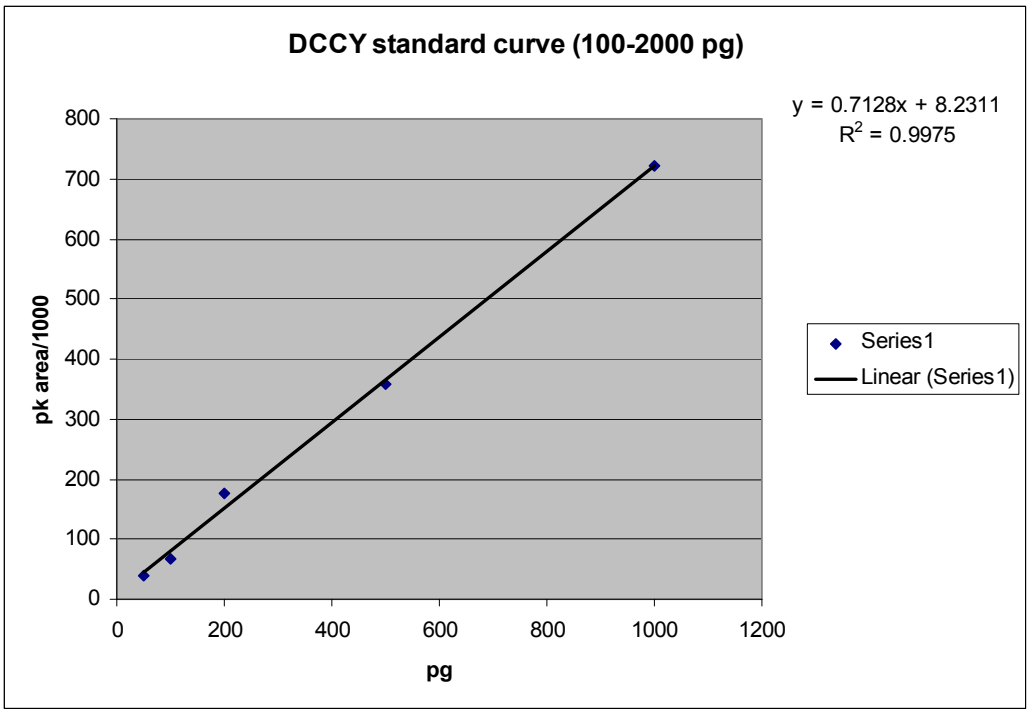

Figure B.4. DCCY standard curve in the concentration range of 100-2000 pg determined by LC-MS.

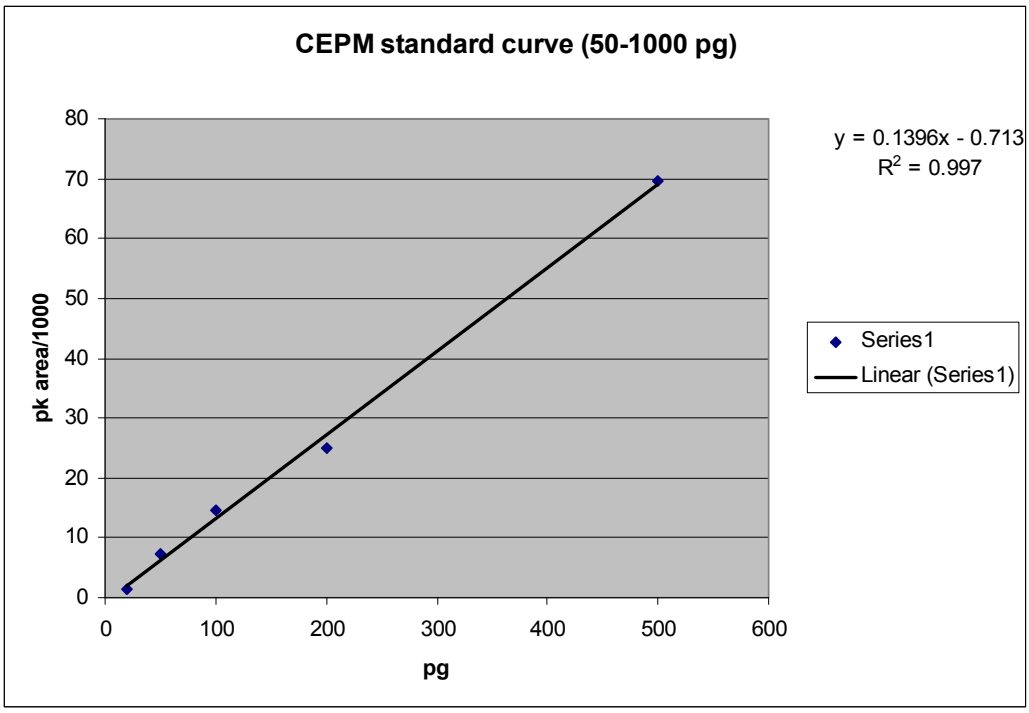

Figure B.5. CEPM standard curve in the concentration range of 50-1000 pg determined by LC-MS.

Appendix C: Detection Recrystallization of Amorphous Formulation by Transmission Electron Microscopy

C.1 INTRODUCTION

Amorphous formulations have been developed in our laboratory to increase the aqueous solubility of poorly water-soluble drugs (i.e. itraconazole (ITZ)), thereby enhance the bioavailability which is limited by the low aqueous solubility [1, 2]. Due to the metastable character of amorphous form, it may automatically transfer to lower energy level of crystalline form during storage. Because of the instability of amorphous state, the supposed improvement of dissolution rate and extent will be affected. Conventionally, powder X-ray diffraction (XRD), differential scanning calorimetry (DSC) and dissolution test can be used to detect recrystallization of amorphous pharmaceutical products. However, they all have limitations in detecting low percentage of morphological change. It is generally accepted that only when the content of crystal is higher than 5%, it can be differiented by XRD [3]. For the nanomaterials, the sensitivity is even lower, due to the weaker diffraction by the smaller particles of crystal. DSC is relatively more sensitive, it can quantify the amount of recrystallized material based on the energy change in a thermal event. However, it is too complicated to predict for systems with more than two components.

Solid state NMR can determine molecular structure and Intermolecular packing, therefore has been reported to use to monitor recrystallization. However, it has not been reported to detect the recrystallization of pharmaceutical amorphous nanomaterials. The

application in detecting small amount of crystal in amorphous nanomaterials will be another research focus.

With advancements in spatial and temporal resolution, instruments such as transmission electron microscopes (TEM), scanning transmission electron microscopes (STEM) have been developed with the ability to observe the evolution of material microstructure and properties [4]. We therefore explored the application of TEM in detecting small amount of recrystallization of an amorphous nano-structured aggregate of ITZ made by URF technology (i.e. URF-ITZ).

C.2 METHODS

The preparation of URF-ITZ was described in previous chapters using the URF technology.

C.2.1 XRD

The crystallinity of freshly made URF-ITZ powder and URF-ITZ powder stored for 12-month was examined using wide angle XRD as described in previous chapters.

C.2.2 TEM

The freshly made URF-ITZ powder and URF-ITZ powder stored for 6-month were examined using TEM. The dry sample powder was placed on a Holey Carbon Support Film with 200 Mesh Copper Grids (Jed Pella, Inc., Redding, CA) and viewing on a JEOL 2010F transmission electron microscope (JEOL USA, Inc., Peabody, MA).

The TEM images were taken by Dr. Paulo Ferreira in the Materials Science and Engineering Program at The University of Texas at Austin.

C.3 RESULTS

C.3.1 XRD profiles

From the XRD patterns shown in Figure C.1., the freshly prepared URF-ITZ powder exhibited broad, diffuse haloes in absence of the characteristic crystalline peaks of ITZ and mannitol, indicating its amorphous nature [5]. The URF-ITZ powder that stored for 6 months also demonstrated no appreciable characteristic crystalline peaks, suggesting its amorphousness.

C.3.2 TEM in detecting recrystallization

The TEM image in Figure C.2. illustrated a disordered mass of the freshly prepared URF-ITZ powder, indicating its complete amorphous state. In contrast, for the URF-ITZ powder that stored for 6 months as shown in Figure C.3., some areas at the edge of the powder displayed ordered morphology. Within the blue circle, regular crystal plates can be seen, compared to the disordered area within the red frame, indicating recrystallization at a few nm level. TEM can "see" the morphological difference at few nm. Compared to XRD and other techniques, TEM is highly sensitive to detect trace amount of recrystallization of amorphous product.

C.4 REFERENCES

1. R.H. Muller, C. Jacobs, and O. Kayser. Nanosuspensions as particulate drug formulations in therapy Rationale for development and what we can expect for the future. Adv Drug Deliver Rev. 47:3-19 (2001).

2. V.B. Patravale, A.A. Date, and R.M. Kulkarni. Nanosuspensions: a promising drug delivery strategy. J Pharm Pharmacol. 56:827-840 (2004).

3. G.P. Johari, S. Ram, G. Astl, and E. Mayer. Characterizing Amorphous and Microcrystalline Solids by Calorimetry. Journal of Non-Crystalline Solids. 116:282-285 (1990).

4. B.G. Clark, P. Ferreira, and I.M. Robertson. In Situ Electron Microscopy Methods. Microscopy Research and Technique. 72:121-121 (2009).

5. L.R. Hildenand K.R. Morris. Physics of amorphous solids. J Pharm Sci. 93:3-12 (2004).

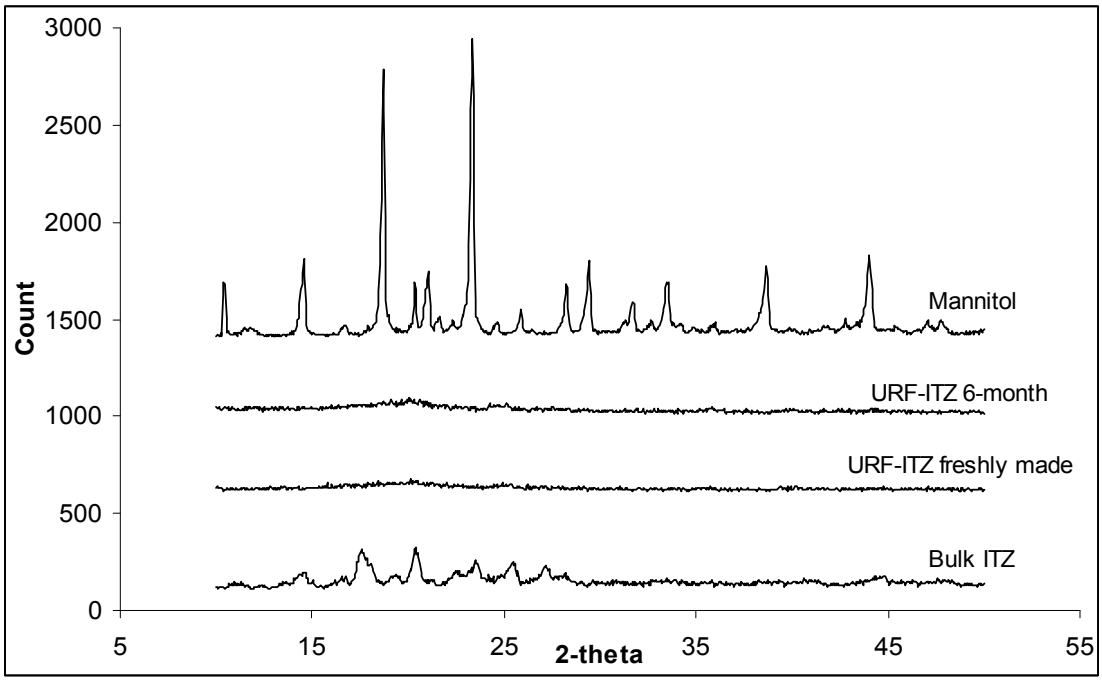

Figure C.1. XRD patterns of Bulk ITZ, URF-ITZ powder freshly prepared, URF-ITZ stored for 6 months, and mannitol.

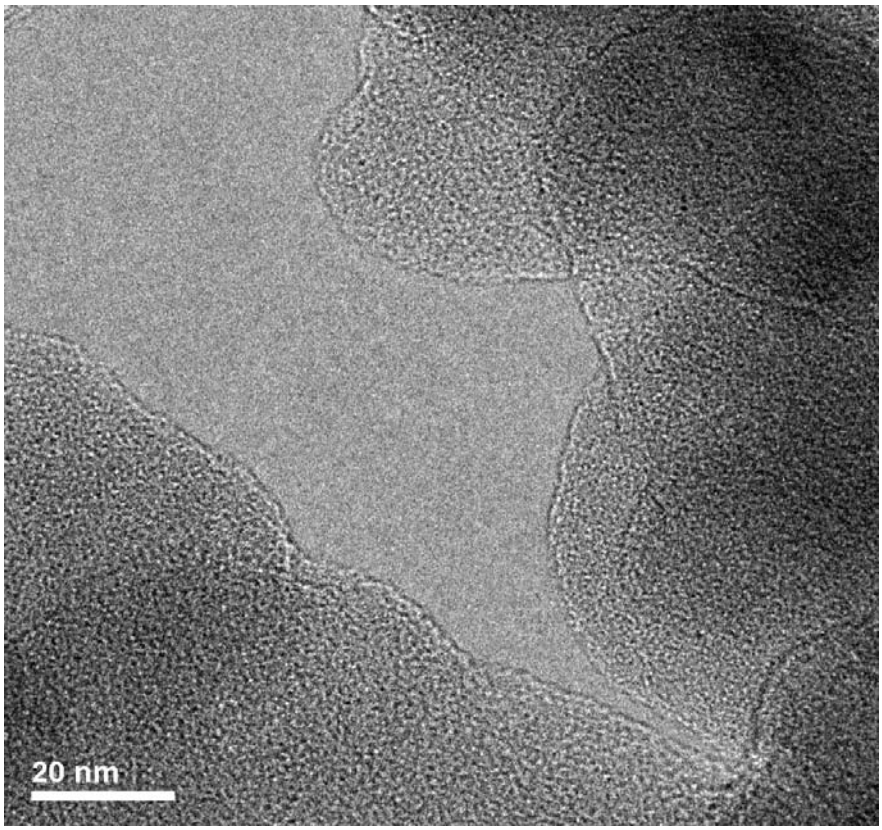

Figure C.2. TEM image of URF-ITZ powder freshly prepared.

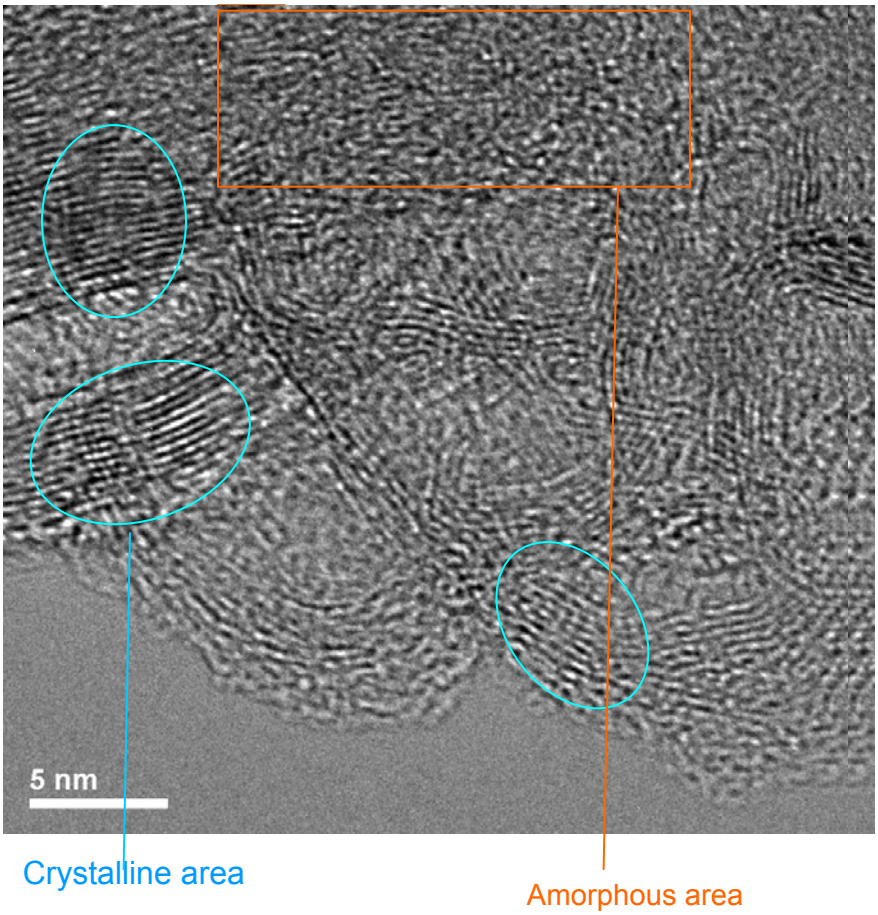

Figure C.3. TEM image of URF-ITZ powder stored for 6 months.

Appendix D: scanning Electron Microscopy images of lyophilized dry powders of itraconazole formulations

D.1 INTRODUCTION

To make biocompatible and biodegradable ITZ nanoparticle formulations for pulmonary delivery, various sugars, sugar alcohols, bovine serum albumin (BSA), lecithin and polysorbate 20 (Tween 20) were tested with different weight ratios. ITZ and excipients were first dissolved in a mixed solvent; the formed solution was then applied to URF process, lyophilized to obtain dry powders. The samples were mounted onto an aluminum stage using conductive carbon tape. Samples were coated using a model K575 sputter coater (Emitech Products, Inc., Houston, TX) with gold/palladium for 20 sec in a high vacuum evaporator. Scanning Electron Microscopy (SEM) was performed using a Hitachi S-4500 field emission scanning electron microscope (Hitachi High-Technologies Corp., Tokyo, Japan) operating at an accelerating voltage of 10-15 kV. SEM images are presented as follows.

D.2 RESULTS

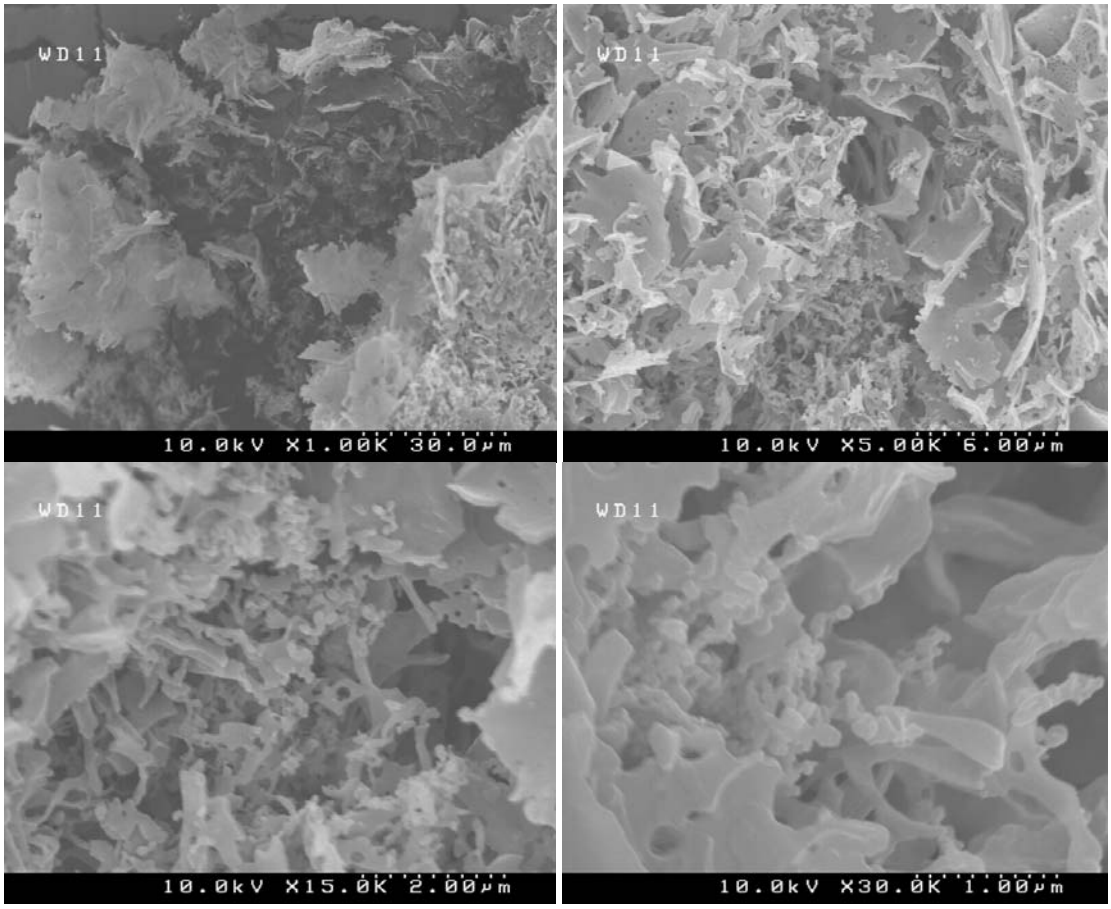

Figure D.1. SEM images of URF processed dry powder of ITZ/Lecithin=1/0.2 (w/w).

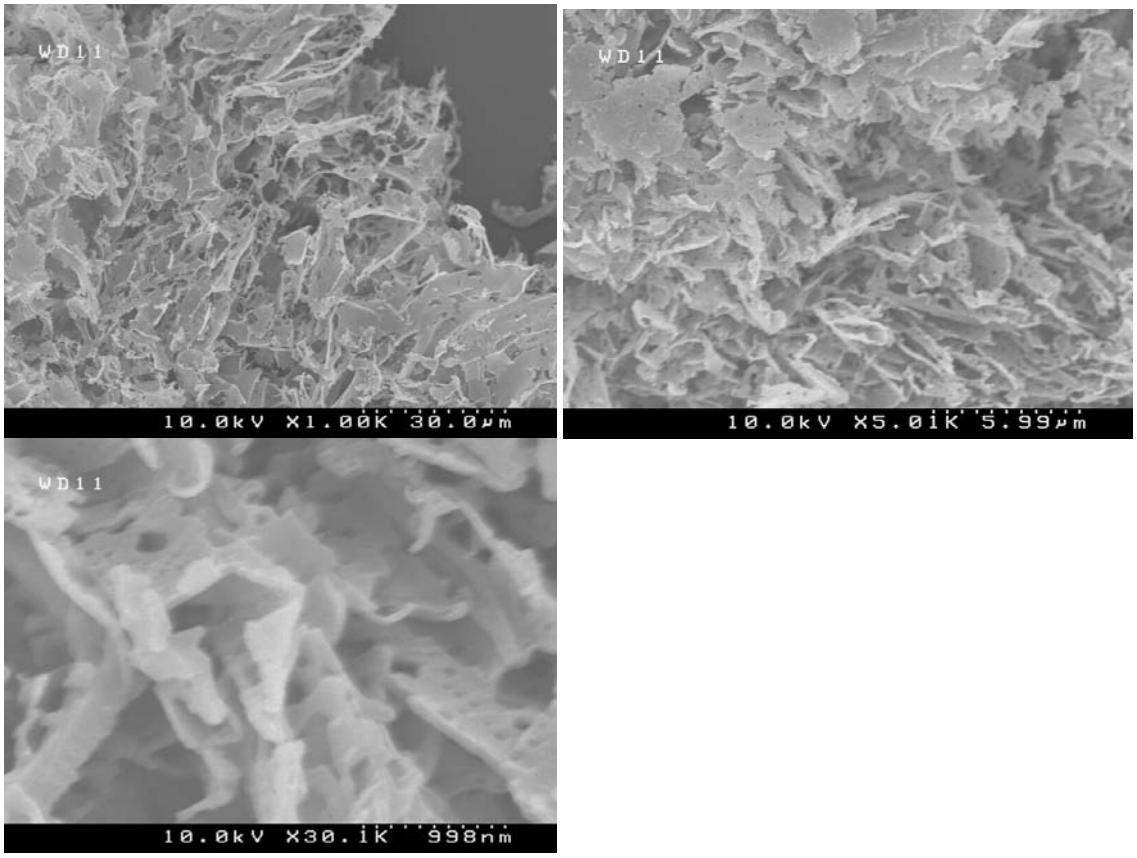

Figure D.2. SEM images of URF processed dry powder of ITZ/Lecithin=1/0.3 (w/w).

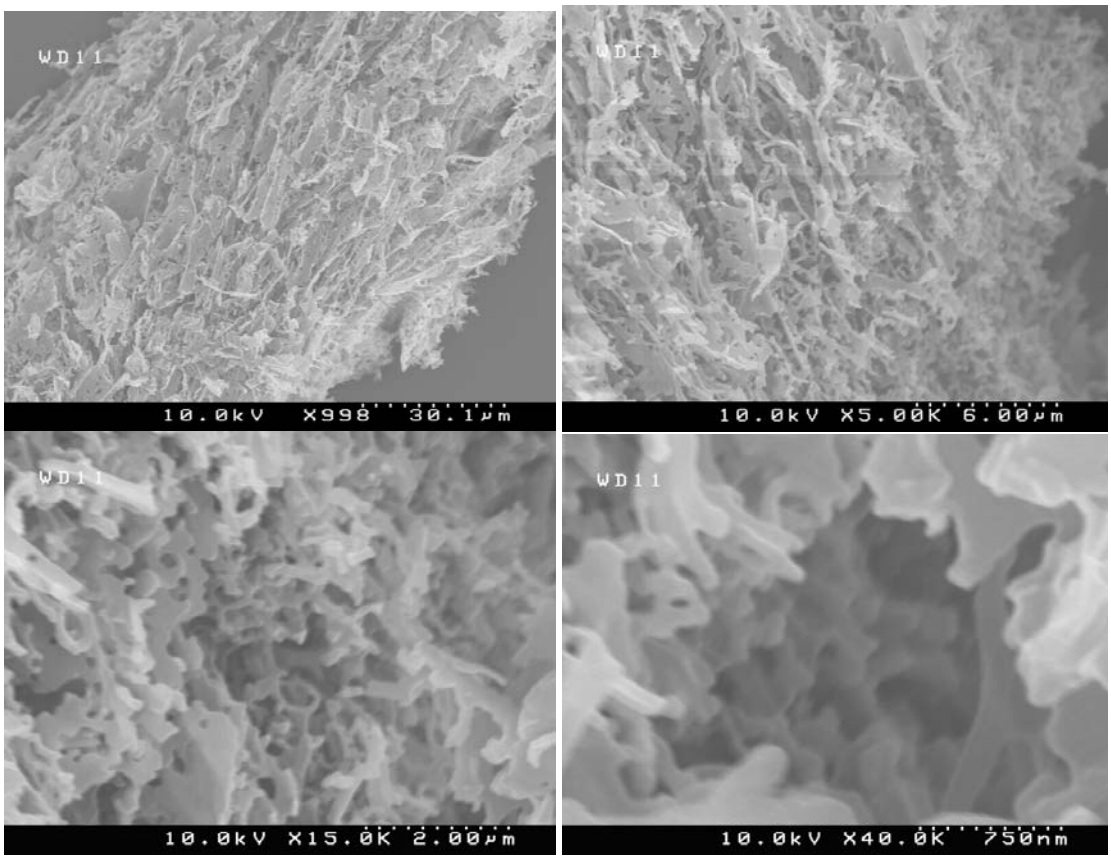

Figure D.3. SEM images of URF processed dry powder of ITZ/Lecithin=1/0.4 (w/w).

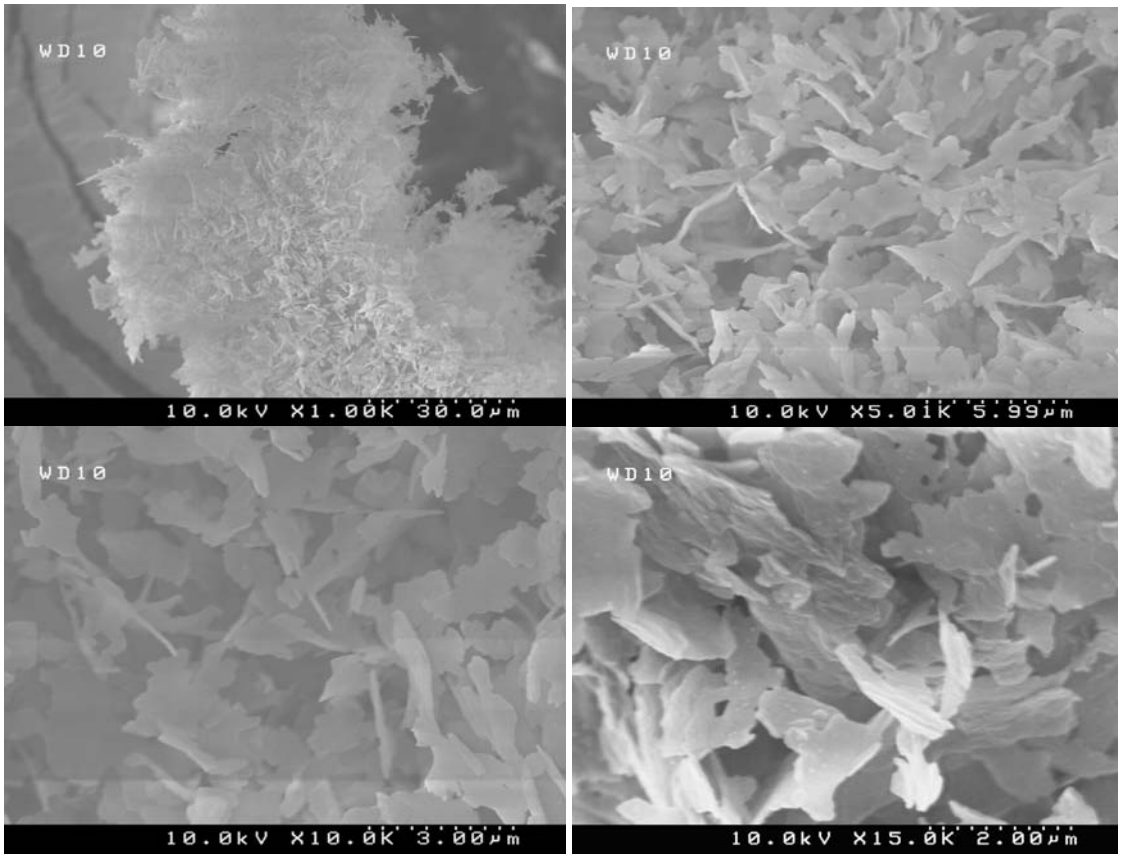

Figure D.4. SEM images of URF processed dry powder of ITZ/BSA/Lecithin=1/0.063/0.2 (w/w/w).

Note: BSA has low solubility in the mixed solvent of Dioxane/water=0.65/0.35 (v/v).

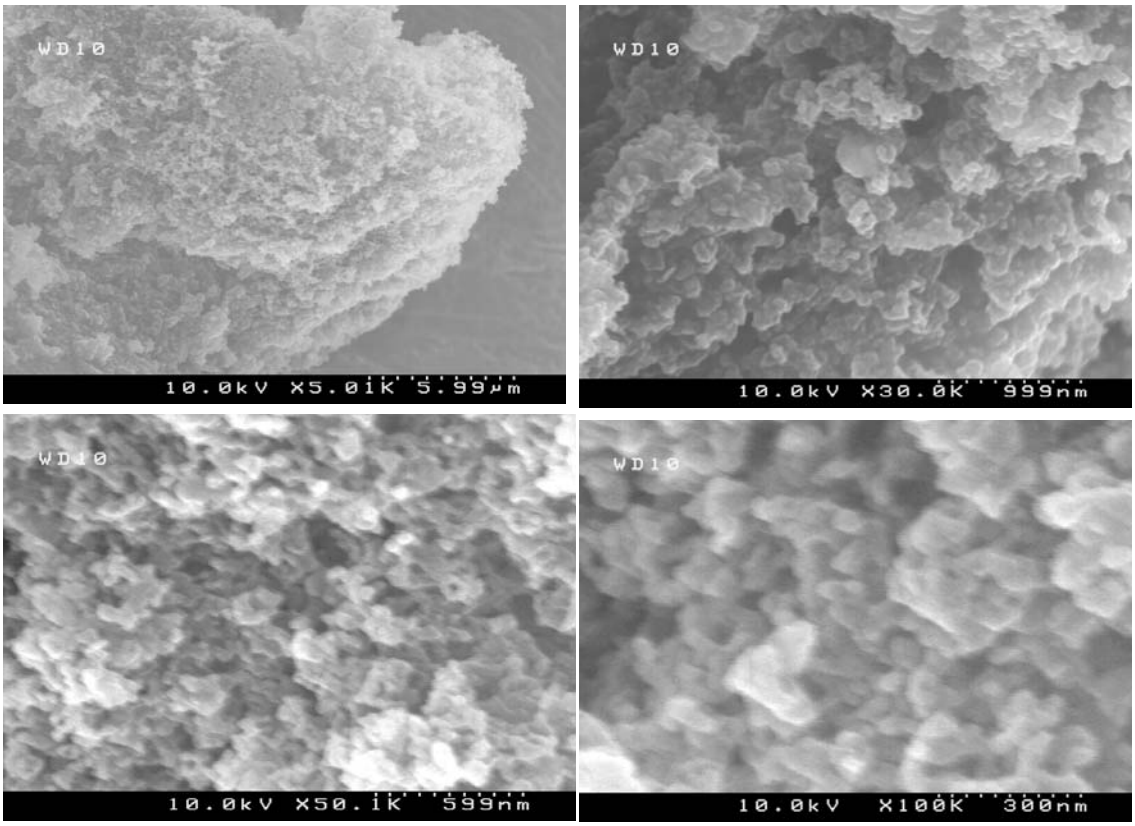

Figure D.5. SEM images of URF processed dry powder of ITZ/Dextrose/Lecithin=1/0.5/0.1 (w/w/w).

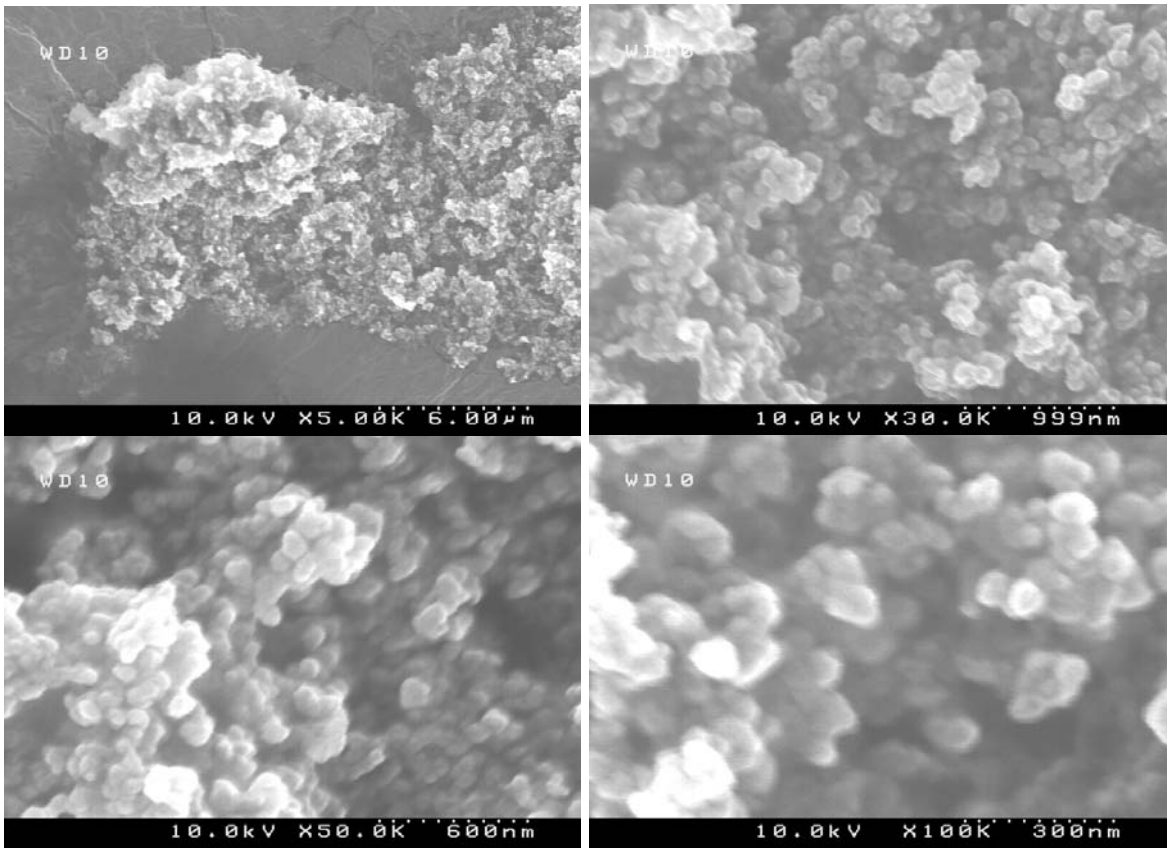

Figure D.6. SEM images of URF processed dry powder of ITZ/Lactose/Lecithin=1/0.5/0.1 (w/w/w).

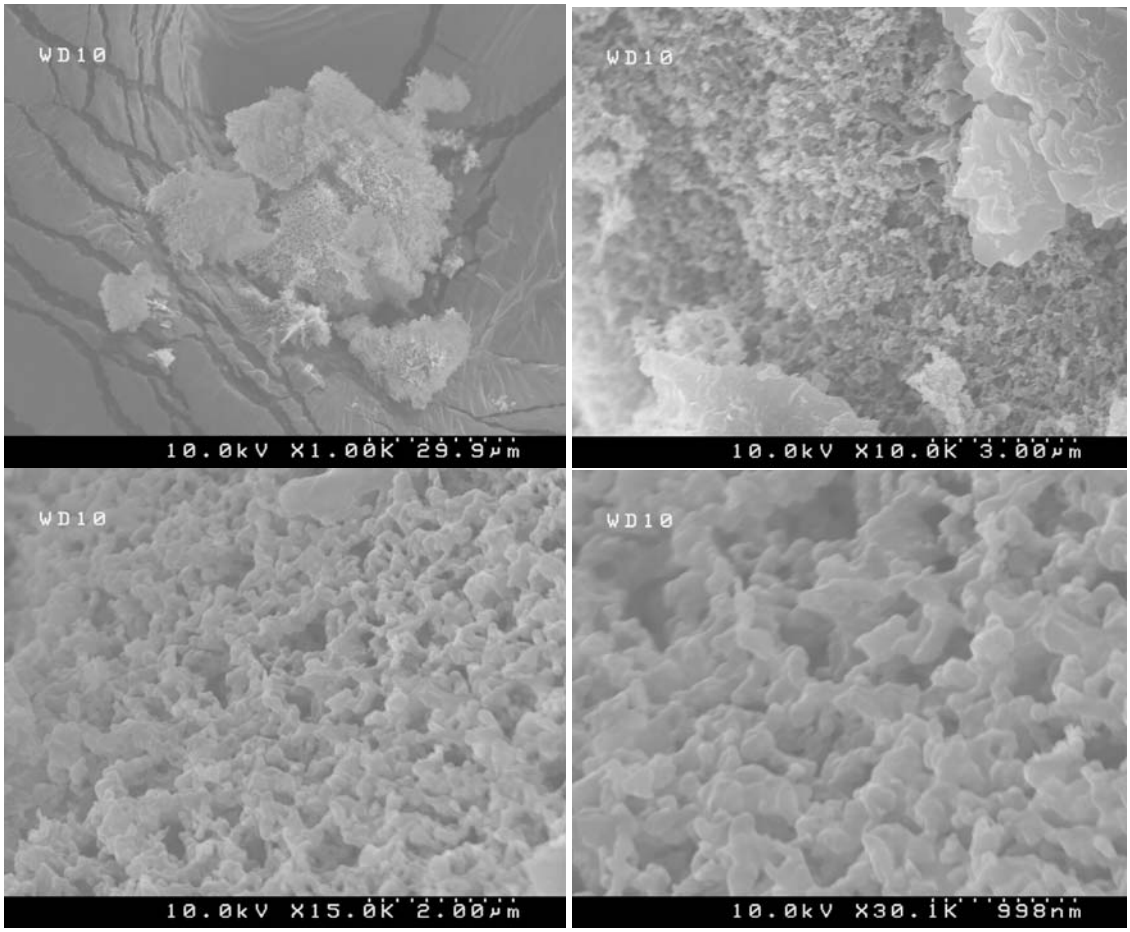

Figure D.7. SEM images of URF processed dry powder of ITZ/Lactose/Lecithin=1/0.5/0.2 (w/w/w).

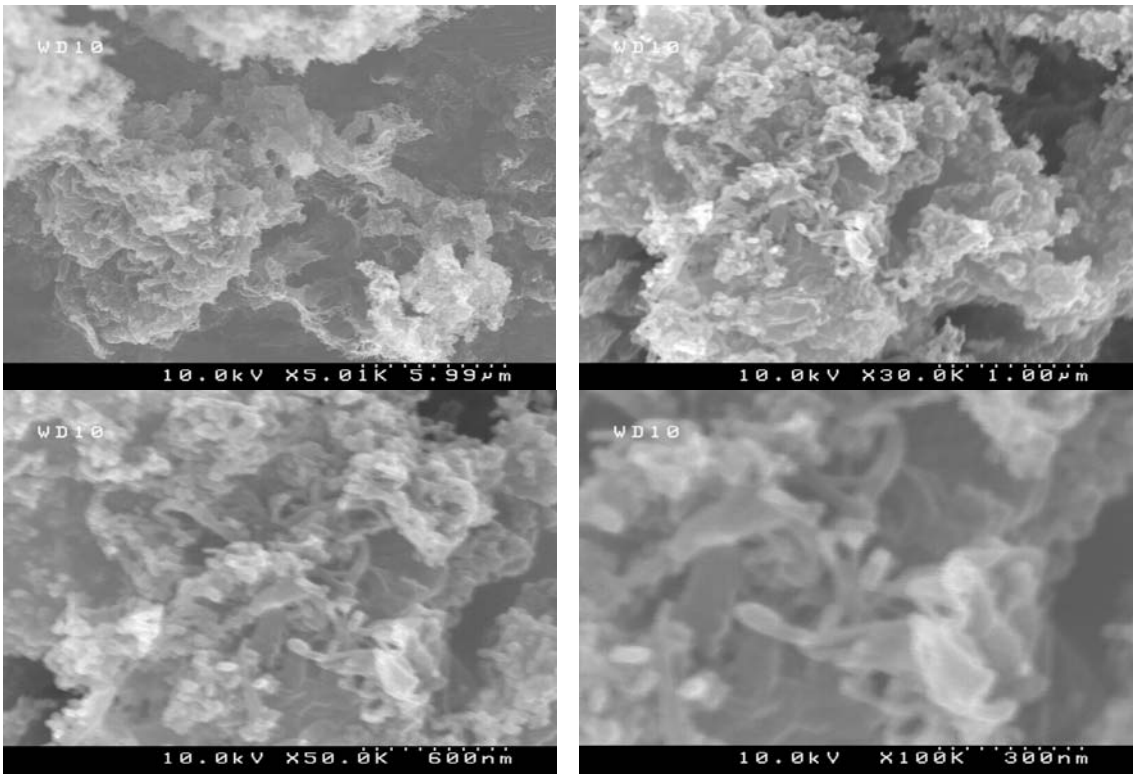

Figure D.8. SEM images of URF processed dry powder of ITZ/Meltose/Lecithin=1/0.5/0.1 (w/w/w).

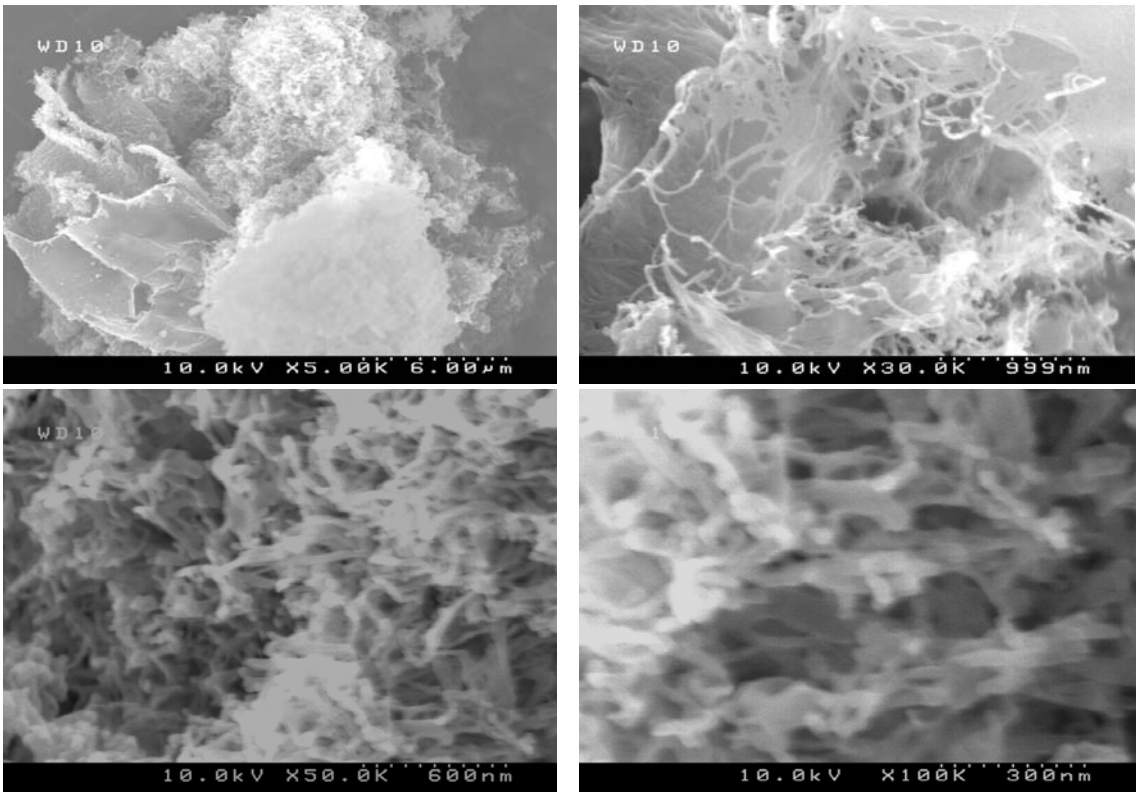

Figure D.9. SEM images of URF processed dry powder of ITZ/Sucrose/Lecithin=1/0.5/0.1 (w/w/w).

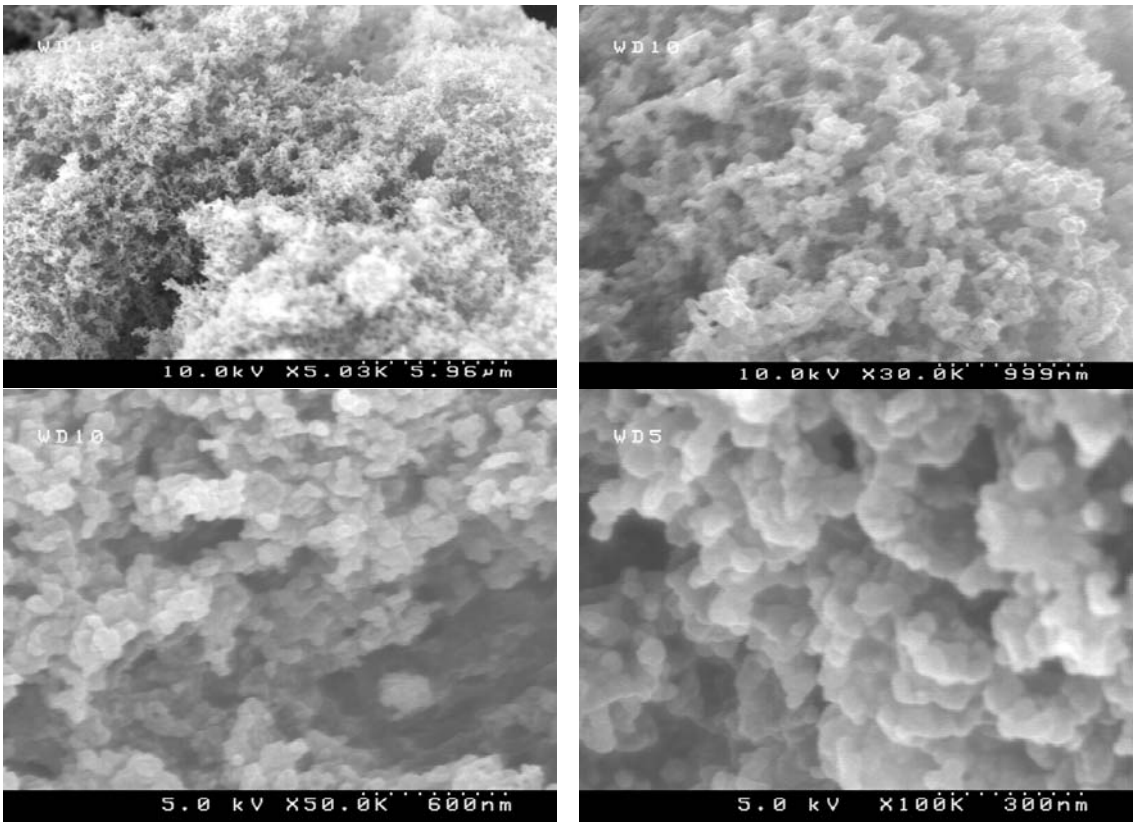

Figure D.10. SEM images of URF processed dry powder of ITZ/Trehalose/Lecithin=1/0.5/0.1 (w/w/w).

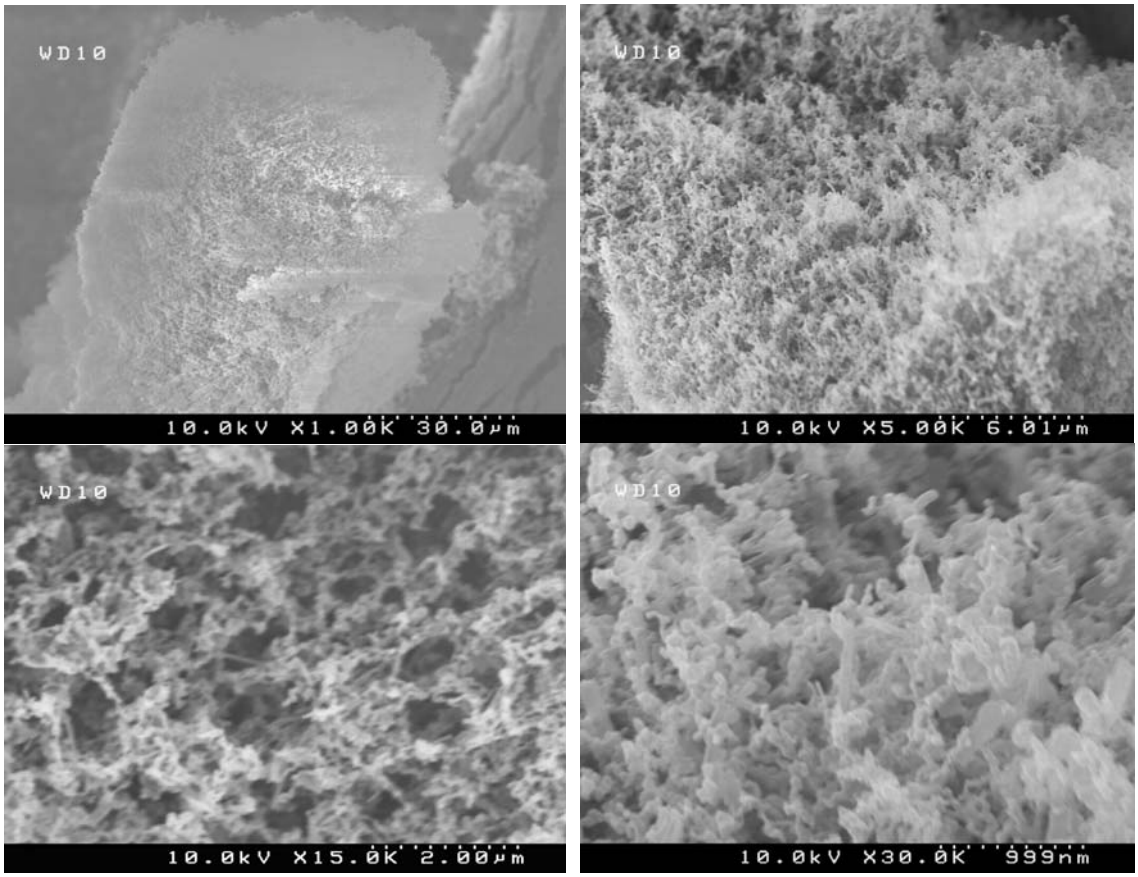

Figure D.11. SEM images of URF processed dry powder of ITZ/Mannitol/Lecithin=1/0.5/0.2 (w/w/w).

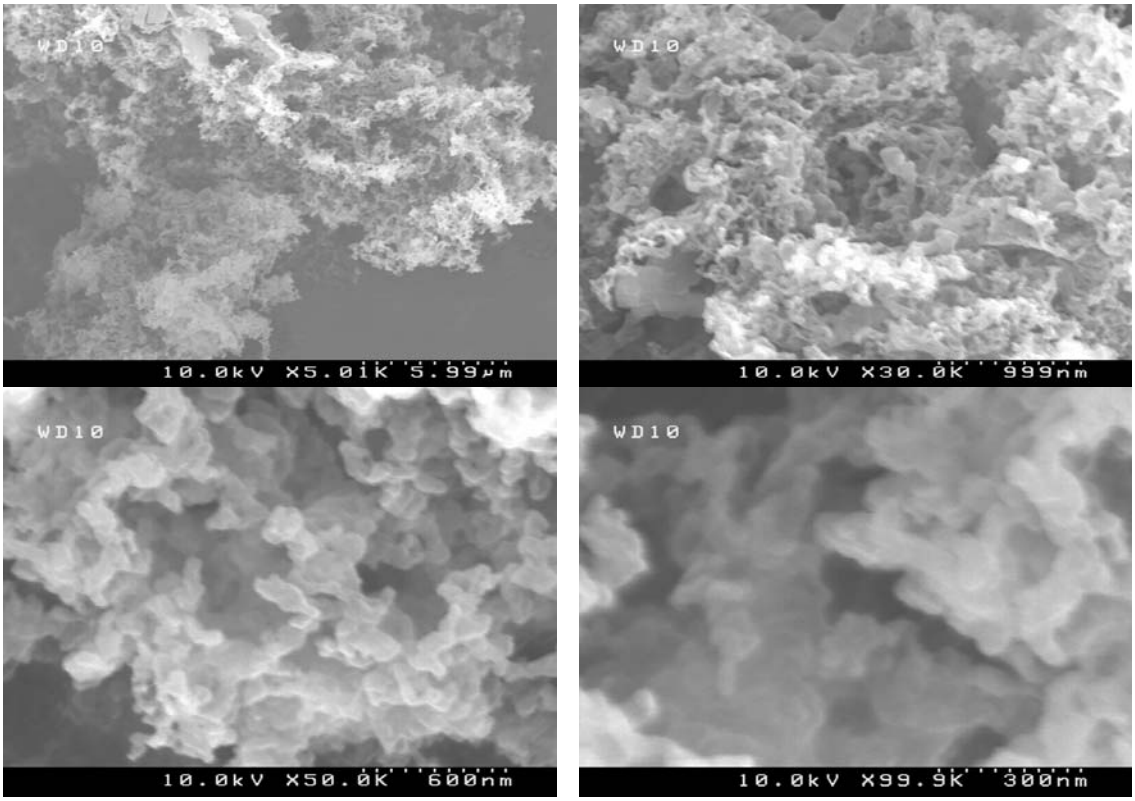

Figure D.12. SEM images of URF processed dry powder of ITZ/Erythritol/Lecithin=1/0.3/0.1 (w/w/w).

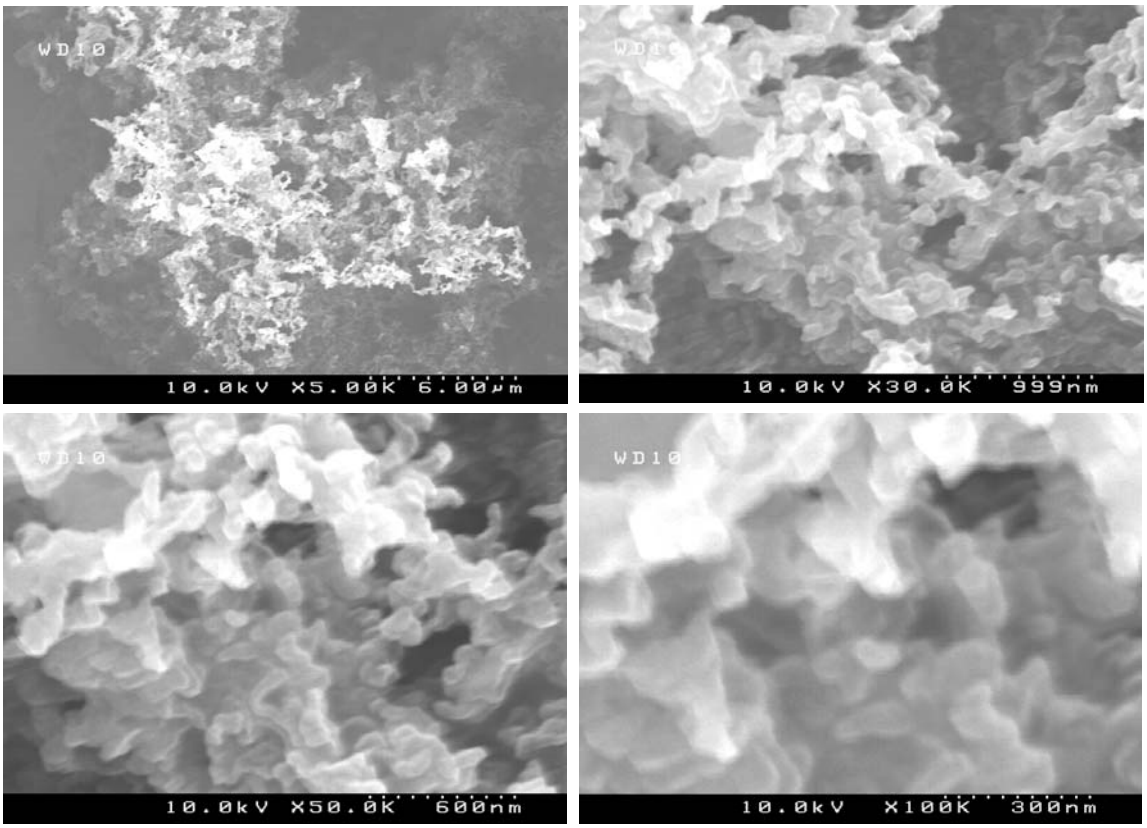

Figure D.13. SEM images of URF processed dry powder of ITZ/Xylitol/Lecithin=1/0.3/0.1 (w/w/w).

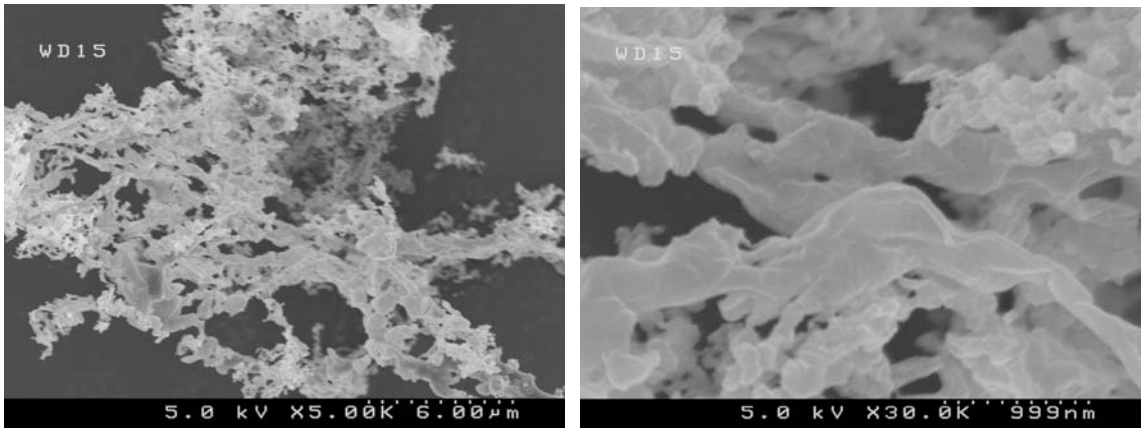

Figure D.14. SEM images of URF processed dry powder of ITZ/Erythritol/Tween20=1/5/0.0038 (w/w/w).

Note: the critical micelle concentration (CMC) of Tween 20 is 7.6×10^{-5} g/mL. When the powder dispersed into water to form a dispersion of 20 mg ITZ/mL equivalent, concentration of Tween 20 is at CMC.

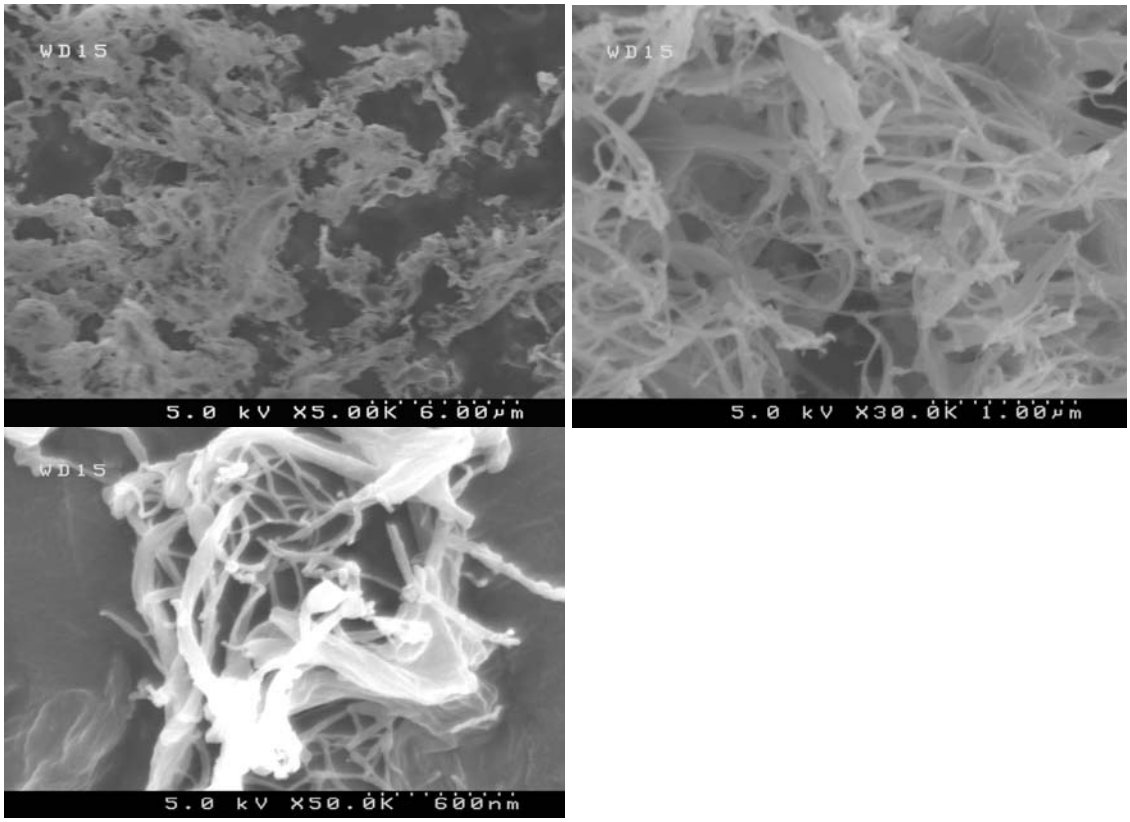

Figure D.15. SEM images of URF processed dry powder of ITZ/Glucose/Tween20=1/5/0.0038 (w/w/w).

Note: the critical micelle concentration (CMC) of Tween 20 is 7.6×10^{-5} g/mL. When the powder dispersed into water to form a dispersion of 20 mg ITZ/mL equivalent, concentration of Tween 20 is at CMC.

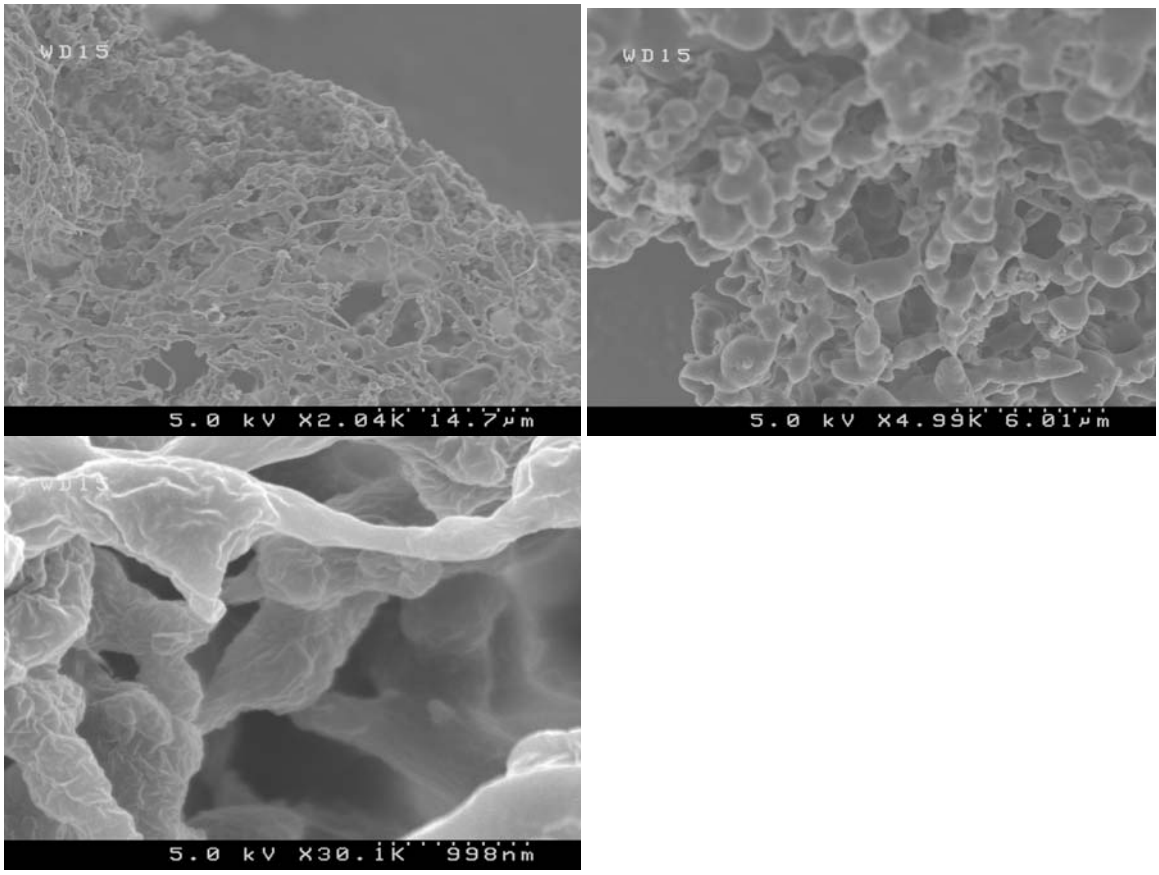

Figure D.16. SEM images of URF processed dry powder of ITZ/Lactose/Tween20=1/5/0.0038 (w/w/w).

Note: the critical micelle concentration (CMC) of Tween 20 is 7.6×10^{-5} g/mL. When the powder dispersed into water to form a dispersion of 20 mg ITZ/mL equivalent, concentration of Tween 20 is at CMC.

Bibliography

Adje, A. L., & Gupta, P. K. (1997). Inhalation Delivery of Therapeutic Peptides and Proteins. In A. A. F. Mahmoud (Ed.), *Parasitic Lung Diseases* (pp. 89-125). New York: Marcel Rcel Dekker Inc.

Agharkar, S., Lindenbaum, S., & Higuchi, T. (1976). Enhancement of Solubility of Drug Salts by Hydrophilic Counterions - Properties of Organic Salts of an antimalarial Drug. *Journal of Pharmaceutical Sciences, 65*(5), 747-749.

Aguiar, A. J., Krc, J., Jr., Kinkel, A. W., & Samyn, J. C. (1967). Effect of polymorphism on the absorption of chloramphenicol from chloramphenicol palmitate. *Journal of Pharmaceutical Sciences, 56*(7), 847-853.

Aguiar, A. J., & Zelmer, J. E. (1969). Dissolution behavior of polymorphs of chloramphenicol palmitate and mefenamic acid. *Journal of Pharmaceutical Sciences, 58*(8), 983-987.

Al-Marzouqi, A. H., Elwy, H. M., Shehadi, I., & Adem, A. (2009). Physicochemical properties of antifungal drug-cyclodextrin complexes prepared by supercritical carbon dioxide and by conventional techniques. *J Pharm Biomed Anal, 49*(2), 227-233.

Al-Marzouqi, A. H., Shehatta, I., Jobe, B., & Dowaidar, A. (2006). Phase solubility and inclusion complex of itraconazole with beta-cyclodextrin using supercritical carbon dioxide. *Journal of Pharmaceutical Sciences, 95*(2), 292-304.

Altiere, R., & Thompson, D. (1996). hysiology and pharmacology of the airways. In A. Hickey (Ed.), *Inhalation aerosols—Physical and biological basis for therapy* (pp. 85–138). New York: Marcel Dekker, Inc.

Alvarez, C. A., Wiederhold, N. P., McConville, J. T., Peters, J. I., Najvar, L. K., Graybill, J. R., et al. (2007). Aerosolized nanostructured itraconazole as prophylaxis against invasive pulmonary aspergillosis. *Journal of Infection, 55*(1), 68-74.

Amidon, G. L., Lennernas, H., Shah, V. P., & Crison, J. R. (1995). A theoretical basis for a biopharmaceutic drug classification: the correlation of in vitro drug product dissolution and in vivo bioavailability. *Pharmaceutical research, 12*(3), 413-420.

Amin, K., Dannenfelser, R. M., Zielinski, J., & Wang, B. (2004). Lyophilization of polyethylene glycol mixtures. *Journal of Pharmaceutical Sciences, 93*(9), 2244-2249.

Ariyananda, P. L., Agnew, J. E., & Clarke, S. W. (1996). Aerosol delivery systems for bronchial asthma. *Postgraduate Medical Journal, 72*(845), 151-156.

Arredouani, M., Yang, Z., Ning, Y., Qin, G., Soininen, R., Tryggvason, K., et al. (2004). The scavenger receptor MARCO is required for lung defense against pneumococcal pneumonia and inhaled particles. *J Exp Med, 200*(2), 267-272.

Azarmi, S., Tao, X., Chen, H., Wang, Z., Finlay, W. H., Lobenberg, R., et al. (2006). Formulation and cytotoxicity of doxorubicin nanoparticles carried by dry powder aerosol particles. *International Journal of Pharmaceutics, 319*(1-2), 155-161.

Barone, J. A., Koh, J. G., Bierman, R. H., Colaizzi, J. L., Swanson, K. A., Gaffar, M. C., et al. (1993). Food Interaction and Steady-State Pharmacokinetics of Itraconazole Capsules in Healthy Male-Volunteers. *Antimicrobial Agents and Chemotherapy, 37*(4), 778-784.

Bernhard, W., Haagsman, H. P., Tschernig, T., Poets, C. F., Postle, A. D., vanEijk, M. E., et al. (1997). Conductive airway surfactant: Surface-tension function, biochemical composition, and possible alveolar origin. *American Journal of Respiratory Cell and Molecular Biology, 17*(1), 41-50.

Betageri, G. V., & Makarla, K. R. (1995). Enhancement of dissolution of glyburide by solid dispersion and lyophilization techniques. *International Journal of Pharmaceutics, 126*(1-2), 155-160.

Bitonti, A. J., Dumont, J. A., Low, S. C., Peters, R. T., Kropp, K. E., Palombella, V. J., et al. (2004). Pulmonary delivery of an erythropoietin Fc fusion protein in non-human primates through an immunoglobulin transport pathway. *Proc Natl Acad Sci U S A, 101*(26), 9763-9768.

Blagden, N., de Matas, M., Gavan, P. T., & York, P. (2007). Crystal engineering of active pharmaceutical ingredients to improve solubility and dissolution rates. *Advanced Drug Delivery Reviews, 59*(7), 617-630.

Bodey, G. P. (1992). Azole Antifungal Agents. *Clinical Infectious Diseases, 14*, S161-S169.

Borm, P., Klaessig, F. C., Landry, T. D., Moudgil, B., Pauluhn, J., Thomas, K., et al. (2006a). Research strategies for safety evaluation of nanomaterials, part V: role of dissolution in biological fate and effects of nanoscale particles. *Toxicological Sciences, 90*(1), 23-32.

Borm, P. J., & Kreyling, W. (2004). Toxicological hazards of inhaled nanoparticles--potential implications for drug delivery. *J Nanosci Nanotechnol, 4*(5), 521-531.

Borm, P. J., Robbins, D., Haubold, S., Kuhlbusch, T., Fissan, H., Donaldson, K., et al. (2006). The potential risks of nanomaterials: a review carried out for ECETOC. *Part Fibre Toxicol, 3*, 11.

Bosquillon, C., Lombry, C., Preat, V., & Vanbever, R. (2001). Influence of formulation excipients and physical characteristics of inhalation dry powders on their aerosolization performance. *Journal of Controlled Release, 70*(3), 329-339.

Bradford, C. R., Prentice, A. G., Warnock, D. W., & Copplestone, J. A. (1991). Comparison of the multiple dose pharmacokinetics of two formulations of itraconazole during remission induction for acute myeloblastic leukaemia. *J Antimicrob Chemother, 28*(4), 555-560.

Brewster, M. E., & Loftsson, T. (2007). Cyclodextrins as pharmaccutical solubilizers. *Advanced Drug Delivery Reviews, 59*(7), 645-666.

Brewster, M. E., Neeskens, P., & Peeters, J. (2007). Solubilization of itraconazole as a function of cyclodextrin structural space. *Journal of Inclusion Phenomena and Macrocyclic Chemistry, 57*(1-4), 561-566.

Brewster, M. E., Simpkins, J. W., Hora, M. S., Stern, W. C., & Bodor, N. (1989). The Potential Use of Cyclodextrins in Parenteral Formulations. *Journal of Parenteral Science and Technology, 43*(5), 231-240.

Brewster, M. E., Vandecruys, R., Peeters, J., Neeskens, P., Verreck, G., & Loftsson, T. (2008). Comparative interaction of 2-hydroxypropyl-beta-cyclodextrin and sulfobutylether-beta-cyclodextrin with itraconazole: phase-solubility behavior and stabilization of supersaturated drug solutions. *European Journal of Pharmaceutical Sciences, 34*(2-3), 94-103.

Brigger, I., Dubernet, C., & Couvreur, P. (2002). Nanoparticles in cancer therapy and diagnosis. *Adv Drug Deliv Rev, 54*(5), 631-651.

Brown, D. M., Wilson, M. R., MacNee, W., Stone, V., & Donaldson, K. (2001). Size-dependent proinflammatory effects of ultrafine polystyrene particles: a role for surface area and oxidative stress in the enhanced activity of ultrafines. *Toxicol Appl Pharmacol, 175*(3), 191-199.

Brown, J. S., Zeman, K. L., & Bennett, W. D. (2002). Ultrafine particle deposition and clearance in the healthy and obstructed lung. *Am J Respir Crit Care Med, 166*(9), 1240-1247.

Byron, P., & Phillips, E. (1990). Absorption, clearance and dissolution in the lung. In P. R. Byron (Ed.), *Respiratory Drug Delivery* (pp. 107–141). Boca Raton FL: CRC.

Byron, P. R. (1986). Prediction of drug residence times in regions of the human respiratory tract following aerosol inhalation. *Journal of Pharmaceutical Sciences, 75*(5), 433-438.

Byron, P. R. (1993). Physicochemical effects on lung disposition of pharmaceutical aerosols. *Aerosol Science and Technology 18*, 223–229.

Byron, P. R., & Patton, J. S. (1994). Drug delivery via the respiratory tract. *J Aerosol Med, 7*(1), 49-75.

Chalupa, D. C., Morrow, P. E., Oberdorster, G., Utell, M. J., & Frampton, M. W. (2004). Ultrafine particle deposition in subjects with asthma. *Environ Health Perspect, 112*(8), 879-882.

Chan, H. K., & Gonda, I. (1988). Development of a Systematic Theory of Suspension Inhalation Aerosols .2. Aggregates of Monodisperse Particles Nebulized in Polydisperse Droplets. *International Journal of Pharmaceutics, 41*(1-2), 147-157.

Chiang, P. C., Alsup, J. W., Lai, Y. R., Hu, Y. D., Heyde, B. R., & Tung, D. (2009). Evaluation of Aerosol Delivery of Nanosuspension for Pre-clinical Pulmonary Drug Delivery. *Nanoscale Research Letters, 4*(3), 254-261.

Chiou, W. L. (1977). Pharmaceutical applications of solid dispersion systems: X-ray diffraction and aqueous solubility studies on griseofulvin-polyethylene glycol 6000 systems. *Journal of pharmaceutical sciences, 66*(7), 989-991.

Chono, S., Tanino, T., Seki, T., & Morimoto, K. (2006). Influence of particle size on drug delivery to rat alveolar macrophages following pulmonary administration of ciprofloxacin incorporated into liposomes. *J Drug Target, 14*(8), 557-566.

Chow, A. H. L., Tong, H. H. Y., Chattopadhyay, P., & Shekunov, B. Y. (2007). Particle engineering for pulmonary drug delivery. *Pharmaceutical Research, 24*(3), 411-437.

Clark, B. G., Ferreira, P., & Robertson, I. M. (2009). In Situ Electron Microscopy Methods. *Microscopy Research and Technique, 72*(3), 121-121.

Clark, T. A., & Hajjeh, R. A. (2002). Recent trends in the epidemiology of invasive mycoses. *Current Opinion in Infectious Diseases, 15*(6), 569-574.

Codrons, V., Vanderbist, F., Ucakar, B., Preat, V., & Vanbever, R. (2004). Impact of formulation and methods of pulmonary delivery on absorption of parathyroid hormone (1-34) from rat lungs. *Journal of pharmaceutical sciences, 93*(5), 1241-1252.

Colburn, D. E., Giles, F. J., Oladovich, D., & Smith, J. A. (2004). In vitro evaluation of cytochrome P450-mediated drug interactions between cytarabine, idarubicin, itraconazole and caspofungin. *Hematology, 9*(3), 217-221.

Cook, R. O., Pannu, R. K., & Kellaway, I. W. (2005). Novel sustained release microspheres for pulmonary drug delivery. *Journal of Controlled Release, 104*(1), 79-90.

Corry, D., Kulkarni, P., & Lipscomb, M. F. (1984). The migration of bronchoalveolar macrophages into hilar lymph nodes. *Am J Pathol, 115*(3), 321-328.

Courrier, H. M., Butz, N., & Vandamme, T. F. (2002a). Pulmonary drug delivery systems: Recent developments and prospects. *Critical Reviews in Therapeutic Drug Carrier Systems, 19*(4-5), 425-498.

Courrier, H. M., Butz, N., & Vandamme, T. F. (2002b). Pulmonary drug delivery systems: recent developments and prospects. *Crit Rev Ther Drug Carrier Syst, 19*(4-5), 425-498.

Crisp, M. T., Tucker, C. J., Rogers, T. L., Williams, R. O., 3rd, & Johnston, K. P. (2007). Turbidimetric measurement and prediction of dissolution rates of poorly soluble drug nanocrystals. *Journal of Controlled Release, 117*(3), 351-359.

Crisp, M. T., Tucker, C. J., Rogers, T. L., Williams, R. O., & Johnston, K. P. (2007). Turbidimetric measurement and prediction of dissolution rates of poorly soluble drug nanocrystals. *Journal of Controlled Release, 117*, 351-359.

Dahlberg, C., Millqvist-Fureby, A., & Schuleit, M. (2008). Surface composition and contact angle relationships for differently prepared solid dispersions. *European Journal of Pharmaceutics and Biopharmaceutics, 70*(2), 478-485.

Dailey, L. A., Schmehl, T., Gessler, T., Wittmar, M., Grimminger, F., Seeger, W., et al. (2003). Nebulization of biodegradable nanoparticles: impact of nebulizer technology and nanoparticle characteristics on aerosol features. *Journal of Controlled Release, 86*(1), 131-144.

Damian, F., Blaton, N., Naesens, L., Balzarini, J., Kinget, R., Augustijns, P., et al. (2000). Physicochemical characterization of solid dispersions of the antiviral agent UC-781 with polyethylene glycol 6000 and Gelucire 44/14. *European Journal of Pharmaceutical Sciences, 10*(4), 311-322.

Davies, N. M., & Feddah, M. R. (2003). A novel method for assessing dissolution of aerosol inhaler products. *International journal of pharmaceutics, 255*(1-2), 175-187.

De Beule, K., & Van Gestel, J. (2001). Pharmacology of itraconazole. *Drugs, 61*, 27-37.

de Jonge, M. E., Huitema, A. D. R., Rodenhuis, S., & Beijnen, J. H. (2005). Clinical pharmacokinetics of cyclophosphamide. *Clinical Pharmacokinetics, 44*(11), 1135-1164.

Deng, Z., Xu, S., & Li, S. (2008). Understanding a relaxation behavior in a nanoparticle suspension for drug delivery applications. *International Journal of Pharmaceutics, 351*(1-2), 236-243.

Donaldson, K., Stone, V., Tran, C. L., Kreyling, W., & Borm, P. J. (2004). Nanotoxicology. *Occup Environ Med, 61*(9), 727-728.

Donaldson, K., Tran, L., Jimenez, L. A., Duffin, R., Newby, D. E., Mills, N., et al. (2005). Combustion-derived nanoparticles: a review of their toxicology following inhalation exposure. *Part Fibre Toxicol, 2*, 10.

Dowling, A., Clift, R., Grobert, N., Hutton, D., Oliver, R., O'Neill, O., et al. (2004). *Nanoscience and nanotechnologies: opportunities and uncertainties*. London, UK: The Royal Society and the Royal Academy of Engineering

Dowling, A. P. (2004). Development of nanotechnologies. *Materials Today, 7*(Suppl. 1), 30-35.

Driscoll, K. E., Deyo, L. C., Carter, J. M., Howard, B. W., Hassenbein, D. G., & Bertram, T. A. (1997). Effects of particle exposure and particle-elicited inflammatory cells on mutation in rat alveolar epithelial cells. *Carcinogenesis, 18*(2), 423-430.

Ebbesen, M., & Jensen, T. G. (2006). Nanomedicine: techniques, potentials, and ethical implications. *Journal of Biomedical Biotechnology, 2006*(5), 51516.

Echezarreta-Lopez, M., Torres-Labandeira, J. J., Castineiras-Seijo, L., Santana-Penin, L., & Vila-Jato, J. L. (2000). Complexation of the interferon inducer, bropirimine, with hydroxypropyl-beta-cyclodextrin. *European Journal of Pharmaceutical Sciences, 9*(4), 381-386.

Edwards, D. A., Ben-Jebria, A., & Langer, R. (1998). Recent advances in pulmonary drug delivery using large, porous inhaled particles. *J Appl Physiol, 85*(2), 379-385.

Edwards, D. A., & Dunbar, C. (2002). Bioengineering of therapeutic aerosols. *Annu Rev Biomed Eng, 4*, 93-107.

Elder, E. J., Hitt, J. E., Rogers, T. L., Tucker, C. J., Saghir, S., Kupperblatt, G. B., et al. (2006). Particle engineering of poorly water soluble drugs by controlled

precipitation. *Polymeric Drug Delivery Ii: Polymeric Matrices and Drug Particle Engineering, 924*, 292-304.

Ely, L., Roa, W., Finlay, W. H., & Lobenberg, R. (2007). Effervescent dry powder for respiratory drug delivery. *Eur J Pharm Biopharm, 65*(3), 346-353.

Engstrom, J. D., Lai, E. S., Ludher, B. S., Chen, B., Milner, T. E., Williams, R. O., 3rd, et al. (In Press). Formation of Stable Submicron Protein Particles by Thin Film Freezing. *Pharmaceutical Research*.

Evans, J. C., Scherzer, B. D., Tocco, C. D., Kupperblatt, G. B., Becker, J. N., Wilson, D. L., et al. (2006). Preparation of nanostructured particles of poorly water soluble drugs via a novel ultra-rapid freezing technology. *in: S. Svenson (Ed.), Polymeric Drug Delivery – Polymeric Matrices and Drug Particle Engineering,* , ACS Symposium Series 924, American Chemical Society, Washington, DC, pp320–328.

Forbes, B., & Ehrhardt, C. (2005a). Human respiratory epithelial cell culture for drug delivery applications. *European Journal of Pharmaceutics and Biopharmaceutics, 60*(2), 193-205.

Forbes, B., & Ehrhardt, C. (2005b). Human respiratory epithelial cell culture for drug delivery applications. *European Journal of Pharmaceutics and Biopharmaceutics, 60*(2), 193-205.

Forsgren, P., Modig, J., Gerdin, B., Axelsson, B., & Dahlback, M. (1990). Intrapulmonary Deposition of Aerosolized Evans Blue-Dye and Liposomes in an Experimental Porcine Model of Early Ards. *Upsala Journal of Medical Sciences, 95*(2), 117-136.

Ganta, S., Paxton, J. W., Baguley, B. C., & Garg, S. (2009). Formulation and pharmacokinetic evaluation of an asulacrine nanocrystalline suspension for intravenous delivery. *International Journal of Pharmaceutics, 367*(1-2), 179-186.

Geelhaar, A., & Weibel, E. R. (1971). Morphometric estimation of pulmonary diffusion capacity. 3. The effect of increased oxygen consumption in Japanese Waltzing mice. *Respiratory Physiology, 11*(3), 354-366.

Gehr, P., Bachenfren, M., & Weibel, E. (1978). The normal human lung: ultrastructure and morphometric estimations of diffusion capacity. *Respiratory Physiology, 32*, 121-140.

Gehr, P., Green, F. H., Geiser, M., Im Hof, V., Lee, M. M., & Schurch, S. (1996). Airway surfactant, a primary defense barrier: mechanical and immunological aspects. *J Aerosol Med, 9*(2), 163-181.

Geiser, M., Schurch, S., & Gehr, P. (2003). Influence of surface chemistry and topography of particles on their immersion into the lung's surface-lining layer. *J Appl Physiol, 94*(5), 1793-1801.

Gelperina, S., Kisich, K., Iseman, M. D., & Heifets, L. (2005). The potential advantages of nanoparticle drug delivery systems in chemotherapy of tuberculosis. *Am J Respir Crit Care Med, 172*(12), 1487-1490.

Gill, S., Lobenberg, R., Ku, T., Azarmi, S., Roa, W., & Prenner, E. J. (2007). Nanoparticles: characteristics, mechanisms of action, and toxicity in pulmonary drug delivery - a review. *J. Biomed. Nanotechnology, 3*(2), 107-119.

Goerke, J. (1998). Pulmonary surfactant: functions and molecular composition. *Biochim Biophys Acta, 1408*(2-3), 79-89.

Grant, D. J. W., & Brittian, H. G. (1995). *Physical Characterisation of Pharmaceutical Solids*. New York: Marcel Dekker.

Groneberg, D. A., Witt, C., Wagner, U., Chung, K. F., & Fischer, A. (2003). Fundamentals of pulmonary drug delivery. *Respiratory Medicine, 97*(4), 382-387.

Gumbleton, M. (2001). Caveolae as potential macromolecule trafficking compartments within alveolar epithelium. *Adv Drug Deliv Rev, 49*(3), 281-300.

Gupta, P., Chawla, G., & Bansal, A. K. (2004). Physical stability and solubility advantage from amorphous celecoxib: The role of thermodynamic quantities and molecular mobility. *Molecular Pharmaceutics, 1*(6), 406-413.

Hancock, B. C., & Parks, M. (2000). What is the true solubility advantage for amorphous pharmaceuticals? *Pharmaceutical Research, 17*(4), 397-404.

Hancock, B. C., & Zograf, G. (1997). Characteristics and significance of the amorphous state in pharmaceutical systems. *Journal of Pharmaceutical Sciences, 86*(1), 1-12.

Heyder, J., Gebhart, J., Rudolf, G., Schiller, C. F., & Stahlhofen, W. (1986). Deposition of Particles in the Human Respiratory-Tract in the Size Range 0.005-15-Mu-M. *Journal of Aerosol Science, 17*(5), 811-825.

Heyder, J., & Rudolf, G. (1984). Mathematical-Models of Particle Deposition in the Human Respiratory-Tract. *Journal of Aerosol Science, 15*(6), 697-707.

Heykants, J., Vanpeer, A., Vandevelde, V., Vanrooy, P., Meuldermans, W., Lavrijsen, K., et al. (1989). The Clinical Pharmacokinetics of Itraconazole - an Overview. *Mycoses, 32*, 67-87.

Hilden, L. R., & Morris, K. R. (2004). Physics of amorphous solids. *Journal of Pharmaceutical Sciences, 93*(1), 3-12.

Hinds, W. C. (1998). *Aerosol Technology: Properties, Behavior, and Measurement of Airborne Particles*. New York: Wiley.

Hintz, R. J., & Johnson, K. C. (1989). The Effect of Particle-Size Distribution on Dissolution Rate and Oral Absorption. *International Journal of Pharmaceutics, 51*(1), 9-17.

Hitzman, C. J., Wattenberg, L. W., & Wiedmann, T. S. (2006). Pharmacokinetics of 5-fluorouracil in the hamster following inhalation delivery of lipid-coated nanoparticles. *J Pharm Sci, 95*(6), 1196-1211.

Hoeben, B. J., Burgess, D. S., McConville, J. T., Najvar, L. K., Talbert, R. L., Peters, J. I., et al. (2006). In vivo efficacy of aerosolized nanostructured itraconazole formulations for prevention of invasive pulmonary aspergillosis. *Antimicrobial Agents and Chemotherapy, 50*(4), 1552-1554.

Hoet, P. H., Bruske-Hohlfeld, I., & Salata, O. V. (2004). Nanoparticles - known and unknown health risks. *J Nanobiotechnology, 2*(1), 12.

Hoet, P. H., Gilissen, L., & Nemery, B. (2001). Polyanions protect against the in vitro pulmonary toxicity of polycationic paint components associated with the Ardystil syndrome. *Toxicol Appl Pharmacol, 175*(2), 184-190.

Hoet, P. H., Gilissen, L. P., Leyva, M., & Nemery, B. (1999). In vitro cytotoxicity of textile paint components linked to the "Ardystil syndrome". *Toxicol Sci, 52*(2), 209-216.

Hong, J. Y., Kim, J. K., Song, Y. K., Park, J. S., & Kim, C. K. (2006). A new self-emulsifying formulation of itraconazole with improved dissolution and oral absorption. *Journal of Controlled Release, 110*(2), 332-338.

Hostetler, J. S., Hanson, L. H., & Stevens, D. A. (1992). Effect of cyclodextrin on the pharmacology of antifungal oral azoles. *Antimicrobial Agents Chemotherapy, 36*(2), 477-480.

Hostetler, J. S., Hanson, L. H., & Stevens, D. A. (1993). Effect of hydroxypropyl-beta-cyclodextrin on efficacy of oral itraconazole in disseminated murine cryptococcosis. *J Antimicrobial Chemotherapy, 32*(3), 459-463.

http://www.accessdata.fda.gov/scripts/cder/iig/getiigWEB.cfm.

Hu, J., Johnston, K. P., & Williams, R. O., 3rd. (2004). Nanoparticle engineering processes for enhancing the dissolution rates of poorly water soluble drugs. *Drug Dev Ind Pharm, 30*(3), 233-245.

Irie, T., & Uekama, K. (1997). Pharmaceutical applications of cyclodextrins .3. Toxicological issues and safety evaluation. *Journal of Pharmaceutical Sciences, 86*(2), 147-162.

Jacobs, C., & Muller, R. H. (2002a). Production and characterization of a budesonide nanosuspension for pulmonary administration. *Pharmaceutical Research, 19*(2), 189-194.

Jacobs, C., & Muller, R. H. (2002b). Production and characterization of a budesonide nanosuspension for pulmonary administration. *Pharmaceutical Research, 19*(2), 189-194.

Jaques, P. A., & Kim, C. S. (2000). Measurement of total lung deposition of inhaled ultrafine particles in healthy men and women. *Inhal Toxicol, 12*(8), 715-731.

Johansson, J., Curstedt, T., & Robertson, B. (1994). The proteins of the surfactant system. *Eur Respir J, 7*(2), 372-391.

Johari, G. P., Ram, S., Astl, G., & Mayer, E. (1990). Characterizing Amorphous and Microcrystalline Solids by Calorimetry. *Journal of Non-Crystalline Solids, 116*(2-3), 282-285.

Jones, S., & Parr, G. (1987). The acetotoluides as models for studying cyclodextrin inclusion complexes *International Journal of Pharmaceutics, 36*(2-3), 223-231.

Kalhorn, T. F., Ren, S., Howald, W. N., Lawrence, R. F., & Slattery, J. T. (1999). Analysis of cyclophosphamide and five metabolites from human plasma using liquid chromatography-mass spectrometry and gas chromatography-nitrogen-phosphorus detection. *Journal of Chromatography B, 732*(2), 287-298.

Kantola, T., Backman, J. T., Niemi, M., Kivisto, K. T., & Neuvonen, P. J. (2000). Effect of fluconazole on plasma fluvastatin and pravastatin concentrations. *European Journal of Clinical Pharmacology, 56*(3), 225-229.

Kapsi, S. G., & Ayres, J. W. (2001). Processing factors in development of solid solution formulation of itraconazole for enhancement of drug dissolution and bioavailability. *Int J Pharm, 229*(1-2), 193-203.

Kassem, M. A., Rahman, A. A. A., Ghorab, M. M., Ahmed, M. B., & Khalil, R. M. (2007). Nanosuspension as an ophthalmic delivery system for certain glucocorticoid drugs. *International Journal of Pharmaceutics, 340*(1-2), 126-133.

Kato, T., Yashiro, T., Murata, Y., Herbert, D. C., Oshikawa, K., Bando, M., et al. (2003). Evidence that exogenous substances can be phagocytized by alveolar epithelial cells and transported into blood capillaries. *Cell Tissue Res, 311*(1), 47-51.

Kim, A. I., Akers, M. J., & Nail, S. L. (1998). The physical state of mannitol after freeze-drying: effects of mannitol concentration, freezing rate, and a noncrystallizing cosolute. *J Pharm Sci, 87*(8), 931-935.

Kipp, J. E. (2004). The role of solid nanoparticle technology in the parenteral delivery of poorly water-soluble drugs. *International Journal of Pharmaceutics, 284*(1-2), 109-122.

Koushik, K., Dhanda, D. S., Cheruvu, N. P., & Kompella, U. B. (2004). Pulmonary delivery of deslorelin: large-porous PLGA particles and HPbetaCD complexes. *Pharm Res, 21*(7), 1119-1126.

Kraft, W. K., Steiger, B., Beussink, D., Quiring, J. N., Fitzgerald, N., Greenberg, H. E., et al. (2004). The pharmacokinetics of nebulized nanocrystal budesonide suspension in healthy volunteers. *Journal of Clinical Pharmacology, 44*(1), 67-72.

Kreyling, W. G., Semmler, M., Erbe, F., Mayer, P., Takenaka, S., Schulz, H., et al. (2002). Translocation of ultrafine insoluble iridium particles from lung epithelium to extrapulmonary organs is size dependent but very low. *J Toxicol Environ Health A, 65*(20), 1513-1530.

Labhasetwar, V. (2005). Nanotechnology for drug and gene therapy: the importance of understanding molecular mechanisms of delivery. *Current Opinion in Biotechnology, 16*(6), 674-680.

Lauweryns, J. M., & Baert, J. H. (1977). Alveolar clearance and the role of the pulmonary lymphatics. *Am Rev Respir Dis, 115*(4), 625-683.

Leak, L. V., & Ferrans Lee, V. J. (1991). Lymphatics and lymphoil tissue. In R. G. Crystal, J. B. West, N. S. Cherniack & E. R. Weibel (Eds.), *The Lung: Scientific Foundations* (pp. 779–786). New York: Raven Press.

Lee, K. P., Kelly, D. P., Schneider, P. W., & Trochimowicz, H. J. (1986). Inhalation toxicity study on rats exposed to titanium tetrachloride atmospheric hydrolysis products for two years. *Toxicol Appl Pharmacol, 83*(1), 30-45.

Leuner, C., & Dressman, J. (2000). Improving drug solubility for oral delivery using solid dispersions. *European Journal of Pharmaceutics and Biopharmaceutics, 50*(1), 47-60.

Li, J., Rayner, C. R., Nation, R. L., Owen, R. J., Spelman, D., Tan, K. E., et al. (2006). Heteroresistance to colistin in multidrug-resistant Acinetobacter baumannii. *Antimicrob Agents Chemother, 50*(9), 2946-2950.

Lin, S. J., Schranz, J., & Teutsch, S. M. (2001). Aspergillosis case - Fatality rate: Systematic review of the literature. *Clinical Infectious Diseases, 32*(3), 358-366.

Lindmark, T., Kimura, Y., & Artursson, P. (1998). Absorption enhancement through intracellular regulation of tight junction permeability by medium chain fatty acids in Caco-2 cells. *J Pharmacol Exp Ther, 284*(1), 362-369.

Lipinski, C. A. (2000). Drug-like properties and the causes of poor solubility and poor permeability. *Journal of Pharmacological and Toxicological Methods, 44*(1), 235-249.

Lipinski, C. A., Lombardo, F., Dominy, B. W., & Feeney, P. J. (1997). Experimental and computational approaches to estimate solubility and permeability in drug discovery and development settings. *Advanced Drug Delivery Reviews, 23*(1-3), 3-25.

Liu, F. Y., Shao, Z., Kildsig, D. O., & Mitra, A. K. (1993). Pulmonary delivery of free and liposomal insulin. *Pharmaceutical Research, 10*(2), 228-232.

Liu, R. (2000). *Water-insoluble drug formulation*. Englewood: CO Interpharm Press.

Liversidge, G. G., & Cundy, K. C. (1995). Particle-Size Reduction for Improvement of Oral Bioavailability of Hydrophobic Drugs .1. Absolute Oral Bioavailability of Nanocrystalline Danazol in Beagle Dogs. *International Journal of Pharmaceutics, 125*(1), 91-97.

Loftsson, T., & Masson, M. (2004). The effects of water-soluble polymers on cyclodextrins and cyclodextrin solubilization of drugs. *Journal of Drug Delivery Science and Technology, 14*(1), 35-43.

Loftsson, T., Masson, M., & Sigurjonsdottir, J. F. (1999). Methods to enhance the complexation efficiency of cyclodextrins. *Stp Pharma Sciences, 9*(3), 237-242.

Lombry, C., Edwards, D. A., Preat, V., & Vanbever, R. (2004). Alveolar macrophages are a primary barrier to pulmonary absorption of macromolecules. *Am J Physiol Lung Cell Mol Physiol, 286*(5), L1002-1008.

Lum, H., & Mitzner, W. (1987). A species comparison of alveolar size and surface forces. *J Appl Physiol, 62*(5), 1865-1871.

Marques, H. M. C., Hadgraft, J., & Kellaway, I. W. (1990). Studies of cyclodextrin inclusion complexes .1. the salbutamol-cyclodextrin complex as studied by phase solubility and DSC *International Journal of Pharmaceutics, 63*(3), 259-266.

Marques, H. M. C., Hadgraft, J., Kellaway, I. W., & Taylor, G. (1991). Studies of Cyclodextrin Inclusion Complexes .3. The Pulmonary Absorption of Beta-Cyclodextrin, Dm-Beta-Cyclodextrin and Hp-Beta-Cyclodextrin in Rabbits. *International Journal of Pharmaceutics, 77*(2-3), 297-302.

Marr, K. A., Carter, R. A., Crippa, F., Wald, A., & Corey, L. (2002). Epidemiology and outcome of mould infections in hematopoietic stem cell transplant recipients. *Clinical Infectious Diseases, 34*(7), 909-917.

Marr, K. A., Leisenring, W., Crippa, F., Slattery, J. T., Corey, L., Boeckh, M., et al. (2004). Cyclophosphamide metabolism is affected by azole antifungals. *Blood, 103*(4), 1557-1559.

Martin, A. (1993). *Physical Pharmacy. Fourth ed.* Baltimore: Williams&Wilkins.

Martonen, T. B., & Katz, I. M. (1993). Deposition Patterns of Aerosolized Drugs within Human Lungs - Effects of Ventilatory Parameters. *Pharmaceutical Research, 10*(6), 871-878.

Matilainen, L., Toropainen, T., Vihola, H., Hirvonen, J., Jarvinen, T., Jarho, P., et al. (2008). In vitro toxicity and permeation of cyclodextrins in Calu-3 cells. *Journal of Controlled Release, 126*(1), 10-16.

Matteucci, M. E., Brettmann, B. K., Rogers, T. L., Elder, E. J., Williams, R. O., 3rd , & Johnston, K. P. (2007). Design of Potent Amorphous Drug Nanoparticles for Rapid Generation of Highly Supersaturated Media. *Molecular Pharmaceutics 4*(5), 782-793.

Matteucci, M. E., Hotze, M. A., Johnston, K. P., & Williams, R. O. (2006). Drug nanoparticles by antisolvent precipitation: Mixing energy versus surfactant stabilization. *Langmuir, 22*(21), 8951-8959.

Matteucci, M. E., Miller, M. A., Williams, R. O., & Johnston, K. P. (2008). Highly Supersaturated Solutions of Amorphous Drugs Approaching Predictions from Configurational Thermodynamic Properties. *Journal of Physical Chemistry B, 112*(51), 16675-16681.

Matteucci, M. E., Paguio, J. C., Miller, M. A., Williams, R. O., & Johnston, K. P. (2009). Highly Supersaturated Solutions from Dissolution of Amorphous Itraconazole Microparticles at pH 6.8. *Molecular Pharmaceutics, 6*(2), 375-385.

Mauludin, R., Muller, R. H., & Keck, C. M. (2009). Development of an oral rutin nanocrystal formulation. *International Journal of Pharmaceutics, 370*(1-2), 202-209.

Mawson, S., Yates, M. Z., ONeill, M. L., & Johnston, K. P. (1997). Stabilized polymer microparticles by precipitation with a compressed fluid antisolvent .2. Poly(propylene oxide)- and poly(butylene oxide)-based copolymers. *Langmuir, 13*(6), 1519-1528.

Maynard, A., & Kuempel, E. (2005). Airborne Nanostructured Particles and Occupational Health. *Journal of Nanoparticle Research, 7*, 587-614.

McCabe, W. L., Smith, J. C., & Harriott, P. (2001). *Unit Operations of Chemical Engineering*. Boston, MA: McGraw Hill Inc.

McCallion, O. N., Taylor, K. M., Thomas, M., & Taylor, A. J. (1995). Nebulization of fluids of different physicochemical properties with air-jet and ultrasonic nebulizers. *Pharmaceutical Research, 12*(11), 1682-1688.

McCallion, O. N. M., Taylor, K. M. G., Thomas, M., & Taylor, A. J. (1996). Nebulisation of monodisperse latex sphere suspensions in air-jet and ultrasonic nebulizers. *International Journal of Pharmaceutics, 133*, 203–214.

McConville, J. T., Overhoff, K. A., Sinswat, P., Vaughn, J. M., Frei, B. L., Burgess, D. S., et al. (2006a). Targeted high lung concentrations of itraconazole using nebulized dispersions in a murine model. *Pharmaceutical Research, 23*(5), 901-911.

McConville, J. T., Williams, R. O., Carvalho, T. C., Iberg, A. N., Johnston, K. P., Talbert, R. L., et al. (2005). Design and evaluation of a restraint-free small animal inhalation dosing chamber. *Drug Development and Industrial Pharmacy, 31*(1), 35-42.

McDonald, G. B., Slattery, J. T., Bouvier, M. E., Ren, S., Batchelder, A. L., Kalhorn, T. F., et al. (2003). Cyclophosphamide metabolism, liver toxicity, and mortality following hematopoietic stem cell transplantation. *Blood, 101*(5), 2043-2048.

McIntire, G. L., Bacon, E. R., Toner, J. L., Cornacoff, J. B., Losco, P. E., Illig, K. J., et al. (1998). Pulmonary delivery of nanoparticles of insoluble, iodinated CT X-ray contrast agents to lung draining lymph nodes in dogs. *J Pharm Sci, 87*(11), 1466-1470.

Mehnert, W., & Mader, K. (2001). Solid lipid nanoparticles: production, characterization and applications. *Adv Drug Deliv Rev, 47*(2-3), 165-196.

Mehrad, B., Paciocco, G., Martinez, F. J., Ojo, T. C., Iannettoni, M. D., & Lynch, J. P., 3rd. (2001). Spectrum of Aspergillus infection in lung transplant recipients: case series and review of the literature. *Chest, 119*(1), 169-175.

Meyer, M., Persson, O., & Power, Y. (2001). *Mapping excellence in nanotechnologies, Preparatory study (Nanotechnology expert group and Eurotech data)*. Brussels: European Commission.

Miller, D. A., DiNunzio, J. C., Yang, W., McGinity, J. W., & Williams, R. O. (2008). Targeted intestinal delivery of supersaturated itraconazole for improved oral absorption. *Pharmaceutical Research, 25*(6), 1450-1459.

Miller, D. A., McConville, J. T., Yang, W., Williams, R. O., 3rd, & McGinity, J. W. (2007). Hot-melt extrusion for enhanced delivery of drug particles. *J Pharm Sci, 96*(2), 361-376.

Mills, N. L., Amin, N., Robinson, S. D., Anand, A., Davies, J., Patel, D., et al. (2006). Do inhaled carbon nanoparticles translocate directly into the circulation in humans? *Am J Respir Crit Care Med, 173*(4), 426-431.

Mitra, R., Pezron, I., Li, Y., & Mitra, A. K. (2001). Enhanced pulmonary delivery of insulin by lung lavage fluid and phospholipids. *Int J Pharm, 217*(1-2), 25-31.

Moghimi, S. M., & Hunter, A. C. (2001). Capture of stealth nanoparticles by the body's defences. *Crit Rev Ther Drug Carrier Syst, 18*(6), 527-550.

Moore, M. N. (2002). Biocomplexity: the post-genome challenge in ecotoxicology. *Aquat Toxicol, 59*(1-2), 1-15.

Mu, L., & Seow, P. H. (2006). Application of TPGS in polymeric nanoparticulate drug delivery system. *Colloids Surf B Biointerfaces, 47*(1), 90-97.

Muller, R. H., Jacobs, C., & Kayser, O. (2001). Nanosuspensions as particulate drug formulations in therapy Rationale for development and what we can expect for the future. *Advanced Drug Delivery Reviews, 47*(1), 3-19.

Muranishi, S., Fujita, T., Murakami, M., & Yamamoto, A. (1996). Lymphatic transfer of macromolecules after intrapulmonary administration in the presence or absence of various absorption enhancers in rats. *Pharmazie, 51*(5), 331-336.

Myers, M. A., Thomas, D. A., Straub, L., Soucy, D. W., Niven, R. W., Kaltenbach, M., et al. (1993). Pulmonary effects of chronic exposure to liposome aerosols in mice. *Exp Lung Res, 19*(1), 1-19.

Nel, A., Xia, T., Madler, L., & Li, N. (2006). Toxic potential of materials at the nanolevel. *Science, 311*(5761), 622-627.

Nemmar, A., Vanbilloen, H., Hoylaerts, M. F., Hoet, P. H., Verbruggen, A., & Nemery, B. (2001). Passage of intratracheally instilled ultrafine particles from the lung into the systemic circulation in hamster. *Am J Respir Crit Care Med, 164*(9), 1665-1668.

Nesseem, D. I. (2001). Formulation and evaluation of itraconazole via liquid crystal for topical delivery system. *J Pharm Biomed Anal, 26*(3), 387-399.

Newman, S. P. (1991). Aerosol generators and delivery systems. *Respir Care, 36*(9), 939-951.

Newman, S. P., Pavia, D., Garland, N., & Clarke, S. W. (1982). Effects of various inhalation modes on the deposition of radioactive pressurized aerosols. *Eur J Respir Dis Suppl, 119*, 57-65.

Niven, R. W. (1992). *Pharmaceutical Inhalation Aerosol Technology*. New York: Marcel Dekker, Inc.

Oberdorster, G. (2002). Toxicokinetics and effects of fibrous and nonfibrous particles. *Inhal Toxicol, 14*(1), 29-56.

Oberdorster, G., Ferin, J., & Lehnert, B. E. (1994). Correlation between particle size, in vivo particle persistence, and lung injury. *Environ Health Perspect, 102 Suppl 5*, 173-179.

Oberdorster, G., Oberdorster, E., & Oberdorster, J. (2005). Nanotoxicology: an emerging discipline evolving from studies of ultrafine particles. *Environ Health Perspect, 113*(7), 823-839.

Oberdorster, G., Sharp, Z., Atudorei, V., Elder, A., Gelein, R., Lunts, A., et al. (2002). Extrapulmonary translocation of ultrafine carbon particles following whole-body inhalation exposure of rats. *J Toxicol Environ Health A, 65*(20), 1531-1543.

Oberdorster, G., & Yu, C. P. (1999). Lung dosimetry--considerations for noninhalation studies. *Exp Lung Res, 25*(1), 1-6.

Oh, D. M., Curl, R. L., & Amidon, G. L. (1993). Estimating the Fraction Dose Absorbed from Suspensions of Poorly Soluble Compounds in Humans - a Mathematical-Model. *Pharmaceutical Research, 10*(2), 264-270.

Oren, I., Rowe, J. M., Sprecher, H., Tamir, A., Benyamini, N., Akria, L., et al. (2006). A prospective randomized trial of itraconazole vs fluconazole for the prevention of

fungal infections in patients with acute leukemia and hematopoietic stem cell transplant recipients. *Bone Marrow Transplantation, 38*(2), 127-134.

Ostrander, K. D., Bosch, H. W., & Bondanza, D. M. (1999a). An in-vitro assessment of a NanoCrystal (TM) beclomethasone dipropionate colloidal dispersion via ultrasonic nebulization. *European Journal of Pharmaceutics and Biopharmaceutics, 48*(3), 207-215.

Ott, P., Hope, M. J., Verkleij, A. J., Roelofsen, B., Brodbeck, U., & van Deenen, L. L. (1981). Effect of dimyristoyl phosphatidylcholine on intact erythrocytes. Release of spectrin-free vesicles without ATP depletion. *Biochim Biophys Acta, 641*(1), 79-87.

Overhoff, K. A., Engstrom, J. D., Chen, B., Scherzer, B. D., Milner, T. E., Johnston, K. P., et al. (2007). Novel ultra-rapid freezing particle engineering process for enhancement of dissolution rates of poorly water-soluble drugs. *European Journal of Pharmaceutics and Biopharmaceutics, 65*(1), 57-67.

Overhoff, K. A., Moreno, A., Miller, D. A., Johnston, K. P., & Williams, R. O., 3rd. (2007). Solid dispersions of itraconazole and enteric polymers made by ultra-rapid freezing. *Int J Pharm, 336*(1), 122-132.

Park, M. J., Ren, S., & Lee, B. J. (2007). In vitro and in vivo comparative study of itiraconazole bioavailability when formulated in highly soluble self-emulsifying system and in solid dispersion. *Biopharmaceutics & Drug Disposition, 28*(4), 199-207.

Pass, G. J., Carrie, D., Boylan, N., Lorimore, S., Wright, E., Houston, B., et al. (2005). Role of hepatic cytochrome P450s in the pharmacokinetics and toxicity of cyclophosphamide: Studies with the hepatic cytochrome P450 reductase null mouse. *Cancer Research, 65*(10), 4211-4217.

Patravale, V. B., Date, A. A., & Kulkarni, R. M. (2004). Nanosuspensions: a promising drug delivery strategy. *Journal of Pharmacy and Pharmacology, 56*(7), 827-840.

Patterson, T. F. (2005). Advances and challenges in management of invasive mycoses. *Lancet, 366*(9490), 1013-1025.

Patton, J. (1996a). Mechanisms of macromolecule absorption by the lungs. *Advanced Drug Delivery Review 19*, 3–36.

Patton, J. (1996b). Mechanisms of macromolecule absorption by the lungs. *Adv Drug Del Rev, 19*, 3–36.

Patton, J., Fishburn, C., & Weers, J. (2004). The lungs as a portal of entry for systemic drug delivery. *The Proceedings of the American Thoracic Society 1*(4), 338-344.

Patton, J. S. (1996). Mechanisms of macromolecule absorption by the lungs. *Adv Drug Deliv Rev 19*(1), 3-36.

Patton, J. S. (2005). Unlocking the opportunity of tight glycaemic control. Innovative delivery of insulin via the lung. *Diabetes Obes Metab, 7 Suppl 1*, S5-8.

Patton, J. S., & Byron, P. R. (2007). Inhaling medicines: delivering drugs to the body through the lungs. *Nat Rev Drug Discov, 6*(1), 67-74.

Patton, J. S., McCabe, J. G., Hansen, S. E., & Daugherty, A. L. (1989). Absorption of human growth hormone from the rat lung. *Biotechnol Ther, 1*(3), 213-228.

Peeters, J., Neeskens, P., Tollenaere, J. P., Van Remoortere, P., & Brewster, M. E. (2002). Characterization of the Interaction of 2-hydroxypropyl-beta-cyclodextrin with itraconazole at pH 2, 4, and 7. *Journal of Pharmaceutical Sciences, 91*(6), 1414-1422.

Pekkanen, J., Peters, A., Hoek, G., Tiittanen, P., Brunekreef, B., de Hartog, J., et al. (2002). Particulate air pollution and risk of ST-segment depression during repeated submaximal exercise tests among subjects with coronary heart disease: the Exposure and Risk Assessment for Fine and Ultrafine Particles in Ambient Air (ULTRA) study. *Circulation, 106*(8), 933-938.

Peters, K., Leitzke, S., Diederichs, J. E., Borner, K., Hahn, H., Muller, R. H., et al. (2000). Preparation of a clofazimine nanosuspension for intravenous use and evaluation of its therapeutic efficacy in murine Mycobacterium avium infection. *Journal of Antimicrobial Chemotherapy, 45*(1), 77-83.

Pignatello, R., Bucolo, C., Ferrara, P., Maltese, A., Puleo, A., & Puglisi, G. (2002). Eudragit RS100 (R) nanosuspensions for the ophthalmic controlled delivery of ibuprofen. *European Journal of Pharmaceutical Sciences, 16*(1-2), 53-61.

Pitha, J., Szente, L., & Szejtli, J. (1983). Molecular encapsulation of drugs by cyclodextrins and congeners. In S. D. Bruck (Ed.), *Controlled drug delivery*. Boca Raton, Fla: CRC Press, Inc.

Poirier, J. M., & Cheymol, G. (1998). Optimisation of itraconazole therapy using target drug concentrations. *Clinical Pharmacokinetics, 35*(6), 461-473.

Poirier, J. M., Hardy, S., Isnard, F., Tilleul, P., Weissenburger, J., & Cheymol, G. (1997). Plasma itraconazole concentrations in patients with neutropenia: advantages of a divided daily dosage regimen. *Therapeutic Drug Monitoring, 19*(5), 525-529.

Powell, M. C., & Kanarek, M. S. (2006a). Nanomaterial health effects--part 1: background and current knowledge. *WMJ, 105*(2), 16-20.

Powell, M. C., & Kanarek, M. S. (2006b). Nanomaterial health effects--Part 2: Uncertainties and recommendations for the future. *WMJ, 105*(3), 18-23.

Rabinow, B. E. (2004). Nanosuspensions in drug delivery. *Nature Reviews Drug Discovery, 3*(9), 785-796.

Rajewski, R. A., & Stella, V. J. (1996). Pharmaceutical applications of cyclodextrins. 2. In vivo drug delivery. *Journal of Pharmaceutical Sciences, 85*(11), 1142-1169.

Rao, G. C., Kumar, M. S., Mathivanan, N., & Rao, M. E. (2004). Nanosuspensions as the most promising approach in nanoparticulate drug delivery systems. *Pharmazie, 59*(1), 5-9.

Rejman, J., Oberle, V., Zuhorn, I. S., & Hoekstra, D. (2004). Size-dependent internalization of particles via the pathways of clathrin- and caveolae-mediated endocytosis. *Biochem J, 377*(Pt 1), 159-169.

Ren, S., Kalhorn, T. F., McDonald, G. B., Anasetti, C., Appelbaum, F. R., & Slattery, J. T. (1998). Pharmacokinetics of cyclophosphamide and its metabolites in bone marrow transplantation patients. *Clinical Pharmacology & Therapeutics, 64*(3), 289-301.

Rex, J. H., Pfaller, M. A., Galgiani, J. N., Bartlett, M. S., Espinel-Ingroff, A., Ghannoum, M. A., et al. (1997). Development of interpretive breakpoints for antifungal susceptibility testing: conceptual framework and analysis of in vitro-in vivo correlation data for fluconazole, itraconazole, and candida infections. Subcommittee on Antifungal Susceptibility Testing of the National Committee for Clinical Laboratory Standards. *Clin Infect Dis, 24*(2), 235-247.

Roelofsen, B., Kuypers, F. A., Op den Kamp, J. A., & van Deenen, L. L. (1989). Influence of phosphatidylcholine molecular species composition on stability of the erythrocyte membrane. *Biochem Soc Trans, 17*(2), 284-286.

Rogers, T. L., Johnston, K. P., & Williams, R. O., 3rd. (2001). Solution-based particle formation of pharmaceutical powders by supercritical or compressed fluid CO2 and cryogenic spray-freezing technologies. *Drug Dev Ind Pharm, 27*(10), 1003-1015.

Rowland, M., & Tozer, T. (1995). Absorption and disposition kinetics. In M. Rowland & T. Tozer (Eds.), *Clinical pharmacokinetics: Concepts and applications* (3rd ed., pp. 11–52). Baltimore: Lippincott Williams & Wilkins.

Sakagami, M. (2006). In vivo, in vitro and ex vivo models to assess pulmonary absorption and disposition of inhaled therapeutics for systemic delivery. *Adv Drug Deliv Rev, 58*(9-10), 1030-1060.

Sanna, V., Gavini, E., Cossu, M., Rassu, G., & Giunchedi, P. (2007). Solid lipid nanoparticles (SLN) as carriers for the topical delivery of econazole nitrate: in-vitro characterization, ex-vivo and in-vivo studies. *Journal of Pharmacy and Pharmacology, 59*(8), 1057-1064.

Sarkari, M., Brown, J., Chen, X., Swinnea, S., Williams, R. O., 3rd, & Johnston, K. P. (2002). Enhanced drug dissolution using evaporative precipitation into aqueous solution. *International Journal of Pharmaceutics, 243*(1-2), 17-31.

Sarver, L. W. (1996). SEM and EDS analyze materials. *Advanced Materials & Processes, 150*(1), 19-21.

Schief, W. R., Antia, M., Discher, B. M., Hall, S. B., & Vogel, V. (2003). Liquid-crystalline collapse of pulmonary surfactant monolayers. *Biophys J, 84*(6), 3792-3806.

Schuler, U., Waidelich, P., Kolb, H., Wagner, T., & Ehninger, G. (1991). Pharmacokinetics and Metabolism of Cyclophosphamide Administered after Total-Body Irradiation of Bone-Marrow Transplant Recipients. *European Journal of Clinical Pharmacology, 40*(5), 521-523.

Schurch, S., Gehr, P., Im Hof, V., Geiser, M., & Green, F. (1990). Surfactant displaces particles toward the epithelium in airways and alveoli. *Respir Physiol, 80*(1), 17-32.

Sham, J. O. H., Zhang, Y., Finlay, W. H., Roa, W. H., & Lobenberg, R. (2004). Formulation and characterization of spray-dried powders containing nanoparticles for aerosol delivery to the lung. *International Journal of Pharmaceutics, 269*(2), 457-467.

Shao, Z. H., Li, Y. P., Chermak, T., & Mitra, A. K. (1994). Cyclodextrins as Mucosal Absorption Promoters of Insulin .2. Effects of Beta-Cyclodextrin Derivatives on Alpha-Chymotryptic Degradation and Enteral Absorption of Insulin in Rats. *Pharmaceutical Research, 11*(8), 1174-1179.

Shargel, L., & Yu, A. (1999). *Applied Biopharmaceutics & Pharmacokinetics, fourth ed.* New York McGraw Hill.

Shehatta, I., Al-Marzouqi, A., Jobe, B., & Dowaidar, A. (2005). Enhancement of aqueous solubility of itraconazole by complexation with cyclodextrins using supercritical

carbon dioxide. *Canadian Journal of Chemistry-Revue Canadienne De Chimie, 83*(10), 1833-1838.

Shekunov, B. Y., Chattopadhyay, P., Yim, D., Cippola, D., & Boyd, B. (2006). *Formulation and in vitro performance of drug-lipid nanosuspensions for pulmonary delivery.* Paper presented at the Conference on Respiratory Drug Delivery, Boca Raton, Florida.

Sheppard, D. C., Rieg, G., Chiang, L. Y., Filler, S. G., Edwards, J. E., & Ibrahim, A. S. (2004). Novel inhalational murine model of invasive pulmonmy aspergillosis. *Antimicrobial Agents and Chemotherapy, 48*(5), 1908-1911.

Sibille, Y., & Reynolds, H. Y. (1990). Macrophages and polymorphonuclear neutrophils in lung defense and injury. *Am Rev Respir Dis, 141*(2), 471-501.

Singh, N., & Husain, S. (2003). Aspergillus infections after lung transplantation: clinical differences in type of transplant and implications for management. *Journal of Heart and Lung Transplantation, 22*(3), 258-266.

Sinswat, P., Overhoff, K. A., McConville, J. T., Johnston, K. P., & Williams, R. O. (2008). Nebulization of nanoparticulate amorphous or crystalline tacrolimus - Single-dose pharmacokinetics study in mice. *European Journal of Pharmaceutics and Biopharmaceutics, 69*(3), 1057-1066.

Six, K., Daems, T., de Hoon, J., Van Hecken, A., Depre, M., Bouche, M. P., et al. (2005). Clinical study of solid dispersions of itraconazole prepared by hot-stage extrusion. *European Journal of Pharmaceutical Sciences, 24*(2-3), 179-186.

Six, K., Verreck, G., Peeters, J., Augustijns, P., Kinget, R., & Van den Mooter, G. (2001). Characterization of glassy itraconazole: a comparative study of its molecular mobility below T(g) with that of structural analogues using MTDSC. *International Journal of Pharmaceutics, 213*(1-2), 163-173.

Smith, D., van de Velde, V., Woestenborghs, R., & Gazzard, B. G. (1992). The pharmacokinetics of oral itraconazole in AIDS patients. *Journal of Pharmacy and Pharmacology, 44*(7), 618-619.

Smith, S., & Bernstein, J. (1996). Inhalation Aerosols: Physical and Biological Basis for Therapy. In A. Hickey (Ed.), *Lung Biology Health Diseases* (pp. 233–269). New York Marcel Dekker.

Sobel, J. D. (2000). Practice guidelines for the treatment of fungal infections. For the Mycoses Study Group. Infectious Diseases Society of America. *Clinical Infectious Diseases, 30*(4), 652.

Somasundaran, P., Chakraborty, S., Qiang, Q., Deo, P., Wang, J., & Zhang, R. (2004). Surfactants, polymers and their nanoparticles for personal care applications. *J Cosmet Sci, 55 Suppl*, S1-17.

Spiekermann, G. M., Finn, P. W., Ward, E. S., Dumont, J., Dickinson, B. L., Blumberg, R. S., et al. (2002). Receptor-mediated immunoglobulin G transport across mucosal barriers in adult life: functional expression of FcRn in the mammalian lung. *J Exp Med, 196*(3), 303-310.

Sporanox®, p. l. Package insert. Sporanox capsules/oral solution/Sporanox I.V. (itraconazole). Janssen-Ortho Inc. Toronto, Ontario

Stella, V. J., & He, Q. (2008). Cyclodextrins. *Toxicol Pathol, 36*(1), 30-42.

Stella, V. J., Rao, V. M., Zannou, E. A., & Zia, V. (1999). Mechanisms of drug release from cyclodextrin complexes. *Advanced Drug Delivery Reviews, 36*(1), 3-16.

Stevens, D. A. (1999). Itraconazole in cyclodextrin solution. *Pharmacotherapy, 19*(5), 603-611.

Stone, K. C., Mercer, R. R., Gehr, P., Stockstill, B., & Crapo, J. D. (1992). Allometric relationships of cell numbers and size in the mammalian lung. *Am J Respir Cell Mol Biol, 6*(2), 235-243.

Stuart, D., Lobenberg, R., Ku, T., Azarmi, S., Ely, L., Roa, W., et al. (2006). Biophysical investigation of nanoparticle interactions with lung surfactant model systems. *J. Biomed. Nanotechnology 2*(3/4), 245-252.

Tam, J. M., McConville, J. T., Williams, R. O., & Johnston, K. P. (2008). Amorphous Cyclosporin Nanodispersions for Enhanced Pulmonary Deposition and Dissolution. *Journal of Pharmaceutical Sciences, 97*(11), 4915-4933.

Thiel, M. A., Zinkernagel, A. S., Burhenne, J., Kaufmann, C., & Haefeli, W. E. (2007). Voriconazole concentration in human aqueous humor and plasma during topical or combined topical and systemic administration for fungal keratitis. *Antimicrobial Agents and Chemotherapy, 51*(1), 239-244.

Thompson, P. J. (1998). Drug delivery to the small airways. *Am J Respir Crit Care Med, 157*(5 Pt 2), S199-202.

Tinke, A. P., Vanhoutte, K., De Maesschalck, R., Verheyen, S., & De Winter, H. (2005). A new approach in the prediction of the dissolution behavior of suspended particles by means of their particle size distribution. *Journal of pharmaceutical and biomedical analysis, 39*(5), 900-907.

Tolman, J. A., Nelson, N. A., Son, Y. J., Bosselmann, S., Wiederhold, N. P., Peters, J. I., et al. (2009). Characterization and pharmacokinetic analysis of aerosolized aqueous voriconazole solution. *European Journal of Pharmaceutics and Biopharmaceutics, 72*(1), 199-205.

Torchilin, V. P. (2007). Micellar nanocarriers: Pharmaceutical perspectives. *Pharmaceutical Research, 24*(1), 1-16.

Tsapis, N., Bennett, D., Jackson, B., Weitz, D. A., & Edwards, D. A. (2002). Trojan particles: Large porous carriers of nanoparticles for drug delivery. *Proceedings of the National Academy of Sciences of the United States of America, 99*(19), 12001-12005.

Upton, A., McCune, J. S., Kirby, K. A., Leisenring, W., McDonald, G., Batchelder, A., et al. (2007). Fluconazole coadministration concurrent with cyclophosphamide conditioning may reduce regimen-related toxicity postmyeloablative hematopoietic cell transplantation. *Biol Blood Marrow Transplant, 13*(7), 760-764.

USP. (2008). Aerosols, Nasal Sprays, Metered-dose Inhalers, and Dry Powder Inhalers, In *United States Pharmacopeia 31 - NF 26. The United States Pharmacopeial Convention*. Rockville, MD.

Valeyre, D., Soler, P., Basset, G., Loiseau, P., Pre, J., Turbie, P., et al. (1991). Glucose, K+, and Albumin Concentrations in the Alveolar Milieu of Normal Humans and Pulmonary Sarcoidosis Patients. *American Review of Respiratory Disease, 143*(5), 1096-1101.

Van den Mooter, G., Wuyts, M., Blaton, N., Busson, R., Grobet, P., Augustijns, P., et al. (2001). Physical stabilisation of amorphous ketoconazole in solid dispersions with polyvinylpyrrolidone K25. *European Journal of Pharmaceutical Sciences, 12*(3), 261-269.

van Drooge, D. J., Hinrichs, W. L., & Frijlink, H. W. (2004). Anomalous dissolution behaviour of tablets prepared from sugar glass-based solid dispersions. *J Control Release, 97*(3), 441-452.

Varma, M. V., Sateesh, K., & Panchagnula, R. (2005). Functional role of P-glycoprotein in limiting intestinal absorption of drugs: contribution of passive permeability to P-glycoprotein mediated efflux transport. *Mol Pharm, 2*(1), 12-21.

Vaughn, J. M., Gao, X., Yacaman, M. J., Johnston, K. P., & Williams, R. O., 3rd. (2005). Comparison of powder produced by evaporative precipitation into aqueous solution (EPAS) and spray freezing into liquid (SFL) technologies using novel Z-

contrast STEM and complimentary techniques. *European Journal of Pharmaceutics and Biopharmaceutics 60*(1), 81-89.

Vaughn, J. M., McConville, J. T., Burgess, D., Peters, J. I., Johnston, K. P., Talbert, R. L., et al. (2006). Single dose and multiple dose studies of itraconazole nanoparticles. *European Journal of Pharmaceutics and Biopharmaceutics, 63*(2), 95-102.

Vaughn, J. M., Wiederhold, N. P., McConville, J. T., Coalson, J. J., Talbert, R. L., Burgess, D. S., et al. (2007). Murine airway histology and intracellular uptake of inhaled amorphous itraconazole. *International Journal of Pharmaceutics, 338*, 219-224.

Veldhuizen, R., Nag, K., Orgeig, S., & Possmayer, F. (1998). The role of lipids in pulmonary surfactant. *Biochim Biophys Acta, 1408*(2-3), 90-108.

Verreck, G., Six, K., Van den Mooter, G., Baert, L., Peeters, J., & Brewster, M. E. (2003). Characterization of solid dispersions of itraconazole and hydroxypropylmethylcellulose prepared by melt extrusion--Part I. *International Journal of Pharmaceutics, 251*(1-2), 165-174.

Videira, M. A., Botelho, M. F., Santos, A. C., Gouveia, L. F., de Lima, J. J., & Almeida, A. J. (2002). Lymphatic uptake of pulmonary delivered radiolabelled solid lipid nanoparticles. *J Drug Target, 10*(8), 607-613.

Vincent, J. H., Johnston, A. M., Jones, A. D., Bolton, R. E., & Addison, J. (1985). Kinetics of deposition and clearance of inhaled mineral dusts during chronic exposure. *Br J Ind Med, 42*(10), 707-715.

Wall, D. A., Marcello, J., Pierdomenico, D., & Farid, A. (1994). Administration as Hydroxypropyl-Beta-Cyclodextrin Complexes Does Not Slow Rates of Pulmonary Drug Absorption in Rat. *Stp Pharma Sciences, 4*(1), 63-68.

Weibel, E. (1963). *Morphometry of the Human Lung* New York: Academic.

Widdicombe, J. H., & Widdicombe, J. G. (1995). Regulation of human airway surface liquid. *Respir Physiol, 99*(1), 3-12.

Wiedmann, T. S., DeCastro, L., & Wood, R. W. (1997). Nebulization of NanoCrystals(TM): Production of a respirable solid-in-liquid-in-air colloidal dispersion. *Pharmaceutical Research, 14*(1), 112-116.

Willems, L., van der Geest, R., & de Beule, K. (2001). Itraconazole oral solution and intravenous formulations: a review of pharmacokinetics and pharmacodynamics. *J Clin Pharm Ther, 26*(3), 159-169.

Yamashita, K., Nakate, T., Okimoto, K., Ohike, A., Tokunaga, Y., Ibuki, R., et al. (2003a). Establishment of new preparation method for solid dispersion formulation of tacrolimus. *International Journal of Pharmaceutics, 267*(1-2), 79-91.

Yang, W., Peters, J. I., & Williams, R. O. (2008a). Inhaled nanoparticles - A current review. *International Journal of Pharmaceutics, 356*(1-2), 239-247.

Yang, W., Tam, J., Miller, D. A., Zhou, J., McConville, J. T., Johnston, K. P., et al. (2008). High bioavailability from nebulized itraconazole nanoparticle dispersions with biocompatible stabilizers. *International Journal of Pharmaceutics, 361*(1-2), 177-188.

Yang, W., Wiederhold, N. P., & Williams, R. O., 3rd. (2008). Drug delivery strategies for improved azole antifungal action. *Expert Opin Drug Deliv, 5*(11), 1199-1216.

Yokoyama, M. (2005). Drug targeting with nano-sized carrier systems. *J Artif Organs, 8*(2), 77-84.

Yu, L., & Waxman, D. J. (1996). Role of cytochrome P450 in oxazaphosphorine metabolism - Deactivation via N-dechloroethylation and activation via 4-hydroxylation catalyzed by distinct subsets of rat liver cytochromes P450. *Drug Metabolism and Disposition, 24*(11), 1254-1262.

Yule, S. M., Walker, D., Cole, M., McSorley, L., Cholerton, S., Daly, A. K., et al. (1999). The effect of fluconazole on cyclophosphamide metabolism in children. *Drug Metabolism and Disposition, 27*(3), 417-421.

Zhou, H. Y., Zhang, Y. L., Biggs, D. L., Manning, M. C., Randolph, T. W., Christians, U., et al. (2005). Microparticle-based lung delivery of INH decreases INH metabolism and targets alveolar macrophages. *Journal of Controlled Release, 107*(2), 288-299.

Vita

Wei Yang was born in Yinchuan, Ningxia province, P.R. China on December 12, 1975 to Mr. Jingsen Yang and Mrs. Fengqing Wang. After she graduated from Yinchuan No. 9 High School in China in 1994, she began her undergraduate education at China Pharmaceutical University, Nanjing, China. She received the degree of Bachelor of Science (Pharmacology) in July 1999 with the honor of Top Graduate. She then pursued her graduate study in China Pharmaceutical University, and transferred to the Graduate Program in the School of Pharmacy at Memorial University of Newfoundland, St. John's, Newfoundland, Canada. She obtained her Master of Science in Pharmacy in December 2003, and worked as a Research Associate in North Atlantic Biopharma Inc. at St. John's, Canada thereafter. In September 2005, she was admitted into the Graduate School in the College of Pharmacy at The University of Texas at Austin to pursue her Ph.D. under the supervision of Dr. Williams. During Wei's graduate career she has presented her research at scientific conferences in U.S. and Canada. In 2008 and 2009 Wei was awarded the University of Texas Continuing Fellowship and Jaime N. Delgado Endowed Graduate Fellowship in Pharmacy. Parts of the chapters presented in this dissertation will be submitted for publication in several high impact pharmaceutical journals.

Permanent address: 2501 Lake Austin Blvd. Apt H202, Austin, TX, 78703

This dissertation was typed by the author.